APPLICATION OF STEREOLOGY AND MORPHOMETRY ON SYNAPSES AND NEURONS IN THE HIPPOCAMPUS OF AGEING RATS

APPLICATION OF STEREOLOGY AND MORPHOMETRY ON SYNAPSES AND NEURONS IN THE HIPPOCAMPUS OF AGEING RATS

an illustration of problems and solutions

Toepassing van stereologie en morfometrie
op synapsen en neuronen
in de hippocampus van verouderende ratten

een illustratie van problemen en oplossingen

PROEFSCHRIFT

Ter verkrijging van de graad van doctor
aan de Erasmus Universiteit Rotterdam
op gezag van de rector magnificus
Prof. dr P.W.C. Akkermans M. Lit.
en volgens het besluit van het college van dekanen.
De openbare verdediging zal plaatsvinden
op woensdag 9 maart 1994 om 11.45 uur
door

Didima Maurice Gerarda de Groot
geboren te St. Anthonis

Promotiecommissie

Promotores	:	Prof. dr J. Voogd Prof. dr T.M. Mayhew (Nottingham)
Overige leden	:	Prof. dr W.R.F. Notten Prof. dr H.J.G. Gundersen (Århus)

to Gijs Vrensen
for setting me on the track of this research
and
to the teachers
of the annual courses in morphometry and stereology
for keeping me on it

In memory of my parents

This research was carried out at the Department of Pharmacology, TNO-MBL, Head: Dr. O.L. Wolthuis. Succeeded (January, 1993) by Dr. P.L.B. Bruijnzeel.

CONTENTS

PART IV DESCRIPTION OF PRACTICAL APPROACHES FOR THE QUANTIFICATION OF NEURONAL STRUCTURES (Appendix)

Quantification of synapses and synaptic substructures

Quantification of synapses

- *Total number of synapses per unit disector volume, $N_v(s)$*
- *Maximum intercept length of the synapses, Emaxl(s)*
- *Synapse perimeter length, EL(s)*
- *Synapse (presynaptic) surface area, ES(s)*
- *Projected height (=linear projection) of the synapses, EH(s)*

Quantification of synapse perforations

- *Number of perforations per perforated synapse, Ep_0*
- *Maximum intercept length of the perforations, E(maxl)(p)*
- *Perforation perimeter length, EL(p) and perforation surface area, ES(p)*
- *Projected height (=linear projection) of the perforations, EH(p)*

PART I

GENERAL INTRODUCTION

GENERAL INTRODUCTION

Didima M.G. De Groot

TNO Medical Biological Laboratory, PO Box 5815, 2280 HV Rijswijk,The Netherlands

INTRODUCTION

It is generally accepted that synaptic contact zones are dynamic structures able to modify their chemical, physiological and functional properties throughout the lifespan of an organism. Such changes have been shown to be accompanied by alterations in the morphology of synapses. For example, modifications in synaptic ultrastructure have been reported to be involved in learning and memory, in sensitization and in other functions of the CNS (Central Nervous System). However, qualitative changes, if not extreme, are difficult to detect and compare. Therefore, quantification of synaptic ultrastructural features is of prime importance in neurobiology.

Compared to what is known about the clinical and pathological lesions encountered in various age-related diseases, such as Alzheimer's disease, little is known about structural, biochemical and functional changes that occur in the brain as a consequence of the *normal aging process*. Yet, to get more insight into the mechanisms responsible for the clinical and pathological changes in age-related diseases but also in e.g. environmental toxicology, it seems relevant to obtain baseline knowledge of what constitutes normal ageing.

One of the major problems with regard to normal ageing is the question of whether the synaptic connectivity of neurons that survive in the senescent brain is impaired. This problem has been studied most frequently in the hippocampal formation because of its relatively simple anatomy and its rather well known pattern of synaptic connections. The hippocampal formation seems to be very vulnerable to the ageing process and it plays a crucial role in the aquisition of certain types of new information, particularly for memory formation, which is commonly disrupted during normal ageing (Barnes, 1983, 1988; Landfield et al., 1986; deToledo-Morell et al., 1988a, 1988b).

Electrophysiological studies of the hippocampal formation have indicated that the potential of particular subfields for functional synaptic plasticity is diminished in senescence. However, with respect to quantitative data on the morphology of the synapses at young versus old age, the results of different studies are very conflicting and, consequently, difficult to interpret.

There are several reasons for these discrepancies of the various results on quantitative data of synapse morphology.

A main problem was the finding that synapse shape may deviate from the classically presumed *disc-shape* (West et al., 1972). For several brain regions, including the hippocampal formation, it has been shown that many synaptic contact zones are not flat, round structures. They may have a very complex morphology and may even show interruptions in their pre- and post synaptic densities (De Groot and Bierman, 1983, 1986; De Groot, 1988; Geinisman et al., 1986; Geinisman, 1993). The latter, so called *perforated* synapses (Peters and Kaiser-Abramof, 1969), can only be distinguished

from *non-perforated* synapses with the use of *serial* sections (see below) (De Groot and Bierman, 1983).
Older stereological methods to estimate number and size of synapses use information from *random* sections and start from the assumption that synapses are disc-like structures. In addition, they may fail to account for differences in size of the investigated particles -although the more advanced *unfolding* methods do (Cruz-Orive, 1983)- and may ignore the effect of section thickness. Microscopical sections have a finite thickness whereas some stereological methods start from the assumption that structures are measured and counted in a 2-dimensional plane. The use of tissue sections introduces *truncation* problems (Cruz-Orive, 1983). One of these problems results from *overprojection*, the so called *Holmes' effect* (Weibel, 1979). Because of the 3-dimensional character of a tissue section, the projected image or *profile* of a transected structure may be observable in the section whereas it is not actually present at the upper surface of the section which would be a true 2-dimensional plane. In addition, the projected image of the structure may seem larger than its actual size at the upper surface of the section. Another truncation phenomenon is that of *'lost caps'* where small profiles may go unrecognized in the section.
Clearly, the results obtained with such methods have been biased to an unknown extent and part of the discrepancies between the results of earlier studies will originate from these biases.

Another bias has been introduced by the *reference space*. Numbers of synapses were usually expressed in numbers per unit tissue area or tissue volume whereas *changes in the reference tissue* such as procedural shrinkage or changes in the volume of the neuropil which might have resulted from the ageing process, were not taken into account.

There is also the problem of individual variability in the memory capacity intrinsic to aged animals (Geinisman et al., 1986). One has to realize that, depending on species and strain, only a certain percentage of a population of individuals will reach old age; the proportion reaching senescence will be even smaller. The question remains whether or not the survivors comprise a selected group of physically and/or mentally stronger individuals, not representative of the "average" individual.

OUTLINE OF THE THESIS

This thesis has two main themes.

1) To assess the applicability and value of quantitative stereological/morphometrical methods for the detection of subtle -but relevant- differences in number, size and shape of different types of complex-shaped synapses (Part II, Chapters 1 to 5), and

2) To apply quantitative stereological/morphometrical methods to test whether synaptic plasticity occurs in the hippocampus of the rat during normal ageing (Parts III and IV).

In Part II the methodological problems outlined above have been studied experimentally, using synapses in the hippocampus of young and aged rats.
In chapter 1, the bias introduced into the estimation of synapse number and size when *perforated* synapses are not recognized as such is studied. Results, obtained in random sections are compared with results obtained in serial sections.
In Chapter 2, improvements of the protocol for serial sectioning are described, as is the application of the *serial section technique* to estimate numerical densities of arbitrarily-shaped synapses (Cruz-Orive, 1980).
In Chapter 3, different methods to estimate the thickness of (ultra)thin tissue sections are described, evaluated and compared.
In Chapter 4, the conventional *unfolding procedure* (Cruz-Orive, 1983) to estimate the numerical density of synapses is compared with two recent methods, i.e. the *serial section technique* (Cruz-Orive, 1980) and the *disector technique* (Sterio, 1984), which do not rely on assumptions regarding the size, shape and orientation of the synapse.
In Chapter 5, a method is described providing information on *differences in the shape* of synapses using *measurements on 2-dimensional reconstructions of synapse shadows.*

In Part III the effect of age on several ultrastructural features of neurons, of non-perforated and of perforated synapses in the hippocampus of 3, 12, 24 and 30 months old rats is studied. To estimate number and size of these structures, some of the methods evaluated in Part II have been applied. Also the number and size of *synapse perforations* has been estimated. Synapses and neurons have been counted in serial sections according to an *unbiased counting rule* (Gundersen, 1977). To avoid biases introduced by age-related or procedure-related changes in the reference volume, number fractions of neurons and synapses have been calculated since number fractions do not depend on changes in the reference space.
Methods to estimate the number of *presynaptic dense projections* (Cruz-Orive, 1985) are compared. In addition, synapse shadows are reconstructed and are studied both qualitatively and quantitatively (De Groot et al., 1992), to obtain (indirect) information about differences in the shape of the actual synapse.

The relevance of the results with regard to synaptic plasticity and the ageing process is discussed.

Part IV, the Appendix, includes an extensive description of all the stereological/morphometrical procedures and formulae, used in Part III to quantify neural structures.

The present part of the thesis closes with a brief description of the structural organization of the hippocampus and recent views on the relevance of "perforated" synapses.

STRUCTURAL ORGANIZATION OF THE HIPPOCAMPUS.

Functions of the hippocampus.
Definition and nomenclature.

The hippocampus is one of the most extensively studied areas of the brain. At first, the hippocampus was considered as an important olfactory centre, belonging to the rhinencephalon or "smell brain" (Ramon y Cajal, 1903; Brodal, 1947). This theory was superseded by the Papez hypothesis, suggesting that the hippocampus is part of a circuit interconnecting hippocampus, hypothalamus, thalamus and neocortex and forming the neural substrate of emotional behaviour (Papez, 1937). Later, MacLean (1952) extended the Papez hypothesis by introducing the term "limbic system".

The term "limbic" stems from Broca's (1878) description of the structures near the border (limbus) of the neocortical mantle surrounding the base of the cerebral hemisphere, structures which Broca found to be relatively constant in their development in the brains of all mammals. The "limbic system" concept was based on the assumption that visceral and non-visceral systems in the brain can clearly be distinguished (Maclean, 1952). MacLean included the cerebral cortex surrounding the medial part of the cerebral hemisphere and the subcortical nuclei to which it is connected, suggesting that these areas are all related to non-visceral functions.

Since the introduction of the term limbic system, many brain regions have been shown to have connections with the limbic cortex. In fact, essentially all of the major functional systems in the brain share direct connections with the limbic lobe (Brodal, 1981). This has made it particularly difficult to define the limits of the limbic system. However - although there are variations in definition- the limbic structures generally involve the cingulate and hippocampal gyri, the hippocampal formation, the orbito-insulo temporal polar region, amygdala, septum, hypothalamus, epithalamus and the dorsomedial and anterior thalamic nuclei.

With regard to synaptic functioning, present knowledge suggests that the hippocampal formation may be responsible for integration of information from the sensory modalities and for transformation of this information before it is relayed to cortical association areas and to visceral and motor control systems. In the broadest functional terms it seems to be in the unique position of influencing somatomotor, visceral, motivational, affective and cognitive mechanisms (Swanson, 1983).

Cytoarchitecture and topography of the hippocampal formation.

The hippocampus is a bilaterally symmetrical structure, shaped somewhat like a torsed banana (fig. 1). Its long or septotemporal axis runs from the septal nuclei rostrally to the temporal cortex ventrocaudally. The short or transverse axis is oriented perpendicular to the septotemporal axis.

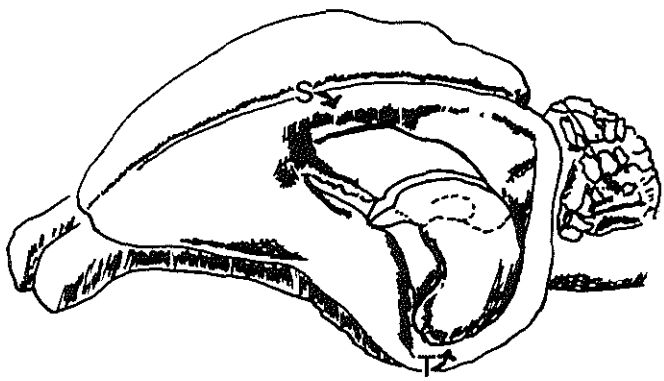

Figure 1. Drawing of the position of the hippocampal formation in the rat brain. The cortical surface overlying the hippocampus has been removed. The hippocampus is an elongated, banana-shaped structure with the long or septotemporal axis running from the septal nuclei rostrally (S) to the temporal cortex (T) ventrocaudally. The short or transverse axis is oriented perpendicular to the septotemporal axis. A slice taken approximately midway along the septotemporal axis is indicated. Such a slice includes the major neuronal connections of the hippocampal formation (compare fig. 2). *Modified after Andersen, 1981b.*

It consists of two interlocking -in transverse sections 'C-shaped'- archicortical fields: the hippocampus proper or cornu ammonis and the dentate gyrus or fascia dentata (fig. 2).

Each region contains a densely packed sheet of "principal" cells.

The principal cells are pyramidal cells. The continuous layer of pyramidal cell bodies is called the pyramidal layer (see below).

The major neurons of the dentate gyrus are the granule cells. The continuous layer containing their cell bodies is called the granular layer (see below).

The hippocampus and the fascia dentata contain a variety of interneurons with their dendrites intermingling with those of the principal cells. Different layers can be distinguished in both regions.

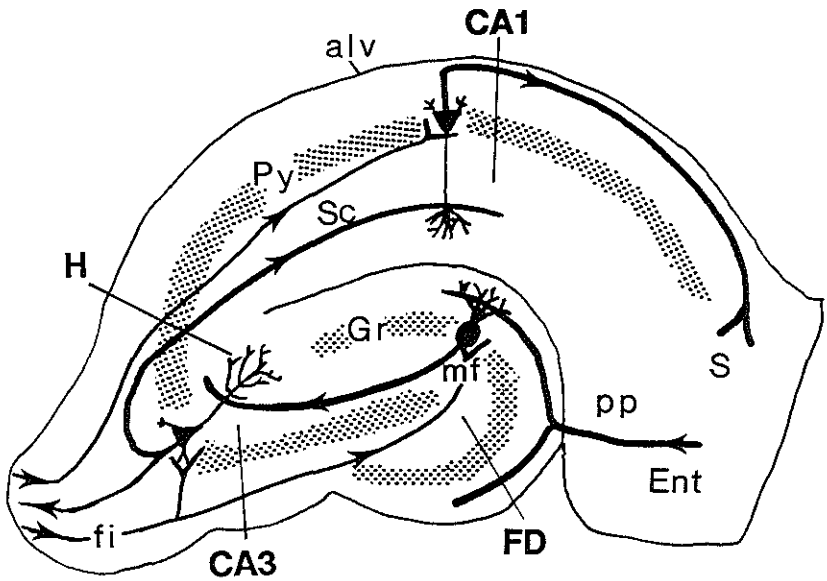

Figure 2. Diagram of a transverse section of the hippocampal formation showing the main neuronal elements of the structure. The hippocampus consists of two interlocking C-shaped archicortical fields: the hippocampus proper (H) and the fascia dentata (FD). The principle cells of H and FD are the pyramidal and granular cells, respectively.
alv, alveus; ent, entorhinal area; fi, fimbria; Gr, granular layer; mf, mossy fibers; pp, perforant path; Py, pyramidal layer; sc, schaffer collaterals; S, subiculum.
Modified after Andersen et al., 1971.

The hippocampus consists of seven layers, from periphery to centre (fig. 3):

1) The ependymal zone, which forms the lining of the ventricular surface of the hippocampus;
2) The alveus, consisting mainly of axons of pyramidal cells and incoming fibers. A few cell bodies, apparently displaced from the adjacent stratum oriens, are present here;
3) Stratum oriens contains the tufts of the basal dendritic arborizations of the pyramidal cells, different types of cell bodies and the collaterals of the axons of the CA3 pyramidal cells that are in parallel with the Schaffer collaterals of the stratum radiatum;
4) Stratum pyramidale represents the continuous layer of densely packed pyramidal cell bodies. The dendrites of the pyramidal cells are located in the stratum oriens, stratum radiatum and stratum lacunosum moleculare (Andersen et al.,

1971);

5) Stratum radiatum, characterized by rather sparse cell bodies and several fiber systems, the most important of which is formed by the Schaffer collaterals, i.e. the collaterals of axons of CA3 pyramidal cells that form synapses with the dendrites of the CA1 pyramidal cells. These collaterals are also called association fibers;

6) Stratum lacunosum, consisting mainly of bundles of parallel fibers. Some of these bundles are collaterals of the pyramidal cells, whereas others are extrinsic to the hippocampus.

7) The most superficial layer is the stratum moleculare, lying directly adjacent to the hippocampal fissure. It contains predominantly fibers and dendritic terminals.

In a number of studies the latter two layers are combined into stratum lacunosum-moleculare (Hjorth-Simonsen, 1977).

The fascia dentata consists of three layers:

1) The molecular or dendritic layer. This molecular layer can be further subdivided based upon the distribution of different afferent systems;

2) The granular cell layer, containing the granule cell bodies (the principle cells of the fascia dentata) with their excitatory axons, the mossy fibers (Blackstad et al, 1970);

3) The polymorph layer or "hilar region" characterized by widely scattered, polymorph neurons (see below area CA4). This hilar region is found between the, so called, upper and lower blades that the fascia dentata possesses because of its geometry.

The hippocampus proper is subdivided into the subfields CA1 to CA4 (Lorente de No, 1934). Each of the subfields contains apical and basal dendritic areas.

Area CA4 corresponds to the so called 'polymorph zone of the dentate gyrus', described earlier by Ramon y Cajal (1911), and to the 'hilar region of the dentate

---

Figure 3. Epon sections (200 nm thick) from the hippocampal CA1 (left) and CA3 regions (right) of a 3 month old rat, stained with toluidine blue. The tissue has been block-stained with E-PTA (ethanolic phosphotungstic acid) prior to embedding.
Different layers can be distinguished in the hippocampus. In CA1, from periphery (ventricular surface; top) to centre (hippocampal fissure; bottom):
epithelial zone (ez), alveus (alv), stratum (str.) oriens (Or), str. pyramidale (Py), str. radiatum (Rad), str. lacunosum (L), stratum moleculare (Mol).
In addition to the layers that can be distinguished in the hippocampal CA1 region (compare CA1 and CA3), the CA3 region contains stratum lucidum (Lu). The mossy fibers, the zinc-rich afferents of the granule cells of the fascia dentata project to this layer and to the pyramidal layer of CA3 as well.
fi, fimbria.
Modified after De Groot, 1988.

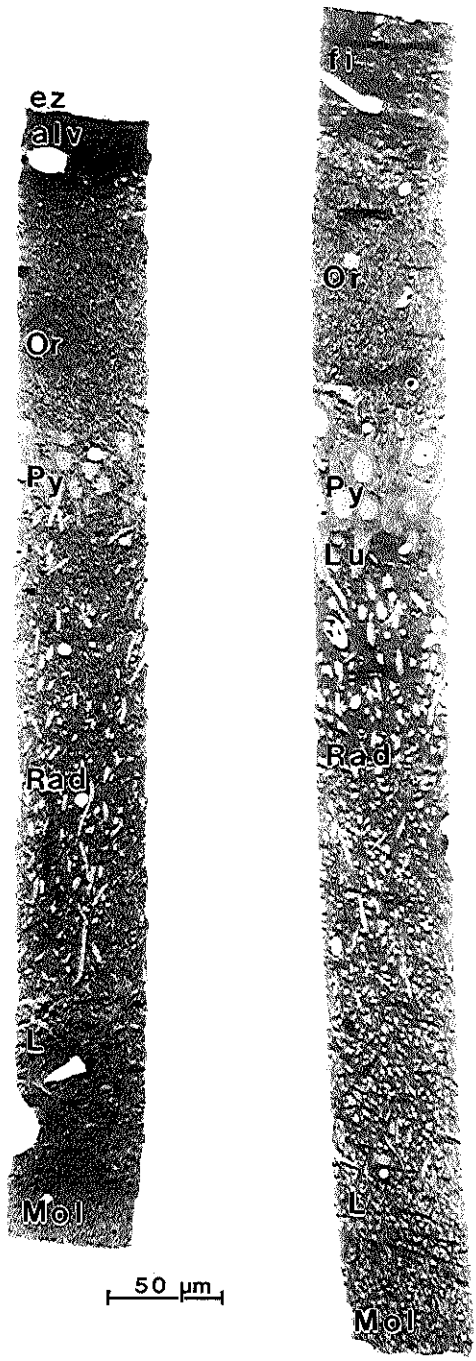

3

gyrus' (Lopez da Silva et al., 1990). The fields CA3 and CA2 together correspond to the 'regio inferior' (Ramon y Cajal, 1911) whereas field CA1 corresponds to the 'regio superior'.

In the rat the CA2 area is often included in CA3 (Blackstad, 1956).

Connections of the hippocampal formation.

The main afferent projections to the hippocampus include (fig. 2):

1) the perforant pathway (Lorento de No, 1934; Hjort-Simonsen, 1972) which originates in the stellate layer of the entorhinal cortex and terminates in the outer two third of the molecular layer of the fascia dentata and
2) the septo-hippocampal projections mediated through the fimbria and fornix. The latter originate in the medial septal nucleus and distribute to the whole hippocampal formation and the adjacent cortical areas (Swanson and Cowan, 1979).

Both CA1 and CA3 pyramidal cells project to the lateral septum via the fimbria (Swanson and Cowan, 1977). The lateral septum projects to the medial septum which, in turn, projects back to the hippocampal subfields as well as to the granule cells of the fascia dentata and the subicular complex (Swanson, 1978; Swanson and Cowan, 1979).

In the hippocampus, integration of all kinds of incoming cortical and subcortical information takes place.
The principal extrinsic cortical afferent inputs to the hippocampal formation terminate in the molecular layer of the hippocampal areas CA1 to CA4 and in the molecular layer of the fascia dentata. In the same regions projections from subcortical areas like amygdala, thalamic nuclei and basal forebrain exist. Other important extrinsic afferents terminate in areas that are dominated by major intrinsic afferent systems.

Lamellar organization of the hippocampus.

A striking feature of the hippocampal formation is the highly ordered and serially aranged chain of intrinsic connections that link adjacent cytoarchitectonically defined subfields. Impulses entering the granule cells of the fascia dentata through the perforant path are further processed through the hippocampal formation by a three-membered pathway, so called "lamella", consisting of the following elements (fig. 2)
1) the mossy fibers
2) the CA3 axons and
3) the CA1 axons.
The mossy fibers, the zinc-rich efferents of the granule cells of the fascia dentata, project to the stratum pyramidale and stratum lucidum of the CA3 area (Blackstad et

al, 1970) (fig. 3).
The CA3 neurons propagate the impulses from the mossy fibers both to the ipsilateral CA1 region through the Schaffer collaterals, an intrinsic projection system identified by classical Golgi impregnation studies, as well as to the contralateral CA1 and CA3 areas through the commissural fibers (Blackstad, 1956; Laurberg, 1979).
The excitatory CA1 pyramidal cells send most of their axons caudally into the subicular complex (Andersen et al, 1973) via the alveus.

All these excitatory pathways appear to be monosynaptically connected (Andersen, 1975) but they are also influenced by recurrent inhibition at each step (Andersen et al, 1964). Local neurons are present both in the fascia dentata and in the stratum pyramidale of the hippocampus (Storm-Mathisen, 1972; Fonnum and Walaas, 1978).

The orientation of the lamellae as regards the longitudinal or septotemporal axis of the hippocampus differs among species (Andersen, 1983). In rat the plane of the lamellae has long been thought to be transverse to the longitudinal axis (cf. figs. 1 and 2). However, increasing evidence indicates that projections in the longitudinal axis are as prominent and well organized as those which run in the transverse axis (Amaral and Witter,1989).

The connections, mentioned above, represent the quantitatively most important part of the hippocampal circuitry. More detailed descriptions are given in reviews by e.g. Amaral and Witter (1989), Andersen (1975, 1981a), Lopez Da Silva et al. (1985, 1990), Teyler and Discenna (1984) and Walaas (1983).

RECENT VIEWS ON STRUCTURE AND FUNCTION OF "PERFORATED" SYNAPSES.

Morphology of perforated synapses.

The term "perforated" synapse was first introduced by Peters and Kaiserman-Abramof (1969), for synapses upon dendritic spines in the cerebral cortex of the rat. In serial sections, these synapses appear to exhibit a discontinuous or *perforated* PSD (Post Synaptic Density) profile in at least one serial section, while *non-perforated* synapses show continuous PSD profiles in all consecutive sections. The perforations (also called *holes)* in the PSD appear to correspond to local interruptions in the presynaptic membrane densities of the synapse, i.e. to interruptions in the so called *presynaptic grid of dense projections* (cf. De Groot and Bierman, 1983, fig. 3; Part II, Chapter 1 of this thesis and De groot, 1988, fig. 9; Part II Chapter 2 of this thesis).

In subsequent years, the presence of perforated synapses was reported for several parts of the brain of different mammals (for a review cf. Calverley and Jones, 1990). It was demonstrated further that perforated synapses are morphologically heterogeneous and may be subdivided according to the appearance of their PSD into 1) segmented 2) horseshoe-shaped or 3) fenestrated perforated synapses (Peters and Kaiserman-Abramof, 1969; Cohen and Siekevitz, 1978; Vrensen and Nunez Cardozo, 1981; Spacek and Hartmann, 1983; Calverley and Jones, 1987; Geinisman et al., 1987, 1991b, 1992a, 1992b).

In *segmented* synapses complete separation of the active zone has occurred. In *horseshoe-shaped* synapses, invaginations in the outer border of the transmission zone are observed and *fenestrated* synapses are characterized by a local interruption in the PSD (fig. 4A-C).

Recently Geinisman (1993), using three-dimensional (3D) reconstructions from serial sections, distinguished additional subtypes of axospinous perforated synapses in the molecular layer of the fascia dentata. These reconstructions showed that some synapses exhibited *partitions*. These partitions are composed of a ridge on the postsynaptic spine head, which invaginates the presynaptic axon terminal. Geinisman distinguished 3 different types of partitions: 1) complete, 2) sectional and 3) focal partitions (fig.4A-C).

Complete spine partitions are observed in *segmented* synapses (fig. 4A). These spine partitions span the entire extend of a transmission zone and divide the area of the axon terminal contacted by the spine into distinct entities. Such complete spine partitions provide barriers between two to four discrete transmission zones, each one being formed by a separate axon terminal protrusion and delineated by a separate segment of the postsynaptic density (PSD).

Sectional partitions are present in *horseshoe-shaped* synapses, i.e. the base of the partition is placed between the arms of a horseshoe-shaped PSD (fig. 4B).

Focal partitions have been observed in *fenestrated* synapses; in this case the base of the partition is restricted to a perforation (fig. 4C).

In the latter two synapse types, contrary to the segmented ones, the base of the spine partition does not extend beyond a perforation area. Although both sectional and focal partitions invaginate a presynaptic axon terminal, they do not divide it into separate protrusions and do not split a single transmission zone into disjoint entities.

In Geinisman's study all three subtypes of *partitioned* synapses appeared to have *nonpartitioned* companions exhibiting segmented, horseshoe-shaped or fenestrated PSDs, but no ridge on the postsynaptic spine head invaginating the presynaptic axon terminal (cf fig. 4A-C).

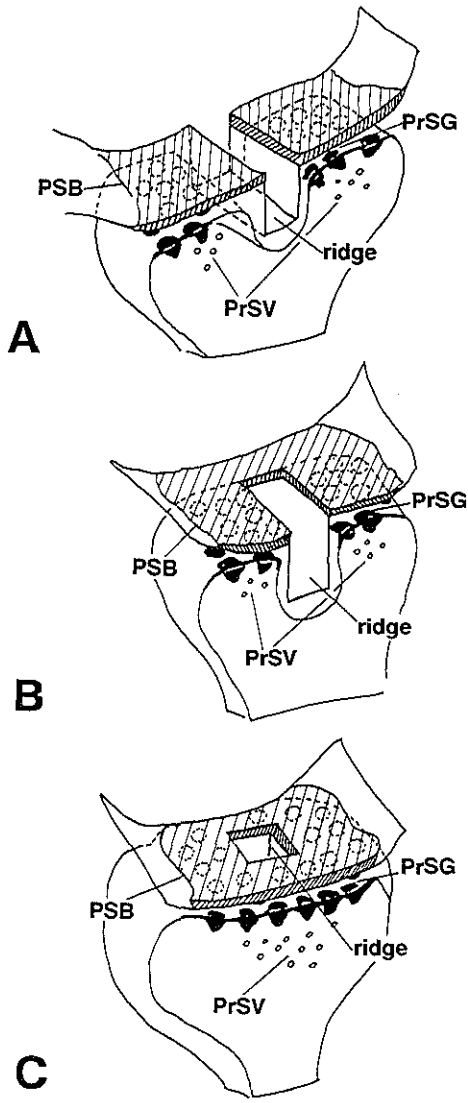

Figure 4. Schematic drawings of distinct sub-types of perforated synapses with 'partitions'. The partitions are formed by a band of cytoplasm (ridge), forth coming from the postsynaptic spine and invaginating the presynaptic axon terminal.

A. Segmented synapse with *complete* partition.

B. Horseshoe-shaped synapse with a *sectional* partition.

C. Fenestrated (annulated) synapse with a *focal* partition.

PSB, shaded area representing the post synaptic band (or postsynaptic 'density'); ridge, band of cytoplasm forth coming from the postsynaptic spine and invaginating the presynaptic axon terminal; PrSG, presynaptic 'grid' of dense projections; PrSV, presynaptic vesicles.

NB. All three subtypes, shown here, may appear also in a non-partitioned form.

The perforated synapse and its possible role in synaptic plasticity.

Synaptic plasticity refers to alterations in the efficacy of synaptic transmission and is likely to involve structural modifications of synapses. The general pattern of synaptic restructuring associated with synaptic plasticity is unknown. However, changes in the number and morphology of synapses and alterations in synaptic strength have been shown to exist (for reviews see Desmond and Levy, 1988; Greenough and Bailey, 1988; Calverley and Jones, 1990; Geinisman et al., 1991a; Wallace et al., 1991; Bailey and Kandel, 1993). Especialy *perforated* synapses are shown to be involved in synaptic plasticity (Nieto-Sampedro et al., 1982; Carlin and Siekevitz, 1983; Dyson and Jones, 1984; Geinisman et al., 1986, 1988, 1990; Petit, 1988; Calverley and Jones, 1990). It has been hypothesized that such synapses may split along PSD perforations into non-perforated synapses having a continuous PSD and that the resulting increase in synaptic numbers may underlie an enduring augmentation of synaptic transmission (Nieto-Sampedro et al., 1982; Carlin and Siekevitz, 1983; Dyson and Jones, 1984; Petit, 1988).

Another explanation for the role of perforated synapses (cf. Vrensen, 1989) is an increase in synaptic efficacy due to the induction of perforations. If neurotransmission indeed takes place at the edges of the PSD (Peters and Kaiserman-Abramof, 1969), induction of perforations will increase the total perimeter length of the PSD. Hence, increased synaptic transmission will take place.

As a result of his observations on reconstructed serial sections, Geinisman (1993) suggested a novel model of the structural modifications which may underly synaptic plasticity.

According to this model, the assembly of spine partitions separating discrete transmission zones, rather than the process of synapse splitting and division, may account for persistent alterations in synaptic efficacy. Remodelling of preexisting synapses which eventually results in the formation of such synapses with multiple, completely partitioned transmission zones is proposed. These synapses, which appear to be designed as elements of an unusual high strength, represent the pivotal structures in synaptic plasticity. Formation of such synapses is postulated to result in a sustained increase in efficacy of synaptic transmission. Conversely, a disassembly of complete partitions with the transformation of multiple transmission zones into a single one is proposed to lead to a persistent depression of synaptic responses.

Evidence, supporting this hypothesis was given by the finding that in the fascia dentata of the rat the induction of LTP (long Term Potentiation) which is a widely accepted experimental model of synaptic plasticity, was followed by a higly specific increase in the number of only those axospinous perforated synapses, exhibiting multiple, completely partitioned transmission zones (Geinisman et al., 1993). This highly selective modification of synaptic connectivity, involving only one particular synaptic subtype in the potentiated synaptic field may represent a structural substrate of the

long-lasting enhancement of synaptic responses which characterizes LTP.

It seems likely that at least the last-mentioned perforated synaptic contact zones represent structures of unusually high efficacy. An increase in their numbers would be expected to augment permanently synaptic responses. However, more evidence should be gathered to support this suggestion.

REFERENCES

Amaral, D.G. and Witter, M.P. (1989) The three-dimensional organization of the hippocampal formation: a review of anatomical data, Neuroscience, 31: 571-591.

Andersen P. (1975) Organization of hippocampal neurons and their interconnections. In R.L. Isaacson and K.H. Pribram (Eds.), The Hippocampus vol 1: Structure and development, Plenum, New York, pp. 155-176.

Andersen, P. (1981a) Properties of glutamate excitation of hippocampal pyramidal cells. In P.J. Roberts, J. Storm-Mathisen and G.A.R. Johnston, Neurobiology of the hippocampus, Wiley, Chichester, U.K., pp.25-33.

Andersen, P. (1981b) Brain slices - a neurobiological tool of increasing usefulness. Trends in Neurosci., 4: 53-57.

Andersen, P. (1983) Operational principles of hippocampal neurons, a summary of synaptic physiology. In W. Seifert (Ed.), Neurobiology of the hippocampus, Academic, London, pp. 81-86.

Andersen, P., Bliss, T.V.P. and Skrede, K.K. (1971) Lamellar organization of hippocampal excitatory pathways, Exp. Brain Res., 13: 222-238.

Andersen, P., Eccles, J.C. and Loyning Y. (1964) Pathways of postsynaptic inhibition in the hippocampus, J. Neurophysiol. 27: 608-619.

Andersen, P., Bland B.H. and Dudar, J.D. (1973) Organization of the hippocampal output, Exp. Brain Res., 17: 152-168.

Bailey, C.G. and Kandel, E.R. (1993) Structural changes accompanying memory storage, Annu. Rev. Physiol., 55: 397-426.

Barnes, C.A. (1983) The physiology of the senescent hippocampus. In W. Seifert (Ed.), Neurobiology of the hippocampus, Academic Press, London, pp. 87-108.

Barnes, C.A. (1988) Selectivity of neurological and mnemonic deficits in aged rats. In T.L. Petit and G. Ivy (Eds.), Neural plasticity: A lifespan approach, Alan Liss, New York, pp. 235-264.

Blackstad, T.W. (1956) Commissural connections of the hippocampal region of the rat, with special referress, ence to their mode of termination, J. Comp. Neurool., 105: 417-538.

Blackstad, T.W., Brink, K., Hem, J. and Jeune B. (1970) Distribution of hippocampal mossy fibers in the rat. An experimental study with silver impregnation methods, J. Comp. Neurol., 138: 433-450.

Broca P. (1878) Anatomie comparee des circonvolutions cerebrales. Le grand lobe limbique et la scissure dans la serie des mammiferes, Rev. Anthropol. Paris, 2: 285-498.

Brodal, A. (1947) The hippocampus and the sense of smell, a review, Brain, 70: 179-222.

Brodal, A. (1981) Neurological anatomy in relation to clinical medicine, 3rd Edition, Oxford University Press, New York, Oxford.

Calverley, R.K.S. and Jones, D.G. (1987) A serial section study of perforated synapses in rat neocortex, Cell Tissue Res., 247: 565-572.

Calverley, R.K.S. and Jones, D.G. (1990) Contribution of dendritic spines and perforated synapses to synaptic plasticity, Brain Res. Rev., 15: 215-249.

Carlin, P.K. and Siekevitz, P. (1983) Plasticity in the nervous system: do synapses divide?, Proc. Natl. Acad. Sci. U.S.A., 80: 3517-3521.

Cohen, R.S. and Siekevitz, P. (1983) Form of the postsynaptic density. A serial section reconstruction, J. Cell. Biol., 78: 36-46.

Cruz-Orive, L.M. (1980) On the estimation of particle number, J. Microsc., 120: 15-27.

Cruz-Orive, L.M. (1983) Distribution-free estimation of sphere size distributions from slabs showing overprojection and truncation with a review of previous methods. J. Microsc., 131: 265-290.

Cruz-Orive, L.M. (1985) Estimating particle number and size. In L.F. Agnati and K. Fuxe (Eds.), Quantitative Neuro-anatomy in Transmitter Research, MacMillan Press, London, pp. 11-24.

De Groot, D.M.G. With an appendix by L.M. Cruz-Orive (1988) Improvements of the serial section method in relation to the estimation of the numerical density of complex-shaped synapses. In A. Reith and T.M. Mayhew (Eds.), Stereology and Morphometry in Electron Microscopy. Problems and Solutions. Hemisphere Publishing Corporation, New York, London, pp. 135-158.

De Groot, D.M.G. and Bierman, E.P.B. (1983) The complex-shaped "perforated" synapse, a problem in quantitative stereology of the brain, J. Microsc., 131: 355-360.

De Groot, D.M.G. and Bierman, E.P.B. (1986) A critical evaluation of methods for estimating the numerical density of synapses, J. Neurosc. Methods, 18: 79-101.

Desmond, N.L. and Levy, W.B. (1988) Anatomy of associative long-term synaptic modification. In: P.W. Landfield and S.A. Deadwyler (Eds.), Liss, New York, NY, pp. 265-305.

DeToledo-Morrell, L., Geinisman, Y. and Morrell, F. (1988a) Age-dependent alterations in hippocampal synaptic plasticity: Relation to memory disorders, Neurobiol. Aging, 9: 581-590.

deToledo-Morrell, L., Geinisman, Y. and Morrell, F. (1988b) Individual differences in hippocampal plasticity as a function of aging: Behavioral, electrophysiological and morphological evidence. In T.L. Petit and G. Ivy (Eds.), Neural plasticity: A lifespan approach, Alan Liss, New York, pp. 283-328.

Dyson, S.E. and Jones, D.J. (1984) Synaptic remodelling during development and maturation: Junction differentiation and splitting as a mechanism of modifying connectivity, Dev, Brain. Res., 13: 125-137.

Fonnum, F. and Walaas, I. (1978) The effect of intrahippocampal kainic acid injections and surgical lesions on neurotransmitters in hippocampus and septum, Acta Physiol. Scand., 76: 35A-37A.

Geinisman, Y. (1993) Perforated axospinous synapses with multiple, completely partitioned transmission zones: probable structural intermediates in synaptic plasticity, Hippocampus, 3: 417-434.

Geinisman, Y, De Toledo-Morrell, L. and Morrell, F. (1986) Aged rats need a preserved compliment of perforated axospinous synapses per hippocampal neuron to maintain good spatial memory, Brain Res., 398: 266-275.

Geinisman, Y, De Toledo-Morrell, L. and Morrell, F. (1991a) Induction of long-term potentiation is associated with an increase in the number of axospinous synapses with segmented postsynaptic densities, Brain Res., 566: 77-88.

Geinisman, Y, De Toledo-Morrell, L. and Morrell, F. (1991b) Structural synaptic substrates of kindling and long-term potentiation. In: F. Morrell (Ed.), Kindling and synaptic plasticity. The legacy of Graham Goddard, Birkhauser, Boston, MA, pp. 124-159.

Geinisman, Y, DeToledo-Morrell, L. Morrell, F., Heller, R.E., Rossi, M. and Parshall, R.F. (1993) Structural synaptic correlate of long-term potentiation: formation of axospinous synapses with multiple, completely partitioned transmission zones, Hippocampus, 3: 435-446.

Geinisman, Y, DeToledo-Morrell, L. Morrell, F., Persina, I.S. and Rossi, M. (1992a) Structural synaptic plasticity associated with the induction of long-term potentiation is preserved in the dentate gyrus of aged rats, Hippocampus, 2: 445-456.

Geinisman, Y, Morrell, F. and DeToledo-Morrell, L. (1987) Axospinous synapses with segmented postsynaptic densities: A morphologically distinct synaptic subtype contributing to the number of profiles of "perforated" synapses visualized in random sections, Brain Research, 423: 179-188.

Geinisman, Y, Morrell, F. and DeToledo-Morrell, L. (1988) Remodelling of synaptic architecture during hippocampal "kindling", Proc. Natl. Sci. U.S.A., 85: 3260-3264.

Geinisman, Y, Morrell, F. and DeToledo-Morrell, L. (19907) Alterations in synaptic ultrastructure induced by hippocampal kindling. In: J.A. Wada (Ed.), Kindling 4, Plenum, New York, NY, pp. 75-88.

Geinisman, Y, Morrell, F. and DeToledo-Morrell, L. (1992b) Increase in the number of axospinous synapses with segmented postsynaptic densities following hippocampal kindling, Brain Research, 569: 341-347.

Greenough, W.T. and Bailey, C.H. (1988) The anatomy of memory: Convergence of results across a diversity of tests, Trends Neurosci., 11: 142-147.

Gundersen, H.J.G. (1977) Notes on the estimation of the numerical density of arbitrarily profiles: the edge effect, J. Microsc., 111: 219-223.

Hjorth-Simonsen A. (1972) Projection of the lateral part of the entorhinal area to the hippocampus and fascia dentata, J. Comp. Neurol. 146: 219-232.

Hjorth-Simonsen, A. (1977) Distribution of commissural afferents to the hippocampus oof the rabit, J. Comp. Neuroll., 176: 495-514.

Hjorth-Simonsen A. and Jeune B. (1972) Origin and termination of the hippocampal perforant path in the rat studied by silver impregnation, J. Comp. Neurol., 144: 215-232.

Landfield, P.W., McGaugh, G. and Lynch, G. (1986) The aged hippocampus: A model system for studies on mechanisms of behavior plasticity and brain aging. In R.L. Isaacson and K.H. Pribram (Eds.), The hippocampus, Plenum, New York, pp. 323-367.

Laurberg, S. (1979) Commissural and intrinsic connections of the rat hippocampus, J. Comp. Neurol., 184: 685-708.

Lömo, T. (1971) Patterns of activation in a monosynaptic cortical pathway: The perforant path input to the dentate area of the hippocampal formation, Exp. Brain Res., 12: 18-45.

Lopez da Silva, F.H., Witter, M.P., Boeyinga, P.H. and Lohman, A.H.M. (1990) Anatomic organization and physiology of the limbic cortex, Physiol. Rev., 70: 453-511.

Lopez da Silva, F.H., Groenewegen, H.J., Holsheimer, J., Room,P., Witter, M.P., Van Groen, Th. and Wadman, W.J., (1985) The hippocampus is a set of partially overlapping segments with a topographically organized system of inputs and outputs: The entorhinal cortex as a sensory gate, the medial septum as a gain-setting system and the ventral striatum as a motor interface. In G. Buzsaki and C.H. Vanderwolf (eds.), Electrical activity of the archicortex, Acad. Kiado, Budapest, pp. 83-106.

Lorente de Nó, R. (1934) Studies on the structure of the cerebral cortex II. Continuation of the study of the Ammonic system, J. Psychol. Neurol., 46: 113-177.

MacLean, P.D. (1952) Some psychiatric implications of physiological studies on frontotemporal portion of limbic system (visceral brain), Electroenceph. Clin. Neurophysiol., 4: 407-418.

Nieto-Sampedro, M., Hoff, S.W. and Cotman C.W. (1982) Perforated postsynaptic densities: Probable intermediates in synapse turnover, Proc. Natl. Acad. Sci. U.S.A., 79: 5718-5722.

Papez, J.W. (1937) A proposed mechanism of emotion, Arch. Neurol. Psychiat., 38: 725-743.

Peters, A. and Kaiserman-Abramof, I.R. (1969) The small pyramidal neuron of the rat cerebral cortex. The synapses upon dendritic spines, Z. Zellforsch., 100: 487-506.

Petit, T.L. (1988) Synaptic plasticity and the structural basis of learning and memory. In T.L. Petit and G. Iny (Eds.), Neural plasticity: A lifespan approach, Liss, New York,NY, pp. 201-234.

Ramon y Cajal, S. (1903) Die Riechrinde beim Menschen und Saugetier, Studien uber die Hirnrinde des Menschen, 4. Heft, Verlag von Johann Ambrosius Barth, Leipzig.

Spacek, J. and Hartman, M. (1983) Three-dimensional analysis of dendritic spines. I. Quantitative observations related to dendritic spine and synaptic morphology in cerebral and cerebellar cortices, Anat. Embryol., 167: 289-310.

Sterio, D.C. (1984) Estimating number, mean sizes and variations in size of particles in 3-D specimens using disectors, J. Microsc. 134: 127-136.

Storm-Mathiesen, J. (1972) Glutamate decarboxylase in the rat hippocampal region after lesions of the afferent fiber systems. Evidence that the enzyme is localized in intrinsic neurones, Brain Res., 40: 215-235.

Swanson, L.W. (1978) The anatomical organization of septo-hippocampal projections. In Cïba Foundation Symposium, Fuctions of the septohippocampal system, Vol. 58, Elsevier/North-Holland, Amsterdam, pp. 25-43.

Swanson, L.W. (1983) The hippocampus and the concept of the limbic system. In W. Seifert (Ed.), Neurobiology of the hippocampus, Academic Press, London, pp.3-19.

Swanson L.W. and Cowan W.M. (1977) An autoradiographic study of the organization of the efferent connections of the hippocampal formation in the rat, J. Comp. Neurol., 172: 49-84.

Swanson, L.W. and Cowan W.M. (1979) The connections of the septal region in the rat, J. Comp. Neurol., 186: 621-656.

Teyler T.J. and Discenna P. (1984) The topological anatomy of the hippocampus: a clue to its function, Brain Res. Bull., 12: 711-719.

Vrensen, G. and Nunez Cardozo, J. (1981) Changes in size and shape of synaptic connections after visual training, Brain Res., 218: 79-97.

Walaas, I. (1983) The hippocampus. In P.C. Emson, Chemical Neuroanatomy, Raven Press, New York, pp. 337-358

Wallace, C., Hawrylak, N. and Greenough, W.T. (1991) Studies of synaptic structural modifications after long-term potentiation and kindling: context for a molecular morphology. In M. Baudry and J.L. Davies (Eds.), Long-term potentiation: A debate of current issues, MIT Press, Cambridge, New York, NY, pp. 189-232.

West, M.J., Coleman, P.D. and Wyss, U.R. (1972) A computerized method of determining the number of synaptic contacts in a volume of cerebral cortex, J. Microsc. 95: 277-283.

PART II

STEREOLOGY AND MORPHOMETRY IN SYNAPTOLOGY

PROBLEMS AND SOLUTIONS

PART II

Chapter 1

THE COMPLEX-SHAPED "PERFORATED" SYNAPSE, A PROBLEM IN QUANTITATIVE STEREOLOGY OF THE BRAIN

Journal of Microscopy, Vol. 131, *Pt* 3, *September* 1983, *pp.* 355–360.
Received 3 *October* 1982; *accepted* 2 *February* 1983

The complex-shaped 'perforated' synapse, a problem in quantitative stereology of the brain

by DIDIMA M. G. DE GROOT *and* EGBERTUS P. B. BIERMAN, *Medical Biological Laboratory TNO, P.O. Box* 45, 2280 *AA Rijswijk, The Netherlands*

KEY WORDS. Synaptic density, synaptic length, perforated synapses, quantitative electron-microscopy, stereology, hippocampus.

SUMMARY

Failure to appreciate the consequences for stereological work of the simultaneous presence of complex-shaped perforated and disc-like non-perforated synapses in brain tissue results in underestimation of synaptic profile length and overestimation of synaptic density when measured in randomly selected ultrathin E-PTA slices. This problem can be solved by using serial slices and a calculation method which makes no assumptions about synaptic size and shape. A three-dimensional reconstruction is unnecessary.

INTRODUCTION

The aim of quantitative stereology is to derive numerical three-dimensional data from measurements in two-dimensional microscopical slices. Stereological methods are used in neuroanatomy for quantitative morphological analyses of neuronal structures such as neurons, dendrites, axons and synapses. Parameters of interest are, for example, volume, surface and number of the structures investigated. When estimating the numerical density of synapses the existence of complex-shaped synapses described by many authors (Gray, 1959; Peters & Kaiserman-Abramof, 1969; Akert, 1973; Greenough *et al.*, 1978; Cohen & Siekevitz, 1978; Dyson & Jones, 1980; Vrensen *et al.*, 1980; Müller *et al.*, 1981; Vrensen & Nunes Cardozo, 1981; Verwer & De Groot, 1982) has to be taken into account. These complex-shaped synapses are thought to have a functional significance, since increases in their number were found in the occipital cortex of rats reared in an 'enriched' environment (Greenough *et al.*, 1978) and in the visual cortex of rabbits after visual training (Vrensen & Nunes Cardozo, 1981). Some of the complex-shaped synapses have a presynaptic grid arranged in such a way that one or more parts of the presynaptic membrane are devoid of dense projections. This gives the impression that these synapses are 'perforated' (Greenough *et al.*, 1978).

The present investigation concerns a quantitative stereological evaluation of synapses in the CA1 and CA3 areas of the hippocampus of rats in relation to the age of the animals. This paper focuses on the errors that can be made if the differences in size and shape of synapses are not taken into account when their numerical density is to be estimated. Both 'classical' disc-like (West *et al.*, 1972) synapses and perforated synapses appeared to be present in all four layers of the hippocampus CA1 and CA3 areas of the rats in the present study (Fig. 1).

Quantitative analysis of the synapses was carried out in slices treated with ethanolic phosphotungstic acid (E-PTA) in which synapses appear against a practically unstained background, a feature which facilitates their detection. The term 'slices', generally used for tissue sections

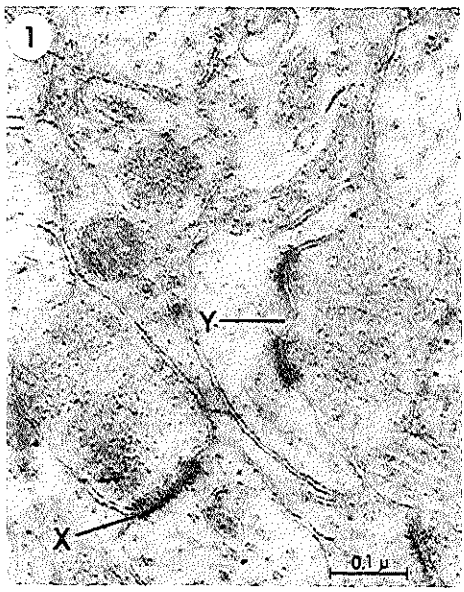

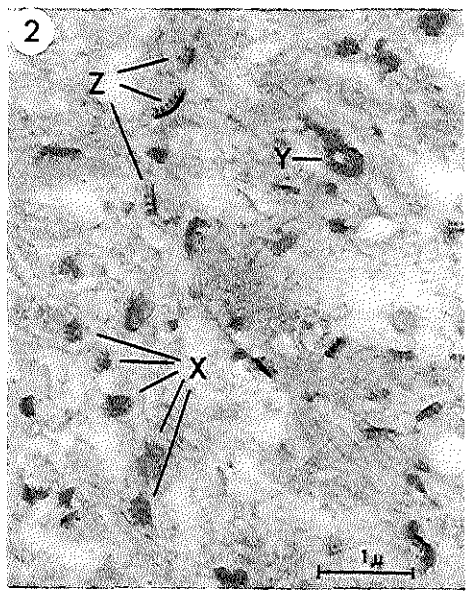

Fig. 1. An OsO_4 treated ultrathin (50 nm) slice showing a perforated (Y) and a possible non-perforated synapse (X).

Fig. 2. An E-PTA treated semi-thin (500 nm) slice showing a large complex-shaped perforated synapse (Y) and smaller disc-like non-perforated (X) synapses. Z, transversely cut synapses.

which have a thickness of more than 100 μm, is used in the present paper for all ultrathin and semithin sections, to avoid confusion with the term 'sections of synapses'. From the images in semi-thin (500 nm) slices it is clear that the perforated synapses in the hippocampi are larger than the disc-like synapses and are often irregularly shaped (Fig. 2). In ultrathin (50 nm) slices the synapses will almost always be transversely cut since the diameter of the presynaptic grid is 100–450 nm. In such a 50 nm slice of osmicated (OsO_4) hippocampal tissue the perforated synapses seem to have an interrupted contact zone, when the cut runs through the 'perforation' (Fig. 1). Only in this case can the perforated synapse be distinguished from the disc-like non-perforated synapse which does not have an interruption (Fig. 1). Obviously one can never be sure if a synapse is a perforated one when a 'perforation' is not present in the plane of the slice. This problem is also encountered in E-PTA treated 50 nm slices. It appears, however, that in the E-PTA treated ultrathin slices an interrupted contact zone often goes unrecognized and is therefore counted as two or more separate synapses instead of one perforated synapse.

The aim of the present report is to show the extent to which this lack of recognition of perforated synapses may affect the measurement of synaptic density and synaptic profile length in random ultrathin E-PTA treated slices of tissue.

MATERIALS AND METHODS

Female, small Wistar (WAG/Rij) rats of 12 (two animals) and 30 (two animals) months respectively were examined. Under ether anaesthesia the animals were fixed by transcardial perfusion with glutaraldehyde/paraformaldehyde mixture (Peters, 1970). When the hippocampi were taken from the brain, a transverse section of approximately 5 mm was taken from the middle of the left hippocampus and 75 μm vibratome slices were cut from this sample. A vibratome slice was put under the dissecting microscope and subsequently three distinct areas

were sampled. After rinsing in sodium cacodylate buffer the slices were blockstained with ethanolic phosphotungstic acid (E-PTA) according to Vrensen & De Groot (1974). Embedding was orientated so that cutting with the ultramicrotome occurred parallel to the ventricular surface. Ultrathin (50 nm) serial slices (thirty slices per series) from the stratum pyramidale of the hippocampus CA3 area (Fig. 3) were prepared on one-hole grids covered with a Pyoloform F (Wacher-Chemie) film and a carbon-coating and were examined with a Philips 201 electron microscope. From each serial slice a square area was photographed which was almost as large as the small slice itself. It should be mentioned that in view of the necessarily large number of slices within one series the size of the pyramid-shaped slice was as small as possible (400–800 μm^2). In these photographed areas the number of synapses per unit area were counted and their profile lengths measured. By tracing the synapses in the adjacent serial slices, a distinction was made between perforated and non-perforated ones. This analysis was carried out as follows: (a) in the centre slice of a series the number of synaptic contact zones (called 'sections of synapses') was counted, applying Gundersen's (1977) unbiased counting rule. Each contact

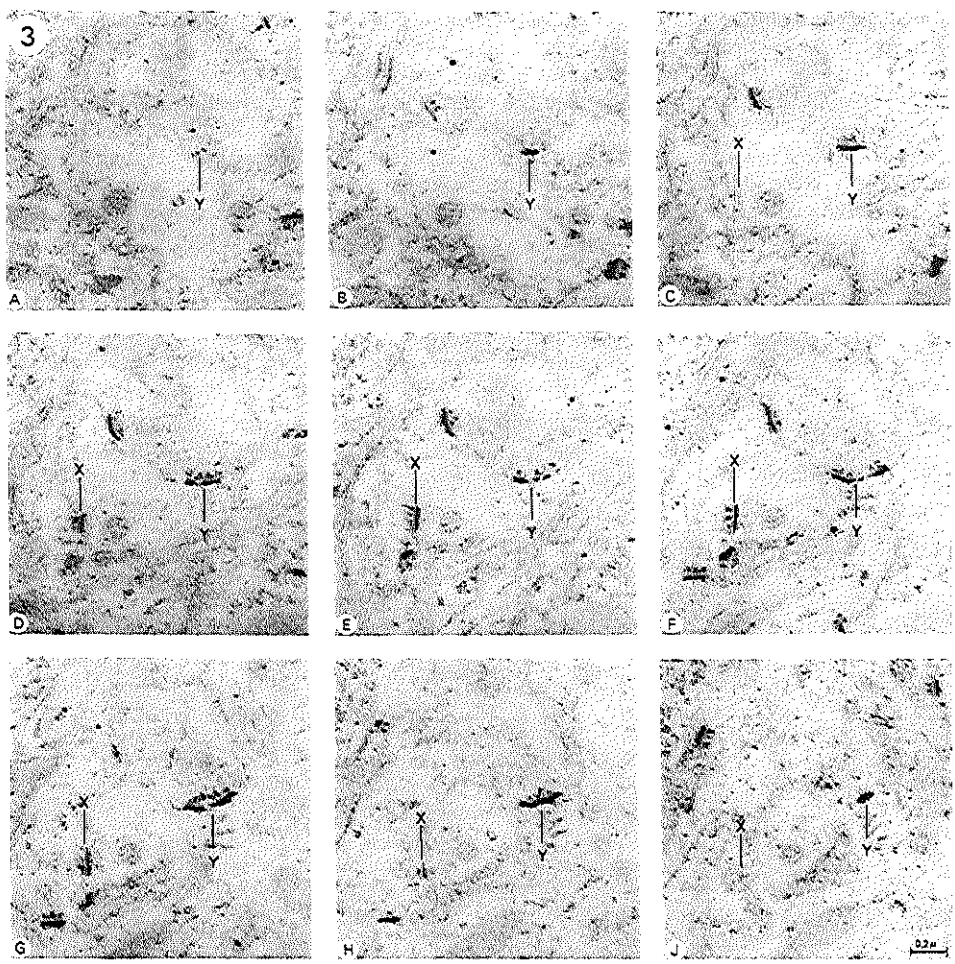

Fig. 3. A series of E-PTA treated ultrathin (50 nm) slices showing from A to J a perforated (Y) and non-perforated (X) synapse.

zone in the photograph, whether curved or not, was traced precisely and its profile length was measured using a Videoplan (Kontron Messgerate, Eching, FDR); (b) subsequently, it was established in how many of the adjacent slices these 'sections of synapses' were present and if they belonged to perforated or non-perforated synapses. Thus, the number of 'true' synapses was counted, thereby distinguishing between perforated and non-perforated synapses.

The number of synapses per unit volume was calculated according to the method of Cruz-Orive (1980a and personal communication), since this method is the only one that does not make an assumption about the shape of the investigated particle. Standard errors were calculated according to Cruz-Orive (1980b).

RESULTS

The number of 'sections of synapses' per unit area was significantly higher than that of the 'true synapses' (Table 1). The majority of true synapses were non-perforated. The measurements showed that the mean profile length of perforated synapses was significantly higher ($P > 0{\cdot}05$, two tailed, Student's *t*-test) than that of the non-perforated ones (Table 1), indicating that the perforated synapses were larger. Clearly, the average profile length of the 'true synapses', depending on the numerical relation between the large perforated and the smaller non-perforated synapses, is larger than the profile length of the 'sections of synapses'. Calculated per unit volume of tissue, 10–20% of the synapses in these rats appeared to be perforated (Table 1).

Taken together, the results show that the number of synapses per unit area of tissue is overestimated, while the average profile length is underestimated, if no account is taken of the effects of the differences in size and shape of the synapses. As a consequence of these systematic errors, the estimate of the number of synapses per unit volume of tissue will be even more erroneous—i.e. overestimated—since this parameter depends on the quotient: number per area/diameter, of which the first is overestimated and the second is underestimated (Table 1).

Table 1. The number of synapses per unit area N_A (10^{-3} μm^{-2}), the synaptic profile length $\bar{l}$(nm) and number of synapses per unit volume N_V (10^{-12} cm^{-3}) in the stratum pyramidale* of the hippocampus CA3 area of four rats.

Number per unit area N_A (10^{-3} μm^{-2})

Age/rat No.	Sections of synapses	True synapses	Non-perforated synapses	Perforated synapses
12 M/No. 58	271	262	241	21
12 M/No. 61	406	359	281	78
30 M/No. 43	242	215	156	59
30 M/No. 45	318	280	210	70

Profile length of synapses $\bar{l}$ (nm)

	Sections of synapses			True synapses			Non-perforated synapses			Perforated synapses		
Age/rat No.	Mean	SEM	*n*	Mean	SEM	*n*	Mean	SEM	*n*	Mean	SEM	*n*
12 M/No. 58	189	6	90	199	7	87	192	6	80	279	42	7
12 M/No. 61	208	7	146	248	10	129	218	8	101	361	29	28
30 M/No. 43	214	8	119	256	11	106	224	9	77	340	28	29
30 M/No. 45	182	6	164	224	10	144	192	7	108	322	26	36

Number per unit volume N_V (10^{-12} cm^{-3})

	True synapses		Non-perforated synapses		Perforated synapses	
Age/rat No.	Mean	SEM	Mean	SEM	Mean	SEM
12 M/No. 58	1·313	0·146	1·239	0·170	0·075	0·038
12 M/No. 61	1·770	0·573	1·526	0·643	0·244	0·077
30 M/No. 43	1·041	0·273	0·866	0·250	0·158	0·053
30 M/No. 45	1·207	0·213	1·013	0·324	0·194	0·072

* Cells and large neurites are excluded from the measurements.

DISCUSSION

It could well be that the discrepancy noted between the counting of synapses in osmicated and in E-PTA-stained ultrathin slices of the developing hippocampus of rabbits (Schwartzkroin *et al.*, 1982) is due to this source of systematic error and is particularly relevant when an increase is noted in the number of complex-shaped synapses, as has been reported by Müller *et al.* (1981) in the developing visual cortex of the rabbit. These authors as well as Vrensen *et al.* (1980) and Vrensen & Nunes Cardozo (1981), found, in semi-thin E-PTA slices, that the size of the complex-shaped synapses was larger than that of disc-like synapses. This finding is in good agreement with our results and those of Peters & Kaiserman-Abramof (1969) obtained in ultrathin serial slices. Unfortunately, from their measurements on semi-thin slices, Müller *et al.* (1981) and Vrensen & Nunes Cardozo (1981) also drew conclusions with respect to the frequency of complex-shaped and disc-like synapses, and ignored the fact that the large complex-shaped synapses stood a smaller chance of being fully incorporated in the slice. Therefore, they stood a smaller chance of being counted, since only fully incorporated synapses were measured. Moreover, these authors calculated the number of synapses per unit volume using the conventional method of Abercrombie (1946). When complex-shaped synapses are present in a tissue, the conventional calculations for the number of synapses per unit volume, based on the assumption that synapses are disc-like structures, is inadequate and may lead to erroneous results. This was shown by Verwer & De Groot (1982), who compared the conventional calculations according to Abercrombie (1946) and to Fullman (1953) with the one proposed by Cruz-Orive (1980a). The latter method does not imply that synapses have a particular and constant shape, size and orientation. This method requires serial sectioning which makes it rather laborious. Since the present measurements were not carried out as a routine investigation, and improvements are envisaged as to the efficiency of the procedure, no fair estimate can yet be given about the time involved. The results described, however, show that this method is essential when complex-shaped perforated synapses are present in the tissue.

ACKNOWLEDGMENTS

The authors wish to thank Drs T. M. Mayhew (University of Aberdeen) and L. M. Cruz-Orive (University of Bern) for their helpful discussion and Drs O. L. Wolthuis and E. M. Meeter for their critical reading of the manuscript. Mr M. J. M. Boermans is acknowledged for his photographic assistance. This project was supported by Shell International Research Company Ltd.

REFERENCES

Abercrombie, M. (1946) Estimation of nuclear population from microtome sections. *Anat. Rec.* **94**, 239–247.

Akert, K. (1973) Dynamic aspects of synaptic ultrastructure. *Brain Res.* **49**, 511–518.

Cohen, R.S. & Siekevitz, P. (1978) Form of the postsynaptic density: a serial section study. *J. Cell Biol.* **78**, 36–46.

Cruz-Orive, L.M. (1980a) On the estimation of particle number. *J. Microsc.* **120**, 15–27.

Cruz-Orive, L.M. (1980b) Best-linear unbiased estimators for stereology. *Biometrics*, **36**, 595–605.

Dyson, S.E. & Jones, D.G. (1980) Quantitation of terminal parameters and their inter-relationships in maturing central synapses. A perspective for experimental studies. *Brain Res.* **183**, 43–59.

Fullman, R.L. (1953) Measurement of particle sizes in opaque bodies. *Trans. AIME*, **197**, 447–452.

Gray, E.G. (1959) Axosomatic and axodendritic synapses of the cerebral cortex: an electron microscope study. *J. Anat. (Lond.)*, **93**, 420–433.

Greenough, W.T., West, R.W. & De Voogd, T.J. (1978) Subsynaptic plate perforations: changes with age and experience in the rat. *Science*, **202**, 1096–1098.

Gundersen, H.J.G. (1977) Notes on the estimation of the numerical density of arbitrary profiles: the edge effect. *J. Microsc.* **111**, 219–223.

Müller, L., Pattiselanno, A. & Vrensen, G. (1981) The postnatal development of the presynaptic grid in the visual cortex of rabbits and the effect of dark-rearing. *Brain Res.* **205**, 39–48.

Peters, A. (1970) The function of cerebral nervous tissue and the analysis of electron micrographs of the neuropil, with special references to the cerebral cortex. In: *Contemporary Research Methods in Neuroanatomy* (Ed. by W. J. H. Nauta and S. O. E. Ebbeson), p. 56. Springer, Berlin.

Peters, A. & Kaiserman-Abramof, J.R. (1969) The small pyramidal neuron of the rat cerebral cortex: the synapses upon the dendritic spines. *Z. Zellforsch.* **100**, 487–506.

Schwartzkroin, P.A., Kunkel, D.D. & Mathers, L.H. (1982) Development of rabbit hippocampus: anatomy. *Develop. Brain Res.* 2, 453–468.

Verwer, R.W.H. & De Groot, D.M.G. (1982) The effect of shape assumptions on the estimation of the numerical density of synapses from thin sections. *Progr. Brain Res.* 55, 195–203.

Vrensen, G. & De Groot, D. (1974) Phosphotungstic acid staining and the quantitative stereology of synapses. In: *Electron Microscopy and Cytochemistry* (Ed. by E. Wisse, W. T. Daems, J. Molenaar and P. van Duyn), Proc. 2nd Int. Symp., p. 255. North-Holland, Amsterdam.

Vrensen, G. & Nunes Cardozo, J. (1981) Changes in size and shape of synaptic connections after visual training: an ultrastructural approach of synaptic plasticity. *Brain Res.* **218**, 79–97.

Vrensen, G., Nunes Cardozo, J., Müller, L. & Van der Want, J. (1980) The presynaptic grid: a new approach. *Brain Res.* **184**, 23–40.

West, M.J., Coleman, P.D. & Wyss, U.R. (1972) A computerized method of determining the number of synaptic contacts in a volume of cerebral cortex. *J. Microsc.* 95, 277–283.

PART II

Chapter 2

IMPROVEMENTS OF THE SERIAL SECTION METHOD IN RELATION TO THE ESTIMATION OF THE NUMERICAL DENSITY OF COMPLEX-SHAPED SYNAPSES

Part II, Chapter 2 was published as Chapter 12 In:
A. Reith and T.M. Mayhew (Eds) Stereology and Morphometry in Electron Microscopy, Problems and Solutions. Hemisphere Publishing Corporation, New York. 1988.

chapter 12

improvements of the serial section method in relation to estimation of the numerical density of complex-shaped synapses

Didima M. G. de Groot*

INTRODUCTION

In estimating the numerical density (N_V) of a type of particles in a tissue sample, both the number per unit area (N_A) and the particle size must be taken into account. The particle size is described by the mean projected height, tangent, or caliper diameter ($\overline{H}$) averaged over all orientations. Under ideal conditions, N_V equals the ratio N_A over $\overline{H}$ [Eq. (2.79) in Ref. 1]. Whereas the determination of N_A is a relatively simple task, the estimation of $\overline{H}$ may cause considerable problems. Most conventional methods for estimating N_V start by making strict assumptions regarding particle shape. Then N_V is estimated on the basis of N_A and a simplified measure of particle size. However, such assumptions may cause serious errors. Cruz-Orive (Ref. 2 and Appendix) described a method for estimating N_V without making any assumptions about size, shape, and orientation of the particles. In essence, this method makes use of serial sections for the estimation of the "effective projected height" ($\tilde{H}$). The quantity $\tilde{H} + T$ is obtained by multiplying the total number of sections in which a particle appears by the thickness of a section.

In studies on synapses in the cerebellum[3] and the hippocampus[4] of the rat, it has been shown that calculations of N_V based on the simple shape assumption that synapses are disklike structures may lead to erroneous biased results. In addition, it appeared that the method of Cruz-Orive must be applied when

* With an appendix by Luis M. Cruz-Orive.

Mr. E. Bierman is gratefully acknowledged for technical assistance and Mr. M. Boermans for photography. Gratitude is expressed to Dr. G. Vrensen (Netherlands Ophthalmic Research Institute, Amsterdam) for constructive comments on the manuscript. Dr. J. Bleichrodt and Dr. O. Wolthuis are acknowledged for critical reading of the manuscript and Mrs. R. Engelen and W. Roelofs for careful typing. This work was supported by Shell Internationale Research Maatschappij B.V.

the numerical density of complex-shaped synapses has to be estimated. A disadvantage of the Cruz-Orive method is that serial sectioning and inspection are rather laborious and time-consuming. The aim of the present chapter is to show how the efficiency of the method can be improved to make it more suitable for routine application. A common problem in serial sectioning is that the size of the pyramid-shaped section is kept very small in view of the necessarily large number of sections within one series.[4] With such small sections the sample size is extremely small, so several series must be cut for quantitative studies. Nevertheless, the statistical relevance of the results obtained from such serial section samples may sometimes be questioned. The use of large sections overcomes this problem to a large extent and considerably reduces the time spent on ultramicrotomy. In the present chapter a serial sectioning technique is described in which large sections are cut.

Another problem in serial sectioning of small tissue samples is the orientation within the tissue, especially when layered or polarized tissues are to be investigated. Large sections, preinspection at the light microscopic (LM) level, the use of specific grids, and the use of a rotation holder and calibrated micrometer with the electron microscope greatly overcome the problem of orientation within the tissue and facilitate recognition of the areas of interest in sequential sections. These points will be dealt with in detail. In addition, the application of the method of Cruz-Orive (Refs. 2 and 5 and Appendix) is shown in a simplified example. The improved method will be illustrated using an example from the author's laboratory on the synaptic density in the hippocampus of the rat as calculated with Cruz-Orive's formulas (Appendix). The advantages and disadvantages inherent in the application of the whole procedure are discussed. To avoid an excess number of illustrations, the hippocampus is also used to illustrate the general aspects of the serial sectioning and sampling technique.

GENERAL PROCEDURES

Fixation, Tissue Sampling, and Embedding

After a proper perfusion fixation, e.g., according to Peters,[6] the brain is taken from the skull. Brain structures are dissected (Fig. 1a) and stored in buffer. The structures in one hemisphere are used for quantitative studies. In some instances it can be important to use the contralateral counterpart to measure the reference volume of the particular brain structure. Slabs of tissue are removed from the brain structure by making transverse cuts of approximately 4 mm with a set of razor blades (Fig. 1b). Depending on the size of the brain structure to be investigated, three to five slabs containing all the layers are selected randomly for further quantitative studies. From the appropriate tissue samples, 75-μm slices are cut on a Vibratome (Oxford Instruments) (Fig. 1c). The Vibratome slices can be examined under a dissecting microscope when it is desirable to sample distinct areas within the slice (Fig.

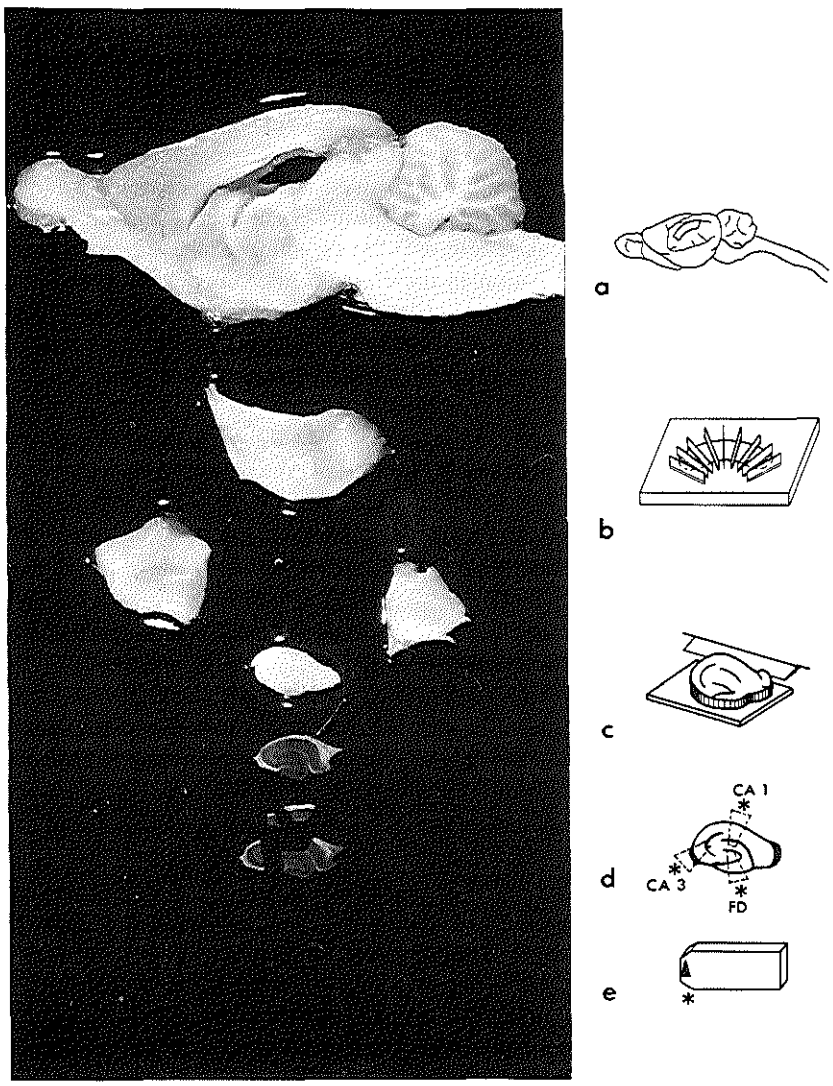

FIGURE 1. Tissue sampling, illustrated for the hippocampus. Embedding of the tissue samples occurs in an orientated way so that cutting with the ultramicrotome starts perpendicular to the outer surface—i.e., the ventricular surface for the hippocampus—of the brain structure (note asterisks). See text for further details. FD, Fascia dentata.

1d). After thorough rinsing in buffer, the slices can be block stained. Embedding is carried out in an orientated way in flat embedding molds (Fig. 1e).

Ultramicrotomy

Embedding occurs in such a way that ultramicrotome cutting is carried out perpendicular to the outer surface of the brain structure. Semithin (500-nm) sections reaching from the surface down to the center of the brain structure are cut on an ultramicrotome using glass knives. These sections are post-stained with toluidine blue. They are examined in a light microscope and the thickness of each layer is measured as illustrated in Fig. 2 for the hippocampal CA1 and CA3 areas. These data are essential for the subsequent selection of areas for examination in the electron microscope. Ultrathin (50-nm) serial sections from the same blocks are cut using a diamond knife. The distance between the first and the last sections of a series should be more than twice the largest particle diameter (Ref. 2 and Appendix, note N2). The sec-

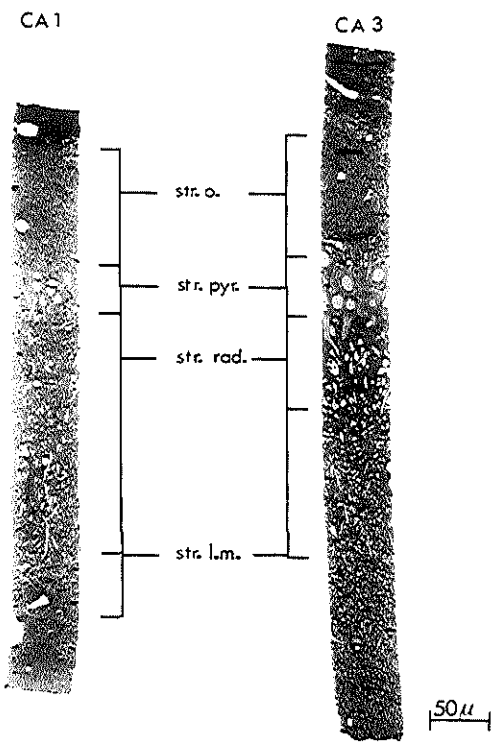

FIGURE 2. Semithin toluidine blue-stained sections of the hippocampus, illustrating the thickness of the distinct layers within the CA1 and CA3 areas. Str. o., stratum oriens; str. pyr., stratum pyramidale; str. rad., stratum radiatum; str. l. m., stratum lacunosum moleculare.

tions are 75 μm wide—the thickness of the Vibratome slice—and can be up to 1500–2000 μm high. Several methods are available for measuring the thickness of the sections, e.g., the Small fold method,[7] densitometry and interferometry,[8–10] and comparison of exposure densities with those of calibrated specimens in the electron microscope.[11–13]

In the Small fold technique the first and last three to five sections adjacent to the series collected for quantitative analysis of the particles of interest are used. The other techniques can be applied to all sections of the series. Serial sectioning is carried out as shown in Fig. 3. The letters of the list below correspond to the letters in the figure.

(a) The specimen block is trimmed in such a way that the bottom edge of the block is orientated parallel to the knife edge during sectioning. However, in contrast to what is usually done, the top edge of the block is not parallel to the bottom edge but is arrow-shaped (Fig. 4). As a result, the sections cut are in contact with the knife edge at only a single point. Consequently, they can easily and quickly be removed one by one from the water surface in the knife boat.

(b) The time interval between two subsequent sections is kept as long as possible by using the lowest speed of the reverse stroke of the ultramicrotome. This allows just enough time to pick up each section individually from the water surface with the aid of a platinum loop held between a pair of tweezers.

(c) The platinum loop containing the section on a water surface is carefully placed on Pyoloform-FN50 (Wacker Chemie) coated and systematically coded glass slides. To avoid damaging the support film, the loop is "dropped" when it is a few millimeters above the support film.

(d) The water in the loop is drawn off by touching the outer edge of the loop with a wedge-shaped piece of filter paper, thereby depositing the floating section on the Pyoloform film. The section is then alowed to dry. Subsequently, the loops are dropped off the slides by turning the slides upside down. If necessary, the sections can be poststained in a tightly closed petri dish. Drops of stain, e.g., lead or uranyl, are then placed over the individual sections and are flushed off with distilled water after a proper staining time.

(e) The Pyoloform support film carrying the sections is removed from the slide by stripping off onto a water surface.

(f) Grids are then placed over the sections under a dissecting microscope in an orientated way while the support film is still floating on the water surface. Slotted grids (pitch 250 μm, hole 200 μm, and bar 50 μm; VECO, R100A, Cu 3.05 mm; 175, 841) from which one bar has been dissected under the dissecting microscope are used.* As shown in Fig. 5,

* Currently, these grids are produced commercially by Oscar Stolk Scientific, Capelle a/d ijssel, The Netherlands.

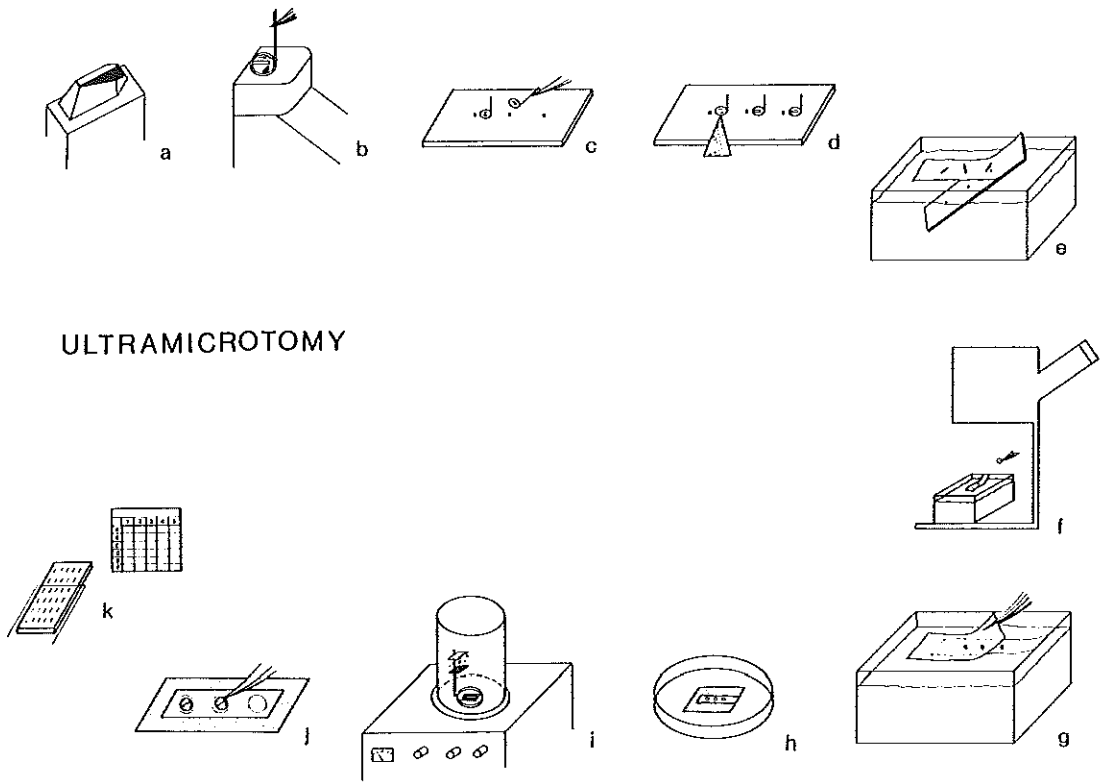

FIGURE 3. Serial sectioning procedure. For details see the section on "Ultramicrotomy." (a) *, Outer surface of the brain structure.

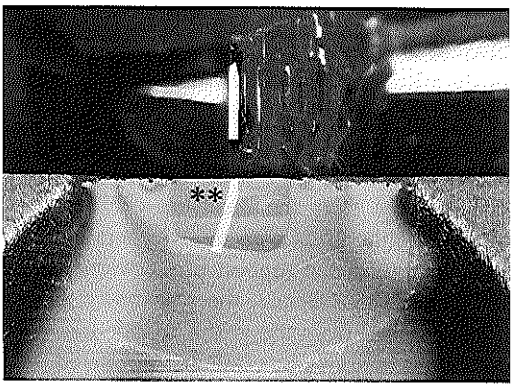

FIGURE 4. Survey picture of a specimen block mounted in the ultramicrotome, showing that the top edge of the pyramid-shaped specimen block is arrow-shaped. Note that the bottom edge of the block (*) is parallel to the knife edge and that the cut section (**) is in contact with the knife edge at a single point only.

the oblong section is placed with its longitudinal axis between and parallel to the two bars adjacent to the removed one, i.e., on the place of the removed bar.

(g) The Pyoloform support film with the overlying grids is picked up from

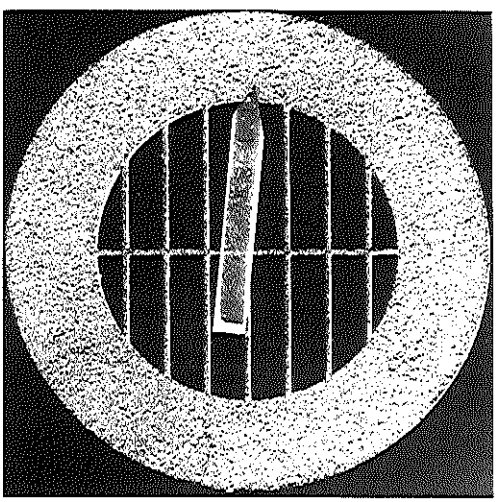

FIGURE 5. Specimen grid, illustrating the carefully oriented position of the section with respect to the grid bars. (Arrowhead indicates the position of the removed bar.)

the water surface with a piece of Parafilm ("M," American Can Company, Greenwich, Conn.).

(h) The piece of Parafilm carrying the Pyoloform film with the sections and grids is put in a closed petri dish with the Parafilm side down.

(i) After thorough drying over silica gel, the grids are vacuum-coated with a thin layer of carbon.

(j) The grids are detached from the Parafilm with a pair of tweezers. It is important to encircle the grids with the tweezers before detaching them. By doing this, the part of the support film covering the grid is separated from the rest of the film. Hence, the possibility that the film with the section will be detached from the grid is avoided.

(k) The grids are stored in a grid box and are numbered.

Electron Microscopic Sampling

The ultrathin sections are inspected in a conventional transmission electron microscope equipped with a goniometer attachment and a rotation specimen holder. The general procedure for selecting and photographing areas of interest is carried out as shown in Fig. 6. The letters of the list below correspond to the letters in the figure.

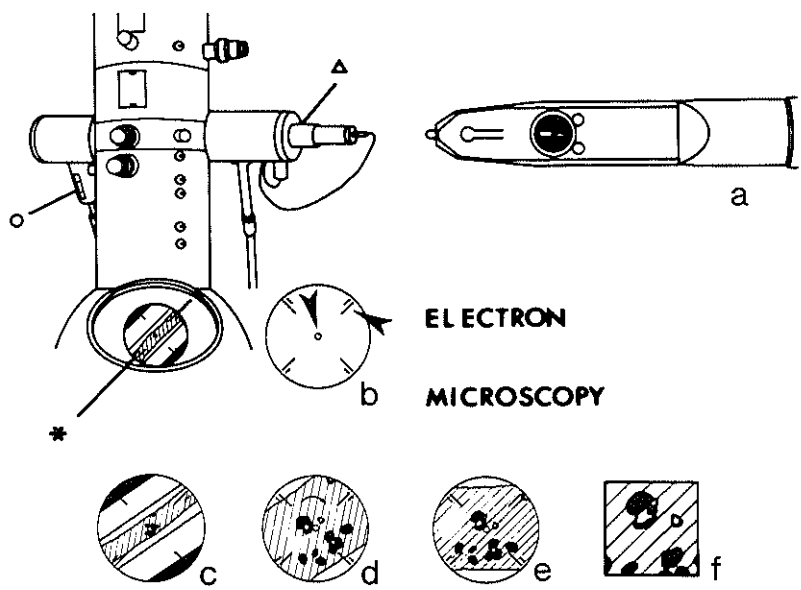

FIGURE 6. Strategy for electron microscopic sampling of serial sections. (a) Note standardized position of the grid with the removed grid bar. (b) *, Direction of movement of micrometer. Note that the longitudinal axis of the oblong section is in the axis of the direction of movement of the micrometer. ○, Calibrated micrometer; △, goniometer attachment and rotation holder; ➤, screen markers and center point on the main screen. See text for further details.

(a) The grid is put in the specimen holder. A standardized position greatly facilitates the orientation in the sequential sections.
(b) At a scanning magnification (e.g., 200× on the main screen) the grid is rotated to a position in which the longitudinal axis of the section is in the axis of the specimen traverse control (Fig. 6b, *) to which the micrometer is connected (Fig. 6b, ○).
(c) The procedure is started in a layer that can easily be recognized at low magnification by the presence of specific landmarks, e.g., cell nuclei. The center of this layer is moved to the center of the main screen. The micrometer value (Fig. 6b, ○) is read and noted. This "starting position" is subsequently used as reference to find other areas of interest that cannot be recognized as such at low magnification.
(d) The magnification is increased to a level appropriate for counting and measuring the structural elements of the particles of interest.
(e) While keeping the center point of this area in the center of the screen, the grid is rotated to another position, i.e., the position in which the upper and lower borders of the layer run parallel to the upper and lower edges of the photograph to be taken. The resulting image on the main screen is drawn diagrammatically. Special attention is paid to the relative position of larger structures, such as blood vessels, cell nuclei, and myelin sheets, with respect to the screen markers (Fig. 6b, arrowheads). Large structures, of course, reappear in a large number of sections and will facilitate orientation in the sequential sections of the series.
(f) The image is photographed. It appears to be helpful for the final analysis to list in a simple table whether or not a particular area was photographed and not missed due to, e.g., folds or dirt on the sections.

Knowing the thickness of each layer from the light microscopic measurements (cf. Fig. 2), any area within a certain layer can be selected. If desired, steps b and c are then repeated in order to return to the starting position. From this starting position the image is moved to reach another area of interest. The distance to be covered is known from the light microscopic measurements. This distance is read on the micrometer, which is connected to the specimen traverse control. Subsequently, steps d to f are repeated. After sufficient areas within one section in different layers have been photographed, an adjacent section is taken and put in the specimen holder in the standardized position and the procedure is repeated. The drawings obtained in step e are used to select and to photograph identical areas in the sequential sections of the series.

The same micrographs can be used for quantitative analysis of much smaller objects, which, although they can be counted, need much higher magnification to be measured. To achieve this, the micrographs are placed on an illuminated screen and a video camera is placed over them. The enlarged image is projected on a monitor. To facilitate orientation within the micro-

graph after enlargement on the monitor, a homemade square lattice was found to be very useful. The image on the monitor represents one of the numbered square areas of the lattice (Fig. 7).

Stereological Analyses

The parameter N_V is estimated according to the method of Cruz-Orive (Appendix).

To illustrate the application of this procedure and the formulas, a simplified imaginary example on more or less "curved" synapses of different sizes is shown in Fig. 8. A series of nine sections is drawn with a reference area (A_i) of 225 μm^2. All synaptic contact zones (N_i) in the center section—i.e., the fifth section—are counted, applying Gundersen's unbiased counting rule.[14] This results in six synaptic contact zones. Two of these synaptic profiles are serially tracked. The quantity $\tilde{H}_{ij} + T$, where $\tilde{H}_{ij}$ is a particle's "effective projected height" (see Appendix) is estimated by multiplying the number of sections in which each particle appears (m_{ij}) (six and four, respec-

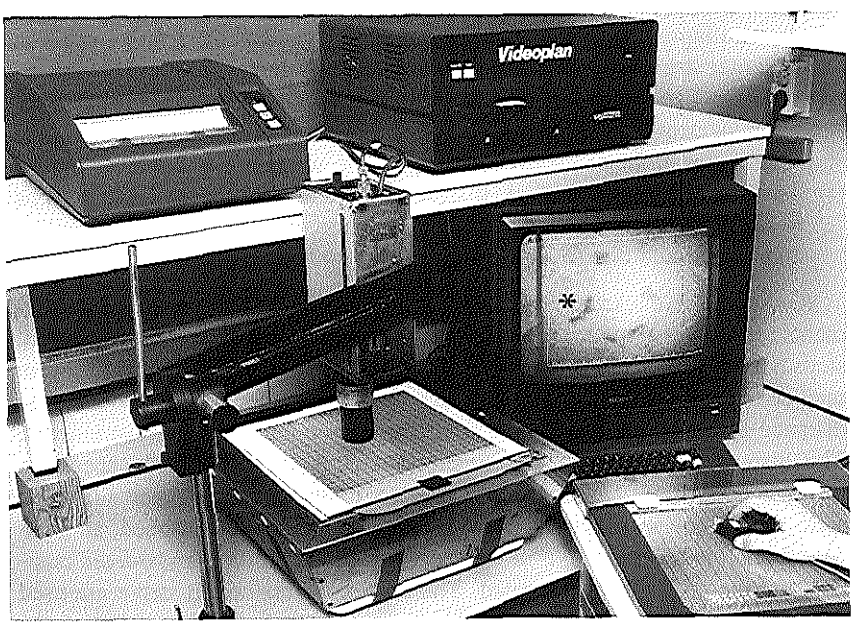

FIGURE 7. Equipment for enlargement of low-power micrographs connected to a semiautomatic image analysis system (Videoplan, Kontron Messgeräte, Eching, FRG). The micrographs on the illuminated screen are covered with an appropriate square lattice. One square is magnified with a video camera and the image is projected on the screen of the monitor. The black lines on the screen of the monitor correspond to the edges of the square of the lattice; the white lines delineate the "active area" of the Videoplan. *, Enlarged transversely cut synaptic contact zone after E-PTA treatment.

tively) by the mean section thickness T_i. The section thickness (T_i) is measured by the Small fold technique[7] and has a mean value of 42 nm.

Data from three other series of the same imaginary brain structure are given, making a total of $m = 4$ series. Values of estN_V(syn, struc), SE{est(N_V)}, and CE{est(N_V)} are calculated using the formulas mentioned in the Appendix. The detailed calculations are shown in Fig. 8.

APPLICATION

A 30-month-old rat was fixed by transcardial perfusion with glutaraldehyde/paraformaldehyde mixtures according to Peters.[6] Both hippocampi were dissected and stored in sodium cacodylate buffer.[6] The right hippocampus was used to estimate the reference volume; the left hippocampus was used for the quantitative study of synapses. Slabs of approximately 4 mm were removed from the left hippocampus by making transverse cuts with a fan-shaped set of razor blades (cf. Fig. 1). This resulted in five slabs of the banana-shaped hippocampus. The two outer slabs did not contain all hippocampal layers. Two other slabs, each containing all the hippocampal layers, were taken for the quantitative studies. Vibratome slices of 75 μm were examined under the dissecting microscope and the CA3 area was dissected for investigation. After thorough rinsing in sodium cacodylate buffer, the slices were block-stained with ethanolic phosphotungstic acid (E-PTA) according to Vrensen and De Groot.[15] With this method, synaptic contact zones are selectively stained, which facilitates their recognition at the electron microscopic level. Semithin and ultrathin serial sections were cut with a Reichert Om U3 ultramicrotome, perpendicular to the ventricular surface and reached to at least the stratum lacunosum moleculare. The semithin toluidine blue sections were examined under a light microscope and the thicknesses of the four distinct layers, i.e., stratum oriens, stratum pyramidale, stratum radiatum, and stratum lacunosum moleculare, were measured with the Videoplan (Kontron Messgeräte, Eching, FRG; Fig. 2). Serial sectioning and photography were carried out as described in the general procedures.

In this study on hippocampal synapses, it was established that the largest synapse had a diameter of approximately 600 nm. Assuming a section thickness of 50 nm on the average, series of 30 sections were collected. The section thickness was estimated by the fold method proposed by Small.[7] For these measurements the first and last three to five sections adjacent to the series of 30 were collected on Pyoloform carbon-coated grids instead of glass slides. The grids were pressed on sections when floating on the water surface in the knife boat. This manipulation caused folds in the section. Small folds in the section that had a parallel outline over a certain distance were photographed at a final magnification of 56,000×. If a fold stands upright, its width equals twice the section thickness and can easily be measured. The ultrathin sections were viewed in a Philips 201 transmission electron micro-

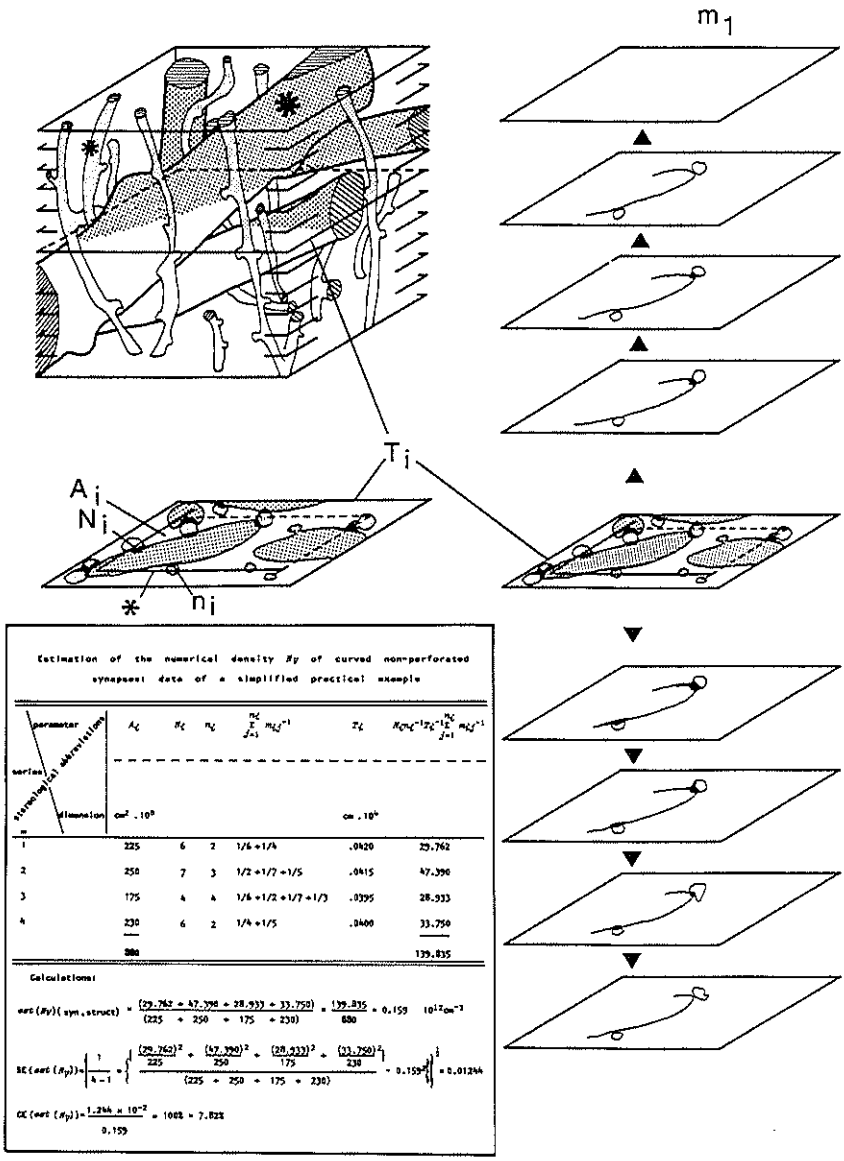

Estimation of the numerical density N_V of curved non-perforated synapses: data of a simplified practical example

serial section m	A_i	N_i	n_i	$\sum_{j=1}^{n_i} m_{ij}^{-1}$	T_i	$N_i m_i^{-1} T_i^{-1} \sum_{j=1}^{n_i} m_{ij}^{-1}$
parameter / abbreviations						
dimension	$cm^2 \cdot 10^5$				$cm \cdot 10^4$	
1	225	6	2	1/6 + 1/4	.0420	29.762
2	250	7	3	1/2 + 1/7 + 1/5	.0415	47.390
3	175	4	4	1/6 + 1/2 + 1/7 + 1/3	.0395	28.933
4	230	6	2	1/4 + 1/5	.0400	33.750
	880					139.835

Calculations:

$$est\,(N_V)(sym.,struct) = \frac{(29.762 + 47.390 + 28.933 + 33.750)}{(225 + 250 + 175 + 230)} = \frac{139.835}{880} = 0.159 \quad 10^{12} cm^{-3}$$

$$SE(est\,(N_V)) = \left\{ \frac{1}{4-1} \cdot \left[\frac{(29.762)^2}{225} + \frac{(47.390)^2}{250} + \frac{(28.933)^2}{175} + \frac{(33.750)^2}{230} - \frac{0.159^2}{(225 + 250 + 175 + 230)} \right] \right\}^{\frac{1}{2}} = 0.01244$$

$$CE(est\,(N_V)) = \frac{1.244 \times 10^{-2}}{0.159} = 100\% = 7.82\%$$

FIGURE 8. Simplified example of application of the method of Cruz-Orive (Ref. 2 and Appendix) for estimation of the numerical density (N_V) of particles in a structure without making assumptions regarding the size, shape, and orientation of the particles. A block of brain tissue containing large (*) and small (*) neurites is shown. Exchange of information between these nerve cell elements occurs via synaptic transmission. The shape of the synapses to be studied does not resemble the ideal shape of a flat circular disk. Their surface is more or less "curved" although not "perforated." To study the numerical density of these synapses, parallel serial sections are cut from the tissue block. In the center section T_i of a series—

scope equipped with a goniometer and a rotation holder. The starting position in the electron microscopic examination (step c) was chosen in the center of the pyramidal layer (Fig. 6). This layer can easily be identified at low magnification by the presence of the large nuclei of the pyramidal cells. The magnification used in step d was approximately 6000× on the main screen. The image in step f was photographed on 35-mm film (Kodak FGP). The electron micrographs were printed at a magnification of 11×, resulting in a final magnification on the micrograph of approximately 6000×. The exact magnification for each series of micrographs was calibrated using a grating replica (2160 lines/mm). The specimen area included in a micrograph was approximately 50 × 50 μm^2. In the example presented in this chapter, per slab one micrograph was taken per layer, i.e., stratum oriens, stratum pyramidale, stratum radiatum, and stratum lacunosum moleculare. Stratified systematic sampling was carried out within one micrograph. As will be outlined below, one to five areas per micrograph were selected for the analyses of the synapses. Both "classical" disklike[16] and larger complex-shaped "perforated" synapses were found in all four layers of the CA3 area. These perforated synapses[17] have a presynaptic grid of regularly arranged dense projections, which is partly disrupted.[4] Since these complex-shaped synapses are thought to have a particular functional significance,[17,18] it was found desirable to distinguish between the disklike nonperforated and the complex-shaped perforated synapses. However, only a small portion (5–30%) of the total synapse population of the hippocampus has been shown to be perforated. By examination of only the center section of a series of micrographs for the analysis of the synapses, it cannot be established whether the profile observed belongs to a perforated or a nonperforated synapse. Therefore, all synaptic profiles present in the center section were tracked through the series to obtain a valid estimation of $\bar{H}$ of the perforated as well as the nonperforated synapses (e.g., see Fig. 9). Stratified systematic sampling was carried out within each micrograph. To be able to do this, a predetermined regular lattice was placed over the micrograph (Fig. 10). The analysis of the synapses was always started in area 3, situated in the center of the micrograph. Subsequently, areas 1 and 5, situated closer to the upper and lower border of the layer, were analyzed. Then if fewer than a dozen synapses—nonperforated as well as perforated—were analyzed the analysis was continued in areas 2 and 4.

in the example the series (m_1) is taken approximately at the middle of the tissue block—all synaptic contact zones N_i are counted using Gundersen's[14] frame (*) for unbiased counting. The straight lines of this frame indicate Gundersen's "forbidden line"; synapses lying on the edge of reference area A_i are counted, provided they do not touch the forbidden line. Some of the synapses (n_i) within A_i are tracked forward (▼) and backward (▲) in the adjacent sections of the series to obtain an estimate of the effective projected height of the synapses. For simplicity, only synapses that are tracked (n_i) are drawn in the adjacent sections of the series. For further details, see the Appendix and the section on "Stereological Analyses."

Three to five areas per layer within one micrograph were thus analyzed, except for the stratum pyramidale, which contains large cell bodies. In this case it was found necessary to analyze in one slab the total area of the micrograph. After obtaining a reliable approximation of $\bar{H}$ for both types of synapses, N_V was calculated. Since all synaptic profiles in the center sections were serially traced, n_i (number of synapses tracked) equals N_i (total number of synapses present in the reference area). Hence, the formula used for the estimation of N_V(syn) was (see Appendix)

$$\text{est}(N_V) = \frac{\sum_{i=1}^{m} T_i^{-1} \sum_{j=1}^{n_i} M_{ij}^{-1}}{\sum_{i=1}^{m} A_i}$$

where

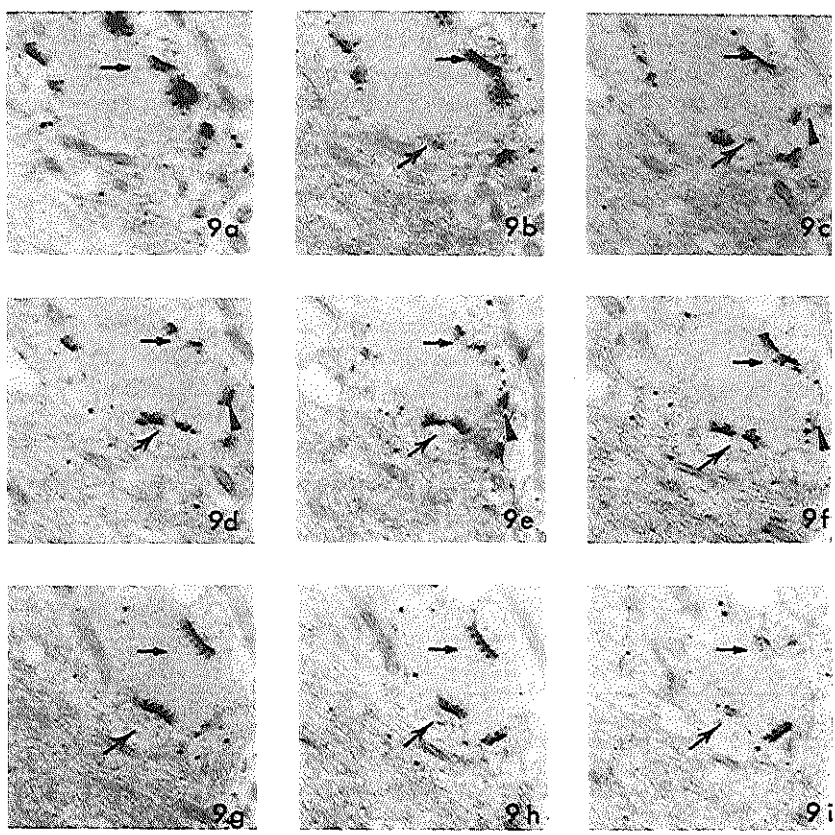

FIGURE 9. Example of E-PTA-treated serial sections in the stratum radiatum of the hippocampal CA3 region of the rat, showing two transversally cut perforated (arrows) and a nonperforated (arrowheads) synapse.

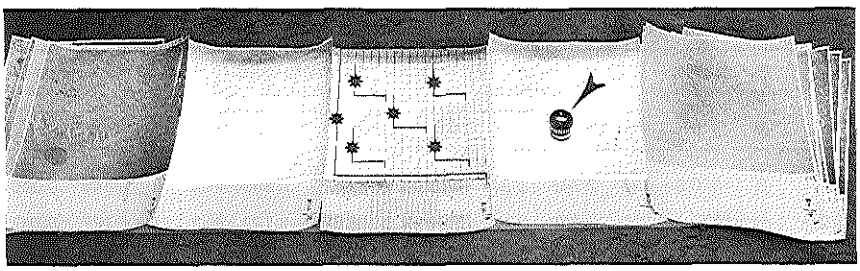

FIGURE 10. Analysis of a series of micrographs for estimation of the numerical density (N_V) according to Cruz-Orive (Ref. 2 and Appendix). Five square areas (1–5) were analyzed using Gundersen's unbiased counting rule (*, Gundersen's frame). Putting the micrographs on an illuminated screen greatly facilitates the measurements. Areas in the sequential sections corresponding to the five analyzed reference areas are identified by putting the adjacent micrograph on top of the previous one. In this way exactly identical areas are analyzed in the sequential sections. A loupe (arrowhead) may be helpful; for example, in the case of the hippocampal synapses it is used to distinguish, in case of doubt, between perforated and nonperforated synapses or to count the number of presynaptic dense projections along the corresponding synaptic contact zone.

- N_V = number of particles per unit volume
- m = number of series
- n_i = number of particles counted within A_i and tracked through the series
- T_i = thickness of the sections in the ith series
- m_{ij} = number of sections in which the jth tracked particle appears in the ith series
- A_i = reference area

The standard error of est(N_V) is estimated as follows [Appendix, Eq. (A.2)]. Setting

$$y_i = T_i^{-1} \sum_{j=1}^{n_i} m_{ij}^{-1}, \qquad x_i = A_i$$

gives

$$\mathrm{SE}\{\mathrm{est}(N_V)\} = \left\{(m-1)^{-1}\left[\frac{\sum_{i=1}^{m} y_i^2 x_i^{-1}}{\sum_{i=1}^{m} x_i} - \mathrm{est}(N_V)^2\right]\right\}^{1/2}$$

The coefficient of error CE{est(N_V)} was estimated as described in the Appendix and general procedures.

Table 1 shows the results of this study, from which it can be concluded that the different layers of the hippocampal CA3 region contain different numbers of perforated and nonperforated synapses. These regional differ-

TABLE 1. Number of Different Types of Synapses per Unit Volume N_V in Distinct Layers of the Hippocampal CA3 Region of a 30-Month-Old Rat, Obtained from Serial Sections[a,b]

	Parameter		All synapses				Nonperforated synapses				Perforated synapses			
Layer	m	$\sum_{i=1}^{m} A_i$ (μm^2)	n_i	[Mean]	SE	CE	n_i	[Mean]	SE	CE	n_i	[Mean]	SE	CE
Stratum oriens	6	510.6	196	2.766	0.349	12.6	177	2.620	0.309	11.8	19	0.146	0.045	30.5
Stratum pyramidale	5	2875.4	252	0.650	0.132	20.4	231	0.623	0.126	20.2	21	0.027	0.007	26.9
Stratum radiatum	5	425.5	171	3.517	0.426	12.1	136	3.148	0.434	13.8	35	0.368	0.073	19.7
Stratum lacunosum moleculare	8	716.1	206	1.718	0.374	21.8	190	1.647	0.372	22.6	16	0.071	0.025	36.0

[a] m, series; A_i, reference area; n_i, number of particles with A_i tracked through the series; [mean], mean number of synapses per unit volume $N_V(10^{12}\ cm^{-3})$; SE, standard error of the mean; CE, coefficient of error of the mean. The parameters were calculated using the formulas given in this chapter (Appendix).

[b] The CE[mean] in the present example is constant although quite large due to the regional variations within the hippocampus. These variations are mainly the result of including cell bodies and main neurites in our samples. A discussion of that point is presented elsewhere.[31]

ences in perforated and nonperforated synapses cannot be fully appreciated in random sections, because perforated synapses are only partly recognized as such. This leads to biased estimates of N_V of the total synapse population, as was shown by De Groot and Bierman[4] and will be discussed below.

COMMENTS AND DISCUSSION

Methods requiring ultrathin serial sectioning are laborious, which greatly reduces their use for routine application. However, for special purposes serial sectioning may be essential, for example, to estimate the numerical density of nonconvex particles, as shown for complex-shaped synapses in brain tissue by Verwer and De Groot[3] and De Groot and Bierman.[4]

The present chapter shows how the efficiency of the sampling procedures in such stereological studies can be improved. The method described is especially useful in the study of layered structures, which are common in the central nervous system (CNS). The lack of homogeneity of CNS tissues leads to major sampling problems. Adequate sampling can be carried out only at low magnification, which, in turn, introduces problems with respect to discrimination of structural details. So far, this problem has been solved by the use of composites of high-power micrographs. In the procedure described here, electron micrographs are made at low magnification to include large areas. The necessary enlargements for the study of the particles of interest are obtained by means of a video camera. In the example presented, these particles are the substructures of synaptic contact zones. To compensate for regional differences, the tissue blocks are sampled from the organ by a systematic sampling procedure. Stratified systematic sampling is then applied within each layer, which excludes overlap of fields and thus prevents double sam-

pling. The distance between the two borders of a layer is measured in advance at the light microscopic level to make sure that the micrographs are representative for a particular layer. Although this measurement is an extra step in the whole procedure, it is worth the effort since it provides the basis for an unbiased sampling of micrographs at the electron microscopic level. Moreover, this extra step takes little time and may, additionally, lead to the detection of changes in thickness of layers.

Orientation within the section is also improved by including in the section all layers in between the outer surface of the organ and its center. From the histological organization of the neuropil—especially the orientation of large neurites—it can then easily be deduced whether or not the section is cut perpendicular to the outer surface of the organ.

Ultramicrotomy of such large blocks is facilitated by the use of 75-μm Vibratome slices that are embedded in an orientated way and subsequently cut perpendicular to the outer surface of the organ, i.e., the ventricular surface for the hippocampus. Serial sectioning of such large oblong sections is made reliable by trimming the specimen block in such a way that the top edge of the block is not parallel to the knife edge. In contrast to conventional ultramicrotomy, this results in contact of the section with the knife edge at a single point only. The resulting minimal contact, together with a low speed of the reverse stroke of the ultramicrotome and the use of loose platinum loops, guarantees one-by-one removal of a series of sections from the knife boat in the proper sequence. After some practice, complete series of 40 sections or even more can be obtained easily and rather safely.

Orientation in the electron microscope is facilitated by placing each section in an orientated way on a suitable grid. The use of a rotation holder and a calibrated micrometer guarantees quick location of the areas of interest, keeping in mind the measurements of layer thickness. This procedure reduces the time during which the grid is in the electron beam, and illumination and emission can be kept low. Consequently, the damage to sections is minimal and very few are lost. The survival rate of the sections is also enhanced by choosing the best fitting grid with respect to grid bars and holes. On the one hand, the bars should not cover the areas of interest in the section; on the other hand, the holes should not be too large since the support film with the section will then collapse as soon as the grid is brought into the electron beam. Pyoloform support films are much stronger under the electron beam than, e.g., Formvar, collodion, or Parlodion films, but they tend to show more drift. This drift can be prevented by coating with carbon, which has a stabilizing and strengthening effect on the supporting film and the section.

By applying these procedures, a drastic reduction is achieved in the time required for sampling, filing, and documenting the tissues as well as in the cost of photographic materials. These modified procedures bring stereological methods involving serial sectioning within reach of routine application.

With respect to estimation of the numerical density using serial sections, the following critical statements can be made. Conventional derivations of the numerical density of a population of particles (N_V) involve strict assumptions with respect to the shape of the investigated particles. For synapses, it is generally accepted that their shape resembles a flat circular disk.[16] However, deviations from the ideal disk shape, e.g., curved or complex-shaped synapses, have been described in several papers.[3,4,17–25] Synapses may not only be curved or complex-shaped but may also be perforated; i.e., one or more parts of the pre- and postsynaptic surface area may be free of dense projections and postsynaptic densities. This gives the impression that the synapses are perforated.[17,24] It has been suggested by some investigators that these complex-shaped synapses have a particular functional significance since their number has been found to vary. Greenough et al.[17] found an increase in the occipital cortex when rats were reared in an "enriched" environment. Vrensen and Nunez-Cardozo[18] found an increase in perforated synapses in the visual cortex of rabbits after visual training. In the present study of rat hippocampus, large complex-shaped synapses were present side by side with smaller disklike synapses, as was found in the visual cortex of the rabbit.[18,24,25] In the latter studies, semithin (500-nm) E-PTA sections were used to reconstruct a frequency distribution of the synapses. Unfortunately, the authors disregarded the fact that they were underestimating the number of the larger complex-shaped synapses. They counted only synapses that were fully incorporated in the sections. Obviously, larger synapses have a greater chance to be cut by sectioning and, therefore, a smaller chance to be fully incorporated in the section; hence they have a smaller chance to be counted. Moreover, Vrensen and Nunez-Cardozo[18] calculated the numerical density of the synapses by the method of Abercrombie[26] based on the disk-shape assumption. As shown by Verwer and De Groot,[3] the validity of this assumption and consequently of such results is questionable. In a study on undernutrition, they compared the results for synaptic density of curved synapses in the cerebellum obtained by conventional methods[26,27]—based on the disklike shape assumption—with those obtained by a method that makes no assumptions regarding size, shape, and orientation of the synapses (Ref. 2 and Appendix). Erroneous results were obtained when methods were applied assuming synapses to be flat disklike structures. The problem is even more complicated when part of the synapses are perforated, as in the study presented in this chapter. It was previously shown by De Groot and Bierman[4] that the simultaneous presence of larger complex-shaped perforated and disklike nonperforated synapses in the hippocampus of rats resulted in underestimation of the synaptic profile length and overestimation of synaptic density when measured in randomly selected ultrathin E-PTA sections. Since the diameter of the presynaptic grid is 100–500 nm, the synapses will mostly be transversely cut in ultrathin (50-nm) sections. In a 50-nm osmicated section,

the perforated synapses seem to have an interrupted contact zone when the cut runs through the perforation. Only in that case can it be distinguished from the disklike nonperforated synapse, which lacks such an interruption. In the study by Greenough et al.,[17] carried out with random osmicated sections, only synapses that had the perforation in the plane of the section were considered to be perforated. Synapses without perforation in the plane of the section were erroneously counted as nonperforated synapses.

In E-PTA-treated 50-nm random sections, an interrupted contact zone often cannot be recognized as such and, instead of being counted as a perforated synapse, is counted as two or more separate synapses.[4] The differences in synaptic density and synaptic profile length found between the results obtained from random E-PTA and random OsO_4 sections[15,28,29] can be ascribed, at least in part, to the presence of complex-shaped perforated synapses in the tissue. In addition, the reaction of E-PTA with the paramembranous densities most likely differs from that of OsO_4, resulting in less extensive postsynaptic densities.

To estimate the numerical density in synapse populations with a considerable number of perforated or irregularly shaped synapses, conventional methods are inadequate. Serial sections should be used to distinguish between perforated and nonperforated synapses, and for the calculation of N_V a method should be applied that makes no assumptions about synaptic size and shape. For several reasons, outlined in this chapter, the method of preference is the one introduced by Cruz-Orive (Ref. 2 and Appendix). With this method the effective projected height $\bar{H}$ of the synapses is estimated directly from serial sections.

As shown in the imaginary example on curved synapses (Fig. 8), only some of the synapses (20 on the average) counted in the center section of the series must be tracked through the series in order to derive a valid estimate of their effective projected height. However, in the example presented in this chapter all synapses counted in the center section had to be tracked in order to distinguish between perforated and nonperforated synapses. A three-dimensional reconstruction is not necessary.

Complex-shaped particles are not overestimated since the particles are tracked through the series of sections. Since no assumptions are made about the size, shape, and orientation of the particles, this method is unbiased. Obviously, the section thickness must be measured very precisely. In an extensive study (De Groot DMG, submitted), it was found that the results obtained with different techniques—i.e., the Small fold method, an interference microscope, and electron microscopic comparison of exposure densities—did not differ significantly.

The method described in this chapter is no longer more laborious than the conventional random section methods for calculating N_V, especially when it is considered that, in the conventional methods, the mean particle size must

often be derived from the deconvoluted profile size distribution.[1] Apart from being rather laborious, the different deconvolution methods do not lead to identical estimates. In general, conventional methods may be applied only when absolute certainty exists that the real shape of the structure resembles an idealized shape. In all other cases the method of Cruz-Orive (Ref. 2 and Appendix) is to be preferred. It is always advisable to check first whether large variations in size and shape exist among the particles to be studied. Subsequently, one has to decide which method will be used for deriving the numerical density of the particles of interest. In the case of quantification of synapses, no randomly selected E-PTA- and OsO_4-treated sections should be used when perforated and nonperforated synapses are simultaneously present in the tissue. Random semithin (500-nm) E-PTA sections are very useful for a quick examination of variations in size and shape, but they should not be used for quantification of synapses of different sizes and shapes.

APPENDIX: ESTIMATION OF N_v FROM SERIAL SLABS, by Luis M. Cruz-Orive

Introduction

In Cruz-Orive[2] two methods were developed to estimate the numerical density $N_V \equiv N/V$ of a collection of N disjoint particles of arbitrary size, shape, and orientation contained in a solid Ω of volume V. The methods are based on measurements made on m uniform random blocks of material from Ω. From each block, a number of parallel sections a known distance apart are needed. The following assumptions are made: (1) The sections have zero thickness and (2) there are no truncation effects (that is, every particle fragment in a section is observable).

In this Appendix we readapt the most efficient method, namely method I of Cruz-Orive,[2] with assumptions (1) and (2) relaxed. It turns out that the estimate of N_V remains unaffected by truncation effects.

It must be pointed out, however, that an unbiased estimate of particle "caliper length" or linear projection H perpendicular to the sections is not available in general in the presence of truncation without additional assumptions. What is estimable is just $\bar{H}$, the "effective" linear projection, which can be interpreted as H minus the linear projection of the truncated part [for an example pertaining to spheres see Cruz-Orive, Ref. 30, Eq. (8.3)]. Fortunately, it is $\bar{H}$, and not H, that is needed to estimate N_V, as shown below.

The results are given first. Proofs are outlined at the end.

Estimation of N_V

Each of m uniform random blocks from the reference solid Ω is cut into serial sections of a known thickness. A given section toward the middle of the series is taken as the *reference section*. An approximately unbiased estimate of N_V is computed as follows:

$$\text{est}(N_V) = \frac{\sum_{i=1}^{m} N_i n_i^{-1} T_i^{-1} \sum_{j=1}^{n_i} m_{ij}^{-1}}{\sum_{i=1}^{m} A_i} \tag{A.1}$$

where est(θ) denotes the estimate of a fixed quantity θ and

- N_V = number of particles per unit volume of reference solid
- m = number of uniform random blocks cut into series
- A_i = reference area, namely the sampled area of the reference section from the ith block ($i = 1, 2, \ldots, m$)
- N_i = total number of particle sections (not just particle "fragments") counted in A_i, according to an unbiased counting rule (see Ref. 2, Fig. 1; and Ref. 14)
- n_i = number of particles in A_i tracked through the series
- T_i = thickness of sections of the ith series
- m_{ij} = number of serial sections from the ith block in which the jth tracked particle appears. Note that j runs from 1 to n_i

Under certain assumptions[5] a good estimate of the standard error of est(N_V) is

$$\text{SE}\{\text{est}(N_V)\} = \left\{(m-1)^{-1}\left[\frac{\sum_{i=1}^{m} y_i^2 x_i^{-1}}{\sum_{i=1}^{m} x_i} - \text{est}(N_V)^2\right]\right\}^{1/2} \tag{A.2}$$

where we have put $y_i = N_i n_i^{-1} T_i^{-1} \sum_{j=1}^{n_i} m_{ij}^{-1}$, $x_i = A_i$. The coefficient of error in percent is

$$\text{CE}\{\text{est}(N_V)\} = 100 \times \frac{\text{SE}\{\text{est}(N_V)\}}{\text{est}(N_V)} \tag{A.3}$$

Notes:

N1. The orientation of each series may be chosen at will.

N2. The distance between the first and the last sections of a series must be at least twice the longest projection of a particle in a direction perpendicular to the sections.

N3. Instead of using all sections in a series, one out of every two, three, etc. may be used. In this case, T_i must be replaced respectively with $2T_i$, $3T_i$, etc. in Eqs. (A.1) and (A.2).

Outline of a Proof of Eq. (A.1)

A proof of Eq. (A.1) consists of three steps. First, for a uniform random reference section of area A, thickness T, and fixed orientation, hitting Ω, it can be shown that

$$N_V = N_A (E\tilde{H} + T)^{-1} \tag{A.4}$$

where N_A = (number of particle sections captured in A)/A and E(·) denotes the true mean value for all particles in Ω. Second, an unbiased estimate of $(E\tilde{H} + T)^{-1}$ is

$$\text{est}(E\tilde{H} + T)^{-1} = n^{-1} \sum_{j=1}^{n} \{(\tilde{H}_j \mid \uparrow) + T\}^{-1} \tag{A.5}$$

where n is analogous to n_i (see above) and $\tilde{H}_j \mid \uparrow$ denotes the effective linear projection of a tracked particle, that is, of a particle actually hit by the reference section (hence the symbol "$\uparrow$"). Equation (A.5) holds because the probability of hitting and observing a particle is proportional to $\tilde{H} + T$. Third, it can be shown that

$$\text{est}\{(\tilde{H}_j \mid \uparrow) + T)\} = m_j T \tag{A.6}$$

is also unbiased, where m_j is analogous to m_{ij}. Note, however, that $(m_j T)^{-1}$ is only "approximately unbiased" for $\{(\tilde{H}_j \mid \uparrow) + T)\}^{-1}$. Hence Eq. (A.1) is approximately unbiased too. Combining Eqs. (A.4)–(A.6) it follows that an approximately unbiased estimate of N_V is

$$\text{est}(N_V) = N_A \cdot (nT)^{-1} \sum_{j=1}^{n} m_j^{-1} \tag{A.7}$$

If m independent blocks with reference areas $A_1, A_2, \ldots, A_m$ are available, the ith N_V estimate should be weighted by $A_i/(A_1 + \cdots + A_m)$. These weights are preferable to the ones proportional to $n_i A_i$ proposed in Cruz-Orive [Ref. 1, Eq. (28)]. Thus, we obtain Eq. (A.1).

From Eqs. (A.5) and (A.6) we see that we can estimate $E\tilde{H}$ but not EH, as pointed out in the Introduction to this Appendix. Fortunately, it is $E\tilde{H}$ that is needed to estimate N_V, not EH [see Eq. (A.4)].

Note Added in Proof

After this chapter was written, H. J. G. Gundersen (J Microsc 143:3–45, 1986, Section 3.3 and Fig. 3.3, left) made a subtle but important remark concerning the unbiasedness of the estimation of particle height via Eq. (A.6), and hence of N_V using Eq. (A.1). The reader is referred to that paper for details. The remark pertains specifically to the situation described in our Note N3, p. 155. If, on the contrary, the height of the sampled particles is estimated by means of consecutive, adjacent sections (as was the case in the present application), then the unbiasedness of Eq. (A.6) remains unaffected.

REFERENCES

1. Weibel ER: Stereological Methods, volume 1, Practical Methods for Biological Morphometry. London: Academic Press, 1979.

2. Cruz-Orive LM: On the estimation of particle number. J Microsc 120:15–27, 1980.
3. Verwer RWH, De Groot DMG: The effect of shape assumptions on the estimation of the numerical density of synapses from thin sections. Prog Brain Res 55:195–203, 1982.
4. De Groot DMG, Bierman EPB: The complex-shaped "perforated" synapse, a problem in quantitative stereology of the brain. J Microsc 131:355–360, 1983.
5. Cruz-Orive LM: Best-linear unbiased estimators for stereology. Biometrics 36:595–605, 1980.
6. Peters A: The fixation of cerebral nervous tissue and the analysis of electron micrographs of the neuropil, with special references to the cerebral cortex. In: Contemporary Research Methods in Neuroanatomy, edited by Nauta WJH, Ebbeson SOE, p. 56. Berlin: Springer, 1970.
7. Small JV: Measurements of section thickness. In: Proceedings 4th European Congress on Electron Microscopy, edited by DS Bocciarelli, volume 1, p. 609. Roma: Tipografia Poliglotta Vaticana, 1968.
8. Smith FH: A photo-electronic phase-measuring microscope. J R Microsc Soc 87:165, 1967.
9. Gillis J, Wibo M: Accurate measurements of the thickness of ultrathin sections by interference microscopy. J Cell Biol 49:947, 1971.
10. Williams MA: Autoradiography and immunocytochemistry. In: Practical Methods in Electron Microscopy, edited by Glauert AM, volume 6. Amsterdam: North-Holland, 1977.
11. Silverman L, Schreiner B, Glick D: Measurement of thickness within sections by quantitative electron microscopy. J Cell Biol 40:768, 1969.
12. Casley-Smith JR, Crocker KWJ: Estimation of section thickness, etc. by quantitative electron microscopy. J Microsc 103:351–368, 1975.
13. Beertsen W, Everts V, Houtkooper JM: Frequency of occurrence and position of cilia in fibroblasts of the periodontal ligament of the mouse incisor. Cell Tissue Res 163:415–431, 1975.
14. Gundersen HJG: Notes on the estimation of the numerical density of arbitrary profiles: the edge effect. J Microsc 111:219–223, 1977.
15. Vrensen G, De Groot D: Phosphotungstic acid staining and the quantitative stereology of synapses. In: Electron Microscopy and Cytochemistry, Proc 2d Int Symp, edited by Wisse E, Daems WT, Molenaar J, van Duyn P, p. 255. Amsterdam: North-Holland, 1974.
16. West MJ, Coleman PD, Wyss UR: A computerized method of determining the number of synaptic contacts in a volume of cerebral cortex. J Microsc 95:277–283, 1972.
17. Greenough WT, West RW, De Voogd TJ: Subsynaptic plate perforations: changes with age and experience in the rat. Science 202:1096–1098, 1978.
18. Vrensen G, Nunes-Cardozo J: Changes in size and shape of synaptic connections after visual training: an ultrastructural approach to synaptic plasticity. Brain Res 218:79–97, 1981.
19. Gray EG: Axosomatic and axodendritic synapses of the cerebral cortex: an electron microscope study. J Anat 93:420–433, 1959.
20. Peters A, Kaiserman-Abramof JR: The small pyramidal neuron of the rat cerebral cortex: the synapses upon the dendritic spines. Z Zellforsch Mikrosk Anat 100:487–505, 1969.
21. Akert K: Dynamic aspects of synaptic ultrastructure. Brain Res 49:511–518, 1973.
22. Cohen RS, Siekevitch P: Form of the postsynaptic density: a serial section study. J Cell Biol 78:36–46, 1978.
23. Dyson SE, Jones DG: Quantitation of terminal parameters and their inter-relationships in maturing central synapses. A perspective for experimental studies. Brain Res 188:43–59, 1980.
24. Vrensen G, Nunes-Cardozo J, Müller L, Van der Want J: The presynaptic grid: a new approach. Brain Res 184:23–40, 1980.
25. Müller L, Pattiselanno A, Vrensen G: The postnatal development of the presynaptic grid in the visual cortex of rabbits and the effect of dark-rearing. Brain Res 205:39–48, 1981.

26. Abercrombie M: Estimation of nuclear population from microtome sections. Anat Rec 94:239–247, 1946.
27. Fullman RL: Measurement of particle sizes in opaque bodies. Trans AIME 197:447–452, 1953.
28. Burry RW, Lasher RS: A quantitative electron microscope study of synapse formation in dispersed cell cultures of rat cerebellum stained either by Os-Ul or by E-PTA. Brain Res 147:1–15, 1978.
29. Mayhew TM: Stereological approach to the study of synapse morphometry with particular regard to estimating number in a volume and on a surface. J Neurocytol 8:121–138, 1979.
30. Cruz-Orive LM: Distribution-free estimation of sphere size distributions from slabs showing overprojection and truncation, with a review of previous methods. J Microsc 131:265–290, 1983.
31. De Groot DMG, Bierman EPB: A critical evaluation of methods for estimating the numerical density of synapses. J Neurosc Meth 18:79–101, 1986.

PART II

Chapter 3

COMPARISON OF METHODS FOR THE ESTIMATION OF THE THICKNESS OF ULTRATHIN TISSUE SECTIONS

Journal of Microscopy, Vol. 151, *Pt* 1, *July* 1988, *pp.* 23–42.
Received 7 *July* 1987; *revised* 21 *March* 1988; *accepted* 24 *March* 1988

Comparison of methods for the estimation of the thickness of ultrathin tissue sections

by DIDIMA M. G. DE GROOT, *Medical Biological Laboratory TNO, P.O. Box* 45, 2280 *AA Rijswijk, The Netherlands*

KEY WORDS. Section thickness, ultrathin sections, electron microscopy, 'small-fold' technique, 'electron scattering' method, interference microscopy, 're-embedding' method, inter-section variation, intra-section variation.

SUMMARY

For a number of quantitative electron microscopical techniques it is relevant to obtain an estimate of the thickness t' of the section which, in general, will differ from the actual distance t between the two cuts that generate the section. To estimate t' of ultrathin sections, several techniques have been adopted in the past, both with and without the aid of the electron microscope and additional equipment, which are summarized in an appendix. In the present study five methods have been evaluated experimentally using sections of ten different interference colours: (a) the 'small-fold' technique, (b) the 'electron scattering' method, (c) interference microscopy with (A) the Vicker's M86® scanning microinterferometer and (B) the Jenoptik Amplival Interphako® interference microscope and (d) the 're-embedding' method. Reliable, reproducible and comparable results were obtained with the small-fold technique, with the Vickers M86® scanning microinterferometer and with the electron scattering method. For the last method, standard test lines for the different settings of the electron microscope were developed. The results obtained with the Jenoptik Amplival Interphako® interference microscope are reproducible, but show a constant difference, i.e. a factor of 1·36, in thickness compared with the other three techniques. The possible cause of this 'systematic error' is discussed. The re-embedding method proved to be more laborious and slightly less reliable than the other techniques.

The variation in t' between sections of a particular interference colour (inter-section variation) was found to be larger than the variation in t' within a section (intra-section variation).

INTRODUCTION

Quantitative electron microscopical techniques such as three-dimensional reconstruction, stereology, quantitative autoradiography, quantitative enzyme-histochemistry, mass determinations or X-ray energy dispersion analysis aim to derive information about structural quantities from measurements in ultrathin sections. These sections are generally dealt with as if they represent a two-dimensional plane of the three-dimensional specimen. This, however, is not correct: even a very thin section of biological tissue is a slice of finite thickness (e.g. 30 nm) generated by two cuts. With today's high resolution electron microscopes it is possible to obtain an ultimate resolution of 0·5 nm. Therefore, an ultrathin section can hardly be considered as a

true plane. Quantitative electron microscopical techniques can only be applied properly with accurate estimates of the section thickness. One cannot rely on the advance setting of the ultramicrotome since this instrument does not take into account variations due to random thermal and mechanical changes and to compression during sectioning (Mori & Christensen 1980; Ohno, 1980). One must also be aware of the decrease in section thickness upon exposure to the electron beam since all embedding media are modified by electron bombardment *in vacuo*. Hence, the thickness t' of the final section will differ from the actual distance t between the two consecutive cuts by which the section is generated (Gundersen *et al.*, 1983). For many quantifications, e.g. when estimating numbers of particles, an estimate of $\bar{t}$, the overall mean sectioning depth, is the desired parameter which can be obtained by the elegant method described by Gundersen *et al.* (1983). However, when, e.g. the volume of a structure is estimated using systematic sections (Cruz-Orive, 1985) t' should be known. In such a case, the area of the structure in the section is measured and multiplied by the distance from the upper surface of that section to the upper surface of the next section and so forth, to calculate the final volume. Clearly, if the thickness t', of the resulting sections deviates from the actual distance t due to 'deformation', the measured area of the structure in the sections will be 'deformed' to the same extent. To estimate the thickness t' of ultrathin sections, several techniques have been adopted in the past, both with and without the aid of the electron microscope and additional equipment. The Appendix summarizes these methods with reference to studies in which a particular method was either proposed or evaluated. In addition, the general advantages and/or limitations of the methods are given. Ideally, such a technique should be precise, it should not require expensive equipment and should be useful for routine application (Williams, 1981).

In previous studies (De Groot & Bierman, 1983, 1986, 1988; De Groot, 1984, 1985) the 'small-fold' method (Small, 1968) has been used to estimate t'. In these studies the numerical density of complex-shaped (perforated) synapses was estimated and their shape reconstructed, using serial sections (Cruz Orive, 1980, 1984, 1985; De Groot & Bierman, 1983, 1986, 1988; De Groot, 1984; Sterio, 1984). The small-fold method, however, cannot be directly adapted since the tracking of the investigated particles through the series of sections would be hampered by the presence of folds in the sections, a prerequisite for the small-fold method. Hence, small-fold measurements of section thickness always have to be carried out on separate sections. A method which is applicable to any section regardless of the presence of folds in the sections, is the 'electron scattering' (ES) method of Weybull (1970). This method is carried out in the electron microscope and once the so-called 'standard test lines' are prepared, the method is very quick (see below). For the stereology and reconstruction of e.g. complex synapses such a method would be superior to the small-fold method, provided the method generates reliable data.

The goal of the present study was, therefore, to see whether the electron scattering technique could serve as a good alternative for the previously used small-fold method. To test the reliability of both these methods it was decided first of all to compare the results of thickness measurements obtained from the small-fold method with those obtained by interferometric measurements and also from re-sectioned sections (Philips & Shortt, 1964). The interferometric measurements were carried out in two ways: (a) with the Vicker's Instruments M86® scanning micro-interferometer (see e.g. Williams 1977a) and (b) with the Jenoptik Amplival Interphako® interference microscope. Secondly, the results of the method with the highest precision, i.e. the Vicker's Instruments M86® interferometric method (see e.g. Williams, 1977a), were looked upon as 'baseline' data for the comparisons and were subsequently used to develop test lines for the electron scattering technique. Electron scattering was measured by using the exposure meter readings of the electron microscope. To improve the accuracy of this read-out, a current meter—simple and inexpensive, but accurate—with digital read-out was connected to the electron microscope.

In addition, the Vicker's Instruments M86® interferometric measurements were used to obtain information about intra- and inter-section variations within tissue/resin containing sections of a particular interference colour.

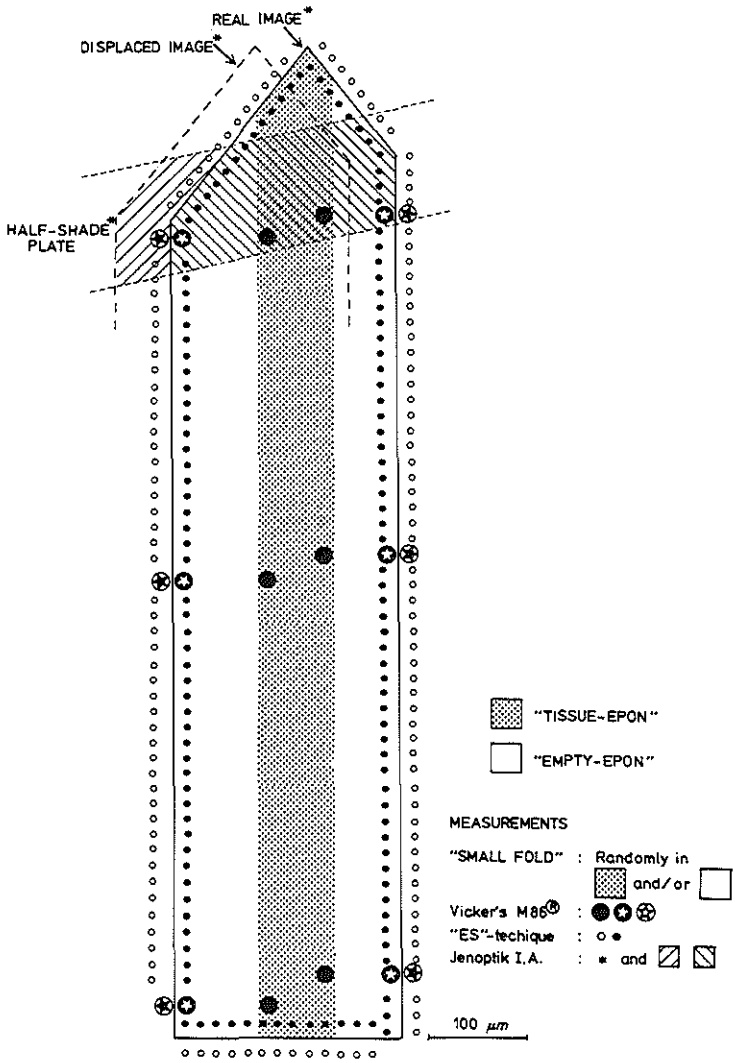

Fig. 1. Oblong, arrow-shaped sections were used in this study. Brain tissue (▨) was present over the total length of the longitudinal axis of the section and over a width of 75 µm, i.e. the thickness of the originally embedded vibratome-slice. 'Empty' Epon resin (□) was left intentionally along both longitudinal edges of the tissue. Section-thickness measurements were made, using different techniques: (a) 'small fold' measurements were carried out in both empty and brain tissue containing resin on folds which are randomly located over the section; (b) the 'electron scattering' of the section on the support-film measured in empty, resin (•) and of the support-film itself (○) was determined directly in the electron microscope by measuring the electron current on the viewing screen with the exposure meter; (A) measurements with the Vicker's M86® scanning micro interferometer were carried out at predetermined spots on (●; ✪) and along side (⊛) the section; (B) for the Jenoptik Amplival Interphako® interference microscope the shearing method with differential image splitting (*) was applied and a half-shade plate was introduced in the microscope. To carry out the measurements the brightness of the phase edge's region of splitting in both the section (▧) and the surrounding (▨) is matched successively to that of the vicinity; (d) a number of sections were re-embedded after the electron scattering technique had been carried out and were cut transversely at intervals of 100 µm. At five previously unexposed points at each interval the thickness of the re-embedded section as measured with the aid of a semi-automatic image analysing system.

MATERIALS AND METHODS

General

To introduce the electron scattering method for section thickness measurements into our laboratory and to use it in future quantitative studies, sections were collected from the same material as commonly used for our quantitative investigations. An adult female, small Wistar (WAG/Rij) rat was fixed by transcardial perfusion with a glutaraldehyde/formaldehyde mixture (Peters, 1970) under ether anaesthesia. 75 μm Vibratome slices of the hippocampal CA3 area were collected, block-stained with ethanolic phosphotungstic acid (E-PTA) and were embedded in Epon 812 (De Groot, 1984; De Groot & Bierman, 1986, 1988). The Epon resin contained a 5:5 mixture of dodecenyl succinic anhydride (DDSA) and methyl nadic anhydride (MNA). Polymerization of the Epon blocks occurred at 35, 45 and 60°C for 24, 24 and 48 h, respectively.

Embedding was orientated in such a way that cutting with the ultramicrotome occurred perpendicular to the ventricular surface of the hippocampal CA3 area. Before ultramicrotomy was carried out the specimen block was trimmed in such a way that oblong, arrow-shaped sections were cut from the block during sectioning (Fig. 1). This particular shape and the rather large size of the sections were chosen, because of the measurements of section thicknesses of serial sections of brain tissue carried out in previous studies (De Groot, 1984; De Groot & Bierman, 1986, 1988) and also those that will be applied in the future.

The sections (see Fig. 1) included brain tissue over the total length of the longitudinal axis of the section and over a width of 75 μm, i.e. the thickness of the originally embedded vibratome-slice. The presence of biological material may introduce larger variations into the thickness of the section (Williams & Meek, 1966). Therefore, 'empty' Epon resin was left intentionally along both longitudinal edges of the tissue in order to make section-thickness measurements in both 'empty' and 'biological material-containing' resin. Sections of different thicknesses displaying interference colours grey, white, silver, yellow, gold, brown, red/brown, violet, blue and green/yellow, respectively, were prepared with a Reichert OmU3® ultramicrotome using a diamond knife. The sections were viewed at a fixed angle since variations in this angle introduce variations in the interference colour scale (Peachy, 1958).

For each interference colour a total of twelve sections, each showing a homogeneous interference colour under the binocular of the ultramicrotome, were selected. For the evaluation and comparison of the different methods for section thickness measurements the sections were collected and sampled as follows. From each set of sections three sections (called series I) were mounted on Formvar/carbon coated 100 mesh copper grids by pressing the grid onto the section while this was floating on the water surface in the knife-boat. By doing so folds, necessary for the application and testing of the small-fold technique (see below: small-fold technique) were introduced into the sections. The remaining nine sections of each interference colour were individually picked up from the water surface with the aid of a loose platinum loop held between a pair of tweezers and were carefully placed on Formvar/carbon coated glass slides. Subsequently, 3 of the 9 sections (called series II) were mounted on slotted grids (pitch 250 μm, hole 200 μm and bar 50 μm; VECO, R100A, Cu 3·05 mm; 841, 175) from which one bar had been removed under the dissecting microscope*. The oblong section was coated over the position of the removed bar, i.e. with its longitudinal axis between and parallel to the two bars neighbouring the removed one. (For a detailed description of this procedure the reader is referred to De Groot, 1984.) Of these 'series II' sections, the Relative number of Electrons Transmitted by the section (R.E.T.) was estimated (see below: electron scattering technique) and thereafter the grids with the orientated sections were re-embedded in Epon. After polymerization 0·5 μm sections were cut normal to the re-embedded sections to measure directly the actual thickness of the sections (see below: re-embedding technique).

*Currently, these grids are commercially produced by Oscar Stolk Scientific, The Netherlands.

The thickness of the remaining six sections per interference colour (series III and series IV) was determined with the aid of interference microscopy (see below: Vicker's Instruments M86® micro-scanning interferometer and the Jenoptik Amplival Interphako® interference microscope) while the sections were still mounted on the glass slides.

After interference microscopy had been carried out, the Formvar/carbon film with the sections was stripped from the glass slides and the sections were mounted on slotted grids as mentioned above for series II. Once the sections were on the grids, the relative number of electrons that had been transmitted through the sections in the electron beam was estimated in the same way as for the sections of series II.

SPECIFIC METHODOLOGIES

(a) *The 'small-fold' technique*

A rather simple method for the estimation of section thicknesses is the 'small-fold' method (Small, 1968). Small proposed to measure the width of the projected image of small folds consisting of two adhering and parallel running parts of a section, i.e. twice the section thickness. The resulting value (nm) is divided by 2 to obtain the thickness (t') of the section:

$$t' = \text{nm}/2$$

Since several objections have been raised against Small's technique we decided to compare the results of the fold technique with those of interferometry and 'electron scattering' ('ES') (see below), all in the same sections (see under series I, Materials and Methods: General).

(b) *The 'electron scattering' method*

Another way to determine the section thickness t' is by measuring electron scattering in the section and comparing the result with a standard test curve (Weybull, 1970). In such a curve the relative electron transmission in sections of varying thicknesses is plotted against 'standard' thickness values of the same sections. These 'standard' values are obtained by a different, reliable technique. Obviously, such a curve is valid only for a particular embedding resin and a particular setting of the electron microscope. Electron scattering is determined directly in the electron microscope by measuring the electron current on the viewing screen with the exposure meter. In this study, standard test lines were made from measurements of the differences in electron scattering between the section on the support-film (ES(s)) and the support-film (ES(f)) itself on the one hand (Fig. 1) and M86 values of the same sections (see below: Interference Microscopy) as standards on the other. Since the exposure meter scale of the Philips 201 electron microscope used in this study is too coarse, a digital multimeter (MM) was connected to the electron microscope, rendering it possible to detect very small differences in electron scattering. Measurements were carried out at accelerating voltages of 40, 60, 80 and 100 kV, respectively. For each measurement (Fig. 1) the reading on the MM was set at an arbitrary value and aimed at an area on the support-film (ES(f)), adjacent to the section. Subsequently, measurements were performed in the section in areas of empty resin (ES(s)) and the change in reading of the MM was used to calculate the relative number of electrons transmitted by the section (R.E.T.):

$$R.E.T. = \{[ES(f) - ES(s)]/ES(f)\} * 100$$

MM settings on the support-film of 30·0, 20·0 and 10·0 mV, respectively, were tested at each accelerating voltage level. A magnification on the main screen of 37·500 was used, together with a condenser aperture of 500 μm and an objective aperture of 30 μm. The log R.E.T. values were plotted against the M86 measurements and a linear regression curve was calculated for each of the above mentioned conditions of the microscope by the method of the least squares.

(c) *Interference microscopy*

Interference microscopy was one of the techniques applied in this study to measure the

thickness of the sections (see under series III and IV Materials and Methods: General). The principle of this technique is as follows. In an interferometer the light beam is split and directed along separate pathways before being recombined finally into a single composite beam. At the point where the two separate beams are combined a phase difference or Optical Path Difference (O.P.D.) occurs, caused by the differences in lengths of the two optic pathways traversed by the two separate beams. Such a difference in length of the optical pathways may be caused by insertion of a transparent refractile object, for example an Epon-section, in the pathway of one of the two separated beams. Then, after recombination of the two beams, the intensity of the composite beam is sinusoidally dependent upon the O.P.D.:

$$I = \cos^2 (\pi.\text{O.P.D.}/\lambda) \qquad (1)$$

where I = intensity of the composite beam, O.P.D. = optical path difference, λ = wavelength. The O.P.D., in turn, depends on the thickness of the inserted object and on the refractive indices of both the object and of the medium. Once the O.P.D. and the refractive indices are known, the thickness of the object can be calculated as follows:

$$t' = \text{O.P.D.}/(\varepsilon - \varepsilon_0) \qquad (2)^*$$

where t' = the thickness of the inserted object; in this case the section-thickness, ε = refractive index (R.I.) of the object; in this case the Epon section, ε_0 = R.I. of the medium; in this case air (= 1·0000). Clearly, the R.I. of the object† and of the medium must be known for the wavelength used.

Two apparatuses were used in the present study: (A) the Vickers M86® scanning micro-interferometer (called: M86), and (B) the Jenoptik Amplival Interphako® interference microscope (called Jenoptik A.I.).

(A) The Vicker's M86® scanning micro-interferometer is a combined microdensitometer and scanning interference microscope that scans with a coherent parallel light beam produced by a He–Ne laser. The laser wavelength is 632·8 nm. The interferometer is the double-refracting plate system according to Jamin, 1868 (Beyer, 1973). Sections, mounted both on coated grids (series I) or on coated glass slides (series III and IV) were measured. The measurements were carried out in distinct spots on and along the section (Fig. 1). The M86 is supplied with a digital wavelength read-out. Thereby objective spotphase (sp) measurements were made both in the section on the support-film (sp(s)) as well as in the support-film only (sp(f)) (Fig. 1). After subtraction the resulting spotphase difference is multiplied with the wavelength used (λ = 632·8 nm) to obtain the O.P.D.:

$$\text{O.P.D.} = [\text{sp(s)} - \text{sp(f)}]\ 0{\cdot}6328\,\mu\text{m} \qquad (3)$$

Subsequently, the thickness (t') of the section was calculated according to formula (2) above.

(B) The other interference microscope used in this investigation was the Jenoptik Amplival Interphako® interference microscope. The shearing method was applied (12·5× shearing objective) with differential image splitting (Beyer, 1973). Thereby the image of the object—i.e. the section—and the displaced image are not completely separated but are partly overlapping (Fig. 1). Monochromatic light (λ = 546 nm) was used and a half-shade plate was introduced in the microscope. This half-shade plate consists of a phase bridge which produces a small relative pathway difference. The phase bridge is set in such a way that it passes across the section to be measured, thereby dividing both the section and its surroundings into two regions of different brightness (Fig. 1). To carry out the measurements the brightness of the phase edge's region of splitting in both the section (a_1) and the surroundings (a_2) is matched successively to that of the

*It must be borne in mind that the intensity I is a periodic function of the thickness I' and that therefore t' is not a unique function of I and that for large thicknesses the results can be ambiguous.

†The refractive index of the Epon, used in this study, was measured with Abbe type refractometers (Abbe Engineering Co., NY); in red light by Prof. Dr M. A. Williams, University of Sheffield, U.K. and in green light by Dr A. Weeda, AKZO-Research Institute, Arnhem, The Netherlands.

vicinity. This is done with the aid of the measuring compensator. The pathway difference or O.P.D. caused by the section is determined from the difference of the scale divisions (ΔT) read on the drum. To calculate the O.P.D. caused by the object the difference between the scale divisions a_1 and a_2 (ΔT) on the drum was multiplied by the calibration factor (K) of the microscope:

$$\text{O.P.D.} = [(a_1 - a_2)/2]K \tag{4}$$

The value of K is represented by the quotient of the wavelength used ($\lambda = 546$ nm) divided by the number of drum divisions (105·8 for this microscope) necessary for the displacement of the interference fringes by one fringe interval. Hence, $K = 5{\cdot}16$. Since the measurements with the half-shade plate were carried out from one partial image to the other, twice the pathway difference (2 O.P.D.) caused by the section and hence double the accuracy is attained.

The thickness (t') of the section was then calculated according to formula (2) written above.

(d) *The 're-embedding' method*

Sections of varying thicknesses were collected on grids as described under Materials and Methods (General) for series II. In the electron microscope the relative number of electrons transmitted by the sections (R.E.T. values) was determined using an accelerating voltage of 100 kV and an arbitrary setting of the multimeter (MM) of 30·0 mV at the level of the support-film, thereby obtaining an appropriate light intensity. Subsequently the grids, carrying the sections on the support-film were re-embedded in Epon and after polymerization 0·5 μm sections (read on the ultramicrotome setting) were cut normal to the re-embedded sections at intervals of 100 μm. At each interval the thickness of the re-embedded section was observed in the electron microscope and at five—previously unexposed—points the image was stored on video-tape. The magnification was calibrated with a grating-replica (2160 l/mm). At each point ten measurements of the thickness of the re-embedded section were carried out with the aid of a semi-automatic image analysing system (Videoplan® Kontron-Messgeräte, Eching, F.R.G.). The resulting mean values were plotted against the log R.E.T. values of the same sections and a linear regression curve was calculated by the method of the least squares. Compression due to cutting was checked by comparing the size of the surface of the tissue block with the size of the sections cut from the block.

RESULTS

The thickness of sections showing a particular interference colour and measured with the M86 (see: series III and IV, Material and Methods: General) are presented in Table 1. The thickness measured over 'empty resin' versus the thickness over 'tissue containing resin' is given. M86 measurements were carried out at six pre-determined points, both in empty Epon resin areas as well as in six pre-determined neighbouring tissue-containing areas (Fig. 1). The results show that for the interference colours brown, red/brown, violet, blue and green/yellow, the mean section thickness determined in tissue-containing areas was significantly larger than the thickness determined in empty resin (paired t-test, $P2 \leqslant 0{\cdot}05$). For the interference colours grey, white, silver, yellow and gold the results did not differ significantly (paired t-test, $P2 > 0{\cdot}05$). These results indicate that for sections in the range of 30–90 nm no significant differences between empty resin areas and tissue-containing resin areas are found, at least not for hippocampal E-PTA tissue. However, above 90 nm the thickness in tissue-containing areas is slightly larger (approximately 2%). Regression analysis with empty Epon resin as the independent variable resulted in $y = -1{\cdot}07 + 1{\cdot}025x$ (significant regression, $P2 < 10^{-4}$); the 95% confidence intervals of the slope and the intercept being (1·014, 1·035) and (−2·23, 0·10), respectively.

Table 2 shows the results of a two-way analysis of variance (six sections per interference colour; six measurements per section at predetermined points) carried out for each interference colour of the sections of Table 1 (empty Epon resin). The results indicate that there is no

Table 1. The mean thickness (±SEM) of ultrathin sections with varying interference colour, i.e. grey (30 nm) to green/yellow (215 nm) ($n = 6$ sections per interference colour). Measurements were carried out with the Vicker's M86® scanning micro-interferometer in empty Epon resin ($n = 6$ measurements per section) and in tissue containing resin ($n = 6$ measurements per section), and the differences were tested with the paired t test (* = significantly different).

	Thickness of section (nm)				
	In empty Epon resin		In tissue containing resin		
Colour	$\bar{x}$	SEM	$\bar{x}$	SEM	P2
Grey	31·39	0·51	31·29	0·62	0·92
White	39·42	1·37	39·08	1·37	0·39
Silver	54·06	1·29	53·89	1·71	0·77
Yellow	70·14	3·06	71·39	2·40	0·16
Gold	90·61	1·93	90·89	1·63	0·84
Brown	108·72	1·96	111·14	1·70	0·037*
Red/brown	128·14	2·26	129·70	2·01	0·028*
Violet	148·75	1·89	151·51	2·49	0·026*
Blue	180·83	0·94	184·24	1·82	0·028*
Green/yellow	215·92	3·48	220·36	2·65	0·016*

Table 2. Results of a two-way analysis of variance for the section thickness of ultrathin sections of varying interference colour, i.e. grey (30 nm) to green/yellow (215 nm) (* = significant difference, $P < 0·05$).

Colour	P values of tested differences between the six sections/colour	P values of tested differences between the six measurements/section
Grey	0·51	0.73
White	0·0019*	0·63
Silver	0·0005	0·80
Yellow	$<10^{-4}$*	0·21
Gold	0·0005*	0·82
Brown	$<10^{-4}$*	0·45
Red/brown	$<10^{-4}$*	0·066
Violet	0·25	0·73
Blue	0·38	0·63
Green/yellow	0·0004*	0·37

difference between the six measurements within the section. In addition the results show that, except for sections of interference colours grey, violet and blue, a difference in section thickness between the six sections of a particular interference colour does exist.

The sections used in Tables 1 and 2, measured with the M86 were also measured with the Jenoptik A.I. interference microscope. The relationship between the section thickness estimates with the Jenoptik A.I. and with the M86 is shown in Fig. 2. The linear regression curve was calculated: $y = -2·39 + 1·365x$, where the intercept of $-2·39$ (95%) confidence limits: $-9·15$, 4·38) was not significantly different from zero (P2 = 0·48) and where the slope of 1·365 (95% confidence limits: 1·30, 1·43) was significantly different from 1 ($P2 < 10^{-4}$). The variation in the data explained by the regression (R^2) was 97·71%. In practice this means that the values of the section thicknesses measured with the Jenoptik A.I. will be approximately 1·36 times higher than the values measured with the M86 when measuring section thicknesses in the range of 30–215 nm.

A standard test line for the electron scattering technique with M86 measurements of series III as 'standards' was made (Fig. 3, closed circles). Conditions of the electron microscope were those generally used in our studies on E-PTA stained nervous tissue: an accelerating voltage of

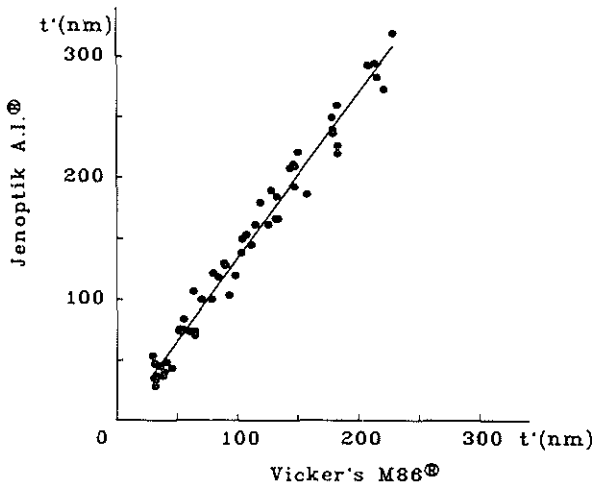

Fig. 2. The relationship between section thickness (t') estimates between the Jenoptik Amplival Interphako® interference microscope (Jenoptik A.I.®) (y-axis) and with the Vicker's M86® scanning micro-interferometer (Vicker's M86®) (x-axis). The scale is in nm. The regression line is $y = -2.39 + 1.365x$ (significant regression, $P2 < 10^{-4}$); the variation in the data explained by the regression (R^2) is 97·71%. The intercept of $-2·39$ (95% confidence limits: -9.15, 4·38) is not significantly different from zero ($P2 = 0·48$); the slope of 1·365 (95% confidence limits: 1·30, 1·43) is significantly different from 1 ($P2 < 10^{-4}$).

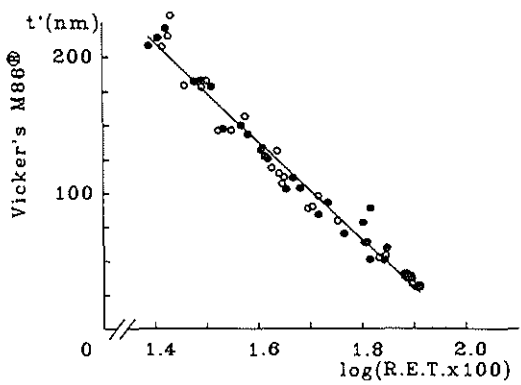

Fig. 3. Representation of the data of two standard test lines (closed and open circles, respectively) for the electron scattering technique with M86 measurements as 'standards'. Conditions of the electron microscope: 40 kV; multimeter setting on the support-film: 30·0 mV. The Relative number of Electrons Transmitted by the section (log R.E.T. values, x-axis) and the section thickness (t') estimates with the Vicker's M86® (in nm, y-axis) are shown. The calculated linear regression curve is: $y = 713.83 - 359·77x$ (significant regression, $P2 < 10^{-4}$); the variation in the data explained by the regression (R^2) is 96.81%.

40 kV and a multimeter setting on the support-film of 30·0 mV. A linear regression curve was calculated: $y = 700·08 - 350·98x$. The variation in the data explained by the regression (R^2) was 97·32%. The regression curve for a second standard test line using a second set (series IV) of ultrathin sections within the same range of thickness was calculated: $y = 717·68 - 362·21x$; $R^2 = 97·18\%$ (Fig. 3, open circles). When comparing the regression lines of these two curves (Hald, 1952) to test their reproducibility, the regression lines were not found to differ significantly ($P2 = 0·92$). In Fig. 3, the data of the sections used for both test lines are taken together in

one graph. The linear regression for this graph is: $y = 713{\cdot}83 - 359{\cdot}77x$ (significant regression, $P2 < 10^{-4}$); $R^2 = 96{\cdot}81\%$. This latter standard test line will be used as a reference line for the estimation of section thicknesses in future stereological studies.

After this method was shown to be reproducible, standard test lines were prepared in the same way with the same sections of series III and IV for different conditions of the electron microscope: 40, 60, 80 and 100 kV, respectively, with varying MM settings over the support-film, i.e. 10·0, 20·0 or 30 mV (Fig. 4). At a constant MM setting over the support-film of 10·0 mV, of 20·0 mV, as well as of 30 mV, the results show different regression equations ($P < 10^{-4}$) for the different accelerating voltages used. In addition, the results show that, at a

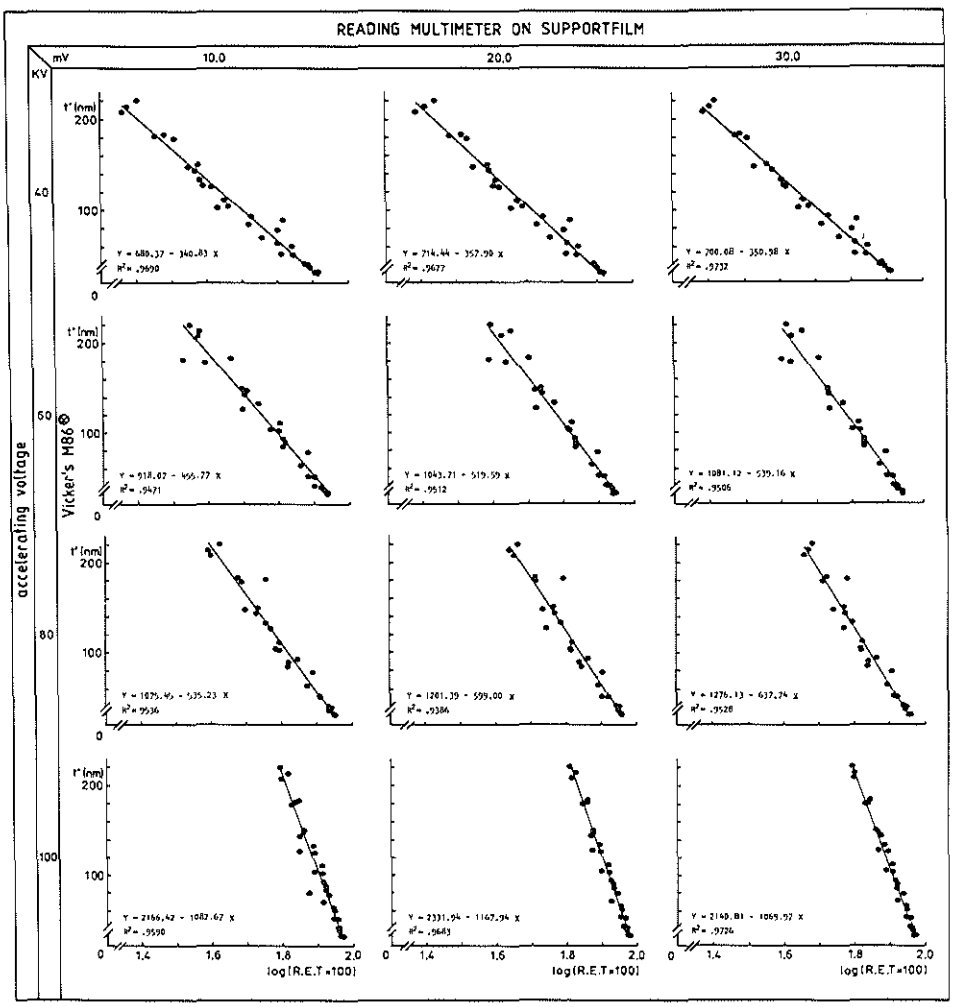

Fig. 4. Standard test lines for the electron scattering technique (log R.E.T. values, *x*-axis) with M86 measurements used as 'standards' (*y*-axis) for different conditions of the electron microscope: 40, 60, 80 and 100 kV, respectively, with varying multimeter settings over the support film, i.e. 10.0, 20.0 or 30 mV. A 500 μm condenser aperture and a 30 μm objective aperture are used; the magnification on the main screen is 37.500. For each test line, the calculated linear regression curve and the variation explained by the regression (R^2) is given in the figure.

constant accelerating voltage of 80 kV ($P = 0{\cdot}00061$) as well as of 60 kV ($P = 0{\cdot}00023$) the different MM settings over the support film result in different regression equations; at 100 kV and at 40 kV the regression equations do not differ significantly ($P = 0{\cdot}16$ and $P = 0{\cdot}31$, respectively). Since the measurements of all the kV/mV combinations were carried out in the same sections, a one-way repeated-measures ANOVA, followed by paired *t*-tests, was applied to the results of each accelerating voltage used. The results of this analysis, shown in Table 3, indicate that a change in MM setting over the support-film indeed contributes to a significant change in log (R.E.T. × 100) values.

In Fig. 5 the relationship between sections thickness estimates with the small-fold tech-

Table 3. Result of a one-way repeated-measures ANOVA, followed by paired *t* tests, for the log (R.E.T. × 100) values for different accelerating voltages (* = significant difference, $P < 0{\cdot}05$).

One-way repeated-measures ANOVA

Accelerating voltage (kV)	*P* values for differences between 30·0, 20·0 and 10.0 mV
100	0·0036*
80	$<10^{-4}$*
60	$<10^{-4}$*
40	$<10^{-4}$*

Paired t *tests*

Accelerating voltage (kV)	P2 values for differences between 30·0 and 20·0 mV	30·0 and 10·0 mV	20·0 and 10·0 mV
100	0·0027*	0·33	0·0082*
80	0·0010*	$<10^{-4}$*	10^{-4}*
60	0·013*	$<10^{-4}$*	10^{-4}*
40	$<10^{-4}$*	0·0012*	10^{-4}*

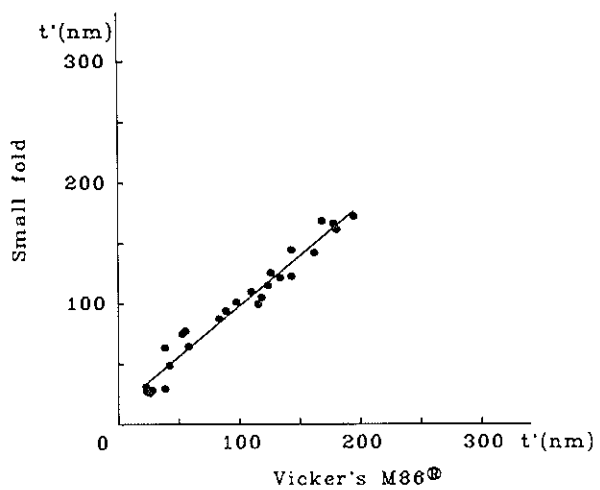

Fig. 5. The relationship between section thickness (*t'*) estimates with the small-fold technique (*y*-axis) and with the Vicker's M86® (*x*-axis). The scale is in nm. The regression line is $y = 14.36 + 0.836x$ (significant regression, $P2 < 10^{-4}$); the variation in the data explained by the regression (R^2) is 96.00%. The intercept of 14.36 (95% confidence limits: 6.28, 22.44) is significantly different from zero ($P2 = 0.0012$); the slope of 0.836 (95% confidence limits: 0.764, 0.908) is significantly different from 1 ($P2 < 10^{-4}$).

nique (see under: series I, Materials and Methods: General) and M86 values of the same sections is shown. The linear regression, curve was calculated: $y = 14{\cdot}36 + 0{\cdot}836x$ (significant regression, $P2 < 10^{-4}$). The variation in the data explained by the regression (R^2) was 96·00%. The intercept of 14·36 (95% confidence limits: 6·28, 22·44) was significantly different from zero ($P2 = 0{\cdot}0012$); the slope of 0·836 (95% confidence limits; 0·764, 0·908) was significantly different from 1 ($P2 < 10^{-4}$). Comparison of the results obtained with both techniques showed that the results did not differ significantly (paired t test: $P2 = 0{\cdot}49$).

The electron scattering in these later sections was measured at 100 kV and a MM setting of 30·0 mV on the support-film. The relationship between the section thickness, determined by the small-fold technique and the results of electron scattering of the same sections is shown in Fig. 6. The corresponding linear regression curve: $y = 570{\cdot}10 - 281{\cdot}42x$ (significant regression, $P2 < 10^{-4}$); $R^2 = 96{\cdot}96\%$, was compared according to Hald (1952) with the test line curve in Fig. 3 100 kV, 30·0 mV (linear regression: $y = 713{\cdot}83 - 359{\cdot}77x$; $R^2 = 96{\cdot}81\%$) in which the log R.E.T. values are plotted against M86 values of the same sections. This comparison showed

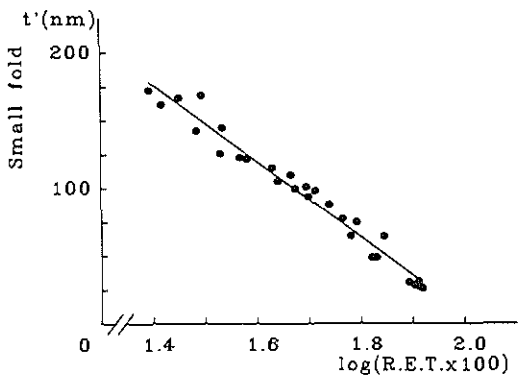

Fig. 6. The relationship between the section thickness (t') determined by the small-fold technique (y-axis) and the results of electron scattering (log R.E.T. values; x-axis) of the same sections. The regression line is $y = 570.10 - 281.42x$ (significant regression, $P2 < 10^{-4}$). The variation in the data explained by the regression (R^2) is 96.96%.

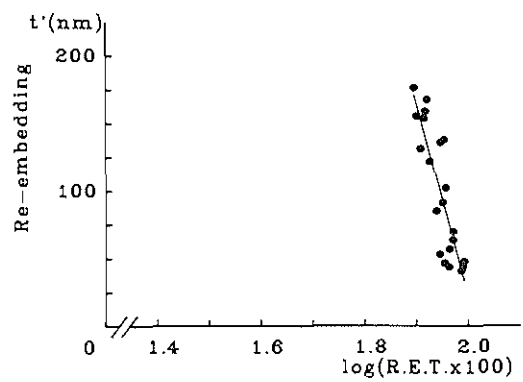

Fig. 7. The relationship between the section thickness (t') of re-embedded sections (y-axis) and the results of their electron scattering (log R.E.T. values; x-axis). The regression line is $y = 2838.0 - 1408.20x$ (significant regression, $P2 < 10^{-4}$); the variation in the data explained by the regression (R^2) is 73.51%.

that neither the regression coefficients (P2 = 0·35) nor the regression lines (P2 = 0·33) differed significantly.

Figure 7 shows the relationship between the section thickness of re-embedded sections and the results of their log R.E.T. values (at 100 kV, 30 mV). The calculated linear regression curve was: $y = 2838{\cdot}0 - 1408{\cdot}2x$ (significant regression, $P2 < 10^{-4}$). The variation in the data explained by the regression (R^2) was 73·51%. Comparison of this line with the standard test line of Fig. 4: 100 kV, 30·0 mV ($y = 2140{\cdot}81 - 1069{\cdot}97x$; $R^2 = 97{\cdot}26\%$) (Hald, 1952) did not show significant differences in the regression coefficients (P2 = 0·70), nor in the regression lines (P2 = 0·13).

DISCUSSION

Interferometry is a technique that has been used extensively in the past to measure the thickness of ultrathin sections (see the Appendix). It is a well-known non-destructive technique and several instruments are commercially available. Accurate measurements of section thickness can be made with the Vicker's Instruments M86® scanning micro-interferometer (M86). According to the user's manual (see: references) a reproducibility of 0·001 nm wavelength can be obtained. With respect to section thickness measurements the error is less than 1%, even in the range of 40–100 nm (Williams, 1977a). In accordance with these data the results can very well be used as 'standards' when preparing standard test lines for the electron scattering (ES) technique (Fig. 4).

The ES method has several advantages. Once standard test lines for different settings of the electron microscope are available, this method is very quick. In contrast to interferometry the thickness of a section can be directly measured in the electron microscope and no additional (expensive) equipment is required. The scattering contrast depends on the accelerating voltage used and the objective aperture size delimited by the aperture at the specimen (Misell & Burdett, 1977). The latter, i.e. the objective aperture size, was kept at constant size in the present study. Edie & Karlsson (1972a) showed that the accelerating voltage, used for the electron microscopical operation, determines the slope of the ES test line curve. Our results (Fig. 4 and Table 3) show that the slope of the ES test line curve is affected by both a change in accelerating voltage and by a change in initial multimeter current setting. As far as the setting of the electron microscope is concerned, there is no reason to prefer a particular setting, as long as the setting is known; although the highest R^2 value is obtained at 100 kV and 30·0 mV and the lowest R^2 value at 80 kV and 20·0 mV, the variation between these two values does not differ significantly. In this context it should be noted that in our experience intermittant changes in accelerating voltage of multimeter current setting, i.e. an increase or a decrease, do not influence the final slope of the ES test line curve, found for a particular setting of the microscope. In this repect, no signs of hysteresis were found. The ES method proved to be very reproducible (Fig. 3) provided care was taken with the following: a first prerequisite for the ES method is that the time during which the section is present in the electron beam before thickness measurements are carried out is kept more or less constant. This is necessasry to avoid variations in thickness due to physical processes in the specimen (e.g. contamination and loss of material) when exposed to an electron beam. As was shown by Edie & Karlsson (1972a), such time effects are last pronounced at low magnification. A second prerequisite for the method is that the thickness measurements are carried out in 'empty resin' areas. This may be in conflict with the choice of a low magnification. Obviously the scattering of electrons is influenced by the presence of tissue in the section. This implies that e.g. the lumen of a blood vessel has to serve as an empty resin area if no extra empty resin has been included in the section as was done in the present investigation. In such a case it may be necessary to work at higher magnification to avoid interference of tissue in the section with electron scattering. Our measurements with the M86 in empty Epon resin versus tissue containing resin (Table 1) show that for sections in the range of 30–90 nm no significant differences between empty resin areas and tissue-containing resin areas are found, at least not for hippocampal E-PTA tissue. However, above 90 nm the

thickness in tissue-containing areas is slightly larger (approximately 2%). This finding should be taken into account when measuring the thickness of sections larger than 100 nm with the ES method.

An interesting finding is that for the preparation of ES standard test lines, small-fold measurements can also be used as standards (Fig. 6). Small-fold measurements appear to be in good agreement with M86 measurements of the same sections (Fig. 5). Small (1968) also found that his method gave the same results as interferometric measurements. Apparently the method is reliable. Unfortunately, folds have to be present in the sections to carry out the measurements. This is obviously a disadvantage when measuring the thickness of serial sections for stereology and/or reconstruction work. Moreover, it is quite laborious to measure the width of folds in many sections. Ideally, measuring a fold may take approximately 30 s. However, one should realize that, even in this relatively short time, changes in the width of the folds may occur due to e.g. drift of the specimen, to contamination and to loss of material. Hence, it is preferable to take photographs of the folds and to measure their width on prints; a procedure which unfortunately is rather time-consuming. Nevertheless, for the preparation of ES standard test lines the small-fold technique provides a simple, cheap and reliable method for those investigators not having access to interferometry and who do need to prepare these ES test lines.

The re-embedding technique is a more laborious and (with an $R^2 = 72{\cdot}96\%$) a slightly less reliable technique (Fig. 7). It is clear that in this re-sectioning/re-embedding technique contamination and sublimation effects as well as shrinkage and compression during embedding and sectioning contribute twice to variations in section thickness (Luther *et al.*, 1987; see also: footnote at the end of the Discussion). In view of the amount of work involved and the resulting variability of the final section thickness the re-embedding technique is not the preferred technique for preparing ES standard test lines.

The constant difference, i.e. a factor 1·36, in thickness found between measurements with the M86 and the Jenoptik A.I. apparently is a systematic error, inherent to one of these two interference techniques. It was found that measurements with the Jenoptik A.I. were liable to error. It turned out that different operators judged the brightness of the colour of the splitted image differently, even though the half-shade plate was introduced into the microscope, which increases the accuracy of the measurements. It should be kept in mind that, when a change is made from the colour of the one image to that of the other the sensitivity of such a visual selection is influenced by the colour of the background. To overcome this optical illusion there is a tendency to set the phase compensator too high or too low and hence the image-matching of objects being measured tends to introduce systematic errors (Pluta, 1971). Subjectivity of the operator implies that the Jenoptik A.I. should not be used e.g. to prepare ES standard test lines unless, as in this case, the systematic error is known from comparison with other techniques.

The average thicknesses found in the present study for sections of a particular interference colour appear to be in good agreement with the thicknesses and colours in the 'continuous interference colour and thickness scale for thin sections' (Reid, 1975). The latter scale is based on measurements made by Peachy (1958). In that paper Peachy (1958) demonstrated that interference colour depends on viewing angle.

The variation in thickness t' found between sections of a particular interference colour (Table 1) is of the same order of magnitude as that previously found for methacrylate sections (Vrensen, 1970), although it is known that methacrylate is more susceptible to compression, etc., than Epon mixtures. In addition, the inter-section variation, i.e. the variation in section thickness between sections of a particular interference colour, appears to be larger than the intrasection variation, i.e. the variation within a section (Table 2). From this finding it was concluded that for serial sections a better estimate of the mean section thickness t' is obtained when e.g. each section is measured just once, rather than making a number of measurements in a selected sample of sections. Although the intra-section variation found in the present study may not exceed the considerable intra-section variation mentioned by e.g. Silverman *et al.* (1969) for Epon–araldite sections, the results show that, when quantifying e.g. the results of a

cytochemical staining or autoradiography, it is always advisable to estimate the section thickness as close as possible to the area of interest (Williams & Meek, 1966).

The statement, mentioned in the introduction that one cannot rely on the advance setting of the ultramicrotome to estimate the section thickness t' is underlined by our own findings. The sections with interference colour green/yellow (Table 1) were obtained by increasing the advance speed of the ultramicrotome with 0·5 μm read on the micrometer setting of the ultramicrotome. The results of t' measured with the different techniques show that the thickness as measured is not even 50%* of the thickness, as indicated. Hereby, 'compression' was checked and was found to be negligible.

The ES method proved to be reliable, especially for stereology and reconstruction of e.g. complex synapses. The method is, for reasons of costs, labour, time and 'non-destructiveness',† superior to any of the other techniques described, including the small-fold method previously used in our studies.

ACKNOWLEDGMENTS

The measurements with the Vicker's Instruments M86® scanning micro-interferometer were carried out at Vicker's Instruments in Yorkshire, U.K. The author is very grateful to the directory of Vicker's company for their hospitality. In particular Mr C. Perrott B.Sc., M.Inst.M. (Vicker's Instruments, Yorkshire, U.K.) is acknowledged for organizing this visit and the skillful assistance of Mr J. M. Smith (Vicker's Instruments, Yorkshire, U.K.) is much appreciated. Dr A. Weeda (AKZO-Research Institute, Arnhem, The Netherlands) introduced us to their Jenoptik Amplival Interphako® interference microscope. The author wants to thank him for his hospitality and helpful discussions. Mrs S. Gravenstein-Koster is acknowledged for her assistance in the laborious re-embedding technique. For his technical assistance and in particular for the preparation of the drawings the author is grateful to Mr E. P. B. Bierman. Mrs M. Saris-Wijnans evaluated the results statistically. Photography was carried out by Mr M. Boermans and Mr M. van Boven. Dr O. L. Wolthuis and Prof. Dr J. Voogd (Erasmus University of Rotterdam, The Netherlands) are gratefully acknowledged for critical reading of the manuscript. The author would like to thank the editors of the Journal, as well as the referees for their valuable suggestions.

*With the most reliable method, i.e. with the Vicker's Instruments M86® scanning micro interferometer, the section thickness t' was measured to be 215·64 nm (3·26 nm) $\bar{x}$ (SEM).

†'Non-destructive' in the sense that, after section thickness measurements, the sections can still be used for ultrastructural studies. Of course, electron bombardment will introduce mass loss, leading to changes in section thickness (see e.g. Luther *et al.*, 1987). In the present study this effect was not assessed since only non-irradiated areas were investigated. However, the importance of distinguishing between irradiated and non-irradiated areas in the section should be borne in mind.

APPENDIX

Method	References
Shadowing sections at a known angle	Porter & Blum (1953); Sjöstrand (1953, 1967); Williams & Meek (1966)
Embedded standard objects	Lenz (1954); Hall (1955); Huxley (1957); Silvester & Burge (1959); Burge & Silvester (1959); Zeitler & Bahr (1962); Bahr & Zeitler (1965); Chandler (1976); Cosslett (1967); Silverman *et al.* (1967, 1969); Casley-Smith (1967, 1972); Spurr (1974); Casley-Smith & Crocker (1975); Halloran *et al.* (1978)
Interferometry/microdensitometry	Deeley (1955); Cosslett (1960a, b); Zelander & Ekholm (1960; Williams & Meek (1966); Bachman & Salpeter (1967); Small (1968); Silverman *et al.* (1969); Vrensen (1970); Gillis & Wibo (1971); Casley-Smith (1972); Edie & Karlsson (1972a); Yang & Shea (1975); Williams (1977a); Robertson *et al.* (1984)
Interference colours	Peachy (1958); Bachman & Sitte (1958); Zelander & Ekholm (1960); Walter (1961)
Re-sectioned sections	Mota (1960); Philips & Shortt (1964); Moretz *et al.* (1968); Beertsen *et al.* (1975); Yang & Shea (1975); Yang & Morrison (1977); Ohno (1980); Jesior (1982); Berriman *et al.* (1984); Frösch & Westphal (1985)
Electron scattering/current and exposure densities/photometry	Hall & Inoue (1957); Zeitler & Bahr (1962); Blümcke *et al.* (1966); Casley-Smith (1967); Misell & Burdett (1977); Weybull (1970, 1972); Casley-Smith (1972); Edie & Karlsson (1972a, b, 1977); Beertsen *et al.* (1975); Casley-Smith & Crocker (1975); Berriman *et al.* (1984)
Autoradiography with labelled resin	Williams & Meek (1966); Vrensen (1970); Williams (1977b)
Minimal folds in sections	Small (1968); Blouin *et al.* (1977); Mori & Christensen (1980)
High-angle tilting stage assessment	Willis (1971)
Microtome setting	Williams (1972); Mori & Christensen (1980); Ohno (1980)

Advantages and limitations
The results along a given edge may vary too much; if the edge is not clear, the shadow is not sharp enough to obtain an accurate measure.
The standard objects should have a mass-thickness resembling that of the embedding resin and should be embedded close to the area of interest. Hence, thickness meaurements can be made close by and errors due to intrasectional thickness variations are avoided. The magnification used depends on the chosen standard. Standards like polystyrene latex spheres proved to be reliable standards; they are relatively insensitive to sublimation and easy to measure. Obviously, such a method is restricted to special cases and is not suitable for routine thickness determination.
Interferometric measurements can be accurate but require special equipment. Different types of instruments are commercially available which are well established and easy to handle. The accuracy of the method depends very much on the type of instrument used and on the type of tissue to be studied. The accuracy may decrease considerably when tissue is embedded in the section. Because of poor resolution it can be hard to distinguish between areas of tissue and areas containing empty re- n and thickness differences between such areas will go unrecognized; this may introduce errors in the final estimate of the section thickness. Incident light interferometers are useful for measuring the thickness of ultrathin sections mounted on glass slides. Sections, mounted on grids, have to be measured in transmitted light using an interference microscope. Hence, the measurement of section thickness and the electron microscopical examination can be carried out on the same section. An additional measurement that has to be done is the determination of the refractive index of the embedding resin which is an essential parameter in interference techniques.
The range of thickness that each colour represents is quite large. Moreover, the interference colour depends on the angle at which the section is viewed. Hence, an estimation of section thickness based on interference colour is not very reliable but it is a good help for a 'first check' during microtome cutting.
The method is laborious and artefacts may be introduced in the re-embedded section due to compression during cutting and sublimation by the electron beam. On the other hand, *in situ* determinations of surface distortions can easily be made.
These methods can be applied directly in the electron microscope or to plates. The optical density of the background (a limiting factor) as well as sublimation problems should be taken into consideration.
Within a limited range of section thicknesses, this method is very reliable. However, it is very laborious and not suitable for routine application.
The measurements are restricted to minimal folds, present in the section. Just a few folds lead to unreliable estimates of section thickness; many folds hamper the acquisition of ultrastructural information. It is a tedious task to measure the thickness of all sections to be used in a quantitative study.
Necessitates the electron microscope to be utilized with special equipment.
The actual thickness of the sections cut with an ultramicrotome depends on the properties of the type of microtome and on those of the block and knive to be used and may deviate from the pre-set thickness to a large extent.

REFERENCES

Bachman, L. & Salpeter, M.M. (1967) Absolute sensitivity of electron microscope autoradiography. *J. Cell Biol.* **33**, 299–305.

Bachman, L. & Sitte, P. (1958) Dickenbestimmung nach Tolansky an Ultradunnschnitten. *Mikroskopie*, **13**, 289–304.

Bahr, G.F. & Zeitler, E. (1965) The determination of the dry mass in populations of isolated particles. *Lab. Invest.* **14**, 955–977.

Beertsen, W., Everts, V. & Houtkooper, J.M. (1975) Frequency of occurrence and position of cilia in fibroblasts of the periodontal ligament of the mouse incisor. *Cell Tissue Res.* **163**, 415–431.

Berriman, J., Bryan, R.K., Freeman, R. & Leonard, K.R. (1984) Methods for specimen thickness determination in electron microscopy. *Ultramicroscopy*, **13**, 351–364.

Beyer, H. (1973) *Handbuch der Mikroskopie*, pp. 174–193. VEB Verlag Technik, Berlin.

Blouin, A., Bolender, R.P. & Weibel, E.R. (1977) Distribution of organelles and membranes between hepatocytes and nonhepatocytes in the rat liver parenchyma. *J. Cell Biol.* **72**, 441–455.

Blümcke, S., Morgenroth, K., Jr. & Backmann, R. (1966) Die Schnittdickenbestimmung mit dem 'Stereoscan'. Messungen an 'semidünnen' Schnitten und ihre Bedeutung für die lichtmikroskopische Autoradioghraphie. *Mikroskopie*, **21**, 263–268.

Burge, R.E. & Silvester, N.R. (1959) The measurement of mass thickness and density in the electron microscope. *J. Biophys. Biochem. Cytol.* **8**, 1–11.

Casley-Smith, J.R. (1967) Quantitative electron microscopy: methods for dry mass determination, avoiding errors introduced by irradiation changes and contaminating films. *J. Ultrastruct. Res.* **18**, 600–604.

Casley-Smith, J.R. (1972) A method for quantifying electron staining, obtaining the dry specific gravity of specimens in sections, and measuring section thickness. *J. Microsc.* **96**, 363–365.

Casley-Smith, J.R. & Crocker, K.W.J. (1975) Estimation of section thickness, etc. by quantitative electron microscopy. *J. Microsc.* **103**, 351–368.

Chandler, J.A. (1976) A method for preparing absolute standards for quantitative calibration and measurement of section thickness with X-ray microanalysis of biological ultrathin specimens in EMMA. *J. Microsc.* **106**, 291–302.

Cosslett, A. (1960a) Some applications of the ultraviolet and interference microscopes in electron microscopy. *J. Roy. Microsc. Soc.* **79**, 263–271.

Cosslett, A. (1960b) The effect of the electron beam, on thin sections. *Proc. Second Eur. Reg. Conf. Electron Microscopy*, Delft, **2**, 678.

Cosslett, A. (1967) Letter to the Editor. *J. Roy. Microsc. Soc.* **86**, 315–316.

Cruz-Orive, L.M. (1980) On the estimation of particle number. *J. Microsc.* **120**, 15–27.

Cruz-Orive, L.M. (1984) *Estimation of Nv from serial slabs*. Internal Report Nr. 111/LC 17. [Will be included as an appendix to D. M. G. De Groot, Improvements of the serial section method in relation to the estimation of the numerical density of complex-shaped synapses. In: *Stereology in Electron Microscopy. An Illustration of Problems and Solutions* (ed. by A. Reith and T. M. Mayhew). Hemisphere/McGraw-Hill, New York (in press).]

Cruz-Orive, L.M. (1985) Estimating particle number and size. In: *Quantitative Neuroanatomy in Transmitter Research* (ed. by L. F. Agnati and K. Fuxe), pp. 11–24. MacMillan Press, London.

Deeley, E.M. (1955) An integrating microdensitometer for biological cells. *J. Sci. Instrum.* **32**, 263–267.

De Groot, D.M.G. (1984) *Improvements of the serial section method in relation to the estimation of the numerical density of complex-shaped synapses*. MBL/TNO Internal Report Nr. DG/84-1. [Included in: *Stereology in Electron Microscopy. An Illustration of Problems and Solutions* (ed. by A. Reith and T. M. Mayhew). Hemisphere/McGraw-Hill, New York (in press).]

De Groot, D.M.G. (1985) Disc-like and complex-shaped synapses: Number, size and dense projections. A critical note. In: *Proceedings of the IV European Symposium on Stereology*, Göteborg, 26–30 August. *Acta Stereol.* **4**, 147–151.

De Groot, D.M.G. & Bierman, E.P.B. (1983) The complex-shaped 'perforated' synapse, a problem in quantitative stereology of the brain. *J. Microsc.* **131**, 355–360.

De Groot, D.M.G. & Bierman, E.P.B. (1986) A critical evaluation of methods for estimating the numerical density of synapses. *J. Neurosci. Methods*, **18**, 79–101.

De Groot, D.M.G. & Bierman, E.P.B. (1988) Numerical changes in rat hippocampal synapses. An effect of 'ageing'? In: *Proceedings of the VII International Congress on Stereology*, Caen, 2–9 September. *Acta Stereol.*, **6/III**, 53–58.

Edie, J.W. & Karlsson, U.L. (1972a) A routine method for object thickness determination in the transmission electron microscope. *J. Microsc.* **13**, 13–30.

Edie, J.W. & Karlsson, U.L. (1972b) Thickness and mass thickness measurements within biological specimens. In: *Proc. Seventh National Conference on Electron Probe Analysis*, San Francisco, CA, 17–21 July 1972, pp. 43A–43D.

Edie, J.W. & Karlsson, U.L. (1977) Contrast and quantitation in uniform regions of thin sections using transmission electron microscopy. *J. Microsc.* **111**, 179–191.

Frösch, D. & Westphal, C. (1985) Choosing the appropriate section thickness in the melamine embedding technique. *J. Microsc.* **137**, 177–183.
Gillis, J.M. & Wibo, M. (1971) Accurate measurement of the thickness of ultrathin sections by interference microscopy. *J. Cell Biol.* **49**, 947–949.
Gundersen, H.J.G., Andersen, B.S. & Floe, H. (1983) Estimation of section thickness unbiased by cutting-deformation. *J. Microsc.* **131**, RP3–RP4.
Hald, A. (1952) *Statistical Theory with Engineering Applications*, pp. 401–406. Wiley, London.
Hall, C.E. (1955) Electron densitometry of stained virus particles. *J. Biophys. Biochem. Cytol.* **1**, 1–12.
Hall, C.E. & Inoue, T. (1957) Experimental study of electron scattering in electron microscope specimens. *J. Appl. Phys.* **28**, 1346–1348.
Halloran, B.P., Kirk, R.G. & Spurr, A.R. (1978) Quantitative electron probe microanalysis of biological thin sections: the use of stem for measurement of local thickness. *Ultramicroscopy,*, **3**, 175–184.
Huxley, H.E. (1957) The double array of filaments in cross-striated muscle. *J. Biophys. Biochem. Cytol.* **3**, 631–647.
Jesior, J.C. (1982) The grid sectioning technique: a study of catalase platelets. *EMBO J.* **1**, 1423–1428.
Lenz, F. (1954) Zur Streuung mittelschneller Elektronen in kleinste Winkel. *Z. Naturforsch.* **9a**, 185–204.
Luther, P.K., Lawrence, M.C. & Growther, R.A. (1987) Use of gold particles for monitoring section shrinkage. *Proceedings RMS*, **22**/5, 261.
Misell, D.L. & Burdett, I.D.J. (1977) Determination of the mass thickness of biological sections from electron micrographs. *J. Microsc.* **109**, 171–182.
Moretz, R.C., Johnson, H.M. & Parsons, D.F. (1968) Thickness estimation of carbon films by electron microscopy of transverse sections and optical density measurements. *J. Appl. Phys.* **39**, 5421–5424.
Mori, H. & Christensen, K. (1980) Morphometric analysis of Leydig cells in the normal rat testis. *J. Cell Biol.* **84**, 340–354.
Mota, M. (1960) Sectioning of sections for determination of thickness in electron microscopy. *Melhoramento*, **13**, 127–134.
Ohno, S. (1980) Morphometry for determination of size distribution of peroxisomes in thick sections by high voltage electron microscopy. I. Studies on section thickness. *J. Electron Microsc.* **29**, 230–235.
Peachy, L.D. (1958) Thin sections. I. A study of section thickness and physical distorsion produced during microtomy. *J. Biophys. Biochem. Cytol.* **4**, 233–242.
Peters, A. (1970) The fixation of cerebral nervous tissue and the analysis of electron micrographs of the neuropil, with special references to the cerebral cortex. In: *Contemporary Research Methods in Neuroanatomy* (ed. by W. J. H. Nauta and S. O. E. Ebbeson), pp. 56–76. Springer, Berlin.
Philips, R. & Shortt, T. (1964) The 're-sectioned section' technique and its application to studies of the topography and thickness of thin sections. *J. Microsc.* **82**, 263–271.
Pluta, M. (1971) On the accuracy of micro-interferometric measurements of optical-path differences by means of the half-shade method. *J. Microsc.* **93**, 83–100.
Porter, K.R. & Blum, J. (1953) A study in microtomy for electron microscopy. *J. Anat. Rec.* **117**, 685–710.
Reid, N. (1975) Ultramicrotomy. In: *Practical Methods in Electron Microscopy* (ed. by A. M. Glauert), table 6.1. North-Holland Publishing Company, Amsterdam.
Robertson, W.M., Storey, B. & Griffiths, B.S. (1984) An interference technique for measuring the thickness of semi-thin and thick sections. *J. Microsc.* **133**, 121–124.
Silverman, L., Frommhagen, L.H. & Glick, D. (1967) Measurements of influenza virus-antibody reaction by quantitative electron microscopy. *J. Cell Biol.* **35**, 61–67.
Silverman, L., Schreiner, B. & Glick, D. (1969) Measurement of thickness within sections by quantitative electron microscopy. *J. Cell Biol.* **40**, 768–772.
Silvester, N.R. & Burge, R.E. (1959) Quantitative estimation of the uptake of two new electron stains by the cytoplasmic membrane of ram-sperm. *J. Biophys. Biochem. Cytol.* **6**, 179–188.
Sjöstrand, F.S. (1953) A new microtome for ultrathin sectioning for high resolution electron microscopy. *Experientia*, **9**, 114–115.
Sjöstrand, F.S. (1967) *Electron Microscopy of Cells and Tissues*, p. 281. Academic Press, New York.
Small, J.V. (1968) Measurement of section thickness. In: *Abstracts Fourth European Regional Conference on Electron Microscopy*, Rome, **1**, 609–610.
Spurr, A.R. (1974) Macrocyclic polyether complexes with alkali elements in epoxy resin as standards for X-rays analysis of biological tissues. In: *Microprobe Analysis as Applied to Cells and Tissues* (ed. by T. Hall, P. Ecklin and R. Kaufmann), p. 213. Academic Press, London.
Sterio, D.C. (1984) Estimating number, mean sizes and variations in size of particles in 3-D specimens using disectors. *J. Microsc.* **134**, 127–136.
Vicker's. M85/M86 scanning microdensitometer and scanning micro-interferometer: instructions for use. Instruments with serial numbers M850069 and proceeding. Part 5, p. 83.
Vrensen, G.F.J.M. (1970) Some new aspects of efficiency of electron microscopic autoradiography with tritium. *J. Histochem. Cytochem.* **18**, 278–290.
Walter, F. (1961) Ultramikrotomie. I. Das Ultramikrotom nach Fernandez-Moran. *Leitz. Mitt, Wiss. Tech.* **1**, 236–243.

Weybull, C. (1970) *Estimation of the thickness of thin sections prepared for electron microscopy*. Philips Analytical Equipment, EM45.

Weybull, C. (1972) Estimation of the thickness of films used in electron microscopy. *Z. Allg. Mikrobiol.* **12**, 487–490.

Williams, M.A. (1972) Autoradiography. In: *Principles and Techniques of Electron Microscopy. Biological Applications*, Vol. 2 (ed. by M. A. Hayat), p. 243. Van Nostrand Reinhold Company, New York.

Williams, M.A. (1977a) Quantitative Methods in Biology. In: *Practical Methods in Electron Microscopy*, Vol. 6 (ed. by A. M. Glauert), pp. 13–17. Elsevier North-Holland Biomedical Press, Amsterdam.

Williams, M.A. (1977b) Quantitative methods in biology. In: *Practical Methods in Electron Microscopy*, vol. 6 (ed. by A. M. Glauert), pp. 151–157. Elsevier North-Holland Biomedical Press, Amsterdam.

Williams, M.A. (1981) Sections of determined thickness for use in stereological estimations on cells. *Stereol. Jugosl.* **3**, suppl. 1, 369–374.

Williams, M.A. & Meek, G.A. (1966) Studies on thickness variation in ultrathin sections for electron microscopy. *J. Roy, Microsc. Soc.* **85**, 337–352.

Willis, R.A. (1971) *In situ* measurement of EM section thickness by use of a high angle tilting stage. *J. Anat.* **109**, 345.

Yang, G.C.H. & Morrison, A.B. (1977) The application of wide-field electron microscopy. Anwendungen der Groszfeld-Elektronenmikroskopie. *Microscopica Acta*, **79**, 277–279.

Yang, G.C.H. & Shea, S.M. (1975) The precise measurement of the thickness of ultrathin sections by a 'resectioned section' technique. *J. Microsc.* **103**, 385–392.

Zeitler, E. & Bahr, G.F. (1962) A photometric procedure for weight determination of microscopic particles. Quantitative electron microscopy. *J. Appl. Phys.* **33**, 847–853.

Zelander, T. & Ekholm, R. (1960) Determination of the thickness of electron microscopy section. *J. Ultrastruct. Res.* **4**, 413–419.

PART II

Chapter 4

A CRITICAL EVALUATION OF METHODS FOR ESTIMATING THE NUMERICAL DENSITY OF SYNAPSES

Journal of Neuroscience Methods, 18 (1986) 79–101
Elsevier

NSM 00636

A critical evaluation of methods for estimating the numerical density of synapses

Didima M.G. de Groot and Egbertus P.B. Bierman

Medical Biological Laboratory TNO, Rijswijk (The Netherlands)

(Received 27 February 1986)
(Revised 11 July 1986)
(Accepted 23 July 1986)

Key words: Numerical density – (Complex) perforated and (simple) non-perforated synapses – Discrete unfolding technique – Serial section technique – Disector technique – Fractionator technique – Selector technique

Several methods for estimating the numerical density (N_V) of particles are described. The usefulness and the limitations of different methods with respect to the estimation of synaptic densities are discussed. These methods are: (1) the discrete unfolding technique, (2) the serial section technique and (3) the disector technique.

From the results it is concluded that it is not advisable to use an unfolding technique to estimate the number and size of synapses since all sorts of assumptions regarding the shape, truncation and overprojection are hazardous.

Consistently lower values for N_V were obtained with the disector technique compared with the results of the serial section technique. This difference, obtained with two unbiased techniques, is discussed. The main conclusion with respect to this point is that both techniques can be used to estimate synaptic densities, provided a reliable estimate of the section thickness is obtained and an appropriate sampling procedure is used.

Introduction

At present several stereological methods are available for estimating particle numbers in a unit volume (N_V). This paper is mainly concerned with the estimation of numbers of synapses and is focussed on the stereological methods used to estimate N_V.

In principle, stereological methods aim to extract information about tissue structures in the three-dimensional space from measurements on two-dimensional (microscopical) sections. The number of synapses in a brain region can be derived from the size of the synapses and their mutual distance. By sectioning for mi-

Correspondence: D.M.G. de Groot, Medical Biological Laboratory TNO, P.O. Box 45, 2280 AA Rijswijk, The Netherlands.

croscopy the synapses will be cut with a probability which is directly related to their size and orientation. A conventional stereological method like the unfolding procedure for deriving N_V requires independent area-weighted random sections (see e.g. Miles and Davy, 1976). This ensures that the probability that a synapse is hit by the section plane is not biased by the location and orientation of the synapses within the brain region. N_V is then calculated from the number of profiles of the transected particles per unit section area (N_A) and a measure describing the size of the particle. On the whole it has been experienced that counting N_A (synapses) is easy, although particularly in EPTA-treated tissue errors can be made when dealing with complex (perforated) synapses (De Groot and Bierman, 1983). In order to obtain an indication of the size, the synapses have usually been treated by applying a 'best fitting' geometric form which was generally accepted to be a disc (West et al., 1972). Such assumptions on the shape of the investigated particle and on its size are inherent to the conventional methods for estimating N_V. In principle, orientation does not play a role whenever area-weighted random sections are used. However, it should be stressed at this point that area-weighted random sections are very hard to obtain and that consequently most investigators assume that the synapses themselves are isotropically oriented. Unfortunately it is never known to what extent such assumptions match reality or are comparable between experimental groups. Another drawback of several conventional methods is the fact that they assume that the random section from which the necessary data for calculating N_V are obtained, basically is a true plane without a thickness (T). Obviously this is not true; even the thickness of an extremely thin section (e.g. 40 nm) can still be quite large in comparison with the size of several ultrastructural features. The effect of non-zero section thickness on the estimation of N_V is called over-projection or Holmes effect (Holmes, 1927).

Another bias may be induced whenever the structures incorporated in the section are not projected onto the observation plane in full extent or whenever the structures cannot be observed completely, i.e. 'truncation' of the theoretically available information. Truncation effects may take place even if $T = 0$. Some conventional formulae for calculating N_V do account for $T > 0$, as well as for truncation effects (see e.g. Cruz-Orive, 1983 and 1985a), but the final bias remains unknown.

More recently, stereological methods have been developed which do not suffer from these disadvantages (Cruz-Orive, 1980, 1984, 1985a; Sterio, 1984; Gundersen, 1986). Despite these advances in stereology which allow unbiased estimations of numerical densities of arbitrarily shaped particles, conventional methods are still widely used for the estimation of synaptic densities. The main reason for this 'preference' is that, apart from the number, many investigators are also interested in a size distribution of the investigated synapses in order to distinguish between different types of synapses. Differences in number and size of synapses most likely reflect a functional change (see e.g. Greenough et al., 1978; Vrensen and Nunez Cardozo, 1981; Fields and Ellisman, 1985). However, it is quite clear nowadays that synapses do not only differ in number and size. In fact, several authors have described synapses that deviate from the assumed disc-shape (Gray, 1959; Peters

and Kaiserman-Abramof, 1969; Akert, 1973; Greenough et al., 1978; Cohen and Siekevitz, 1978; Dyson and Jones, 1980; Vrensen et al., 1980; Müller et al., 1981; Vrensen and Nunez Cardozo, 1981; Verwer and De Groot, 1982; De Groot and Bierman, 1983; De Groot, 1984, 1985). Such synapses may be 'complex-shaped', 'curved' or may have so called 'perforations'. These differences in shape are looked upon as differences in synaptic functioning. It is, therefore, relevant to use an appropriate method to quantify these different types of synapses.

The main objectives of this paper are: (1) to discuss the usefulness, the possibilities and the limitations of both the unfolding technique and the newer (unbiased) methods for estimating numbers of synapses and (2) to show that, with respect to the distinction between different types of synapses a size distribution of synapses, derived by conventional means does not provide satisfactory results since the types and extent of biases are never known.

To illustrate (1) and (2) we used 2 different types of synapses in the stratum lacunosum moleculare of the hippocampal CA_3 area of female adult rats. In principle the numerical density (N_V) of both types of synapses was estimated using the (unbiased) 'serial section' technique of Cruz-Orive (1980, 1984, 1985a; De Groot, 1984). Two other techniques, i.e. the 'disector' technique (Sterio, 1984) and the conventional discrete unfolding technique (see e.g. Abercrombie, 1946; Cruz-Orive, 1983 and 1985a) were also applied to these samples. It should be noted, however, that the sampling technique was not optimal for the two latter techniques.

For the sake of completeness the reasons are given why the 'fractionator' technique (Gundersen, 1986) is not preferred and the 'selector' technique (Cruz-Orive, 1985b) cannot be applied for these estimations of synaptic densities. To enable other investigators to use the methods, the principal steps of the 'serial section', the 'disector' and the 'unfolding' techniques are presented in a 'cookbook' manner with references to the original papers.

Material and Methods

General procedures

Three adult female small Wistar (WAG/Rij) rats, weighing 180–200 g, were used in this study. Under ether anaesthesia they were fixed by transcardial perfusion with glutaraldehyde/paraformaldehyde mixtures according to Peters (1970). After the brain was taken from the skull a transverse slab of approximately 5 mm was taken from the middle of the left hippocampus. Vibratome slices (75 μm thick) were cut from this slab. From each vibratome slice the CA_3 area was sampled, using the dissecting microscope. These samples were treated with ethanolic phosphotungstic acid (EPTA) (Vrensen and De Groot, 1974). Embedding was oriented so that sectioning with the ultramicrotome could be carried out perpendicular to the ventricular surface. Ultrathin serial sections (35 sections/series) including all 4 layers of the hippocampal CA_3 area were cut with a diamond knife and were inspected without additional staining in the transmission electron microscope (Philips 201). The microscope was equipped with a rotation specimen holder and a goniome-

ter attachment enabling orientation of the sections in the microscope and selective photography of the desired areas, respectively. The magnification was calibrated using a grating replica (2160 lines/mm). Each micrograph, containing a specimen area of approximately $50 \times 50\ \mu m^2$, was printed at a final magnification of $6000 \times$. Systematic random sampling was carried out in the desired layer, i.e. stratum lacunosum moleculare, and/or micrograph, thereby aiming at a selection of reference areas for the synapse analysis which was representative for this layer (for details, see De Groot, 1984). All synaptic profiles in the reference areas of the centre section of a series were tracked in the adjacent serial sections. It cannot be established otherwise whether the profiles observed belong to (simple) non-perforated or to (complex) perforated synapses. [A synapse is called 'perforated' when the presynaptic and corresponding postsynaptic membrane thickenings are focally absent (Greenough et al., 1978).] Subsequently, the numerical density of both types of synapses was determined by means of the 'serial section technique' of Cruz-Orive (1980, 1984, 1985a; De Groot, 1984) considering the centre section of a series as the 'reference' section.

For the sake of illustration the 'disector' technique of Sterio (1984) was also applied to the synapses actually sampled for the serial section technique. The centre section of a series was hereby considered as the 'reference plane' of the disector and both adjacent sections as the 'look-up plane', which resulted in two distinct disectors with a common reference plane.

To the (simple) non-perforated synapses a conventional 'unfolding' technique (see e.g. Abercrombie, 1946; Cruz-Orive, 1983, 1985a) was applied. The centre section of the series is treated here as if it had been an independent random section.

The 3 methods applied are summarized in Figs. 1–3 and an extended description follows below.

Procedures for the estimation of synaptic densities (N_V)

(1) The discrete unfolding technique (Fig. 1). As pointed out in the Introduction the conventional methods for deriving N_V require independent area-weighted random sections for collecting the necessary data to estimate N_V. N_V can be calculated from the ratio $N_A/(EH + T)$ (T = constant) (Abercrombie, 1946). For this, (1) the number of identifiable profiles of the transected synapses per unit section area (N_A (synapses)) is counted and (2) the synaptic profile lengths (l(synapses)) in the section area are measured and used to estimate the mean projected height of the synapses (EH(synapses)). With respect to synapses, these methods start from the assumption that synapses are *disc-like* structures (West et al., 1972). Only when identical, isotropic (disc-like) synapses are to be investigated and the section thickness $T = 0$, then El(synapses) = EH(synapses) (see e.g. Hilliard, 1967). In general, however, synapses will differ in size. In that case a frequency distribution of the measured profile lengths ($f(l)$) is made and is subjected to a so-called 'unfolding' procedure (for a review, see e.g. Cruz-Orive, 1983, 1985a). Such unfolding procedures take into account the differences in size of the disc-like synapses and the corresponding 'hit' probabilities and hence the synaptic profile length distribution ($f(l)$) is transformed into the actual synapse diameter distribution ($F(D)$).

From $F(D)$ an estimate of the diameter (ED) of synaptic discs of different size can be derived and the corresponding EH can then be calculated (Hilliard, 1967). If the section thickness (T) and the capping angle (Z) are known and the resolution threshold (Q) is zero, then the disc diameter can be estimated directly from the profile data without unfolding the profile size histogram (Cruz-Orive, 1983, 1985a).

The discrete unfolding procedure described by Cruz-Orive (1983, section 4) has been applied to the example, presented in this paper.

(2) The serial section technique (Fig 2). To calculate N_V (synapses) according to the formula presented in Fig. 2 it is necessary first of all to count the total number (N_i) of synaptic profiles, present in the reference area (A_i) of the centre section. Secondly, these synaptic profiles are serially tracked and for each synapse the number of sections (m_{ij}) in which this synapse appears, is counted.

The chance for a synapse to be hit and to be observed in the reference plane is proportional to the quantity $\tilde{H} + T$, where $\tilde{H}$ denotes the effective projected height of a hit synapse and T denotes the section thickness (Cruz-Orive, 1984, 1985a). The quantity $\tilde{H} + T$ of the hit synapse is calculated by multiplying the number of sections in which the synapse appears (m) with the section thickness (T). The reciprocals, i.e. the harmonic mean, of the quantity mT of the synapses hit by the reference plane are used in the formula for estimating N_V (Cruz-Orive, 1984, 1985a; De Groot, 1984). Obviously, it is important to have a reliable approximation of the section thickness (T) which can be obtained by using e.g. the 'small-fold' technique, (Small, 1968) 'interferometry' (for a review, see e.g. Williams, 1977) or 'electron scattering' (Weybull, 1970), techniques which all proved to result in a good estimate of the thickness (T) of ultrathin sections (De Groot, in preparation). The size of the reference area (A_i) is measured and subsequently N_V (synapses) is calculated using the formula given in Fig. 2.

A requirement for this method is that the total distance between the first and the last section of a series is at least a factor of 2 larger than the maximal projected height of the largest particle (max H_i) in a direction perpendicular to the sections. In the case of perforated and non-perforated synapses each synapse has to be tracked through *every* section of the series in which it appears in order to distinguish correctly between profiles belonging to perforated and profiles belonging to non-perforated synapses. However, in the case one is dealing with quite large synapses which can easily be recognized from any profile through this transected synapse, for example one out of every two sections may be used. T is then replaced with $2T$ in the formula for N_V (Fig. 2). Note also that the orientation of each series may be chosen at will. If these requirements are fulfilled, the method results in an (approximately) unbiased estimate of N_V (see Discussion). Assumptions about the size, shape and orientation of the particle and upon capping (truncation) and overprojection are not necessary, in principle.

(3) The disector technique (Fig. 3). In principle the disector technique uses two planparallel sections a known distance apart, to obtain the necessary data to calculate N_V. The first of these two sections is called the 'reference plane', the second is called the 'look-up plane'. The space which is generated by the reference area (A_i) of both planes and their mutual distance is called the 'disector'. The

NUMERICAL DENSITY OF SYNAPSES DISCRETE UNFOLDING TECHNIQUE

- Formula : $est\ N_V = est\ N_A\ /\ est(EH + T)$ (see ref. 1)
  where
  $est\ N_V$ = estimated mean number of particles, i.e. synapses, per unit volume of reference solid
  $est\ N_A$ = estimated mean number of transected particles per unit reference area
  $est\ EH$ = estimated mean linear projection of the particles
  T = section thickness
- Approach :
  - to obtain $est\ N_A$, count the number of transected synapses n_i in the reference area A_i of a random section and measure the size of the reference area; see ref.2 for an unbiased counting rule
  - to obtain $est\ EH$, measure the profile length, l, of these transected synapses. Then:
    - for discs, i.e. disc-like synapses, of equal size: $El \propto EH$;
    - for discs varying in size:

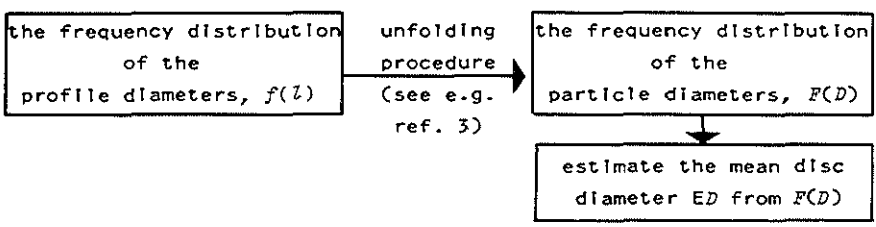

      Then, $\pi/4\ ED = EH$ (see e.g. ref. 4)
    - If section thickness $T>0$ and capping angle $\Im>0$ are known, and if resolution threshold $Q=0$, then the disc diameter can be estimated directly from the profile data without unfolding the disc size histogram (see ref. 3 sect. 5 and ref. 5 equ. 2.9)
  - to obtain T, measure the thickness of the section (see e.g. ref. 6)
- Requirements :
  - the particles are assumed to have a disc-like shape
  - the complete set of profiles belonging to the planar transect through one disc, i.e. a disc-like synapse, must be identifiable as such in the random section
- References :

1. Abercrombie, M., Anat. Rec. 94: 239-247, 1946.
2. Gundersen H.J.G., J. Microsc. 111: 219-223, 1977.
3. Cruz-Orive, L.M., J. Microsc. 131: 265-290, 1983.
4. Hilliard, J.E., In: Stereology (ed. H. Elias), Springer, Berlin Heidelberg New York, p. 211-215,1967.
5. Cruz-Orive, L.M. Internal Report Nr 117/LC 19. Proceedings of the Wenner-Gren International symposium on Quantitative neuroanatomy in Transmitter Research, Stockholm, May 3-4, 1984 Macmillan Press, London (in press) 1986.
6. Small, J.V., In: Proceedings 4th European Congress on Electron Microscopy (ed. D.S. Bocciarelli) Vol. I, Tipografia Poliglotta Vaticana, Roma, p. 609, 1968.

Fig. 1. 'Cookbook' description of a conventional 'discrete unfolding' technique for estimating the numerical density of synapses. For details the reader is referred to the text.

NUMERICAL DENSITY OF SYNAPSES — SERIAL SECTION TECHNIQUE

- Formula : $est\ N_V = \sum_{i=1}^{m} T_i^{-1} \sum_{j=1}^{N_i} m_{ij}^{-1} \Big/ \sum_{i=1}^{m} A_i$ (see refs. 1,2 and 3)

where

$est\ N_V$ = estimated mean number of particles, i.e. synapses, per unit volume of reference solid

m = number of uniform random blocks cut into series

T_i = thickness of the sections of the i-th series

N_i = total number of transected particles present in A_i. Note that, since all synapses in A_i are tracked through the series, $N_i = n_i$ which would represent the number of particles in A_i tracked through the series

m_{ij} = number of serial sections from the i-th block in which the j-th tracked particle appears; j runs from 1 to n_i

A_i = reference area of the reference section from the i-th block (i = 1,2,..., m)

- Approach :
  - to obtain N_i, count the number of transected synapses in the reference area of the centre section of a series according to an unbiased counting rule (see e.g. ref. 4)
  - to obtain m_{ij}, track each of these transected synapses in adjacent sections of the series and count the number of serial sections in which each of them appears
  - to obtain T_i, determine the section thickness (see e.g. ref. 5)
  - to obtain A_i, measure the size of the reference area in the centre section
- Requirements :
  - the distance between the first and the last section of a series must be at least twice the longest linear projection, max H_{ij}, of a particle, i.e. a synapse, in a direction perpendicular to the sections
- References :

1. Cruz-Orive, L.M., J. Microsc. 120: 15-17, 1980.
2. De Groot, D.M.G., with an appendix by Cruz-Orive, L.M., In: Stereology in Electron Microscopy (eds. A Reith and T.M. Mayhew), Hemisphere/McGraw-Hill, New York (in press), 1986.
3. Cruz-Orive, L.M., Internal Report Nr 117/LC 19. Proceedings of the Wenner-Gren International Symposium on Quantitative Neuroanatomy in Transmitter Research, Stockholm, May 3-4, 1984 MacMillan Press, London (in press), 1986.
4. Gundersen, H.J.G., J. Microsc. 111: 219-223, 1977.
5. Small, J.V., In: Proceedings 4th European Congress on Electron Microscopy (ed. D.S. Bocciarelli) Vol. I, Tipografia Poliglotta Vaticana, Roma, p. 609, 1968.

Fig. 2. 'Cookbook' description of the 'serial section' technique for estimating the numerical density of synapses. For details the reader is referred to the text.

number of particles which is present in A_i (reference plane) and not in A_i (look-up plane), called Q^-, represents the number of particles (N) included in the volume (V) of the disector (Sterio, 1984). This volume (V) equals the size of the reference

NUMERICAL DENSITY OF SYNAPSES — DISECTOR TECHNIQUE

- Formula : $est\ N_V = \sum_{i=1}^{n} Q_i^- \ / \ \sum_{i=1}^{n} h_i\ A_i$ (see ref. 1 and footnote)

where

$est\ N_V$ = estimated mean number of particles, i.e. synapses, per unit volume of reference solid

n = number of disectors

Q_i^- = transects of particles, present in A_i (*reference plane*) and absent in A_i (*look-up plane*)

h_i = distance in disector between A_i (*reference plane*) and A_i (*look-up plane*)

A_i = reference area of the reference plane from the i-*th* disector ($i = 1,2,\ldots, n$).

- Approach :
  - to obtain Q_i^-, track in the look-up plane of the i-*th* disector the transected synapses, Q_i, present in A_i (*reference plane*) and note the fraction of particles that is absent in this look-up plane (see ref. 2)
  - to obtain h_i, measure the vertical distance between the reference plane and the look-up plane from the i-*th* disector (see e.g. ref. 3)
  - to obtain A_i, measure the size of the reference area of the reference plane from the i-*th* disector
- Requirements :
  - the distance h in the disector must be less than the smallest linear projection, min H_i, of any particle, i.e. a synapse, in the direction i perpendicular to the planes of the disector
  - the complete set of profiles belonging to the planar transect through one particle, i.e. a synapse, must be identifiable in both the reference plane and the look-up plane
- References :

1. Sterio, D.C., J. Microsc. 134, 127-136, 1984.
2. Gundersen, H.J.G., J. Microsc. 111, 219-223, 1977.
3. Small, J.V., In: Proceedings 4th European Congress on Electron Microscopy (ed. D.S. Bocciarelli) Vol. I, Tipografia Poliglotta Vaticana, Roma, p. 609, 1968.

- N.B. The formula is presented in this way for the sake of comparison with figs. 1 and 2. It should be noted that Sterio (1984) did not suggest that stereological ratios should be measured.

Fig. 3. 'Cookbook' description of the 'disector' technique for estimating the numerical density of synapses. For details the reader is referred to the text.

area (A_i) multiplied by the height of the disector (h_{dis}) which in turn is represented by the distance between the reference plane and the look-up plane. Therefore, Q^- is counted, the size of A_i is measured and h_{dis} is determined in order to calculate N_V according to the formula given in Fig. 3.

Requirements that must be fulfilled are: (1) a set of profiles, representing a transect through one particle, should be identifiable as such in both the reference plane and in the look-up plane and (2) the distance between the two planes (h_{dis}) should be less than the sum of the minimal projected height of the smallest particle (min H_i) and the section thickness (T).

With respect to the estimation of synaptic densities these requirements mean *in practice* that: (1) synapses have to be serially tracked in case (complex) perforated synapses are present in the tissue and (2) adjacent sections have to be used for the reference plane and the look-up plane respectively, when the minimal projected height of the smallest synapse (min H_i) is smaller than the section thickness (T).

TABLE I

The number of non-perforated synapses per unit volume(N_V) and the mean disc diameter ED in the stratum lacunosum moleculare of the hippocampal CA3 region of female adult rats, obtained by the discrete unfolding technique.

rat nr.	bl.	ref. pl.	m	$\sum_{i=1}^{m} A_{\Sigma}$	$est T$	CE	(*)	$est\ Z$	min l_{Σ}	n_{Σ}	E l	CE	$est ED$	CE	$est\ N_V$	CE
1	3	3	6	487.0	36.0	1.9	(44)	46.6	65.9	169	183.1	3.2	230.1	0.9	2.6	8.0
2	2	2	8	716.1	35.0	3.7	(15)	50.1	67.3	190	222.6	2.8	276.7	3.3	1.9	7
3	2	2	4	340.4	38.2	1.9	(54)	56.8	76.2	154	190.5	2.6	238.7	3.2	3.9	8.3

bl. , blocks
ref.pl., reference planes
m , number of random sections
A_{Σ} , reference area (10^{-8} cm^2)
$est\ T$, estimated mean section thickness (10^{-7} cm) (Small, 1968)
CE , coefficient of error of the mean (%)
(*) , number of sections used to estimate T
$est\ Z$, estimated mean capping angle obtained by successive unfolding (Cruz-Orive, 1983)
min l_{Σ} , smallest observable profile length (10^{-7} cm)
n_{Σ} , number of synaptic profiles, counted and measured in A_{Σ}
E l , mean profile length of transected synaptic discs (10^{-7} cm)
$est ED$, estimated mean diameter of synaptic discs (10^{-7} cm) after unfolding according to Cruz-Orive (1983), thereby accounting for overprojection ($Z>0$) and truncation (capping angle$Z$ and positive resolution threshold,Q, determined by minl_{Σ})
$est\ N_V$, estimated mean number of synapses per unit volume (10^{12} cm^{-3}) after unfolding.

The parameters were calculated using the formulae given in this paper.

N.B. 1 Cell-bodies, main neurites and blood vessels are included in the reference area (A_{Σ})
N.B. 2 CE ($est ED$) and CE ($est\ N_V$) are computed from the variation between n_{Σ} synapses within the animal, distributed over 20 size classes (Cruz-Orive, 1983).

Results

Table I summarizes the numerical densities (N_V) of the (simple) non-perforated synapses, obtained with a discrete unfolding technique. In addition, their average profile length (El) is given and an estimate of their particle diameter (ED). In Fig. 4 the frequency distributions of the measured profile length ($f(l)$), and of the particle diameters after unfolding ($F(D)$), are shown. For rat no. 1, both $f(l)$ and $F(D)$ are plotted together in Fig. 5 with the frequency distribution of the maximal profile lengths ($F(\max\ l)$ observed in serial sections, of the synapses counted with the disector technique, i.e. the number Q^-. The numerical densities (N_V) of the

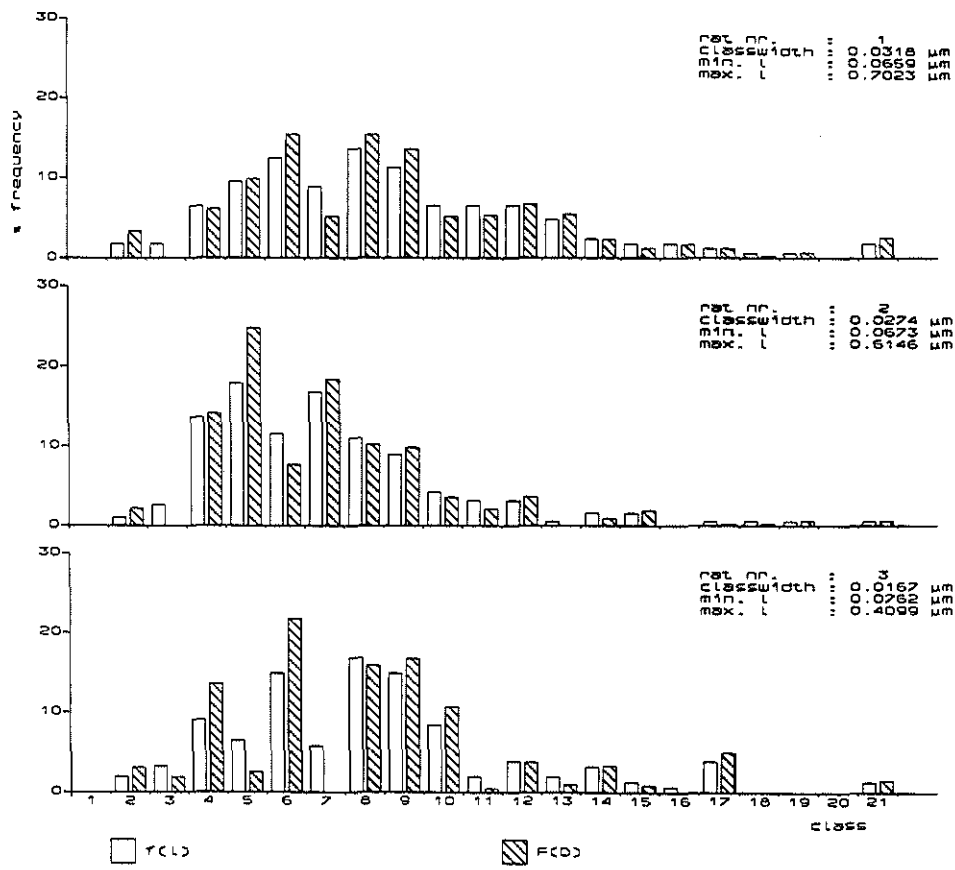

Fig. 4. Results of the application of an 'unfolding' procedure (Cruz-Orive, 1983) to profiles of (simple) non-perforated synapses in the stratum lacunosum moleculare of the hippocampal CA_3 area of 3 female adult rats. The histograms represent the frequency distributions of the measured synaptic profile lengths ($f(l)$) (open bars) and of the particle diameters ($F(D)$) after 'unfolding' (hatched bars). min l and max l respectively indicate the shortest and longest profile length measured in independent area-weighted random sections.

TABLE II

The number of different types of synapses per unit volume (Ny) in the stratum lacunosum moleculare of the hippocampal CA3 region of female adult rats, obtained by the serial section technique.

rat nr.	bl.	ref. pl.	m	$\sum_{i=1}^{m} A_i$	$cat\ T$	CE	(*)	non-perforated synapses n_i	non-perforated synapses $cat\ Ny$	non-perforated synapses CE	perforated synapses n_i	perforated synapses $cat\ Ny$	perforated synapses CE	all synapses n_i	all synapses $cat\ Ny$	all synapses CE
1	3	3	6	487.0	36.0	1.9	(44)	169	3.1	5.9	43	0.39	14	212	3.5	5.7
2	2	2	8	716.1	35.0	3.7	(15)	190	2.2	22	16	0.10	36	206	2.3	22
3	2	2	4	340.4	38.2	1.9	(54)	154	3.5	5.6	33	0.39	55	187	3.8	5.2

bl , blocks
ref.pl., reference planes
m , series
A_i , reference area (10^{-8} cm^2)
$cat\ T$, estimated mean section thickness (10^{-7} cm) (Small, 1968)
CE , coefficient of error of the mean (%)
(*) , number of sections used to estimate T
n_i , number of synapses within in A_i tracked through the series.
$cat\ Ny$, estimated mean number of synapses per unit volume Ny (10^{12} cm^{-3})

The parameters were calculated using the fomulae given in this paper.

N.B. 1 The relatively large CE ($cat\ Ny$) are partly due to regional variations within the hippocampus which are mainly the result of including cellbodies, main neurites and bloodvessels in the reference area (A_i).

N.B. 2 CE ($cat\ Ny$) is computed from the number of synapses within m series.

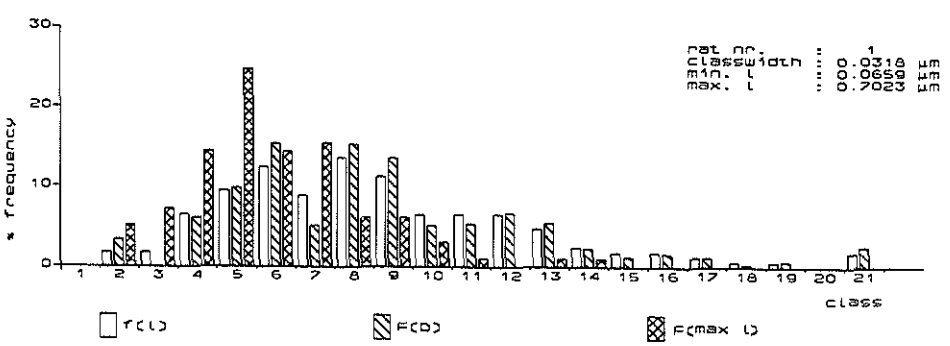

Fig. 5. The histograms of the frequency distributions of the measured synaptic profile lengths ($f(l)$) (open bars) and of the particle diameters ($F(D)$) after 'unfolding' (hatched bars) of rat no. 1 (Fig. 4) are shown together with the frequency distribution of the longest profile lengths ($F(\max l)$) observed in serial sections (double hatched bars). $f(l)$ and $F(D)$ are composed of synapses from independent area-weighted random sections; $F(\max l)$ is composed of 'disector-sampled' synapses i.e. the number Q^- (see Material and Methods and Discussion). Notice that $F(\max l)$ is skewed to the left in comparison with $F(D)$.

TABLE III

The number of different types of synapses per unit volume (N_V) in the stratum lacunosum moleculare of the hippocampal CA3 region of female adult rats, obtained by the disector technique.

rat nr.	bl.	ref. pl.	n	$\sum_{i=1}^{n} A_{\frac{i}{2}}$	$est\ T$	CE	(*)	non-perforated synapses Q^-	non-perforated synapses $est\ N_V$	non-perforated synapses CE	perforated synapses Q^-	perforated synapses $est\ N_V$	perforated synapses CE	all synapses Q^-	all synapses $est\ N_V$	all synapses CE
1	3	3	12	487.0	36.0	1.9	(44)	97	2.8	12	9	0.26	37	106	3.0	7.9
2	2	2	16	716.1	35.0	3.7	(15)	99	2.0	22	2	0.04	68	101	2.0	22
3	2	2	8	340.4	38.2	1.9	(54)	73	2.8	15	7	0.27	40	80	3.1	14

bl , blocks
ref.pl., reference planes
n , disectors
$A_{\frac{i}{2}}$, reference area (10^{-8} cm^2)
$est\ T$, estimated mean section thickness (10^{-7} cm) (Small, 1968)
CE , coefficient of error of the mean (%)
(*) , number of sections used to estimate T
Q^- , number of synapses present in $A_{\frac{i}{2}}$ (*reference plane*) and absent in $A_{\frac{i}{2}}$ (*look-up plane*)
$est\ N_V$, estimated mean number of synapses per unit volume N_V (10^{12} cm^{-3})

The parameters were calculated using the fomulae given in this paper.

N.B. 1 The relatively large CE ($est\ N_V$) are partly due to regional variations within the hippocampus which are mainly the result of including cellbodies, main neurites and bloodvessels in the reference area ($A_{\frac{i}{2}}$).

N.B. 2 CE ($est\ N_V$) is computed from the number of synapses within n disectors.

simple non-perforated, of the complex perforated and of 'all', i.e. non-perforated and perforated synapses, are obtained with both the serial section (Table II) and the disector techniques (Table III).

Comparing the numerical densities of the non-perforated synapses, of the perforated synapses and of 'all' synapses, obtained with either the discrete unfolding

Fig. 6. This figure shows 'orthogonal projections' (hatched areas) of EPTA-treated synapses present in reference area 1 of rat no. 1 of the example presented in this paper. These orthogonal projections are obtained by 'symmetric' reconstruction, thereby using the measurements of the profile lengths in adjacent serial section in which the 'tracked' synapse can be observed and an estimate of the mean section thickness (dotted bars). In the reconstructions the centre-point of all the profile lengths of a tracked synapse are put on top of each other resulting in 'symmetric' reconstructions. The length of the dotted bars represents the size of the profile lengths observed in serial sections; the width of the dotted bars represents the average section thickness; the number of bars in each 'symmetric' reconstruction represents the number of sections in which the synapse is observed, when tracked in adjacent serial sections.To reconstruct an 'orthogonal projection' (hatched area) the upper planes of the profiles in adjacent sections are connected; therefore, the lowest section of each projection remains unhatched. Apparently, a portion of the synapses does not have the assumed 'disc shape'.

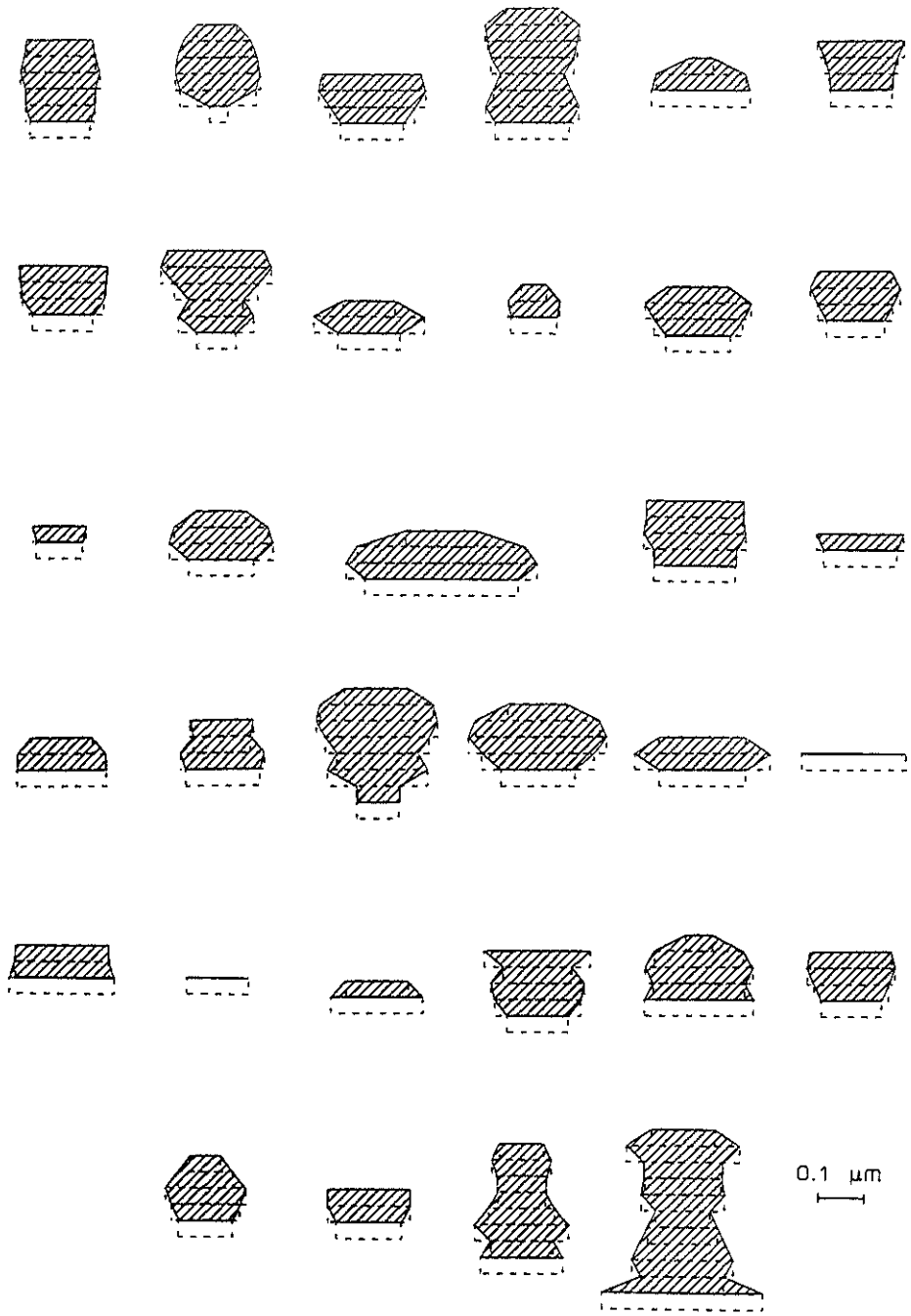
0.1 µm

technique (only the non-perforated ones), the serial section or the disector techniques it was found that the results do not differ significantly [paired t-test, not significant ($\alpha = 0.05$; Bonferroni $P_2 > 0.0167$; see Hald, 1952; Miller, 1966)]. However, consistently lower values are obtained with the disector technique compared with those obtained with the serial section technique (see Discussion).

Provided that the assumptions with respect to the shape of the synapses and those regarding capping and overprojection were correct, $F(D)$ should approximate $F(\max l)$; this resemblance could not be confirmed (Fig. 5). 'Symmetric' reconstruc-

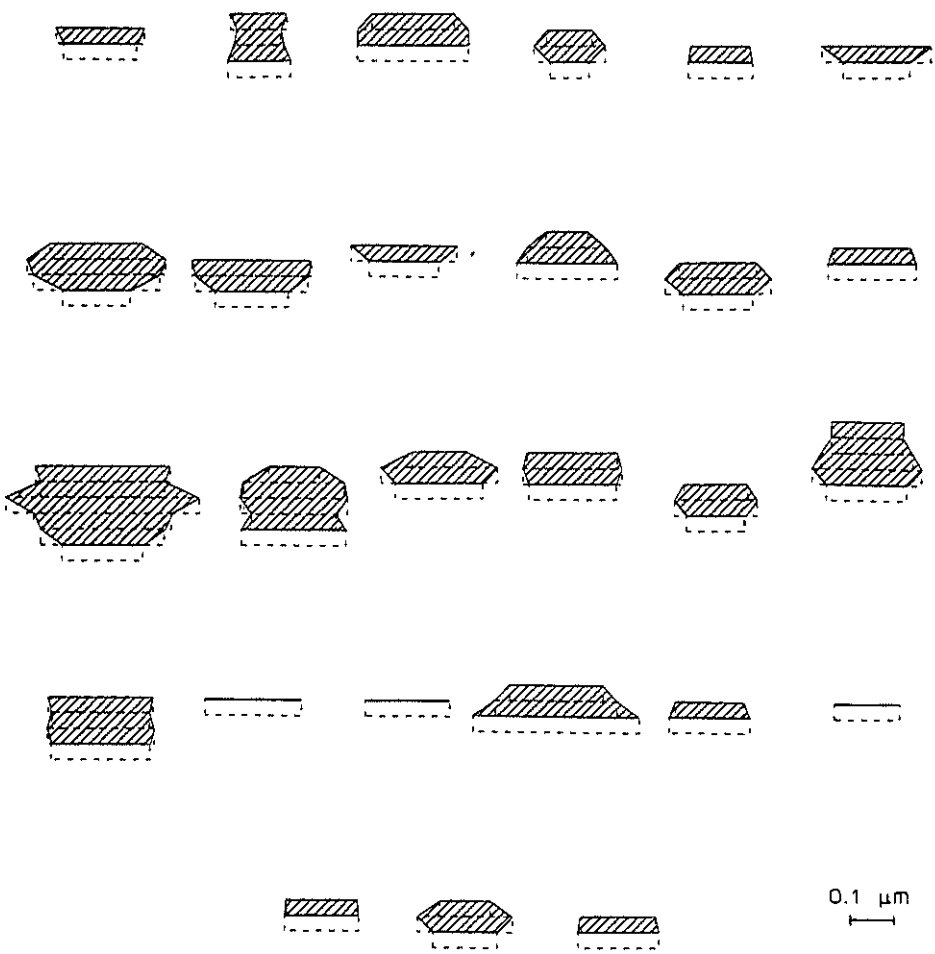

Fig. 7. 'Orthogonal projections' of OsO_4-treated synapses of rat no. 1 of the example, presented in this paper. These synapses were present in an identical area as those, shown in Fig. 6. The sections used were taken from a block (i.e. a 75 µm thick vibratome slice) adjacent to the block used in Fig. 6. For further details, see Fig. 6.

tions of the synapse projections in EPTA (Fig. 6) and OsO_4-treated tissue (Fig. 7) showed that for a portion of the non-perforated synapses the previously assumed disc-shape is incorrect.

Discussion

The conventional methods for the estimation of numerical densities have been, and still are, widely used. It has been long recognized that these methods may be seriously biased and must be considered inferior. The bias may occur if the assumptions that are made regarding the shape and size of the investigated particles and the section thickness are incorrect. Erroneous results are then obtained (Verwer and De Groot, 1982). At present there are 4 methods available that allow an *unbiased* estimation of the numerical density of *arbitrarily shaped* particles. These methods are: (1) the serial section technique (Cruz-Orive, 1980, 1984, 1985a), (2) the disector technique (Sterio, 1984), (3) the fractionator technique (Gundersen, 1986) and (4) the selector technique, 'born' at the Scandinavian Stereology Course preceding the European Stereology Symposium in Göteborg, September 1985 (Cruz-Orive, 1985b). Before starting an experiment in which numerical densities are to be estimated, the advantages and limitations of the various methods should be compared. In general, the fractionator technique as proposed and described in detail by Gundersen (1986) will be the most efficient technique to obtain an unbiased estimate of the numerical density of arbitrarily shaped particles. However, when applying this method it should be kept in mind (a) whether the outcome of such an approach, i.e. in this example the number of synapses in the total brain, is a meaningful neurobiological parameter. This is hardly acceptable taking into account that the brain is a layered structure with different synaptic in and outputs in different layers and in different brain regions. These regions can sometimes only be distinguished on electrophysiological grounds; (b) whether the total reference space is at all available for fractionation; e.g. part of it may be required for other studies for which structural integrity is required; (c) that it may be too laborious to determine the volume fraction of the disectors in the very last subsamples, e.g. in electron microscopy when dealing with rather small particles such as synapses. For these reasons, this technique is not 'the preferred technique' to estimate synaptic densities.

For this specific purpose the selector technique of Cruz-Orive 1985b, however elegant, cannot be used at all. The reason for this is the following. In principle the selector is a disector of *unknown* thickness. Instead of measuring the volume of the disector (see Material and Methods: the disector technique) the ratio of the *mean particle volume* and the reference volume is estimated. If, however the investigated (three dimensional) particle has 1, 2 or 3 extremely small dimensions, the method does not allow a correct estimation of the mean particle volume. This implies that this method is not applicable for the estimation of the numerical density of synapses, since synapses are composed of a pre- and a postsynaptic membrane, separated by a very narrow intercleft space. Such synaptic contact-zones are too

narrow to derive a useful volume of the synapses with the selector technique. Even in synaptic terminals (boutons) which do have a clearcut volume, all three dimensions may still be too small to obtain a reliable and useful estimate of the particle volume with the selector technique.

The main points to consider before making a choice between the remaining two methods are the amount of work involved in: (A) cutting and inspection of serial sections (serial section technique) (B) cutting planparallel sections (serial section and disector technique) and (C) measuring the section thickness (serial section technique and disector technique).

These considerations are discussed in more detail below, with special emphasis on the example presented in this paper.

(A) The serial section technique requires serial sections to obtain the data for calculating N_V, while the disector technique in principle uses only two sections: a 'reference plane' and a 'look-up plane'. In terms of labour and cost one would preferably like to avoid the serial section technique. However, both techniques—like all techniques for estimating N_V—derive a particle number estimate from the number of profiles of the transected particles in the section plane. Therefore, a requirement that must be fulfilled for both these techniques is, that a profile or a set of profiles in a section belonging to the same particle can be recognized as such. If not, the profiles should be tracked in more sections in order to identify them. In the present example a correct distinction between the (simple) non-perforated and the larger (complex) perforated synapses can only be made by using serial sections (De Groot and Bierman, 1983). By tracking each synapse through the adjacent sections it can be determined whether a profile or a set of profiles belongs to one and the same non-perforated or perforated synapse. Since in this particular example serial sections are required anyway, none of the two methods can be excluded on the basis of the amount of work involved. (For improved serial sectioning, see De Groot, 1984.)

(B) In the disector technique the two sections used, i.e. the reference plane and the look-up plane, have to run parallel. The distance between the two sections must be known.

(C) The section thickness is an essential parameter in the disector and serial section techniques. In the serial section technique the 'effective' projected height of the investigated particle is determined by the product of the number of sections in which the particle appears and the thickness of these sections (Cruz-Orive, 1984, 1985a). In the disector technique the height of the disector is determined in a comparable way (Sterio, 1984). Both the effective projected height and the height of the disector are essential parameters for calculating N_V (see Material and Methods). The evaluation of methods for the determination of the thickness of ultrathin sections (De Groot, in preparation) indicated that the methods of 'electron-scattering' (Weybull, 1970), 'small-fold' (Small, 1968) and 'interference microscopy' (for a review, see e.g. Williams, 1977) led to comparable estimates of the section thickness which differed from the values obtained with the 're-embedding' method (see e.g. Beertsen et al., 1975).

Both the serial section and disector technique have been applied to (simple)

non-perforated and (complex) perforated synapses. Only the non-perforated synapses, initially thought to have a disc-like shape, were included in the discrete unfolding technique. It would be unrealistic to apply an unfolding procedure to the complex perforated synapses or to the total population of synapses containing an unknown amount of the latter complex ones. In general, the shape of perforated synapses differs considerably from that of a disc *.

It was found that the final results of the numerical density of the non-perforated synapses (N_V (*np*)) may vary to a rather large extent and that the results obtained with the different methods are not significantly different. At first sight one might conclude that 'therefore' the unfolding technique can be applied, which provides a size distribution of the synapses *in addition* to number estimates. Such a size distribution could be of help to distinguish between different types of synapses. However, from the result of the present comparison one should conclude that with respect to the overall variations, the deviation from the circular disc shape of these non-perforated synapses is not sufficient to result in a wrong estimation of N_V by the unfolding procedure. With respect to these variations it should be noted that cell bodies, main neurites and blood vessels were included in the samples, resulting in — sometimes rather large — variations in N_V. When these structures are excluded from the samples (see e.g. De Groot and Bierman, 1983) or when their volumes are estimated separately when included, the extent of the variations in N_V is reduced considerably. Moreover, the circumstances for the different methods were not necessarily ideal for the present comparison and it is a known fact that the shape of synapses may change to an unknown extent under several experimental conditions (see e.g. Peters and Kaiserman-Abramof, 1969; Greenough et al., 1978; Vrensen and Nunez Cardozo, 1981; Fields and Ellisman, 1985). Therefore, it should be stressed that, since the extent of bias remains unknown it is always unpredictable whether the unfolding procedure will yield the same estimates as the serial section and disector methods. In any case it is scientifically unacceptable to use a method (the unfolding procedure) for the detection of differences in synaptic sizes which assumes that the bias due to deviations from a special shape will be small compared with the overall variation. Definite proof for the type of the investigated synapses is always lacking unless the synapses are three-dimensionally reconstructed.

The section thickness used is rather large in comparison with the size of the smallest synaptic profile measured (Table I and Fig. 4). In the unfolding procedure used (Cruz-Orive, 1983) attempts are made to correct for 'missing profiles' or 'capping' and for overprojection due to finite section thickness, but only for spheres, circular discs and vertical surfaces of revolution cut vertically. If the shape of the synapse is unknown then it is also unknown to what extent the assumptions about capping and overprojection match reality.

If the disc-assumption is correct, the maximal profile length (max l) of a synapse

* Note that in order to extract the non-perforated synapses from the total population, each synaptic profile in the reference area had to be serially tracked in adjacent sections to make a correct distinction between perforated and non-perforated synapses.

observed in serial sections can be used as a measure for the size of this synapse since for circular discs, max l equals the disc diameter. An unbiased estimation of the distribution of the maximal profile lengths ($F(\max l)$) of synaptic 'discs' can serve to distinguish between different types of disc-like synapses if clear-cut differences in size are present. Such a distribution can be obtained using 'disector-sampled' synapses for the max l analysis. Notice that the number of synapses sampled from independent area-weighted random sections (unfolding technique) or those counted in the centre section of a series of sections (serial section technique) cannot be used (as such) to compose an unbiased distribution of maximal profile lengths ($F(\max l)$). Indeed, larger synapses stand a greater chance to be hit by sectioning and unfolding procedures take the differences in size and the corresponding 'hit' probabilities into account. However, this is not done when their max l is used to compose $F(\max l)$. This implies that such a distribution would yield a bigger amount of 'larger' disc diameters than actually present in the total synapse population. With respect to the present example it can be expected that, provided the unfolding procedure (Cruz-Orive, 1983) has been applied to *disc*-like synapses and the corrections for overprojection and truncation have been correct, the estimated particle diameter distribution ($F(D)$) after unfolding approximates the afore-mentioned $F(\max l)$. Conversely, it might be stated that, if $F(D)$ does not approximate $F(\max l)$, then assumptions about shape, capping and/or overprojection were incorrect. These two size distributions have been compared for rat no. 1 in Fig. 5 and clearly show a difference: $F(D)$ yields larger sizes than $F(\max l)$. In fact, the estimated mean synapse diameter (ED) of $F(D)$ (calculated according to Cruz-Orive 1983, section 4) was found to be 230.1 nm ($CE(\text{mean}) = 0.9\%$) (Table I) whereas the mean maximal profile length ($E(\max l)$ was 164.1 nm ($CE(\text{mean}) = 3.6\%$; $n = 97$); a rather large difference. Furthermore, the shape assumption was checked by making 'symmetric' reconstructions of synapse projections from profile lengths of the synapses observed in serial sections. A portion of the synapses clearly deviates from the disc shape (Fig. 6); they may resemble more or less ellipsoidal platelets or they may be really complex-shaped as was previously found for the perforated synapses (De Groot and Bierman, 1983).

Estimations of the capping angle Z for rat no. 1 by repeated unfolding (Cruz-Orive, 1983) and by calculation from the shortest (min l) and longest (max l) profile lengths (see Cruz-Orive, 1985a, Eqns. 1.19 and 1.20) yield values of *est* $Z = 46.6°$ (Table I) and *est* $Z = 34.3°$, respectively. The latter method to obtain *est* Z is acceptable for arbitrarily oriented discs (Cruz-Orive, 1985a). The overprojection effect should not be too large, otherwise Z will be slightly overestimated. The discrepancy found in the present example between est Z obtained with the two above-mentioned methods will partly be the result of the deviations from the disc-shape (see Fig. 6).

Since the section thickness is relatively large as compared with the size of the synapses and since EPTA-treated synapses have been looked upon as opaque structures in a translucent matrix, overprojection was expected. However, ongoing experiments cast some doubt on the occurrence of the phenomenon of overprojection. A study to investigate certain discrepancies is in progress.

As far as the usefulness of the discrete unfolding technique for estimating number and sizes of synapses is concerned, the conclusion from the results discussed so far is the following: if the synaptic number and size are to be estimated from independent random sections it is advisable to check beforehand whether the necessary assumptions regarding the shape of the synapses, regarding truncation and regarding overprojection are correct.

When we return to the application of the serial section and disector techniques to estimate the numerical density of non-perforated, perforated and 'all' synapses, the following can be said.

The fact that for the non-perforated, for the perforated as well as for 'all' synapses, the estimates of N_V calculated with the disector technique are consistently the lowest in each of the 3 rats studied is puzzling. An intriguing question is whether this difference is a methodological 'pitfall' or whether it is due to the experimental conditions of the present example. With these preliminary results we can only speculate about what may actually cause this difference. The essential parameters and requirements in both techniques are: (1) the reference area, (2) the number of sections composing the height of the disector (disector technique) and the effective projected height (serial section technique), and an estimate of the section thickness, and (3) identifiable profiles of the transected synapses.

These 3 points can be detailed as follows:

(1) The reference areas in both techniques were the same in this example. Therefore, the differences in the estimates of N_V will not be caused by areal differences, due to e.g. shrinkage and compression problems.

(2) The size of the profile length of the shortest synaptic profile was found to be of the same order of magnitude as the thickness of an ultrathin section. Therefore, the 'reference plane' and 'look-up plane' (disector technique) have to be taken in adjacent sections. The height of the disector is then equal to the thickness of one ultrathin section, i.e. the 'reference' section. The effective projected height of most synapses (serial section technique) is composed of more than one section. The thickness of the sections, composing the disector height and the effective projected height of the synapses, should be known and used to calculate N_V. Deviations from the actual section thickness will give rise to comparable deviations of N_V with both techniques. Preferably the thickness of the sections used should be measured, rather than the section thickness of a separate set of sections as was done in the present example *. When the height of the disector is composed of only one ultrathin section it is very well possible that the actual thickness of this particular section deviates from the estimated thickness to a rather large extent. The influence of the deviation will be reduced with an increasing number of disectors and will be less pronounced when more sections are used as is generally the case for the effective projected height. It is not unlikely that the differences in N_V, presently found

* The small-fold method cannot be directly adapted to the serial sections since the tracking of the investigated synapses through the series of sections would be hampered by the presence of folds in the sections.

between the two techniques, are to some extent caused by the aforementioned source of bias. Theoretically it is possible that the sections used for the reference planes — for the 3 rats in the present example these were 3,2 and 2 different sections respectively — happened to be thinner than the estimated section thickness.

When it is assumed that the average estimate of the section thickness itself is wrong, this does not explain the consistent differences in N_V between the disector and serial section techniques. In both techniques the same estimate of the section thickness is used. Since the section thickness is introduced in the denominator of both N_V formulae, the relative effect of a deviation of the estimated thickness from the true thickness on the estimate of N_V is the same for both techniques.

As was pointed out by Cruz-Orive (1984) $(mT)^{-1}$ (see Material and Methods: the serial section technique) is only approximately unbiased for $(\tilde{H}+T)^{-1}$ of a synapse hit by the reference plane. Therefore, est N_V (see Fig. 2) will also be approximately unbiased, since $(mT)^{-1}$ of the synapses hit is used in the formula of N_V. Since the mean effective projected height of the synapses is very low, this bias may not be negligible. Further exploration, carried out at present, is required to establish the extent of this bias.

(3) Identification of profiles of transected synapses may be doubtful when perforated and non-perforated synapses are simultaneously present in EPTA-treated tissue. As shown before (De Groot and Bierman, 1983) it is possible that an interrupted profile of a perforated synapse might be identified as two or more profiles of separate synapses. The opposite is also possible. This problem can be largely, if not totally, avoided by tracking the synapses through serial sections. If the first profile of a synapse 'starts to appear' in a series of sections very close to the spot where another synapse is 'disappearing' from the series it is theoretically possible that e.g. two adjacent profiles of two separate synapses are 'recognized' as the perforation focus of a perforated synapse. As a consequence, the effective projected height of the investigated synapse(s) will be incorrect.

Considering the symmetric reconstructions of the EPTA-treated synapses (Fig. 6) one may even be inclined to conclude that e.g. the '8-shaped' orthogonal projections are the result of a reconstruction of two disc-like synapses 'built' on top of each other. However, it should be noted (see Fig. 7) that such 'complex' orthogonal projections of synapses were also reconstructed from OsO_4-treated tissue taken from a block, adjacent to the aforementioned EPTA-treated tissue. Since in OsO_4-treated tissue the unit-membrane is also visualized, there is no doubt in recognizing in serial sections the first and last profile length belonging to a particularly tracked synapse. Whatever the case, this problem of the identification of the synaptic profiles plays a comparable role in the disector and serial section techniques. As a result, the estimated N_V values may be wrong, but the effect is the same for both techniques. The consistent N_V differences between the two approaches can, therefore, not be explained by this 'identification' problem.

In a previous study (De Groot and Bierman, 1983) semithin (500 nm) EPTA sections were used and 'en face' synapses were studied to see whether 'perforated' synapses were present in the tissue. In general, particularly the smaller synapses

appear 'en face': the larger a synapse, the smaller its chance to be fully incorporated in the section. As was already shown by other investigators (see e.g. Peters and Kaiserman-Abramof, 1969) the shape of the synapse generally becomes more complicated with increasing size. This feature can also be deduced from the reconstructions shown in Figs. 6 and 7. This implies that in semithin sections in particular the more complex synapses are underestimated in number. Nevertheless, closer examination of the above-mentioned semithin sections taught us that even among the smaller non-perforated synapses deviations from the disc shape can be observed (see e.g. De Groot and Bierman, 1983, Fig. 2). For these reasons it seems justified to believe that complex shapes of EPTA-treated *non-perforated* synapses actually do exist.

Summarizing the discussion about the actual cause of the 'consistent' differences in numerical densities obtained with either the serial section technique or the disector technique, the following conclusions can be drawn.

A rational explanation for the fact that in this example the results of the numerical densities obtained with the disector technique are consistently the lowest would be that the reference section of the disector was always thinner than the estimated section thickness (est T). Such a problem could be largely overcome when more disectors are used, in which case the mentioned effect will be averaged out. Notice that the sampling design in the present example initially was developed for applying the serial section technique and it is clear that this design was not optimal for applying the disector technique. This explanation for the occurrence of consistent differences between the results obtained with both methods may therefore sound rather trivial, but it points out the importance of a reliable estimate of the section thickness in addition to an appropriate sampling design.

Note that serial sections are required for the identification of the synaptic profiles. The synapses in the present example cannot all be identified in only two sections. This implies that, even though the disector technique probably is to be preferred to estimate N_V, serial sections have to be used. Once the serial sections are available both the disector and the serial section techniques can be applied with the same amount of effort. However, the sampling design should be adjusted to the technique chosen. In addition, serial sections may provide extra information about the size of the investigated particle (see e.g. Sterio, 1984), (max l) and about its shape.

Acknowledgements

The authors wish to express their gratitude to Drs. L.M. Cruz-Orive (University of Bern, Switzerland), H.J.G. Gundersen (University of Aarhus, Denmark), T.M. Mayhew (University of Aberdeen, Scotland) and G.F.J.M. Vrensen (Neth. Opth. Res. Inst., Amsterdam, the Netherlands) for the helpful discussions and for their constructive remarks on the first draft of this paper. Drs. J. Voogd (Erasmus University of Rotterdam, the Netherlands) and O.L. Wolthuis are gratefully

acknowledged for critical reading of the manuscript and Mrs T. Westmaas and H. Wilhelmi for skillful typework; Mr M. Boermans for printing the figures.

The constructive and critical comments of the unknown referee of this Journal are greatly appreciated; his/her efforts have led to a considerably improved manuscript.

References

Abercrombie, M. (1946) Estimation of nuclear population from microtome sections, Anat. Rec., 94: 239–247.

Akert, K. (1973) Dynamic aspects of synaptic ultrastructure, Brain Res., 49: 511–518.

Beertsen, W., Everts, V. and Houtkooper, J.M. (1975) Frequency of occurrence and position of cilia in fibroblasts of the periodontal ligament of the mouse incisor, Cell Tiss. Res., 163: 415–431.

Cohen, R.S. and Siekevitz, P. (1978) Form of the postsynaptic density: a serial section study, J. Cell Biol., 78: 36–46.

Cruz-Orive, L.M. (1980) On the estimation of particle number, J. Microsc., 120: 15–27.

Cruz-Orive, L.M. (1983) Distribution-free estimation of sphere size distributions from slabs showing overprojection and truncation, with a review of previous methods, J. Microsc., 131: 265–290.

Cruz-Orive, L.M. (1984) Estimation of N_V from serial slabs, Internal Report Nr. 111/LC 17. [Will be included as appendix to D.M.G. de Groot, Improvements of the serial section method in relation to the estimation of the numerical density of complex-shaped synapses. In A. Reith and T.M. Mayhew (Eds.), Stereology in Electron Microscopy. An illustration of problems and solutions. Hemisphere/McGraw-Hill, New York, in press.]

Cruz-Orive, L.M. (1985a) Estimating particle number and size. In L.F. Agnati and K. Fuxe (Eds.) Quantitative Neuroanatomy in Transmitter Research, MacMillan Press, London, pp. 11–24.

Cruz-Orive, L.M. (1985b) Arbitrary particles can be counted using a disector of unknown thickness: the selector, Internal Report 147/LC 21, August 26–30, J. Microsc., in press.

De Groot, D.M.G. (1984) Improvements of the serial section method in relation to the estimation of the numerical density of complex-shaped synapses. MBL/TNO Internal Report Nr. DG/84-1. [Included in A. Reith and T.M. Mayhew (Eds.), Stereology in Electron Microscopy. An illustration of problems and solutions, Hemisphere/McGraw-Hill, New York, in press.]

De Groot, D.M.G. (1985) Disc-like and complex-shaped synapses: number, size and dense projections. A critical note. Proceedings of the IV European Symposium on Stereology, Göteborg, August 26–30, 1985. Acta Sterologica, 4: 147–151.

De Groot, D.M.G. and Bierman, E.P.B. (1983) The complex-shaped 'perforated' synapse, a problem in quantitative stereology of the brain, J. Microsc., 131: 355–360.

Dyson, S.E. and Jones, D.G. (1980) Quantitation of terminal parameters and their inter-relationships in maturing central synapses. A perspective for experimental studies, Brain Res., 183: 43–59.

Fields, R.D. and Ellisman, M.H. (1985) Synaptic morphology and differences in sensitivity, Science, 228: 197–199.

Gray, E.G. (1959) Axosomatic and axodendritic synapses of the cerebral cortex: an electron microscope study, J. Anat., 93: 420–433.

Greenough, W.T., West, R.W. and De Voogd, T.J. (1978) Subsynaptic plate perforations: changes with age and experience in the rat, Science, 202: 1096–1098.

Gundersen, H.J.G. (1977) Notes on the estimation of the numerical density of arbitrary profiles: the edge effect, J. Microsc., 111: 219–223.

Gundersen, H.J.G. (1986) Stereology of arbitrary particles: A review of unbiased number and size estimators and the presentation of some new ones, in memory of William R. Thompson, J. Microsc., in press.

Hald, A. (1952) Statistical theory with engineering applications, New York, Wiley, London, pp. 401–406.

Hilliard, J.E. (1967) The calculation of the mean caliper diameter of a body for use in the analysis of the number of particles per unit volume. In H. Elias (Ed.), Stereology, Proc. Second Int. Congress Stereology, Springer, Berlin, pp. 211–215.

Holmes, A. (1927) Petrographic Methods and Calculations, Murby, London.

Miles, R.E. and Davy, P. (1976) Precise and general conditions for the validity of a comprehensive set of stereological fundamental formulae, J. Microsc., 107: 211–226.

Miller Jr., R.G. (1966) Simultaneous statistical inference, McGraw-Hill, New York, pp. 67–70.

Müller, L., Pattiselanno, A. and Vrensen, G. (1981) The postnatal development of the presynaptic grid in the visual cortex of rabbits and the effect of dark-rearing, Brain Res., 205: 39–48.

Peters, A. (1970) The fixation of cerebral nervous tissue and the analysis of electron micrographs of the neuropil, with special references to the cerebral cortex. In W.J.H. Nauta, and S.O.E. Ebbeson, (Eds.), Contemporary Research Methods in Neuroanatomy, Springer, Berlin, pp. 56–76.

Peters, A. and Kaiserman-Abramof, J.R. (1969) The small pyramidal neuron of the rat cerebral cortex: the synapses upon the dendritic spines, Z. Zellforsch., 100: 487–506.

Small, J.V. (1968) Measurement of section thickness. In D.S. Bocciarelli (Ed.), Proceedings 4th European Congress on Electron Microscopy, Tipografia Poliglotta Vaticana, Roma, Vol. 1, p. 609.

Sterio, D.C. (1984) Estimating number, mean sizes and variations in size of particles in 3-D specimens using disectors, J. Microsc., 134: 127–136.

Verwer, R.W.H. and De Groot, D.M.G. (1982) The effect of shape assumptions on the estimation of the numerical density of synapses from thin sections, Prog. Brain Res., 55: 195–203.

Vrensen, G. and De Groot, D.M.G. (1974) Phosphotungstic acid staining and the quantitative stereology of synapses. In E. Wisse, W.T. Daems, J. Molenaar, and P. van Duyn, (Eds.), Electron Microscopy and Cytochemistry, Proc. 2nd Int. Symp., Amsterdam, North-Holland, pp. 255–258.

Vrensen, G. and Nunes Cardozo, J. (1981) Changes in size and shape of synaptic connections after visual training: an ultrastructural approach of synaptic plasticity, Brain Res., 218: 79–97.

Vrensen, G., Nunes Cardozo, J., Müller, L. and Van der Want, J. (1980) The presynaptic grid: a new approach, Brain Res., 184: 23–40.

Weybull, C. (1970) Estimation of the thickness of thin sections prepared for electron microscopy, Philips Analytical Equipment EM 45.

Williams, M.A. (1977) Quantitative Methods in Biology. In A.M. Glauert (Ed.), Practical Methods in Electron Microscopy, North-Holland Publishing Company, Amsterdam, New York, Oxford, pp. 13–17.

West, M.J., Coleman, P.D. and Wyss, U.R. (1972) A computerized method of determining the number of synaptic contacts in a volume of cerebral cortex, J. Microsc., 95: 277–283.

PART II

Chapter 5

2D RECONSTRUCTION OF SYNAPSE ORTHOGONAL PROJECTIONS: ESTIMATION OF DIFFERENCES IN SHAPE USING SECOND ORDER MOMENT INVARIANTS

ACTA STEREOL 1992; 11/SUPPL I: 587-592
PROC 8ICS IRVINE, CA, 1991
ORIGINAL SCIENTIFIC PAPER

2D RECONSTRUCTION OF SYNAPSE ORTHOGONAL PROJECTIONS : ESTIMATION OF DIFFERENCES IN SHAPE USING SECOND ORDER MOMENT INVARIANTS

Didima M.G. de Groot, Egbertus P.B. Bierman and Marja J. Saris-Wijnans

Medical Biological Laboratory TNO, P.O. Box 45, 2280 AA Rijswijk

ABSTRACT

2D reconstruction and quantification of synapse orthogonal projections (shadows) are proposed as a practical approach to obtain information about *differences* in their actual configuration. The quantification of the shadows implies estimation of size parameters (area and perimeter) and shape functions (i.e. second order moment invariants independent of location and size). The method was applied to two synapse types, non-perforated and perforated synapses, in the hippocampal CA3 area of 3-months-old rats.
Significant differences in size and shape between non-perforated and perforated synapses were demonstrated. The perforated synapses are larger and the invaginations in their boundary are significantly more pronounced. This may reflect an increased efficacy of the perforated synapses as compared with the non-perforated ones. The difference in invagination of the boundary of the two synapse types could not be detected from visual inspection of the reconstructed orthogonal projections.

Key-words
geometric moments - moment invariants - (non-)perforated synapses - orthogonal projections

INTRODUCTION

In previous studies (De Groot and Bierman, 1983; 1986) it was shown that two types of synapses can be distinguished in the hippocampus of the rat: (i) non-perforated synapses (nps) with a fully covered regularly organized presynaptic grid with dense projections and (ii) perforated synapses (ps) with an interrupted presynaptic grid. The nps are most numerous ($\approx$ 80%); the ps are largest (diameter $\approx$ 400 nm vs. $\approx$ 200 nm). In addition, synapses may be curved and can have an invaginated outline. In a recent study on the effect of ageing on synapses in the hippocampus of the rat it was shown that the ratio of the nps vs. ps, the number of interruptions ("perforations") per ps and the size of the ps was not affected. The size of the nps increased with age; the total number of synapses (nps+ps) decreased with age. It has been postulated (cf Vrensen, 1989) that an increase of the boundary of the active zones by invaginations or by induction of perforations leads to an increase in Ca^{++} channels and vesicle attachment sites which may account for a more efficacious transmission. Problems in proper alignment of subsequent profiles rendered the use of 3D reconstruction inadequate to investigate changes in synapse boundaries with age. In the present paper we propose 2D reconstruction as a practical alternative. This so called "orthogonal projection" or "shadow" approach is described and its validity for the study of synapses is discussed.

MATERIAL AND METHODS

Female rats (Small Wistar, Wag/Rij; 3-Month-old; n=5) were used for this experiment. Synapses in the stratum radiatum of the hippocampal CA3 area were studied, assuming a random orientation of the synapses. The procedures for perfusion fixation, E-PTA treatment (to facilitate the discrimination of the synapses), embedding, ultramicrotomy of serial sections -"vertical sections" were cut-, selection and photography of the synapses and estimation of section thickness have been described previously (De Groot and Bierman, 1986; De Groot, 1988a; 1988b). To distinguish between perforated and non-perforated synapses, all synapses were tracked in adjacent serial sections. The disector method (Sterio,

1984) was applied to obtain a uniform, unbiased sample of synapses -i.e. the, so called, "Q⁻portions"- of both perforated and non-perforated synapses.

To obtain so called "orthogonal projections" of the synapses, the following procedure was carried out. In each of the serial sections in which the "tracked" Q⁻disector-sampled synapse appeared, the "chord length" (i.e. shortest distance between the outer ends) of the intercepts (i.e. profiles) was measured using a semi-automatic image analysis system "Videoplan" (Kontron Messgeräte, Eching, GFR). "Symmetric" reconstructions (Fig. 1A) of the synapses were performed by a program (SYNMORF-DRAWING V4-90) written in the Fortran language by one of us (EPB B). In a reconstruction the centre-points of all intercept chord lengths of a tracked synapse -i.e. the chord length(s) of the transmission zone(s) including the chord length(s) of possible perforation(s) (open spots in Fig. 1A)- are put on top of each other. The width of a drawn chord length equals the section thickness used. Obviously, the reconstruction depends on a reliable estimate of the section thickness. In this paper, such an estimate was obtained by measuring small folds in the section (cf. De Groot, 1988a). Subsequently, the boundary of the resulting figure is "smoothed" (Fig. 1B). These "symmetric" reconstructions are comparable with "orthogonal projections" or "shadows". The hardware used was a VAX/VMS 8250-computer (Digital Equipment Corporation, Maynard, Massachusetts) and a ZETA8-plotter (NICOLET).

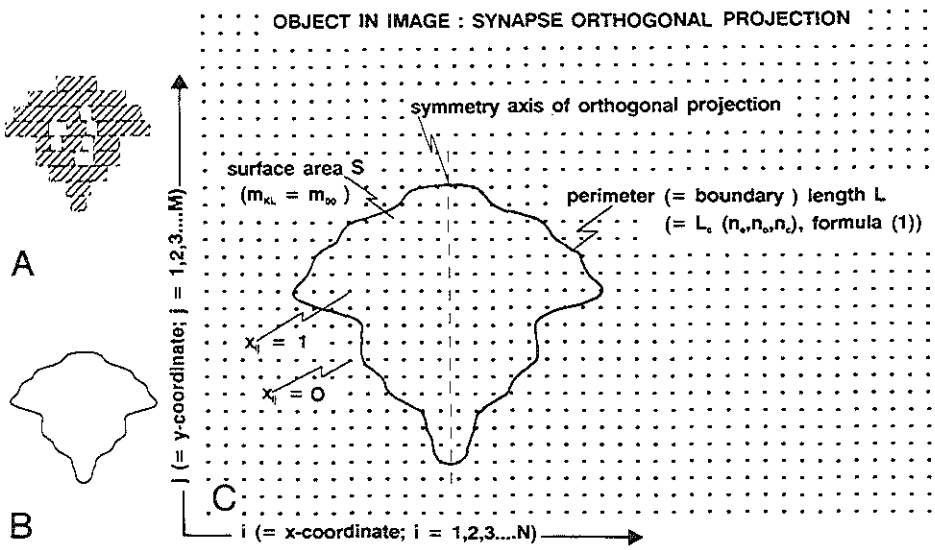

Fig. 1. 2D-symmetric reconstruction of a synapse : A,B) cf. Materials and Methods; C) binary image of B.

To see whether differences in synaptic size and shape exist between perforated and non-perforated synapses the perimeter (i.e. boundary length) L, the surface area S (Fig. 1C) and the moment invariants η_{20} and η_{02} and Φ_1 (Fig. 2) were calculated for each orthogonal projection of the Q⁻ synapses. The latter three variables are functions of geometric moments and are invariant under image translation, scaling and rotation (Fig. 2 and legends). The calculations were performed with a program (AREA-HE V8-90) written in the Pascal language (EPB B). For these calculations an 8-connected-chaincode scheme (Freeman, 1961), coding the contour of the drawn (smoothed) synapse projection (Fig. 2B), was used. This coding was derived from the coordinates of the drawing.

To obtain the perimeter L, the corner count estimator, proposed by Dorst and Smeulders (1987, formula 24) was calculated.

$$L_c(n_e, n_o, n_c) = an_e + bn_o + cn_c \qquad (1)$$

where : L_c = corner count estimator; n_e,n_o = number of even/ odd chaincode elements in the contourstring; n_c = (corner count) number of "knight's moves" (number of occurrences of consecutive unequal i.e. odd-even or even-odd sequences in the contourstring); a,b,c = coefficients for the (n_e, n_o, n_c) characterization; in this case a = 0.980, b = 1.406 and c = -0.091. For the derivation of a, b and c the reader is referred to the original paper of Dorst and Smeulders (1987), formulae 22-24.

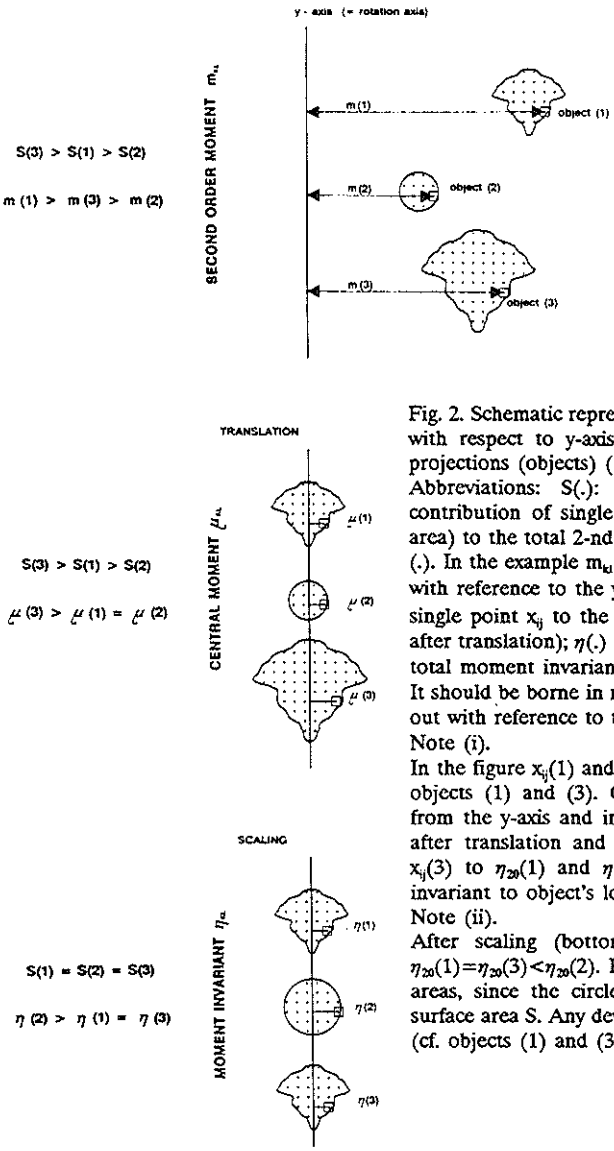

Fig. 2. Schematic representation of the translation and scaling with respect to y-axis of the binary images of orthogonal projections (objects) (1), (2) and (3).
Abbreviations: S(.): surface area of object (.); m(.): contribution of single point x_{ij} (point in delineated square area) to the total 2-nd order geometric moment m_{kl} of object (.). In the example m_{kl} is m_{20} (axial quadratic surface moment with reference to the y-axis ($\Sigma i^2 \cdot j^0 \cdot x_{ij}$); $\mu(.)$=contribution of single point x_{ij} to the total central moment μ_{kl} (i.e. $\mu_{20}=m_{20}$ after translation); $\eta(.)$ = contribution of single point x_{ij} to the total moment invariant η_{kl} (i.e. $\eta_{20}=\mu_{20}$ after scaling).
It should be borne in mind that this procedure is also carried out with reference to the x-axis, resulting in m_{02}, μ_{02} and η_{02}. Note (i).
In the figure $x_{ij}(1)$ and $x_{ij}(3)$ are identically located within the objects (1) and (3). Objects (1) and (3) differ in distance from the y-axis and in size but not in shape. Consequently, after translation and scaling the contribution of $x_{ij}(1)$ and $x_{ij}(3)$ to $\eta_{20}(1)$ and $\eta_{20}(3)$, respectively, is the same (η_{kl} is invariant to object's location, size and orientation!).
Note (ii).
After scaling (bottom figure): S1= S2= S3. However, $\eta_{20}(1)=\eta_{20}(3)<\eta_{20}(2)$. By definition, η_{kl} is minimal in circular areas, since the circle is the "minimal configuration" of a surface area S. Any deviation from this minimal configuration (cf. objects (1) and (3)) will result in an increase of η_{kl}.

In principle L_c is unbiased over an ensemble of long straight strings. In this case, the contour length of the orthogonal projections was approximated as a concatenated series of circular arcs. Although not designed for such situations, L_c is remarkably accurate (Dorst and Smeulders, 1987).

The 0-th order geometric moment m_{00} (=S) and the moment invariants η_{20}, η_{02} and Φ_1 were obtained as follows (Chen, 1990).

Basic knowledge learns that a digital image can be represented by moments of its intensity functions. The discrete form of the (K,L)-th (geometric) moment of an object in an image is defined by

$$m_{KL} = \sum_{i=1}^{N} \sum_{j=1}^{M} i^K j^L x_{ij} \qquad (2)$$

where : m = moment; K,L = order indicators; the order of the moment equals K plus L; N,M =

number of coordinates in x/y direction of image, i = x coordinate; i=1,2,3...N, j = y coordinate; j=1,2,3...M, x_{ij} = binary value at the point (i,j). Note that the point (i,j), by definition, represents the area of the pixel at point (i,j); x_{ij} = 1, if point (i,j) is on or within (the contour of) the object; x_{ij} = 0, if point (i,j) is outside the object.

The area (S) of the binary image of the object is represented by the 0-th order geometric moment m_{00} (K and L zero; $\Sigma i^0 \cdot j^0 \cdot x_{ij}$; note $i^0=1$; $j^0=1$).

m_{00} together with the 1-st order geometric moments m_{10} and m_{01} locate the centroid (i.e. centre of gravity= point i_o,j_o) of an object in the image. The centroid is defined by

$$i_o = m_{10} / m_{00} \qquad j_o = m_{01} / m_{00} \tag{3}$$

The centroid, together with the 2-th order geometric moments m_{20} and m_{02} (i.e. axial quadratic surface moments with reference to y- and x-axis, respectively) were used to compute the central moments μ_{20} and μ_{02}

$$\mu_{20} = m_{20} - m_{10}^2 / m_{00} \qquad \mu_{02} = m_{02} - m_{01}^2 / m_{00} \tag{4}$$

The polar quadratic surface moment I is

$$I = \mu_{20} + \mu_{02} \tag{5}$$

Note In the present study I is calculated, assuming different configurations (i.e. "shapes") of the objects (i.e. the reconstructed orthogonal projections). I for the actual reconstruction, i.e. symmetry in the x-direction, is called I_o (i.e. $I_{observed}$) with surface area S_o (i.e. $S_{observed}$). To estimate deviations of the reconstructed shape from circularity or ellipticity I was calculated, *ignoring the actual shape of the reconstruction and assuming* the object (i) to have the minimal configuration of *a circle* with surface area S_o which, by definition, shows equal symmetry in both x- and y-directions or (ii) to be *an ellipse* with principle axes A and B, i.e. unequal symmetry in x- and y-directions; A and B are calculated from the observed central moments μ_{20} and μ_{02} and zero-th order moment m_{oo} (=S_o): A=4sqrt(μ_{02}/m_{oo}); B=4sqrt(μ_{20}/m_{oo}). The resulting I's are called here: I_c (i.e. I_{circle}) and I_e (i.e. $I_{ellipse}$).

The central moments μ_{20} and μ_{02} were normalized for scaling as follows

$$\eta_{20} = \mu_{20} / \mu_{00}^2 \qquad \eta_{02} = \mu_{02} / \mu_{00}^2 \tag{6}$$

where : η_{KL} = moment invariant

Finally, the moment invariant Φ_1 is

$$\Phi_1 = \eta_{20} + \eta_{02} \tag{7}$$

From the moments mentioned above only the resulting moment invariants η_{20}, η_{02} and Φ_1 are independent upon location, size and orientation of the investigated particles. Differences between the two synapse types in the estimated mean values of the 3 variables can result only from differences in shape. However, it should be borne in mind that- although est $E\eta_{20}$, est $E\eta_{20}$ and est $E\Phi_1$ are unbiased variables characterizing the shape of an object- knowledge on the shape of the orthogonal projections cannot simply be extrapolated to the actual shape of the synapses. Nevertheless *differences* in the shape of orthogonal projections clearly do reflect *differences* in the actual shape of the synapse.

RESULTS AND DISCUSSION

Estimates of the mean surface area (est ES), the mean perimeter (est EL), mean moment invariants with reference to the x-axis (est $E\eta_{02}$) and y-axis (est $E\eta_{20}$) and the mean moment invariant est $E\Phi_1$,(=$\eta_{20}+\eta_{02}$) are shown in Tbl. 1. Between non-perforated and perforated synapses significant differences were found for est ES and est EL (paired t-test, $P2 \leq 0.05$), indicating a significant difference in size. For est $E\eta_{02}$, est $E\eta_{20}$ and $E\Phi_1$, estimates that might reflect differences in shape, significant differences were found only for $E\eta_{20}$ (paired t-test, P2=0.043). Regression analysis of the relationship (x-axis : y-axis) between L and S resulted for the non-perforated synapses in log y=-0.307+1.6604 log x (significant regression, $P < 0.0001$, R^2=86.3%); the 95% confidence limits of the slope and the intercept being (1.57, 1.75) and (-0.57, -0.04), respectively. For the perforated synapses the analysis resulted in log y=-0.122+1.5974 log x (significant regression, $P < 0.0001$, R^2=84.1%); the 95% confidence limits of the slope and the intercept being (1.31, 1.88) and (-1.02, 0.78), respectively. Regression analysis of the relationship (x-axis : y-axis) between η_{02} and η_{20} resulted for the non-

perforated synapses in log y=9.83-0.998 log x (significant regression, $P < 0.0001$, R^2=93.6%); the 95% confidence limits of the slope and the intercept being (-1.03, -0.96) and (9.64, 10.02), respectively. For the perforated synapses log y=10.68-1.153 log x (significant regression, $P < 0.0001$, R^2=88.4%); the 95% confidence limits of the slope and the intercept being (-1.32, -0.98) and (9.77, 11.59), respectively. The significant regression between L and S demonstrates that an increase in S is followed by a comparable increase in L; the significant regression between η_{02} and η_{20} indicates a "uniform" shape for small and larger synapse orthogonal projections. Comparison of the regression equations (Kleinbaum and Kupper, 1978) of both synapse types showed significant differences for the relationship log η_{02} : log η_{20} (P=0.0002). It is noted that the relationship L : S (P=0.81, not significantly different), cannot be used to show differences in shape since differently shaped synapses may have an identical area size and an identical perimeter length. Summarizing, the results indicate that perforated synapses are larger than non-perforated ones and that these types of synapses slightly differ in shape.

Table 1. Estimates of different variables of orthogonal projections of non-perforated and perforated synapses in the stratum radiatum of the hippocampal CA3 area of 3-month-old rats.

		non-perforated		perforated	
variable	dimension	[mean]*	CE	[mean]*	CE
S	10^1 nm^2	3252	10.9	9441	17.1
L	nm^1	761	5.4	1517	7.7
η_{02}**	nm^0	0.151	5.2	0.217	12.1
η_{20}**	nm^0	0.0537	3.7	0.0399	11.6
Q_1	nm^0	0.205	2.9	0.256	8.5

[mean], estimated mean value; CE, coefficient of error of the mean ((sem/mean)•100%); *, n = 5 rats; **, since the orthogonal projections are symmetric with respect to the y-axis and not with respect to the x-axis, the values of η_{20} are smaller than those of η_{02}.

To speculate on the actual shape of both synapse types, the polar quadratic surface moment I was calculated for the reconstructed orthogonal projections, assuming different configurations. Est I, calculated from the *observed* orthogonal projections (I_o) after pooling the projections of the 5 rats used was $248•10^6$ nm^4 and $2506•10^6$ nm^4 for the non-perforated (n=197) and perforated (n=27) synapses, respectively. Assuming circularity (I_c) these values were $204•10^6$ nm^4 and $1608•10^6$ nm^4 and assuming ellipticity (I_e) these values were $264•10^6$ nm^4 and $2696•10^6$ nm^4.

I_o, being significantly *larger* than I_c and *smaller* than I_e, appeared to differ significantly more from circularity (mean 19.0%, CE 5.8% for non-perforated and mean 31.0%, CE 8.0% for perforated synapses) than from ellipticity (mean 4.7%, CE 8.9% for non-perforated and mean 9.3%, CE 16.2% for perforated synapses) (Wilcoxon's signed rank test, $P2 < 0.0001$). As mentioned in Material and Methods, the ellipse-shape implies (unequal) symmetry in the x- and y-directions whereas the actual shape is symmetric only in the x-direction. Nevertheless I_c is larger than I_o. The ratio A : B of the principle axes of the fictive ellipse proved to be for the non-perforated synapses approximately 1.56:1; for the perforated synapses 2.20:1. In conclusion, these findings indicate that the actual shape of S of the synapse orthogonal projections must roughly resemble an ellipse with axial ratio for the non-perforated synapses (1.56>x>1):1; for the perforated synapses (2.20>x>1):1.

If it is assumed that the shape of the actual synapse resembles a disc (cf. West et al., 1972), then the "shape" of their orthogonal projections will range between a line and a circle. The "average" shape will resemble an ellipse with axial ratio (1.57>x>1):1. In principle, the results of the present study are not in conflict with this theoretical approach. The suggestion is made here that the *"rough"* shape of the synapses in this study approximates the shape of a disc. The differences in shape found at present do not point at pronounced variations in the "rough" shape of the synapse but rather in the fine shape. These variations in the "fine" shape include an extension of the boundaries, i.e. border zones, of the synapse by induction of invaginations and perforations. Evidence is increasing that in particular this type of changes at the border zones of the synapse are very important with regard to synaptic functioning.

Regression analysis of the relationship (x-axis : y-axis) between log I_o and log I_c resulted for the non-perforated synapses in log y=-0.288+1.023 log x (significant regression, $P < 10^{-4}$, R^2=95.6%); the 95% confidence limits of the slope and the intercept being (0.99, 1.05) and (-0.54, -0.03), respectively. For

the perforated synapses this analysis resulted in log y=0.446+0.933 log x (significant regression, $P < 0.0001$, $R^2=96.5\%$); the 95% confidence limits of the slope and the intercept being (0.86, 1.01) and (-0.22, 1.11), respectively. Regression analysis of the relationship (x-axis : y-axis) between log I_o and log I_c resulted for the non-perforated synapses in log y=-0.123+1.017 log x (significant regression, $P < 0.0001$, $R^2=99.8\%$); the 95% confidence limits of the slope and the intercept being (1.01, 1.02) and (-0.18, -0.07), respectively. For the perforated synapses log y=0.098+0.993 log x (significant regression, $P < 0.0001$, $R^2=99.6\%$); the 95% confidence limits of the slope and the intercept being (0.97, 1.02) and (-0.14, 0.34), respectively.
Summarizing, the significant regression for the relationships $I_o : I_c$ and $I_o : I_o$ and a variation explained by the regression of more than 95% indicate a "constant" deviation from circularity or ellipticity with increasing size of the synapse orthogonal projections.

In conclusion, whatever the actual shape of the investigated synapses may be, the results of the measurements on their orthogonal projections show that there is a difference in size, but also in shape between the non-perforated and perforated synapses of this study. The deviations from circularity or ellipticity may reflect "invaginations" in the boundary of the orthogonal projections which, in turn, must reflect "irregularities" in the shape of the actual synapse. These irregularities are most pronounced in the perforated synapses and most likely indicate increased efficacy of this synapse type (cf. Vrensen, 1989). It is concluded that, compared with 3D reconstruction, the proposed 2D reconstruction approach is rather simple and differences found in the shape of synapse orthogonal projections demonstrated with this method reflect *differences* in the shape of the synapse. The method certainly has its limitations, in particular, with respect to the orientation and distribution of the synapses in the tissue and it does not permit firm conclusions about the *actual* shape of the synapse as 3D reconstruction does. Nevertheless, the method provided relevant information about synaptic functioning which could not be obtained by other means; 3D reconstruction was hampered by alignment problems which, so far, were unsolvable.

REFERENCES

Chen, K. Efficient parallel algorithms for the computation of two-dimensional image moments. Pattern Recognition 1990; 23(1/2): 109-119.

De Groot, DMG and Bierman, EPB. The complex-shaped "perforated" synapse, a problem in quantitative stereology of the brain. J Microsc 1983; 131: 355-360.

De Groot, DMG and Bierman, EPB. A critical evaluation of methods for estimating the numerical density of synapses. J Neurosc Methods 1986; 18: 79-101.

De Groot, DMG. Comparison of methods for the estimation of the thickness of ultrathin tissue sections. J Microsc 1988a; 151: 23-42.

De Groot, DMG. Improvements of the serial section method in relation to the estimation of the numerical density of complex-shaped synapses. In Reith A. Mayhew TM. eds. Stereology and Morphometry in Electron Microscopy. Problems and Solutions New York, London: Hemisphere Publishing Corporation; 1988b: 135-158.

Dorst, L and Smeulders, AWM. Length estimators for digitized contours. Computer vision, graphics and image processing 1987; 40: 311-333.

Freeman, H. On the encoding of arbitrary geometric configurations. IEEE Trans on Computers 1961; C10: 260-268.

Kleinbaum, DG and Kupper, LL. Applied Regression Analysis and Other Multivariable Methods, North Scituate, Massachusetts: Duxury Press; 1978: 190-192.

Sterio, DC. Estimating number, mean sizes and variations in size of particles in 3-D specimens using disectors. J Microsc 1984; 134: 127-136.

Vrensen, GFJM. Learning, Memory and long-term synaptic plasticity in the mammalian brain. In: Rahmann H. ed. Fundamentals of memory Formation: Neuronal Plasticity and Brain Function Stuttgart, New York: Gustav Fisher Verlag; 1989: 132-147.

West, MJ, Coleman, PD and Wyss, UR. A computerized method of determining the number of synaptic contacts in a volume of cerebral cortex. J Microsc 1972; 95: 277-283.

PART III

QUANTITATIVE ASSESSMENT OF SYNAPSES AND NEURONS IN THE HIPPOCAMPUS OF AGEING RATS

QUANTITATIVE ASSESSMENT OF SYNAPSES AND NEURONS IN THE HIPPOCAMPUS OF AGEING RATS

Didima M.G. De Groot, Egbertus P.B. Bierman and Marja J. Saris-Wijnans

TNO Medical Biological Laboratory,
PO Box 5815, 2280 HV Rijswijk,The Netherlands

SUMMARY

In the present paper different methods are described which, in principle, can be used to quantify any morphological element. Specifically, the effect of age on the number, size and shape of synapses and neurons in the hippocampus of the rat is studied. Wherever possible, methods have been used providing unbiased estimates of the investigated parameters. In general, the effect of age on the parameters measured was found to be mild. The following observations were made:

1) no change in the numerical relation between numbers of CA1 and CA3 pyramidal neurons;
2) no change in the numerical relation between numbers of CA3 synapses (stratum radiatum) and CA3 pyramidal neurons; the apparent decrease in synapse numbers from 12 to 24 months of age is not significant;
3) no change in the numerical relation between numbers of perforated and non-perforated synapses in CA3, stratum radiatum;
4) an increase in size of the non-perforated synapses;
5) no change in the number of perforations per perforated synapse; significantly larger perforations at high age (30 months);
6) an increase in numbers of presynaptic dense projections;
7) no change in size and shape of synapse shadows; the shape of both synapse types deviates considerably from the presumed disc-shape.

Perforated synapses are found to be larger and more 'complex' (presence of perforations and relatively more dense projections) than the non-perforated synapses.

The reliability and value of the different variables are discussed in relation to the effect of age on the neural structures studied.

The results, taken together, suggest that the number of synapses per neuron in the hippocampal CA3 area is not affected by age. The efficacy of the synapses increases with age, expressed by an increase in the number of dense projections in the active zone (transmission zone), an increase in size of the active zone (non-perforated synapses) and a larger size of the perforation area in the active zone (perforated synapses) at high age (30 months). Impairment of the synaptic circuitry in this area in older rats (30 months) is not likely to occur.

INTRODUCTION

Different factors active during development and ageing of the brain, such as training, learning, malnutrition, deprivation, pharmacological treatment or sensitizing lesions, are known to induce changes in synaptic physiology and biochemistry. These lesions most likely have their counterparts in changes in synaptic ultrastructure.

The first studies reporting quantitative data on synaptic ultrastructures appeared in the late sixties/early seventies. In particular, the number of synaptic contact zones per unit section area (n_a(synapses)) (cf. e.g. Aghajanian and Bloom, 1967; Bloom, 1970; Field, 1972; Fifková, 1970; Fisher, 1972; Molliver and Van der Loos, 1970; Nicholson and Altman, 1972; West et al., 1972) and the synaptic intercept length (l(syn)) observed in the tissue section (cf. e.g. Cragg, 1967a, 1967b, 1969, 1971, 1972) were measured. In the years thereafter, stereological formulae (cf. e.g. Weibel, 1979 chapters 2 and 5 and 1980 chapter 8 and references therein; Cruz-Orive, 1983 and references therein) were used to extrapolate these measurements into estimates, describing 3-dimensional aspects of the synapses i.e. the number of synapses per unit tissue volume (N_V(syn)) and the true diameter of the synapse (D(syn)), respectively. Unfortunately, the stereological methods available at that time were based on assumptions about the size, shape and orientation of the particles. Moreover, the methods started from the assumption that the original measurements were obtained from a true plane. However, a tissue section, even an ultrathin section, does not fulfil this requirement. As a consequence, measurements in a tissue section are biased by overprojection and/or truncation effects. Correction formulae for these aberrations were developed (cf. Cruz Orive, 1983 and references therein). However, the final effect of such corrections is always hard to predict since the extent of overprojection and truncation biases is never known. The neurobiologist was confronted with the fact that no method was available to obtain unbiased estimates of numbers and sizes of synapses and/or neurons (let alone their shapes); a fact that would remain so till 1980 (see below).
Another shortcoming of most of the earlier studies is the fact that in those studies, possible changes in the reference volume that might result from the experimental manipulation, were not taken into account.
As a consequence, the interpretations in many of these studies cannot be trusted because the results were biased to an unknown extent.
However, despite all biases, the early studies (still) have an unprecedented value: the fact that changes in synaptic number and size were found under the various experimental conditions mentioned above has contributed to our knowledge about "plasticity" of the nervous system.

In 1980 Cruz-Orive introduced a method for estimating numbers of arbitrarily-shaped particles. This method does not rely on assumptions and is insensitive to overprojection and truncation. Serial sectioning is inherent to this method. Probably because of this tedious serial sectioning only a few papers using this method for estimating synaptic densities appeared in the literature (Bedi et al., 1984; Calverly and Jones, 1987; De Groot, 1985,

1988b; De Groot and Bierman 1983, 1986; Geinisman et al., 1986 a, 1986 b; Verwer and De Groot, 1982). In contrast, papers using conventional stereological methods and producing biased results, kept appearing in increasing numbers.
Fortunately, this policy has started to reverse since the introduction of the disector (Sterio, 1984). As was shown by e.g. De Groot and Bierman (1986) and Braendgaard and Gundersen (1986) the disector provides efficient and unbiased estimates of synaptic number and size.

Changes in the reference volume, due to experimental conditions, have been taken into account more and more (cf. e.g. Cruz-Orive and Myking, 1981; Uylings et al. 1986; De Groot and Bierman, 1987).

In long-term toxicity studies, such as on-going in our institute, the age of the individual may be an important factor. It was considered desirable, therefore, to obtain quantitative data on morphological aspects of the nervous system. In the present study, two key-structures in neuronal transmission, i.e. neurons and synapses, have been studied. The hippocampus was chosen as a structure because it is involved in learning and memory. The characteristic pyramidal neurons of the hippocampus, whose cell bodies are located in stratum pyramidale and whose main dendrites are located in stratum radiatum, have been selected for the quantification of neurons. The quantification of synapses has been carried out in stratum radiatum.

This paper describes

- the estimation of the number of CA1 and CA3 pyramidal neurons and of so called 'non-perforated' and 'perforated' synapses in the hippocampal CA3 area of rats of different ages (3, 12, 24 and 30 months) using the disector technique (Sterio, 1984). A synapse is called perforated when the outline of the array (or 'grid') of presynaptic dense projections clearly is non-convex (e.g. horseshoe-shaped) or not simply connected. In any case the presynaptic grid of dense projections localy is devoid of dense projections. The dense projection free area in the grid is called the 'perforation'. A perforation does not represent a true hole in the cell membrane.
- As a measure of the size of both synapse types, the mean maximum intercept length has been estimated as well as mean projected height (linear projection) (fig. 1). Also for the nuclei of the pyramidal cells, the mean projected height was estimated.
- The number of presynaptic dense projections per synapse (fig. 2) has been determined for both types, in different ways (Cruz-Orive, 1985; De Groot, 1985). These dense projections play a crucial role in transmitter release (Akert, 1973) and their number may be considered as a measure of synaptic efficacy.
- Relevant to synaptic efficacy is the number of perforations per perforated synapse, which is also estimated (fig.2). It has been suggested (cf. Vrensen, 1989) that an increase in boundary (border zones) of the synaptic transmission zone by induction of "perforations" results in a potentially enhanced synaptic transmission.

- An attempt has been made to study indirectly the effect of age on the shape of both types of synapses, using 2D reconstructions of orthogonal projections (shadows) of the synapses (De Groot and Bierman, 1986; De Groot et al.,1992).
- To avoid problems encountered in the estimation of the reference volume (see Discussion), numerical fractions of 1) CA1 to CA3 pyramidal neurons, 2) CA3 synapses to CA3 pyramidal neurons and 3) CA3 perforated to CA3 non-perforated synapses, have been estimated.

The results of these morphological studies of synaptic plasticity in the hippocampus of ageing rats have been compared with those from other studies. Attention has been given to the possible bias in some of the published and present results, inherent to the method(s) used.

MATERIALS AND METHODS

Tissue preparation and tissue sampling

The subjects of this study were female Small Wistar (Wag/Rij) rats, aged 3, 12, 24 and 30 months (7 animals/age group). Mean (± SEM) bodyweights (g) at the time of sacrifice were: 142 ± 4.0 (3M), 214 ± 6.1 (12M), 259 ± 5.9 (24M) and 268 ± 7.1 (30M).

After transcardial perfusion with glutaraldehyde/paraformaldehyde mixtures according to Peters (1970), the brains were removed. This fixative was chosen in view of the ultrastructural studies carried out in the left hemispheres of these rats (see below). The right hemispheres were stored overnight in 4% formalin and were subsequently prepared for embedding in paraplast using standard histological procedures. From the left hemispheres the hippocampi were taken out after fixation by perfusion. Transverse slabs of approximately 4 mm were cut from the hippocampi with a fan-shaped set of razor-blades (cf. De Groot, 1988b, fig. 1). Vibratome slices (Oxford Instruments) of 75 μm were cut from these slabs and under the dissecting microscope both the CA1 and CA3 areas were dissected. The dissected tissue slices were either treated with osmium tetroxide (OsO_4) (Palade, 1952) or with ethanolic phosphotungstic acid (E-PTA) (Vrensen and De Groot, 1973a). For embedding in Epon 812 the OsO_4 and E-PTA treated tissues were oriented in such a way that cutting with the ultramicrotome could start perpendicular to the ventricular surface.

The OsO_4 treated tissue of the left hippocampus was used for a qualitative investigation of the ultrastructure (De Groot and Bierman, 1983). The E-PTA treated slices were used for a quantitative study of the pyramidal cell bodies in stratum pyramidale and the synapses in stratum radiatum. As was shown (De Groot and Bierman, 1983) the E-PTA stained synaptic image is different from the OsO_4 treated one, because the synapse appears against a more or less unstained background, a feature which facilitates their discrimination. Apart from this, E-PTA treated tissue was essential for the quantification of the so called, 'presynaptic dense projections' (see below) which can clearly be distinguished in E-PTA treated synapses. In OsO_4 treated synapses, contrary to E-PTA synapses, the membranes of the transmitter vesicles are visualized (fig.2). Since these vesicles are preferentially positioned around and on top of the dense projections, it is impossible to make a clear distinction between vesicles and dense projections.

The use of 75 μm vibratome slices was essential since incubation in E-PTA of small tissue blocks often results in an uneven staining of synapses throughout the tissue (cf. Vrensen and De Groot, 1973a).

The right hemispheres, embedded in paraplast, were used for other purposes.

Quantification of (pyramidal) neurons (and synapses)

From E-PTA treated tissue of the hippocampal CA1 and CA3 areas, serial sections were cut on an ultramicrotome (Reichert OmU3) at a preset thickness of 0.5 μm (fig. 3). A reliable estimate of the section thickness t' was obtained by measuring the thickness of the sections with the Vicker's M86 scanning microinterferometer (cf. De Groot 1988a).

Every 10-th section of a series of 111 (=k) sections was collected and

stained with toluidine blue. The pyramidal layer was photographed on Panatomic-X film (Eastman Kodak Company, USA) using a photo/light microscope (Zeiss, West Germany) with a 100x oil objective (planapo 100/1.3 oil, 160/-, Zeiss, West Germany). The photographs were printed at a final magnification of 2450x. The magnification was calibrated with an objective-micrometer (1 mm = 100 units).

For the estimation of the number of pyramidal cells (and projected height H of their nuclei (see below) the disector "stack" procedure was performed (Sterio, 1984). In principle, the number of pyramidal cell *nuclei* was counted to obtain information about *cell* numbers, since CA1 and CA3 neurons contain only one nucleus per neuron. Gundersen's (1977) unbiased counting rule was applied during counting. The samling and counting procedure is shown in fig. 3.

A stack of n sections -n = 11* the 10-th section of a series of k sections (see above)- was composed of (n-1) disectors. The section pair, composing a disector, i.e. the reference plane and look-up plane, consisted of two sequential "10-th"-sections, e.g. the 1-st and 11-th section, the 11-th and 21-st section, and so on.

Nuclei present in the reference area A_i of the reference plane are called "Q"; those present in A_i(reference plane) but not in the look-up plane are called "Q^-" (Sterio, 1984). To obtain the Q^- portion of the nuclei of the first disector of the stack (= $Q(1)^-$) the reference area A_i of the first disector (= 1-st section of the series; = 1-st section of the stack) was compared with the look-up area of the first disector (= 11-th section of the series; = 2-nd section of the stack). This latter area, i.e. the look-up area of the first disector, subsequently served as reference area of the second disector and was compared with the 21-st section of the series (= look-up area of the second disector; = third section of the stack) to obtain $Q(2)^-$. This procedure was followed through the complete stack of n sections. Doing so, the look-up plane of one disector is the reference plane of the next. The very first and very last (= n-th) sections of the stack are exceptions; they were used only once.

Since the cells have only one nucleus, an estimate of the number of pyramidal cell neurons per unit disector volume was obtained as follows :

$$\text{est } N_v = \sum_{i=1}^{m} \left(\sum_{j=1}^{n_i} Q^-_{ij} \Big/ \sum_{j=1}^{n_i} h_{ij}\, A_{ij} \right) / \, m \qquad (3.1.)$$

where

est N_v	=	estimated total number of particles per unit disector volume
m	=	number of stacks (= series)
n_i	=	number of disectors in i-th stack
Q^-_{ij}	=	number of pyramidal cell nuclei, present in A_{ij}(reference plane) but not in A_{ij}(look-up plane) of j-th disector in i-th stack
h_{ij}	=	distance in disector between A_{ij}(reference plane) and A_{ij}(look-up

plane).

A_{ij} = reference area of the reference plane in the j-th disector in i-th stack

h_{ij} was obtained as follows

$$h_{ij} = kEt' \qquad (3.2.)$$

where

k = number of sections in the series composing the height of the disector (not to confuse with the number of sections in the stack!)

E^*t' = mean section thickness (cf. De Groot, 1988a)

To avoid problems, resulting from a lack of knowledge about the reference volume (see: Discussion), the following numerical fractions N_N were estimated:

1) N_V(pyr. neurons, CA1 str. pyr.) / N_V(pyr. neurons, CA3 str. pyr.);
2) N_V('all' synapses, CA3 str. rad.) / N_V(pyr. neurons, CA3 str. pyr.).
Estimation of N_V(synapses) is given below.

The size parameter 'projected height' (H) (= linear projection) of the nuclei (n) was also calculated according to Sterio (1984). For this, the Q and Q^- portions determined in the stacks for the estimation of the number of nuclei were used.

Thus, EH(n) is obtained :

$$\text{est } EH = \sum_{i=1}^{m} \left[\left(\sum_{j=1}^{n_i} Q_{ij} \sum_{j=1}^{n_i} h_{ij} \right) / \sum_{j=1}^{n_i} Q^-_{ij} \right] / m \qquad (3.4.)$$

where

est EH = estimated mean projected height of the nuclei

Q_{ij} = number of pyramidal cell nuclei, present in A_{ij}(reference plane of the j-th disector in i-th stack

m, Q_{ij}, Q^-_{ij}, h_{ij} and n_i are as indicated above for formula 3.1.

EH requires a random orientation distribution of either the nuclei or the disectors (Sterio, 1984). Comparison of stratum pyramidale after sectioning in different (random) directions indicated that it is justified to

---

*In this paper and in the corresponding Appendix the notation E is used for 'average mean' instead of for its literal meaning 'Expectatia', which is a mathematical term.

assume a random orientation distribution of the nuclei in stratum pyramidale of both the CA1 and CA3 areas.

Quantification of synapses and synaptic substructures

General approach and requirements.

To distinguish between the two types, i.e. non-perforated and perforated synapses, they were tracked in adjacent serial sections (for details, see De Groot and Bierman, 1983; De Groot, 1988b).

To obtain an estimate of the number of both types of synapses the disector method (Sterio, 1984; Gundersen, 1986) was applied. Since the minimal projected height of the smallest synapse min H_i appeared to be smaller than the section thickness t', adjacent sections were used for the section pair, i.e. the reference plane and the look-up plane, composing a disector.

A reliable estimate of the section thickness t' of the ultrathin sections (< 50 nm) was obtained using the Small fold technique (cf. De Groot, 1988a).

Taking the need of the tracking procedure for identification of the synapses into account, disectors were always taken approximately in the middle of the series of sections so that tracking could occur up and down in the series. The centre section of a series was considered as the 'reference plane' of the disector and both adjacent sections as the 'look-up plane' resulting in two disectors with a common reference plane (cf. De Groot and Bierman, 1986). At least 5 series (= 10 disectors) per animal were analyzed. Per age group the estimates of 4 to 6 rats were averaged. Synapses present in the reference area A_i of the reference plane are called 'Q'; those, present in A_i(reference plane) but not in the look-up plane are called 'Q$^-$' (Sterio, 1984).

When counting and/or measuring in A_i(reference plane) and/or A_i(look-up plane) Gundersen's (1977) unbiased counting rule was applied. The Q$^-$ portion of the synapses was used to estimate the number of non-perforated and perforated synapses and their mean maximum intercept (=profile) length Emax1 with corresponding dense projections E(nDP/max1) (figs. 1 and 2), as well as the mean number of synapse perforations per perforated synapse Ep_0.

In addition, this Q$^-$ portion was used to reconstruct, so called, 'orthogonal projections' (shadows) of the synapses (De Groot and Bierman, 1986; De Groot et al., 1992). Parameters, invariant to size, shape and orientation of the investigated particles were estimated to describe the size and shape of these shadows. These calculations were carried out on the shadows to study (indirectly) whether age-related changes in the shape of both synapse types occur.

Combined information of the Q$^-$ and the Q portions of the synapses and of the synapse perforations was used to estimate their mean projected height EH (Sterio, 1984).

The Q portion of the synapses (and of the synapse perforations) was used to estimate their mean perimeter length EL and their mean (presynaptic) surface area ES (Cruz-Orive, 1985). The latter two parameters are essential to predicte the number of dense projections per presynaptic surface area En_0 according to the, so called, 'tile model' (Cruz-Orive, 1985; De Groot, 1985) (see below).

The formulae used to calculate the quantitative morphological parameters, mentioned above, were mainly adapted from Sterio (1984) and Cruz-Orive (1985). For the sake of completeness the formulae used in the present study are given in an appendix. The reconstruction procedure for the synapse orthogonal projections and the measurements carried out on them are also included in this appendix. The latter procedure is based mainly on the papers of Hu (1962), Chen (1990) and Dorst and Smeulders (1987).

Statistics

The results of this study were tested statistically with one or more of the following tests.
One-way (multiple) analysis of variance ((M)ANOVA) to test differences between the 4 age groups (Hollander and Wolfe, 1973). The Student's-t-test (equal variances) and the Welch test (unequal variances) both with "Bonferroni correction" (Hald, 1952; Miller, 1966) were used to test the origin of possible differences between the age groups. The homogeneity of the variances was tested according to Bartlett (1937; Hald, 1952). Regression analysis (Draper and Smith, 1981; Kleinbaum and Kupper, 1978) was carried out to test a possible increase or decrease with age. In case of hetero scedasticity, a weighted least squares regression analysis was performed. Differences between perforated and non-perforated synapses were tested with the paired t-test (Hald, 1952).

RESULTS

Quantification of (pyramidal) neurons (and synapses)

Figure 4 shows the effect of age on the numerical fractions N_N of A) CA1 to CA3 pyramidal neurons, B) CA3 synapses (non-perforated or perforated) to CA3 pyramidal neurons and C) CA3 perforated to CA3 non-perforated synapses.
Table I shows the numerical densities N_V of the synapses and neurons.
Table II shows the results of the mean projected height (EH) of the CA1 and CA3 pyramidal cell nuclei.

No significant differences exist between the 4 age-groups, neither for any of the numerical fractions or numerical densities, nor for the projected height of the CA1 and CA3 cell nuclei (one-way ANOVA, $P>0.05$).

Quantification of synapses and synaptic substructures

Table III shows for the non-perforated and perforated synapses in stratum radiatum of the hippocampal CA3 area the effect of age on: 1) the mean maximum intercept length (maxl), 2) the mean ratio of the number of dense projections observed along the maximum intercept length and the maximum intercept length itself (E(nDP/maxl) and 3) the mean projected height (EH) (cf. figs. 1 and 2).
Note the distinction that is made between the zone carrying dense projections (= DP zone) and the zone free of dense projections (= perforation) (cf. fig. 2).

Significant differences are found only between the results of (nDP/maxl)(non-perforated synapses) of the 3 months and 30 months age-groups (one-way ANOVA, $P \leq 0.05$, followed by Student's t-test, $\alpha=0.05$; $P2 \leq 0.0083$ (Bonferroni)).
The increase with age of (nDP/maxl) is significant for both types of synapses and so is the increase of EH(non-perforated synapses) (regression analysis, $P \leq 0.05$) (fig. 5).

Figure 6 shows for the synapse perforations in stratum radiatum of the hippocampal CA3 area the effect of age on: A) the mean number of synapse perforations per perforated synapse (Ep_0), B) the maximum intercept length (Emaxl) and C) the projected height (EH).
The estimated mean per age-group is indicated on top of each figure with the coefficient of error among animals (CE=SEM/mean*100%).

Except for Emaxl(synapse perforations), which differs significantly between 12 months and 30 months of age (one-way ANOVA, $P \leq 0.05$, followed by Student's t-test ($\alpha=0.05$; significant if $P2 \leq 0.0083$ (Bonferroni)), no differences between the age-groups exist for the number of perforations per synapse p_0 or for their projected height H.

Table IV shows the effect of age on the mean number of presynaptic dense projections per synapse (En_0) calculated according to two models (tile model and conic model).

No significant differences are found between the 4 age-groups, neither with the tile model nor with the conic model (one-way ANOVA, $P>0.05$). The observed tendency towards an increase in the number of dense projections per synapse with age is significant for En_0(non-perforated synapses) obtained with the conic model (regression analysis, $P2 \leq 0.05$) (fig. 7).

With the tile model significantly lower values of En_0 are obtained as compared with the conic model (paired t-test, $P2 \leq 0.05$). However, the tendency in the results of En_0 obtained with the two models is the same.

Fig. 8 shows examples of so called 'orthogonal projections' (symmetrical reconstructions or shadows) of both synapse types. From visual inspection of these shadows it is concluded that 1) the shape of both synapse types deviates considerably from the presumed disc-shape and 2) perforated synapses are larger than non-perforated ones.

Table V and fig. 9 show the results of measurements on these shadows, i.e. the 'size' estimates of their mean surface area (ES) and their mean perimeter length (EL) and the 'shape' estimates of the normalized central moments with reference to major semi-axis (est $E\eta_a$) and minor semi-axis (est $E\eta_b$) and the mean moment invariant est $E\Phi_1$ ($=\eta_{02}+\eta_{20}$). No significant differences between the 4 age-groups are found for any of these indirect size and shape measurements on the synapse shadows, neither for the non-perforated, nor for the perforated synapses (one-way ANOVA, $P>0.05$).

The estimates est Emax1, est EH, est En_0, ES and EL can all be considered as indicators of size. Statistical evaluation of the combined "size" variables points -at least for the non-perforated synapses- at a significant increase in synaptic size with age; significant differences exist between 3 and 24 months, between 12 and 24 months and between 30 and 24 months (one-way MANOVA, 5 variables; $P \leq 0.05$ (pairwise comparisons, significant if $P2 \leq 0.0083$ (Bonferroni))).

With respect to possible *differences* in size between non-perforated and perforated synapses tables III, IV and V and fig. 5 show that -in all 4 age-groups- the perforated synapses are larger than the non-perforated synapses. The values of the size parameters Emax1 and EH -except those of the 30 months age-group- differ significantly (paired t-test, $P2 \leq 0.05$) (table III and fig.5). The number of dense projections per synapse (En_0) is significantly larger for the perforated synapses and also EL and ES of the synapse shadows (table V) differ significantly.

In general, an increased interindividual variability has been observed in the 3 months and 30 months age-groups.

Regarding the high variability among rats, particularly for the estimated numerical densities of the synapses, it has been noted (table I) that the variability among blocks (series) and disectors within an animal is approximately the same.

DISCUSSION

In the present paper the effects of age on the number and size of synapses and neurons in the hippocampus of the rat are studied. In addition, some fine structural characteristics of the synaptic contact zone ('perforations' and 'dense projections') are investigated. Wherever possible, methods have been used providing unbiased estimates of the parameters.

In general, the effect of age on the parameters measured is mild although definitely present for some of them. The following effects of age were observed:

1) no change in the numerical relation between numbers of CA1 and CA3 pyramidal neurons;
2) no change in the numerical relation between numbers of CA3 synapses (stratum radiatum) and CA3 pyramidal neurons;
3) no change in the numerical relation between numbers of perforated and non-perforated synapses in CA3, stratum radiatum;
4) an increase in size of the non-perforated synapses;
5) no change in the number of perforations per perforated synapse; significantly larger perforations at high age (30 months);
6) an increase in numbers of presynaptic dense projections;
7) no change in size and shape of synapse shadows; the shape of both synapse types deviates considerably from the presumed disc-shape.

Perforated synapses are found to be larger and more 'complex' (presence of perforations and relatively more dense projections) than the non-perforated synapses.

In this discussion, the reliability and value of the different variables will be discussed in relation to the effects of age which, in turn, will be compared with the literature. Headings are used to facilitate comparison with the text in 'Materials and Methods' and 'Results'.

Estimation of synapse and neuron fractions

In the initial phase of this study we reported the effect of age on synaptic densities in the rat hippocampus (De Groot, 1981; De Groot and Bierman, 1981; 1983), not appreciating the bias inherent to the method used to estimate N_V (De Groot, 1984; De Groot and Bierman, 1983) and the fact that N_V is subject to changes in the reference volume. By the time it was realized that *absolute numbers* should be estimated, which can be obtained by multiplying N_V with the volume V of the reference space, an unknown number of sections of the embedded tissue blocks had been "lost" during sectioning so that a proper estimate of the reference volume could not any more be derived from this material. Recognizing this problem, we decided to estimate the numerical fractions (N_V(particle X)/(N_V(particle Y)) of different neurons and synapses since such fractions will at least indicate whether the numerical relation between neurons and/or synapses has been affected by age. The numerical fractions, thus estimated, i.e. CA1 neurons/CA3 neurons, CA3

synapses/CA3 neurons and CA3 perforated synapses/CA3 non-perforated synapses appear not to be affected by the age of the rats (fig. 4). This implies that, if the *absolute numbers* of these synapses and neurons are at all affected by the age, this effect has been the same for the investigated neurons and synapses of this study. However, the *actual extent* of this effect remains unknown since this can *only* be obtained from *absolute numbers* which are *not affected by changes in the reference volume.*

In another ageing study using sulfide perfusion fixed, and subsequently *deep frozen* brain tissue of ageing F 344 rats (4, 12, 20, 27, 33 and 37 months), Coleman et al. (1987) found only a mild increase in the volume of some hippocampal regions between 4 months and 12 months of age. From 12 months of age and older no changes in volume of the different areas of the hippocampal region were detected.

Measuring the total volume of the unfixed ('fresh') brain in male F 344 rats of 3 months and 24 months of age (18 rats/group), Geinisman (personal communication) observed a slight (difference between group means is 11%), but statistically highly significant increase in the total brain volume in aged animals as compared to young adults and there was no overlap in the values obtained from young to old animals.

In the rats of the present study (Small Wistar, Wag/Rij) the total volumes of the hippocampus and dentate gyrus of the right, paraplast embedded hemisphere were also found to increase with age (34% and 29%, respectively), particularly between 12 months and 24 months of age (23% and 19%, respectively). The layers of the hippocampal CA3 area did not change in volume with age; the volume of CA1 stratum pyramidale showed a mild increase (13%). At least part of the increase in total volume will originate from differential shrinkage of young and old brains during processing of the tissue for paraplast embedding. It is known that this shrinkage is stronger in the brains of younger individuals than in older ones (Haug, 1980, 1984, 1985; Sass, 1982; Uylings et al., 1986) particularly when methylbenzoate or chloroform are used as intermedium. However, since we used xylene as intermedium which does not show age-related changes of shrinkage (Haug, 1986), it is also possible that (part of) the measured increase in hippocampal volume results as a function of ageing.

Taken together the findings that the numerical fractions of the neurons and synapses in the present study do not change with age and the data which indicate no change or a mild increase in brain volume with age, we are inclined to conclude that there is no absolute loss of the neurons and synapses analysed in the present study.

The apparent -but not significant- decrease in synaptic density N_V, reported here (table I) is comparable with the (apparent) decrease in N_V obtained previously with conventional quantitative methods (cf. De Groot and Bierman, 1986) such as the 'unfolding' (De Groot, 1981; De Groot and Bierman, 1981) and 'serial section' technique (De Groot and Bierman, 1983, 1987). Apparently, the decrease in N_V must be explained by a *relative* loss of

synapses resulting from an increase in reference volume with age rather than by an *absolute* loss of synapses resulting from 'ageing'.

In another study on ageing also using the disector technique, but on OsO_4 treated tissue, Calverley and Jones (1988) found that the numerical densities N_V of perforated and non-perforated synapses in the parietal cortex of the rat did not change with age. Possible changes in the reference volume were not taken into account.

In an early study in the molecular layer of the dentate gyrus using a conventional quantitative method (Cruz-Orive, 1980; Verwer and De Groot, 1982) and OsO_4 treated tissue, Geinisman et al. (1986b) found apparent decreases with age (5 months → 27 months) of 10.7% and 3.1% for the number fractions of non-perforated and perforated synapses per granule cell, which were not significant. In a later study (Geinisman et al., 1992a) using the disector technique instead of the conventional counting method these authors concluded that there was an age-dependent decrease in the number fractions of perforated and non-perforated synapses which was significant for both synapse types in the middle molecular layer and for the non-perforated synapses in the inner molecular layer. Subsequently, Geinisman et al. (1992b) subdivided the perforated synapses into 1) fenestrated, 2) horseshoe-shaped, and 3) segmented synapses. An apparent decrease with age was found for all subtypes, which was significant in the middle molecular layer for the horseshoe-shaped and segmented synapses.

Segmented synapses, also called 'multifocal' synapses (Vrensen and Nunez-Cardozo, 1981), cannot be recognized in E-PTA treated tissue. Since only the membrane thickenings are 'stained' with E-PTA rather than the cell membrane itself, such a synapse will be counted as 2 or more separate non-perforated synapses. *Even serially tracking of the synapses cannot avoid this identification problem.* This problem is a serious drawback of the E-PTA treatment for counting synapses. In the hippocampus, the percentage of this type of synapses compared to the total number of perforated synapses is unknown. In the dentate gyrus it has been shown that in young rats about 50% of the perforated synapses belong to the population of segmented synapses. In addition, there is evidence that especially this synaptic sub-type is involved in synaptic plasticity (Geinisman et al., 1991; 1992b; 1993). *However, it should be borne in mind that E-PTA treatment was essential in the present study for the quantification of presynaptic dense projections as an indirect measure for synaptic efficacy (see below).*

A comparison between E-PTA treated and OsO4 treated synapses was made in an earlier paper (Vrensen and De Groot, 1973b). It was concluded that the number of E-PTA synapses corresponds to the number of membrane thickenings of the OsO_4 synapses. The average size of the E-PTA synapse, however, always was slightly smaller than that of the membrane thickening of the OsO_4 synapse. So far, it is not precisely known which components of the synapse are stained precisely by either OsO_4 or E-PTA.

Quantification of the size of synapses and pyramidal cell nuclei

Unbiased estimates, indicative for the size of arbitrarily-shaped synapses are the maximum intercept length maxl and the projected height H (cf fig. 1). The first is measured in all 'q⁻' disector-sampled synapses; the latter is obtained from the ratio q/q^- of the disector-sampled synapses (Sterio, 1984). In this study, EH(non-perforated synapses) increases significantly with age (table III and fig. 5) indicating an increase in size of the *total contact zone*. The apparent increase in Emaxl(non-perforated synapses) is not significant. It is noted that, for the non-perforated synapses, the total contact zone equals the DP-zone; the total contact zone of the perforated synapses equals the DP-zone plus the perforation zone (cf. fig. 2). No significant changes in the size of the perforated synapses is found.

Attention is drawn to the finding that the ratio est Emaxl/est EH found for the non-perforated synapses approximates the $4/\pi$ ratio which is valid for circular discs (Fullmann, 1953) whereas that of the perforated synapses does not (table III). This result at least indicates that the shape of perforated synapses deviates more from the classically presumed disc-shape than that of the non-perforated synapses does.

In a study on ageing, using OsO_4 treated tissue, Geinisman et al. (1990b) found that maxl of the perforated axospinous synapses in the dentate gyrus of the rat is 2.15 times larger than maxl of the non-perforated synapses. For E-PTA treated synapses in CA3 stratum radiatum the ratio maxl(perforated synapses)/maxl(non-perforated synapses) is 1.57 on the average (table III).

With regard to effects of age on the size of the pyramidal neurons we observed here that the projected height H of pyramidal cell nuclei in CA1 and CA3 is not affected by the age of the rats. Since the size of the nucleus remains constant with age and the indication (see above) that the CA1 and CA3 areas probably do not change (much) in volume with age, it is not likely to expect a change in the size of the perikaryon of these cells and may be not even a change in its dendrites. However, it is obvious that such a 'conclusion' must be treated with caution.

Quantification of synapse perforations

The size of the perforations has also been estimated (the maximum intercept length maxl and the projected height H) as well as the number of perforations per synapse Ep_0. As mentioned before, due to the E-PTA treatment, segmented perforated synapses are not recognized as such. Therefore it can be concluded that only perforations of fenestrated and horseshoe-shaped perforated synapses were included in the countings and measurements.

Ep_0 is an unbiased estimate since it represents the numerical fraction of N_V(synapse perforations)/N_V(perforated synapses); both N_V's are obtained by

the disector stack method of Sterio (1984) for which no assumptions have to be made about the shape, size and orientation of the particles (De Groot and Bierman, 1986). As mentioned before, numerical fractions N_N do not depend on changes in reference volume.
No change in the number of perforations per perforated synapse is found (fig. 6A). With respect to their size, the results showed that, at high age (30 months) the size of the perforations is larger, compared with the size at 12 months (fig. 6B).

The *relevance of 'perforations'* regarding synaptic efficacy is as follows. It has been stated in a review by Vrensen (1989) that the formation of complex-shaped synapses such as perforated synapses, results from expansion of the 'active zone' over a larger area of the presynaptic membrane. The active zone is where synaptic transmission takes place; it corresponds with the grid of presynaptic dense projections (DP zone) and the postsynaptic 'band' ('thickening', 'density' or 'plate') (cf. fig. 2). There is evidence that especially the border zones of the presynaptic grid of dense projections are important with regard to synaptic functioning. In this context it is important to realize that perforation of a synapse creates an 'internal' border zone, which accuses for an important increase in total length of the border zones in this type of synapse. As described earlier Peters and Kaiserman-Abramof, 1969; Cohen and Siekevitz, 1978; Spacek and Hartmann, 1983; Calverley and Jones, 1987a; Geinisman et al., 1987, 1991, 1992b, 1992c; Vrensen and Nunez-Cardozo, 1981) the 'perforation' may imply a local 'interruption' in the active zone (so-called 'fenestrated' or 'annulated' synapses), an 'invagination' in the active zone (so-called 'horseshoe-shaped' synapses) or complete separation of the active zone (so called 'segmented' or 'multi-focal' synapses) (cf. e.g. Geinisman et al., 1991, fig. 2). In any case, the outer boundary of the active zone increases with the length of the perforation boundary. Akert and coworkers (cf. Akert and Peper, 1975) showed, by means of freeze etch studies, that presynaptic dense projections, vesicle attachment sites (VASs) and Ca^{2+} channels are complementary structures, involved in the processes of transmitter release. VASs are the sites where the transmitter is exocytosed in the 'intercleft' space between the pre and postsynaptic membranes (cf. fig 2). Venzin and coworkers (1977) demonstrated that the contribution of the periphery of the active zone to the number of VASs and Ca^{2+} channels is larger than that of the centre of the zone. This implies that *an increase in boundary (border zones) of the active zone by means of invagination of the outer boundary or induction of 'perforations' (dense projection free areas in the zone) leads to an increase in Ca^{2+} channels and VASs*. Consequently, a potentially enhanced synaptic transmission results. This idea was also received from the results of Cohen and Siekevitz (1978). Based on their finding that clustering of synaptic vesicles in the presynaptic element arises particularly opposite the edges of the post synaptic densities, they suggested a concentration of receptors for transmitters at the edges of the postsynaptic thickenings. For these reasons it is believed that perforated synapses are more efficient than non-perforated synapses. If true, the former idea would also imply that, in

general, the segmented perforated synapses will be more efficacious than the horseshoe-shaped or fenestrated ones since it is likely that their total boundary is larger. This suggestion is supported by the results of studies, in which particularly the segmented perforated synapses increase in number as a result of a specific stimulus, such as long-term potentiation (LTP) (Geinisman et al., 1991, 1992b) or kindling (Geinisman et al., 1992c; 1993).

Jones and Calverley (1991b), reported a doubling of the projected height H of synapse perforations in the parietal cortex of the rat from 0.5 months to 22 months of age. In groups of comparable age, the size of the perforations was found to be about twice the size of the synapse perforations of the present study (cf. fig. 6): 104 nm (4 months), 102 nm (12 months) and 133 nm (22 months).

Since, in our study, the ratio est Emaxl/est EH found for the perforations does not equal the $4/\pi$ ratio which is valid for circular discs (Fullmann, 1953) it seems likely that the shape of the perforations is rather complex. Jones and Calverley (1991a) reported in a study on ageing in the parietal cortex of the rat that, at early age (0.5 and 1 months) the perforations tend to be discrete (just like fenestrated synapses); later (4 months), so called 're-entrant' perforations are mainly observed, i.e. perforations which are co-extensive with the surrounding synaptic contact zone (like e.g. the typical horseshoe-shaped synapses) and the perforations tend to branch (7 and 10 months). At higher ages (19 and 22 months) large synapses with large perforations are found. Frequently the perforations are co-extensive with the synaptic contact zone outside the DP zone and are continuous with other extensive perforations; one or more small synaptic grids belonging to one and the same synaptic terminal (segmented synapses) may be observed.

In the study presented here, *qualitative visual inspection* of the perforations in the reconstructed synapse shadows (see below) did not allow a prediction about differences between the age-groups in number, size and shape of the perforations. At each age perforated synapses with one or more perforations, all or not co-extensive with the outer boundary of the DP zone, are present. However, as mentioned already, segmented synapses are not included.

As a consequence of the fact that segmented synapses go unrecognized and are counted as two or more non-perforated synapses, the number of non-perforated synapses will be overestimated whereas the number of perforated synapses -although to a lesser extent- will be underestimated. In addition, the number of perforations per synapse will be underestimated and the size of the perforations may actually be different. However, the *relative* differences between age-groups are only affected when differences in the number of segmented synapses between the age-groups exist.

The results of the study of Jones and Calverley (1991a) in the rat parietal cortex -oldest age group being 22 months- suggest that the number of segmented perforated synapses in the rat parietal cortex and the number of

'segments' per synapse increase with age. However, the synapses selected for the analysis do not comprise an unbiased number since the selection of up to 10 synapses, used for the reconstructions, was carried out in one section of a section series. This implies that larger synapses had a larger chance to be incorporated in the analysis. It is clear from the reported results that the segmented synapses particularly belong to the category of larger synapses. Hence, their number has unavoidably been overestimated.

Estimating *unbiased* numbers of synapses, Geinisman et al. (1992b) reported for the molecular layer of the dentate gyrus, a decrease in the number of segmented synapses from 5 months to 27 months of about 23%; horseshoe-shaped and fenestrated synapses decreased in number as well (30% and 11%, respectively). In 5 months old rats, segmented synapses were found to comprise 51% of the total population of perforated synapses (Geinisman, 1993a).

Inspection of synapse shadows

Indirect information about synaptic size and shape, is obtained from reconstructions of their shadows (figs. 8 and 9).
Qualitative inspection of these 2D reconstructions showed that the shape of both synapse types clearly deviates from the classically presumed disc-shape. They also showed that the perforated synapses are larger than the non-perforated synapses.
Qualitative inspection of the synapse shadows does not allow to draw conclusions about changes in size and shape, resulting from ageing. Quantitative inspection of the synapse shadows did not point at changes with age, neither for the size parameters S and L, nor for the 'shape factors' η_a, η_b and Φ_1.

As pointed out by De Groot et al., 1992, the results obtained with inspection of synapse shadows do not permit hard conclusions about the actual shape of a synapse. They may provide additional information on the configuration of synapses and the effect of an external stimulus on it and may hence contribute to a better understanding of neuronal plasticity on the whole. It is likely that differences in the actual shape of the synapse, reflect changes in its structural organization and efficacy.

A comparison of the shape of the perforated and non-perforated synapses, using the shadows is not reliable. From inspection of 'en face' profiles of both synapse types (De Groot and Bierman, 1983) it was concluded that the actual shape of the perforated synapses of this study, in general, will be more irregular than that of the non-perforated synapses. It can be stated, that the reduction from actual shape to shadow is larger, the more complex the actual shape of the structure in 3D is. This implies that, relatively, the shadows of the perforated synapses are 'simplified' more than those of the non-perforated synapses.

In a study on ageing in rats using reconstructed synapse shadows (orthogonal projections), Jones and Calverley (1991a) showed that the area

occupied by the perforation(s) is as large as the area, occupied by the postsynaptic band PSB. In the present study, the area occupied by the perforation(s) is smaller compared to that of the PSB (table III). Although it should be borne in mind that, here, segmented (multifocal) synapses are not included in the population of perforated synapses, the results indicate that perforated synapses in the parietal cortex are likely to be larger and more complex than those in stratum radiatum of the hippocampus.

In another study on ageing, using OsO_4 treated tissue, Geinisman et al. (1990b) calculated the area of the post synaptic band (PSB) as an estimate for the size of the synapses. This area was obtained by taking the product of the total length of all PSB profiles and the mean section thickness. This estimate is comparable to ES(synapse shadows) presented here (table V) except that, in our study, the area occupied by the perforation is included in ES. With respect to this estimate it should be noticed that the ratio ES(perforated synapse shadows)/ES(non-perforated synapse shadows) found by Geinisman et al. (1990b) is 3.78 whereas that of the present study is 2.67. The difference between the two studies originates mainly from the fact that the non-perforated synapses in the molecular layer of the dentate gyrus, apparently are much smaller than those in stratum radiatum of the hippocampus; the size of the perforated synapses is more or less the same in the two studies. A larger size for the perforated synapses using synapse shadows, was reported by Jones and Calverley (1991a) for synapses in the parietal cortex of young and old rats.

Quantification of the number of presynaptic dense projections

In the present study, the number of dense projections per synapse En_0 obtained with either the tile model or the conic model show a tendency to increase with age and also the number of dense projections counted along maxl shows an increase with age for both synapse types.
These results suggest that both non-perforated, as well as perforated synapses, become more efficient with age.

As mentioned above, it has been suggested (Akert, 1973) that the dense projections are membrane thickenings 'guiding' the transmitter vesicles to their vesicle attachment sites (VAS), i.e. the sites where the transmitter is exocytosed in the intercleft space. Since the dense projections are supposed to be complementary to the VAS it can be deduced that, the more dense projections there are, the more vesicle attachment sites are present in the synapse. Clearly, the release of transmitter is relevant in the process of transmission of information from one nerve cell to the other. Therefore, the number of dense projections per synapse En_0 is an indirect measure of synaptic efficacy.

In this study, En_0 has been calculated along two different lines, namely the 'tile' and the 'conic' models. Another parameter, providing information on numbers of dense projections is the number of dense

projections along the maximum intercept length, E(nDP/maxl).

For the tile model it is assumed that the dense projections are arranged on the presynaptic surface area according to a regular array. To estimate the number of presynaptic dense projections En_0 with this model the size parameters ES and EL, i.e. the surface area and boundary length of the presynaptic surface area have to be calculated since they are indispensible parameters in the model. However, ES and EL are based on the assumption that synaptic contact zones are round, disc-like structures. Since the tile model starts from this shape assumption and, in addition, starts from assumptions about the distribution array of the dense projections on the presynaptic surface area, the results of En_0 are biased to an unknown extent. It has been observed that, in general, the array of dense projections shows high regularity, at least in the non-perforated synapses. In the perforated synapses the regularity may be disturbed (fig.2).

In the conic model the dense projections are regarded as cone-like structures, sitting on the presynaptic surface area. A closer look makes clear that for this model assumptions are made regarding the shape of the dense projections. However, no assumptions are made about the shape of the synaptic contact zone or about the array of the dense projections on the presynaptic contactzone. The bias in the estimate of En_0 obtained with the conic model will be less than the bias in En_0 obtained with the tile model.

Also the number of dense projections along maxl will be biased since the cutting angle at which the synapse has been hit by sectioning is never known and corrections for capping and under- or overprojection are not made.

Nevertheless, although biased to an unknown extent, En_0 and E(nDp/maxl) are important parameters and no method leading to *unbiased* estimates of numbers of dense projections are available, so far.

The finding that significantly lower values of En_0 were obtained with the tile versus the conic model are in agreement with our earlier data on synapses in the stratum pyramidale of the hippocampal CA3 area of the rat (De Groot, 1985). Most likely this difference originates from the fact that the surface area S and perimeter length L *of the actual synapse*, parameters used in the tile model to calculate N_V(dense projections), were corrected for overprojection (see: Appendix). As a consequence EL and ES become smaller and so does N_V(dense projections).
Apart from the fact that the corrections for overprojection only apply to disc-like structures - which most synapses are not - the question remains whether E-PTA-stained synaptic contact zones are at all *'over'*projected. The findings that the values of EL and ES of the synapse shadows (table V) are approximately of the same size or, in case of the non-perforated synapses, even slightly *larger* than the values calculated for the actual synapse in the tile model, support this suggestion. The size of the surface area and perimeter length of the shadow of a structure can, at the very most, equal the size of the actual structure; in general, however, the surface area and boundary length of the shadow will be *smaller*.

As far as we are aware, no other data on numbers of dense projections in relation to ageing are available in the literature. The tile and conic models presented here have been applied only by Cruz-Orive (1985) and De Groot (1985). Regarding the models presented here the results, taken together, suggest that the conic model is to be preferred.

Another method to quantify numbers of dense projections at the electron microscopical level has been described earlier by Vrensen et al. (1980). For this method, the use of "semi-thin" (i.e. 500 nm thick) sections of E-PTA treated tissue is proposed. The thickness of these sections, in general, will be larger than the 'thickness' of many of the investigated synaptic contact zones and, therefore, a number of synapses will be fully incorporated in the section. These, so called, 'en face' positioned synapses very elegantly show the array of the dense projections in the presynaptic grid (fig. 2) and enable counting and measurement of the dense projections in the grid. However, although very elegant, this method has one main drawback, namely that the population of synapses that will be analysed in this way, is biased in number to an unknown extent because only fully incorporated 'en face' positioned synapses can be analysed in this way. As stated before, larger synapses stand a larger chance to be cut by sectioning and hence they stand a smaller chance to be fully incorporated in the section (De Groot and Bierman, 1983). Hence, the number of dense projections per synapse, analysed and counted with this method, represents the 'average' composition of the presynaptic grid of a *selected* portion of synapses and these may not be representative for the total synapse population.

Theoretically, the method could provide nearly unbiased results with respect to En_0 if for the counting and selection of the synapses for dense projections analysis, the disector 'stack' method could be used. One of the requirements of the disector method is that the minimal size of the investigated particle is smaller than the height of the disector which, in turn, equals the section thickness. Since only those synapses that are fully incorporated in the sections can be used for dense projections analysis, the 'thickness' of the synaptic 'disc' should be considered as minimal height of the investigated particles. This thickness includes the height of the dense projections and postsynaptic plate plus the width of the synaptic intercleft space (cf fig. 2). This total thickness is less than 500nm and thus the disector stack method can not adequately be used to select and count an unbiased number of synapses for the evaluation of the presynaptic grid of dense projections. In practice, only a minor number of synapses will be situated in the section perfectly parallel to the surface of the section. In addition, the application of the disector stack method on semithin sections to quantify non-perforated and perforated synapses separately, has practical limitations: perforations in a complex-shaped synapse may go unrecognized when the synapse is curved or when the synapse is positioned under a certain angle with reference to the section plane. As a result, perforated synapses are identified, counted and further analysed as if they belong to the non-perforated portion.

Regarding the large ***variability among rats***, particularly for the estimated numerical densities of the synapses (table I), it should be noted that the variability among blocks and disectors *within* an animal is of the same order of magnitude. It is suggested that the *main* source for this variability is originating from a pitfall in the sampling procedure for the analysis of the synapses, although the specific problem has not been identified. It is possible that in some photographs, sampled for the synapse countings, complex-shaped mossy fiber terminals have been incorporated which are actually located in the stratum lucidum and should not have been included in the analysis. The location of these synapses is restricted to a small 'band' in stratum lucidum, adjacent to the stratum radiatum. Their *local* density appears to be relatively high. and the majority of these synapses are perforated.

In addition to this (probably main) source for the large variability found among rats, it is noted that in the 3 months old rats the nervous system may or may not yet be fully matured, which may contribute to the interindividual variability. At the age of 30 months, only 50 % of the rats are still alive. Hence, the 30 months survivors represent a selected population of physically stronger rats. Whether such a selection also involves a selection with regard to nervous system functioning, remains unknown.

To summarize, the results of the present study show that quantitative morphological methods enable the detection of neural plasticity. Nowadays, methods are available to obtain *unbiased* estimates of number and size of *arbitrarily-shaped* particles such as synapses and neurons, which are key-structures in the nervous system. In addition, reliable information on synaptic substructures such as pre- and postsynaptic membrane thickenings (presynaptic dense projections and postsynaptic band, respectively) and 'perforations', known to play a relevant role in signal transmission from one nerve cell to the other, can be obtained by morphometric means with reasonable validity.

Our results show that perforated synapses are significantly more efficient than non-perforated ones. Perforated synapses are larger and they have one or more 'perforations'. Hence, their border zones are more extensive, implicating a potentially enhanced synaptic transmission. In addition, they have a relatively larger number of presynaptic dense projections, also suggesting a higher probability of transmitter release.

With respect to ageing in rat hippocampus, four major findings can be deduced from the present results.

1) No loss in numbers of non-perforated or perforated synapses per neuron occurs. Changes in numerical densities of synapses and neurons -if at all present- originate from an increase in reference volume.

2) Structural changes with age occur in non-perforated and perforated synapses, reflecting increased synaptic efficacy with age:
   a) enlargement of the synaptic surface area (non-perforated synapses);
   b) increase in numbers of dense projections composing the presynaptic grid;
   c) a larger size of 'perforations' in the presynaptic grid at high age (30 months).
3) No change in number fractions of CA1 to CA3 pyramidal neurons.
4) Probably no change in size of CA1 and CA3 neurons, although this conclusion must be treated with caution.

Taken together, these results suggest that the number of synapses per neuron in the hippocampal CA3 area is not affected by age. The efficacy of the synapses increases with age, expressed by an increase in size and complexity of the active zone (transmission zone). Impairment of the synaptic circuitry in this area at 30 months is not likely to occur.

The interesting question then, remains: 'Why do aged animals need an enhanced efficacy of synaptic transmission'.
The answer to this question is as yet unknown but it could be a reflection of the compensatory reaction of synapses in the hippocampus proper in response to e.g. a loss of synapses in the dentate gyrus (Geinisman, 1993a; Geinisman, personal communication).

ACKNOWLEDGEMENTS

The authors are grateful to Prof. Dr. J. Voogd (Erasmus University Rotterdam) and Prof. Dr. T.M. Mayhew (University of Nottingham) for critical reading of the manuscript and for their constructive remarks. Prof. Dr. H-J. Gundersen (University of Ärhus) and Prof. Dr. L.M. Cruz-Orive (University of Bern) are acknowledged for their help in the stereological assessment and for their fruitful discussions.
Mr. M. Boermans and Mr. R. Van Boven are thanked for printing the photographs.

REFERENCES

Aghajanian, G.K. and Bloom, F.E. (1967) The formation of synaptic junctions in developing rat brain: a quantitative electron microscopic study, Brain Res., 6: 716-727.

Akert, K. (1973) Dynamic aspects of synaptic ultrastructure, Brain Res., 49: 511-518.

Akert, K. and Peper, K. (1975) Ultrastructure of chemical synapses. In M. Santini (Ed.), Golgi centennial symposium: perspectives in neurobiology, Raven Press, pp. 521-527.

Akert, K. and Pfenniger, K. (1969) Synaptic fine structure and neural dynamics. In S.H. Barondes (Ed.), Cellular dynamics of the neuron, I.S.C.B. Symposium, Vol. 8, Academic Press, New York, pp. 245-260.

Akert, K., Kawana, E. and Bandri, C. (1971) ZIO-positive and ZIO-negative vesicles in nerve terminals. In Eränko (Ed.), Histochemistry of nervous transmission, Progress in Brain Research, Vol 34, Elsevier, Amsterdam, pp. 305-317.

Bartlett, M.S. (1937) Properties of sufficiency and statistical tests, Proc. Roy. Soc. A., 160: 268-282.

Bloom, F.E. (1970) Correlating structure and function of synapses. In F.O. Schmitt (Ed.), The Neurosciences Second Study Program, Rockefeller University Press, New York, pp. 729-746.

Bedi, K.S., Calverley, R.K.S. and Jones, D.G. (1984) Effects of undernutrition on brain morphology: a critical review of methods and results. In D.G. Jones (Ed.), Current topics in research on synapses, Vol.2, Alan R Liss, New York, pp. 93-163.

Braendgaard, H. and Gundersen H.J.G. 1986 The impact of recent stereological advances on quantitative studies of the nervous system, J. Neurosc. Methods, 18: 39-78.

Calverley, R.K.S. and Jones, D.G. (1987a) A serial section study of perforated synapses in rat neocortex, Cell Tissue Res., 247: 565-572.

Calverley, R.K.S. and Jones, D.G. (1987b) Determination of the numerical density of perforated synapses in rat neocortex, Cell Tissue Res., 248: 399-407.

Calverley, R.K.S. and Jones, D.G. (1988) Estimation of numerical density of perforated brain synapses in aging rats, Neurosci. Lett. Suppl. 30: 54.

Chen, K. (1990) Efficient parallel algorithms for the computation of two-dimensional image moments, Pattern Recognition, 23(1/2): 109-119.

Cohen, R.S. and Siekevitz, P. (1983) Form of the postsynaptic density. A serial section reconstruction, J. Cell. Biol., 78: 36-46.

Coleman, P.D., Flood, D.G. and West, M.J. (1987) Volumes of the components of the hippocampus in the aging F344 rat, The Journal of comparative Neurology, 266: 300-306.

Cragg, B.G. (1967a) Changes in visual cortex on first exposure of rats to light, Nature (Lond.), 215: 251-253.

Cragg, B.G. (1967b) The density of synapses and neurones in the motor and visual areas of the cerebral cortex, J. Anat. (Lond.), 101: 639-654.

Cragg, B.G. (1969) The effects of vision and dark-rearing on the size and density of synapses in the lateral geniculate nucleus measured by electron microscopy, Brain Res., 13: 53-67.

Cragg. B.G. (1971) The fate of axon terminals in visual cortex during transsynaptic atrophy in the lateral geniculate nucleus, Brain Res., 34: 53-60.

Cragg, B.G. 1972 The development of cortical synapses during starvation in the rat, Brain Res., 95: 143-150.

Cruz-Orive, L.M. (1980) On the estimation of particle number, J. Microsc., 120: 15-27.

Cruz-Orive, L.M. and Myking, A.O. (1981) Stereological estimation of volume ratios by systematic sections, J. Microsc., 122: 143-157.

Cruz-Orive, L.M. (1983) Distribution-free estimation of sphere size distributions from slabs showing overprojection and truncation with a review of previous methods. J. Microsc., 131: 265-290.

Cruz-Orive, L.M. (1985) Estimating particle number and size. In L.F. Agnati and K. Fuxe (Eds.), Quantitative Neuro-anatomy in Transmitter Research, MacMillan Press, London, pp. 11-24.

De Groot, D.M.G. (1981) Age-related morphometric changes in the CNS of the rat, Acta Anatomica, 111/1-2: 51-52.

De Groot, D.M.G. (1984) Problems in the quantitative stereology of complex-shaped synapses, Ultramicroscopy, 14: 404-405.

De Groot, D.M.G. (1985) Disc-like and complex-shaped synapses: Number, size and dense projections. A critical note, Acta Stereol., 4: 147-151.

De Groot, D.M.G. (1988a) Comparison of methods for the estimation of the thickness of ultrathin tissue sections, J. Microsc., 151: 23-42.

De Groot, D.M.G. With an appendix by L.M. Cruz-Orive (1988b) Improvements of the serial section method in relation to the estimation of the numerical density of complex-shaped synapses. In A. Reith and T.M. Mayhew (Eds.), Stereology and Morphometry in Electron Microscopy. Problems and Solutions. Hemisphere Publishing Corporation, New York, London, pp. 135-158.

De Groot, D.M.G. and Bierman, E.P.B. (1981) Age-related morphometric changes in the CNS of the rat, Neuroscience Letters, 7: S434.

De Groot, D.M.G. and Bierman, E.P.B. (1983) The complex-shaped "perforated" synapse, a problem in quantitative stereology of the brain, J. Microsc., 131: 355-360.

De Groot, D.M.G. and Bierman, E.P.B. (1986) A critical evaluation of methods for estimating the numerical density of synapses, J. Neurosc. Methods, 18: 79-101.

De Groot, D.M.G. and Bierman, E.P.B. (1987) Numerical changes in rat hippocampal synapses. An effect of "ageing", Acta Stereol., 6/III: 53-58.

De Groot, D.M.G., Bierman, E.P.B. and Saris-Wijnans, M.J. (1992) 2D Reconstruction of synapse orthogonal projections: Estimation of differences in shape using second order moment invariants, Acta Stereol., 11/Suppl I: 587-592.

De Hoff, R.T. (1968) Measurement of number and average size in volume. In R.T. de Hoff and F.N. Rhines (Eds.), Quantitative Microscopy, Chapter 5, McGraw-Hill, New York, pp. 128-148.

Dorst, L. and Smeulders, A.W.M. (1987) Length estimators for digitized contours, Computer vision, graphics and image processing, 40: 311-333.

Draper, N. and Smith, H. (1981) Applied regression analysis, 2nd edn., John Wiley and Sons, York, pp. 193-212.

Field, P.M. (1972) A quantitative ultrastructural analysis of the distribution of amygdaloid fibers in the preoptic area and ventromedial hypothalamic nucleus, Exp. Brain Res., 14: 527-538.

Fifková, E. (1970) The effect of monocular deprivation of the synaptic contacts of the visual cortex, J. Neurobiol., 1: 285-294.

Fisher, L.J. (1972) Changes during maturation and metamorphosis in the synaptic organization of the tadpole retina inner plexiform layer, Nature (Lond.), 235: 391-393.

Freeman, H. (1960) On the encoding of arbitrary geometric configurations, IRE Trans. Electr. Comp., C10: 260-268.

Fullmann, R.L. (1953) Measurement of particle sizes in opaque bodies, Trans. AIME, 197: 447-452.

Geinisman, Y. (1993) Perforated axospinous synapses with multiple, completely partitioned transmission zones: probable structural intermediates in synaptic plasticity, Hippocampus, 3: 417-434.

Geinisman, Y, De Toledo-Morrell, L. and Morrell, F.(1986a) Loss of perforated synapses in the dentate gyrus: Morphological substrate of memory deficit in aged rats, Proc. Natl. Acad.Sci. USA, 83: 3027-3031.

Geinisman, Y, De Toledo-Morrell, L. and Morrell, F. (1986b) Aged rats need a preserved compliment of perforated axospinous synapses per hippocampal neuron to maintain good spatial memory, Brain Res., 398: 266-275.

Geinisman, Y, De Toledo-Morrell, L. and Morrell, F. (1989) Perforated synapses on double-headed dendritic spines: a possible structural substrate of synaptic plasticity, Brain Res. 480: 326-329.

Geinisman, Y, De Toledo-Morrell, L. and Morrell, F. (1990b) The brain's record of experience: kindling-induced enlargement of the active zone in hippocampal perforated synapses, Brain Res. 513: 175-179.

Geinisman, Y, De Toledo-Morrell, L. and Morrell, F. (1991) Induction of long-term potentiation is associated with an increase in the number of axospinous synapses with segmented postsynaptic densities, Brain Res., 566: 77-88.

Geinisman, Y, DeToledo-Morrell, L. Morrell, F., Heller, R.E., Rossi, M. and Parshall, R.F. (1993) Structural synaptic correlate of long-term potentiation: formation of axospinous synapses with multiple, completely partitioned transmission zones, Hippocampus, 3: 435-446.

Geinisman, Y, DeToledo-Morrell, L. Morrell, F., Persina, I.S. and Rossi, M. (1992a) Age-related loss of axospinous synapses formed by two afferent systems in the rat dentate gyrus as revealed by the unbiased stereological dissector technique, Hippocampus, 2: 437-444.

Geinisman, Y, DeToledo-Morrell, L. Morrell, F., Persina, I.S. and Rossi, M. (1992b) Structural synaptic plasticity associated with the induction of long-term potentiation is preserved in the dentate gyrus of aged rats, Hippocampus, 2: 445-456.

Geinisman, Y, Morrell, F. and DeToledo-Morrell, L. (1987) Axospinous synapses with segmented postsynaptic densities: A morphologically distinct synaptic subtype contributing to the number of profiles of "perforated" synapses visualized in random sections, Brain Research, 423: 179-188.

Geinisman, Y, Morrell, F. and DeToledo-Morrell, L. (1990a) Increase in the relative proportion of perforated axospinous synapses following hippocampal kindling is specific for the synaptic field of stimulated axons. Brain Research, 507: 325-331.

Geinisman, Y, Morrell, F. and DeToledo-Morrell, L. (1992c) Increase in the number of axospinous synapses with segmented postsynaptic densities following hippocampal kindling, Brain Research, 569: 341-347.

Greenough, W.T., West, K.W. and De Voogd, T.J. (1978) Subsynaptic plate perforations: changes with age and experience in the rat, Science, 202: 1096-109.

Gundersen, H.J.G. (1977) Notes on the estimation of the numerical density of arbitrarily profiles: the edge effect, J. Microsc., 111: 219-223.

Gundersen, H.J.G. (1986) Stereology of the arbitrary particles: A review of unbiased number and size estimators and the presentation of some new ones, J. Micr. (Lond.), 143: 3-45.

Hald, A. (1952) Statistical theory with engineering applications, Wiley, London, pp. 401-406.

Haug, H. (1980) Die Abhangigkeit der Einbettungsschrumpfung des Gehirngewebes vom Lebensalter, Verh. Anat. Ges., 74: 699-700.

Haug, H. (1984) Der Einfluss der sakularen Akzeleration auf das Hirngewicht des Menschen und dessen Anderung wahrend der Alterung, Gegenbaurs, Morph. Jahrb., 130: 481-500.

Haug, H. (1985) Gibt es Nervenzellverluste waehrend der Aelterung in der Menschlicher Hirnrinde? Ein morphometrischen Beitrag zu dieser Frage, Nervenheilkunde, 4: 103-109.

Haug, H. (1986) History of neuromorphometry, J. Neurosc. Methods, 18: 1-17.

Harris, R.M. (1985) Light microscopic depth measurements of thick sections, J. Neurosc. Methods, 14: 97-100.

Hollander, M. and Wolfe, D.A. (1973) Nonparametric statistical methods, John Wiley and Sons, New York, pp. 120-123.

Hu, M.K. (1962) Visual pattern recoqnition by moments invariants, IRE Trans. Inf. Theory, IT-8: 179-187.

Kleinbaum, D.G. and Kupper, L.L. (1978) Applied Regression Analysis and Other Multivariable Methods, Duxury Press, North Scituate, Massachusetts, pp. 190-192.

Jones, D.G. and Calverley, R.K.S. (1991a) Perforated and non-perforated synapses in rat neocortex: three-dimensional reconstructions, Brain Research, 556: 247-258.

Jones, D.G. and Calverley, R.K.S. (1991b) Frequency of occurrence of perforated synapses in developing rat neocortex, Neuroscience Letters, 129: 189-192.

Kohler, C. (1988) Intrinsic connections of the retrohippocampal region in the rat brain. III. The lateral entorhinal area, J. Comp. Neurol., 271: 208-228.

Leitz, E., Inc. (1968) Measurement of specimen thickness in ordinary transmitted light, Tech. Inf. Bull, 8: 1-3.

Lorente de Nó, R. (1934) Studies on the structure of the cerebral cortex II. Continuation of the study of the Ammonic system, J. Psychol. Neurol., 46: 113-177.

Miller Jr., R.G. (1966) Simultaneous statistical inference, McGraw-Hill, New York, pp. 67-70.

Molliver, M.E. and Van Der Loos, H. (1970) The ontogenesis of cortical circuitry: the spatial distribution of synapses in somesthetic cortex of newborn dog, Ergebn. Anat. Entwickl. Gesch., 42: 1-53.

Nicholson, J.L. and Altman, J. (1972) Synaptogenesis in the rat cerebellum: effects of early hypo- and hyperthyroidism, Science, 176: 530-532.

Palade, G.E. (1952) A study of fixation for electronmicroscopy, J. Exp. Med., 95: 285-298.

Paxinos, G. and Watson, C. The rat brain in stereotaxic coordinates, 2nd edn., Academic Press, Sydney, New York, London.

Peters, A. (1970) The fixation of cerebral nervous tissue and the analysis of electron micrographs of the neuropil, with special references to the cerebral cortex. In W.J.H. Nauta and S.O.E. Ebbeson (Eds.), Contemporary Research Methods in Neuroanatomy, Springer, Berlin, pp. 55-76.

Peters, A. and Kaiserman-Abramof, I.R. (1969) The small pyramidal neuron of the rat cerebral cortex. The synapses upon dendritic spines, Z. Zellforsch., 100: 487-506.

Romeis, B. (1948) Mikroskopische Technik, Leibniz Verlag (Bisher R. Oldenbourg Verlag), p. 158.

Spacek, J. and Hartman, M. (1983) Three-dimensional analysis of dendritic spines. I. Quantitative observations related to dendritic spine and synaptic morphology in cerebral and cerebellar cortices, Anat. Embryol., 167: 289-310.

Sass, N-L. (1982) The age-dependent variation of the embedding-shrinkage of neurohistological sections. Mikroskopie (Wien), 39: 278-281.

Sterio, D.C. (1984) Estimating number, mean sizes and variations in size of particles in 3-D specimens using disectors, J. Microsc. 134: 127-136.

Storm-Mathisen, J. (1981) Autoradiographic and microchemical localization of high affinity glutamate uptake. In P.J. Roberts, J. Storm-Mathisen and G.A.R. Johnston (Eds.), Glutamate: Transmitter in the Central Nervous System, John Wiley, Chichester, pp. 89-115.

Storm-Mathisen, J. and Fonnum, F. (1971) Quantitative histochemistry of glutamate decarboxylase in the rat hippocampal region, J. Neurochem., 18: 1105-1111.

Uylings, H.B.M., van Eden, C.G. and Hofman, M.A. (1986) Morphometry of size/volume variables and comparison of their bivariate relations in the nervous system under different conditions, J. Neurosc. Methods, 18: 19-37.

Venzin, M., Sandri, C., Akert, K. and Wyss, U.R. (1977) Membrane associated particles of the presynaptic active zone in rat spinal cord: a morphometric analysis, Brain Res., 130: 393-4004.

Verwer, R.W.H. and De Groot, D.M.G. (1982) The effect of shape assumptions on the estimation of the numerical density of synapses from thin sections, Progress in Brain Res., 55: 196-203.

Vrensen, G.F.J.M. (1989) Learning, memory and long-term synaptic plasticity in the mammalian brain. In H. Rahmann (Ed.), Fundamentals of memory formation: Neuronal plasticity and brain function, Gustav Fisher Verlag, Stuttgart, New York, pp. 132-147.

Vrensen, G. and De Groot, D.M.G. (1973a) Phosphotungstic acid staining and the quantitative stereology of synapses. In E. Wisse, W.T. Daems, J. Molenaar and P. van Duyn (Eds.), Electron Microscopy and Cytochemistry, Proc. 2nd Int. Symp. Amsterdam, North Holland, pp. 225-258.

Vrensen, G. and De Groot, D.M.G. (1973b) Quantitative stereology of synapses: a critical investigation. Brain Res., 58: 25-35.

Vrensen, G. and Nunez Cardozo, J. (1981) Changes in size and shape of synaptic connections after visual training, Brain Res., 218: 79-97.

Vrensen, G., Nunez Cardozo, J., Müller, L. and Van der Want, J. (1980) The pre-synaptic grid: a new approach, Brain Res., 184: 23-40.

Wann, D.F., Woolsey, T.A., Dierker, M.L. and Cowan, W.M. (1973) An on-line digital computer system for the semiautomatic analysis of Golgi-impregnated neurons, IEEE Trans. BME, 20: 233-247.

Weibel, E.R. (1979) Stereological Methods, Vol.1. Practical Methods for Biological Morphometry, Chapter 2, Chapter 5, Academic Press, London.Weibel, E.R. (1980) Stereological Methods, Vol. 2. Theoretical Foundations, Chapter 8, Academic Press, London.

West, M.J., Coleman, P.D. and Wyss, U.R. (1972) A computerized method of determining the number of synaptic contacts in a volume of cerebral cortex, J. Microsc. 95: 277-283.

Table I

Effect of age on the estimated numerical density (N_V)* of synapses and neurons in the hippocampus of female rats (Small Wistar, Wag/Rij)

age (months)	synapses** non-perforated mean	CE	n	perforated mean	CE	n	pyramidal neurons CA1 mean	CE	n	CA3 mean	CE	n
3	13.62	16.0	5	2.14	28.3	5	773	5.7	6	333	10.7	5
12	10.80	14.5	6	2.06	24.9	6	818	6.5	5	280	9.2	6
24	8.12	16.4	5	1.10	20.2	5	769	5.4	5	322	11.4	5
30	8.56	31.4	4	1.98	29.2	4	810	7.8	4	281	5.3	5

n, number of rats; 5 blocks/rat, 2 disectors/block are analysed.
CE, coefficient of error among rats ((SEM/mean)*100%).

* N_V(synapses) ($*10^{11}$ cm^{-3}) and N_V(neurons) ($*10^{6}$ cm^{-3}), estimated mean number of particles per unit volume (Sterio, 1984).

** data are taken from De Groot and Bierman (1987a/b, table I).

Table II

Effect of age on the mean projected height (EH)* of pyramidal cell nuclei in the stratum pyramidale of the hippocampal CA1 and CA3 areas of female rats (Small Wistar, Wag/Rij).

	CA1			CA3		
age (months)	n	mean	CE	n	mean	CE
3	6	5.20	3.5	5	5.86	4.0
12	5	4.91	5.4	6	6.17	5.8
24	5	5.07	2.9	5	5.73	5.0
30	4	5.41	4.1	5	6.64	5.9

n, number of rats; 2 blocks/rat, 2 stacks/block, 10 disectors/stack are analysed.
CE, coefficient of error among rats ((SEM/mean)*100%).

* EH (μm) (Sterio, 1984, formula 4).

Table III

Effect of age on estimates of mean maximum intercept length (Emaxl)*, mean ratio of the number of dense projections** observed along the maximum intercept length and the maximum intercept length itself (E(nDP/maxl)) and mean projected height (EH)*** of non-perforated and perforated synapses in stratum radiatum of the hippocampal CA3 area of female rats (Small Wistar, Wag/Rij).

		non-perforated synapses						perforated synapses****							
		DP zone						DP zone				(DP zone+perforation)			
age		Emaxl		E(nDP/maxl)		EH		Emaxl		E(nDP/maxl)		Emaxl		EH	
(months)	n	mean	CE	mean	CE	mean	CE	mean	CE	mean	CE	mean	CE	mean	CE
3	5	209	4.9	0.99	3.9	151	5.1	386	13.9	1.11	2.8	486	11.0	425	11.9
12	6	209	2.9	1.06	3.8	166	3.3	317	6.5	1.09	13.5	403	4.7	548	10.8
24	5	220	4.8	1.08	5.4	181	9.2	380	11.9	1.29	13.1	478	8.6	755	25.8
30	4	222	6.4	1.23	4.2	195	18.4	271	7.3	1.45	5.4	409	6.9	464	27.4

n, number of rats; 5 blocks/rat, 2 disectors/block are analysed.
CE, coefficient of error among rats ((SEM/mean)*100%).

* Emaxl(nm) -maxl observed when tracking the synapse in serial sections- is determined from disector-sampled (Q^-) synapses and is unbiased by section thickness, lost caps and orientation distribution. For circular (disc-like) synapses maxl represents the diameter of the synapse; for other shapes it is as close to the ideal as one can come (Braendgaard and Gundersen, 1986).

** All dense projections observed along maxl(synapse) are counted (estimated mean section thickness Et'=35.2 nm).

*** EH (nm) (Sterio, 1984, formula 4).

**** Note that (DP zone + perforation) is measured as a whole; DP zone is calculated by substraction of Emaxl(perforation) from Emaxl(perforated synapse).

Table IV

Effect of age on estimates of the mean number of presynaptic dense projections per synapse (En_o^*) -non perforated and perforated- in stratum radiatum of the hippocampal CA3 area of female rats (Small Wistar, Wag/Rij).

age		non-perforated synapses				perforated synapses			
		tile model*		conic model*		tile model*		conic model*	
(months)	n	mean	CE	mean	CE	mean	CE	mean	CE
3	5	3.3	12.4	4.4	7.7	8.5	36.9	11.9	20.9
12	6	3.6	8.0	5.2	5.5	8.1	12.8	12.6	7.5
24	5	4.1	14.4	5.9	8.2	12.9	27.0	20.5	19.4
30	4	4.1	19.4	6.9	21.7	6.9	8.9	12.0	12.5

n, number of rats; 5 blocks/rat, 2 disectors/block are analysed.
CE, coefficient of error among rats ((SEM/mean)*100%).

* $En_o = N_v$(dense projections)/N_v(synapses). Unbiased estimates of Nv(synapses) are used (Sterio 1984). Est N_v(dense projections) is obtained by 2 different methods (cf. Cruz-Orive, 1985; De Groot, 1985): 1. Tile model, where N_v is calculated from the number of conic particles, triangularly arranged on the presynaptic surface area; 2. conic model where N_v is calculated from the number of presynaptic dense projections observed in the reference area, assuming conic particles in space.

Table V

Effect of age on the estimated mean surface area (ES*) and mean perimeter length (EL**) of orthogonal projections*** ('shadows') of non-perforated and perforated synapses in the stratum radiatum of the hippocampal CA3 area of female rats (Small Wistar, Wag/Rij).

age		non-perforated synapses				perforated synapses			
		ES		EL		ES		EL	
(months)	n	mean	CE	mean	CE	mean	CE	mean	CE
3	5	3252	10.9	761	5.4	9441	17.1	1517	7.7
12	6	3069	5.3	748	2.5	7722	7.4	1381	4.4
24	5	3845	10.8	820	4.7	10659	17.2	1649	5.4
30	4	3542	11.9	809	6.8	8753	13.2	1388	6.1

n, number of rats; 5 blocks/rat, 2 disectors/block are analysed.
CE, coefficient of error among rats ((SEM/mean)*100%).

* S(*10^1 nm^2) is zero-th order geometric moment (m_{00}).

** to calculate L (nm^1) (Dorst and Smeulders, 1987, formula 24) the contour length of the orthogonal projections is approximated as a concatenated series of circular arcs.

*** The orthogonal projections are 'symmetric' reconstructions of an unbiased number of (disector-sampled) synapses, i.e. the Q⁻portions (Sterio, 1984).

Figure 1. Schematic drawings of a "synaptic disc" (or "contact zone") to illustrate some of the parameters estimated in the present paper, i.e. the maximum intercept length (profile length) (maxl), a random intercept length (l_i), the actual diameter (D) and projected height (or linear projection) H of the particle. A disc-like particle fixed between two parallel planes (P), e.g. the lower surface of the first, and upper surface of the last section of a "stack" of serial sections with thickness t', is assumed.
x, y and z indicate geometric axes. The section plane is in the x,y directions; z is the direction of cutting (or sectioning).

A. Disc in upright position, i.e. disc face parallel to x,z plane. Note that in this position, maxl = D = H.
B. Orientation of the disc has been changed: compared to A, the disc has been rotated 45° around the z-axis and has been turned towards the x,y plane. Angle between x,y plane and disc is 45°.

Comparison of figures A and B shows that the *maximum intercept length* maxl and the *actual disc diameter* D are not affected by this rotation of the particle, whereas the *projected height* H is. Averaged over all possible orientations the value of H = pi/4 x D for circular discs.

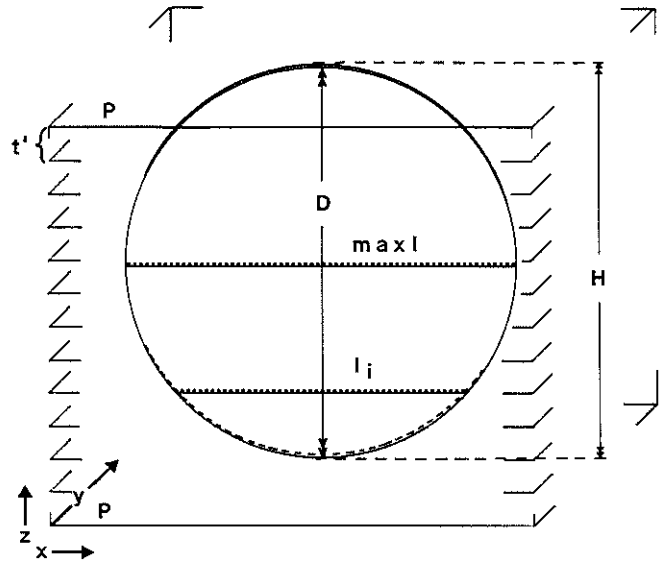

A

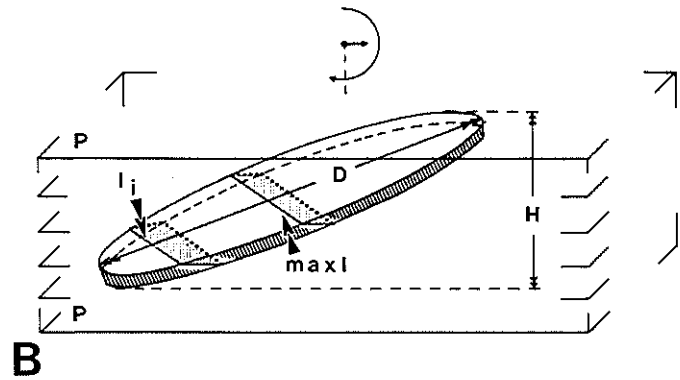

B

Figure 2.

A, B. Photomicrographs of E-PTA treated non-perforated (A) and perforated (B) synapses in stratum radiatum of the hippocampal CA3 area of a 3 months old rat. The section thickness used is 25 nm. The synapses are positioned in the tissue section "en face", i.e. instead of being cut by sectioning, the synapse is fully incorporated in the tissue and the presynaptic "grid" of dense projections is facing the upper plane of the section. The dark (electron dense) areas are dense projections (arrow).
P, perforation.

C, D. Drawings of the synapses, illustrated in A and B. The black dots represent the presynaptic dense projections. Compared to non-perforated synapses, the DPs in perforated synapses are more irregular (note dense projections indicated by open circles) and so is their pattern of distribution (compare A, B, C and D). In addition, the presynaptic grid of dense projections is interrupted at one or more sites in perforated synapses. Such interruptions are called "perforations" (P) (compare A, B, C and D).
The arrows 1 and 2, intersecting the synapses, assume random "cuts" through the synapses. In 1, the cut runs through the dense projections *carrying* zone (DP zone); in 2 the cut, in addition, runs through a dense projections *free* zone (perforation zone or perforation (P); compare C and D with E and F).

E, F. When "cut" by sectioning, the synapses appear in the tissue section "en profile", i.e. the synapse is transversely cut by sectioning and shows the profile of the transected synaptic contact zone (CZ) or "synaptic disc" (= DP-zone + possible P-zone).
The top figures in E and F represent the "en profile" appearance of transections 1 and 2 in figs. C and D, after treatment of the tissue with E-PTA; the lower figures show their appearance after treatment with OsO_4.
After OsO_4 treatment the presynaptic transmitter vesicles (PrSV) and the pre and postsynaptic cell membranes (PrCM and PCM, respectively) are visualized whereas they are not after E-PTA treatment. In contrast, the dense projections (DP) and postsynaptic band (PSB) (density or plate) are perfectly visualized after E-PTA treatment but not after OsO_4 because the, by OsO_4 visualized PrSV, overlie the DPs.
The actual transmission of information from one cell to the other occurs at the "active zone" composed of the presynaptic grid of dense projections and corresponding postsynaptic membrane thickenings which are separated by the intercleft space (ICS). Within the ICS is the intercleft line (ICL) (electron dense material in the middle of the ICS).

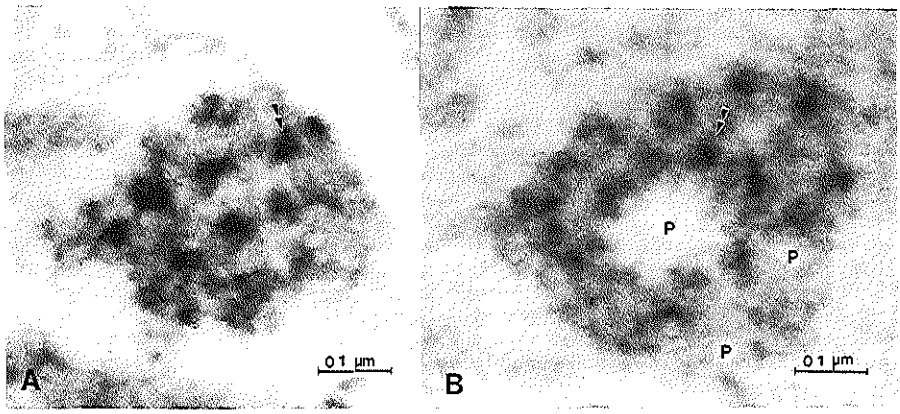
1
0 1 µm
A
2
P
P
P
0 1 µm
B

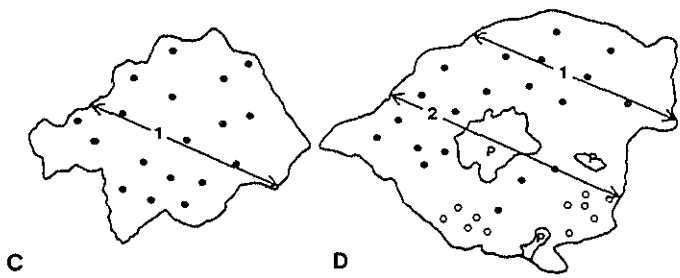
1
C
1
2
P
D

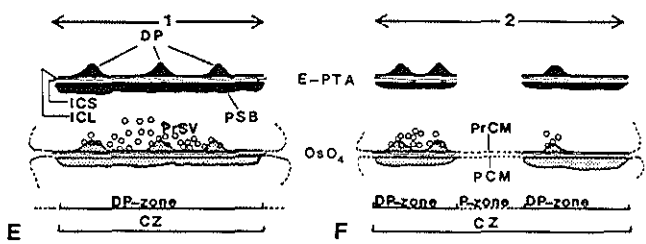
1
DP
ICS
ICL
PSB
PCSV
DP-zone
CZ
E
E-PTA
OsO4
2
PrCM
PCM
DP-zone
P-zone
DP-zone
CZ
F

Figure 3.

A. Diagram, illustrating the sampling scheme for the quantification of the hippocampal pyramidal cell nulei. For the estimation of the number of pyramidal cells (and projected height H of their nuclei the disector "stack" procedure was performed (Sterio, 1984).
A stack of n sections (n = 11* the 10-th section of a series of k sections) was composed of (n-1) disectors. The section pair, composing a disector, i.e. the reference plane and look-up plane, consisted of two sequential "10-th"-sections, e.g. the 1-st and 11-th section, the 11-th and 21-st section, and so on.

B. Disector pair of toluidine blue stained epon sections (0.25 μm thick) of the hippocampal CA3 area of a 3 months old rat showing pyramidal neurons. On the left is the 'reference plane'; on the right is the 'look-up plane' of the disector. To estimate the number of cell nuclei Gundersen's (1977) unbiased counting rule is applied and only the nuclei that are present in the framed reference area of the reference plane, but not in the look-up plane (dotted circle) are counted; there number is unbiased (Sterio, 1984).
Note that, in case the disector would be used in the reversed direction, i.e.: the reference plane on the right and the look-up plane on the left, the nucleus, indicated by the arrows, would have been counted.

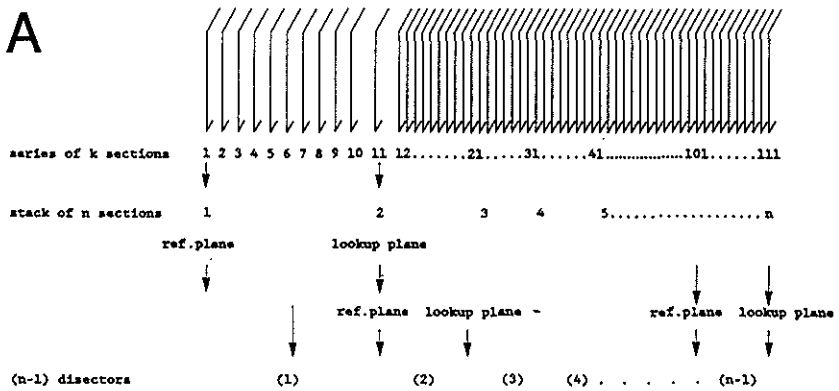
A
series of k sections
1 2 3 4 5 6 7 8 9 10 11 12.....21.....31.....41.....101.....111
stack of n sections
1
2
3
4
5.....n
ref.plane
lookup plane
ref.plane
lookup plane
ref.plane
lookup plane
(n-1) disectors
(1)
(2)
(3)
(4) . . . . . (n-1)

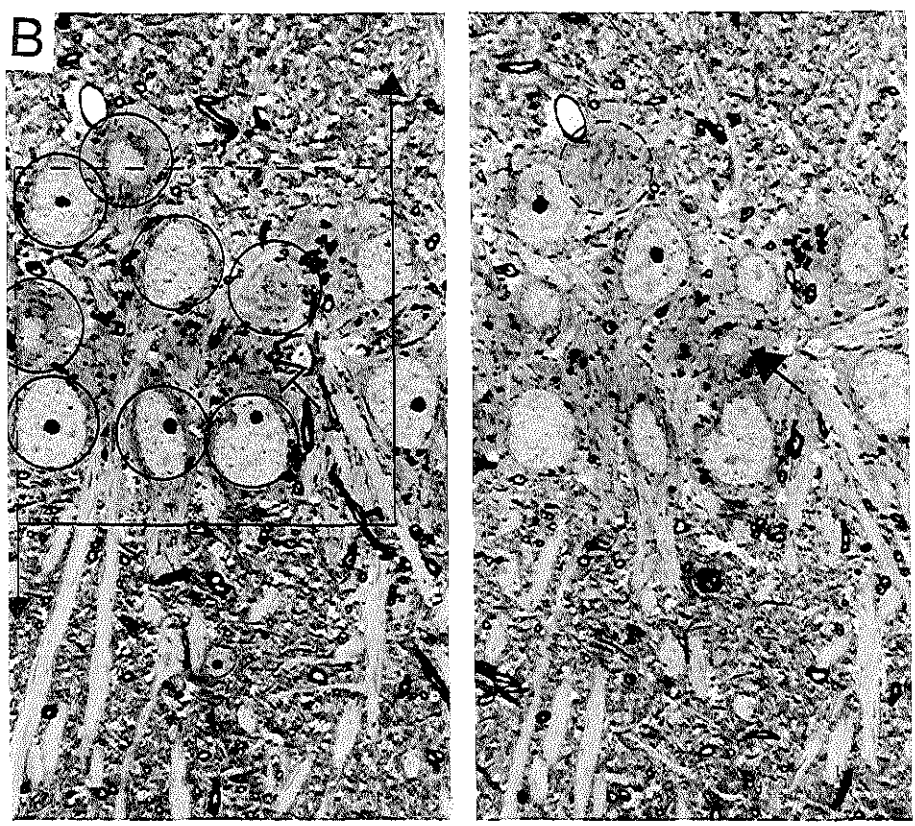
B

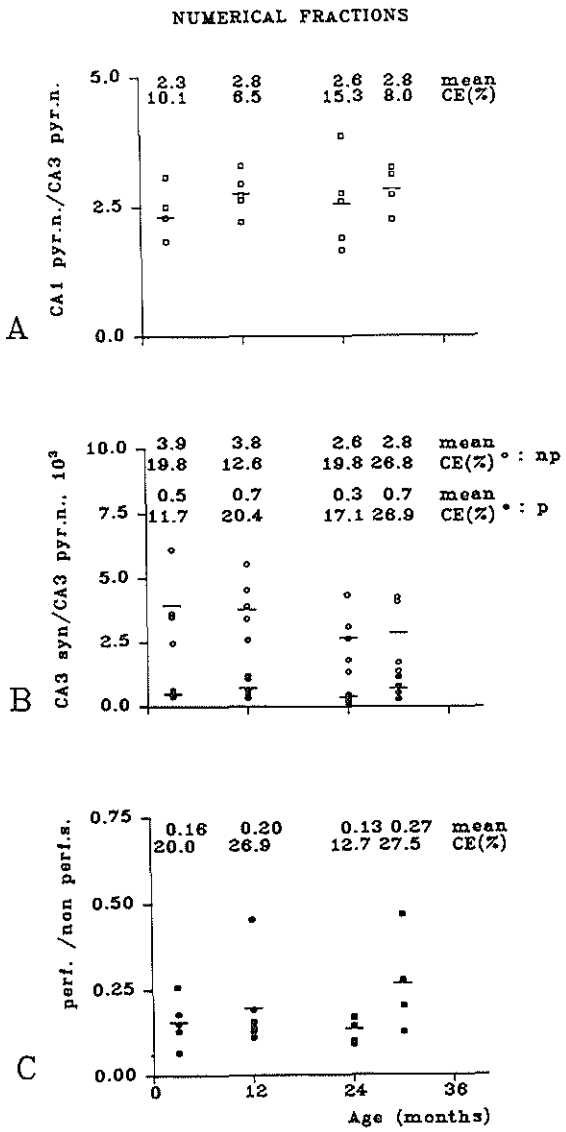

Figure 4. Relationship between the estimated numerical fractions of:

A. CA1 neurons to CA3 neurons (y-axis) and the age of the rats (x-axis),
B. CA3 synapses to CA3 pyramidal neurons (y-axis) and the age of the rats (x-axis),
C. CA3 perforated to CA3 non-perforated synapses (y-axis) and the age of the rats (x-axis).

The estimated number fraction per age-group is indicated on top of each figure with the coefficient of error among rats (CE=SEM/mean*100%). In the figure, the estimated mean numerical fraction is represented by little bars.

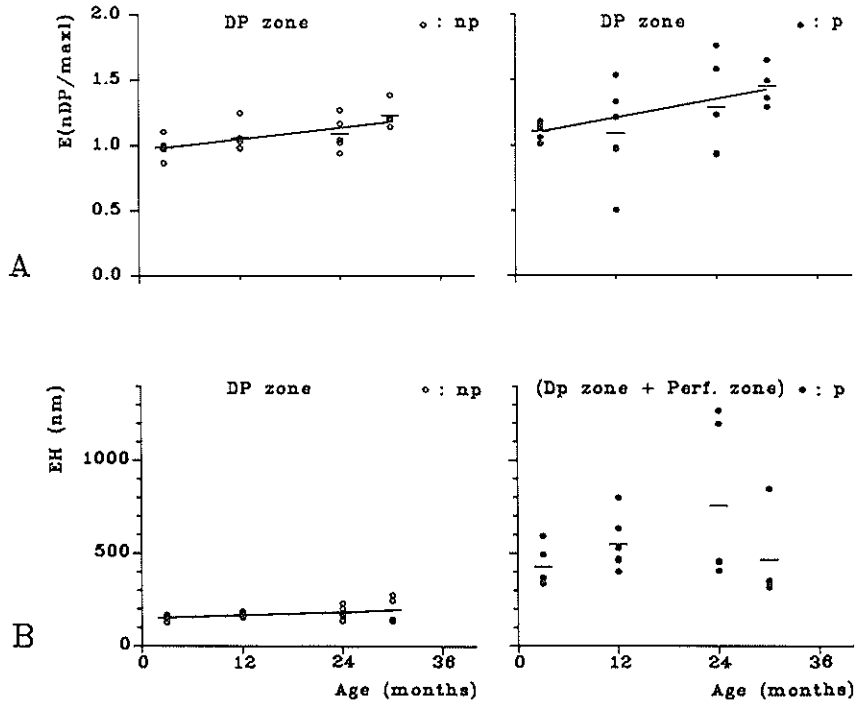

Figure 5. For non-perforated (left; open circles) and for perforated synapses (right; closed circles) in the hippocampal CA3 area (stratum radiatum) of female rats, the relationship is shown between:

A. the expected ratio of the number of dense projections observed along the maximum intercept length and the maximum intercept length of the DP zone itself (E(nDP(maxl)) (y-axis) and the age of the rats (x-axis),

B. the expected projected height of the total synaptic contact zone (y-axis) and the age of the rats (x-axis).

The regression line for E(nDP/maxl)(non perforated synapses) is y=0.960+0.0070x (P2=0.006, significant regression); 95% confidence limits of intercept: 0.865, 1.056; of slope: 0.0024, 0.0124. The variation in the data explained by the regression (R^2) is 35.4%. The regression line for E(nDP/maxl)(perforated synapses) is y=1.0670+0.0119x (significant regression, P2=0.0007); 95% confidence limits of intercept: 0.6081, 1.5249; of slope: 0.0058, 0.0180; R^2=48.5%.
The regression line for EH(non-perforated synapses) is: y=146.6+1.558x (P2=0.031, significant regression); 95% confidence limits of intercept: 129.9, 163.2; of slope: 0.1570, 2.959; R^2=23.3.
The little bars in the figure represent the estimated mean value per age-group of the investigated variables est E(nDP/maxl) and est EH.

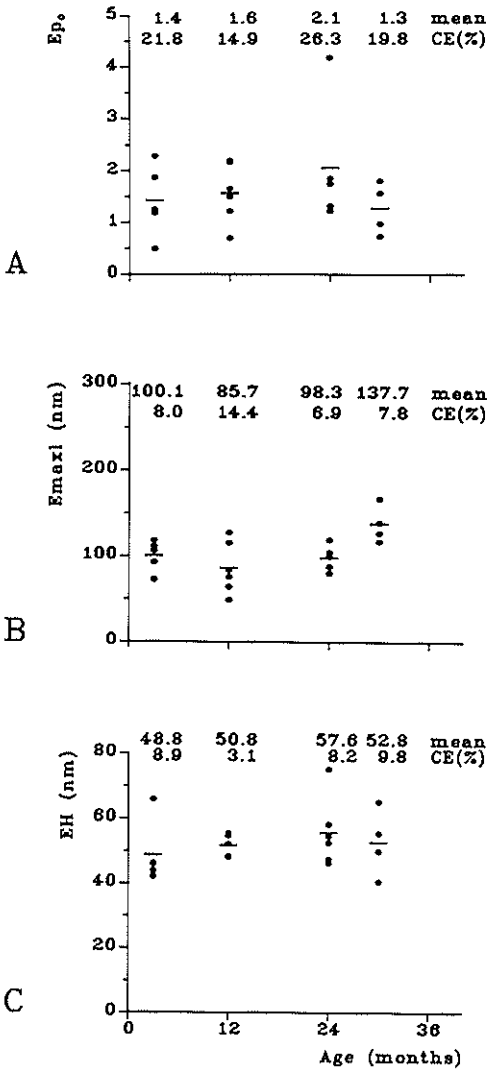

Figure 6. Relationship between (y-axis and x-axis):

A. the expected number of synapse-perforations per perforated synapse (Ep_0)(y-axis) and the age of the rats (x-axis),

B. the expected maximum intercept length (Emaxl) of the synapse-perforations (y-axis) and the age of the rats (x-axis),

C. the expected projected height (EH) of the synapse-perforations (y-axis) and the age of the rats (x-axis).

The estimated mean ratio per age-group is indicated on top of each figure with the coefficient of error among rats (CE=SEM/mean*100%). In the figure, the estimated mean ratio is represented by little bars.

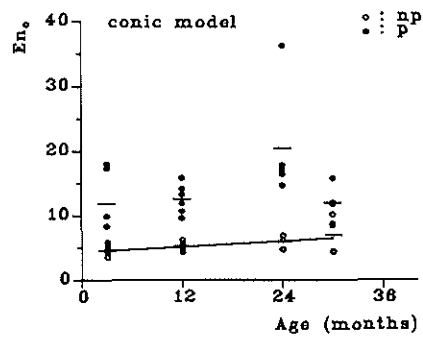

Figure 7. Relationship between the expected number of presynaptic dense projections per synapse (En_0) (y-axis) and the age of the rats (x-axis) of non-perforated (open circles) and perforated (closed circles) synapses in the hippocampal CA3 area (stratum radiatum) of female rats. En_0 is calculated according to the conic model, assuming conic particles in space. The regression line for the non-perforated synapses is: y=4.191+0.0762x (significant regression, P2=0.0067); 95% confidence limits of intercept: 3.4525, 4.9291; of slope: 0.0239, 0.1285; R^2=34.3%.
The little bars in the figure represent the estimated mean value per age group (est En_0).

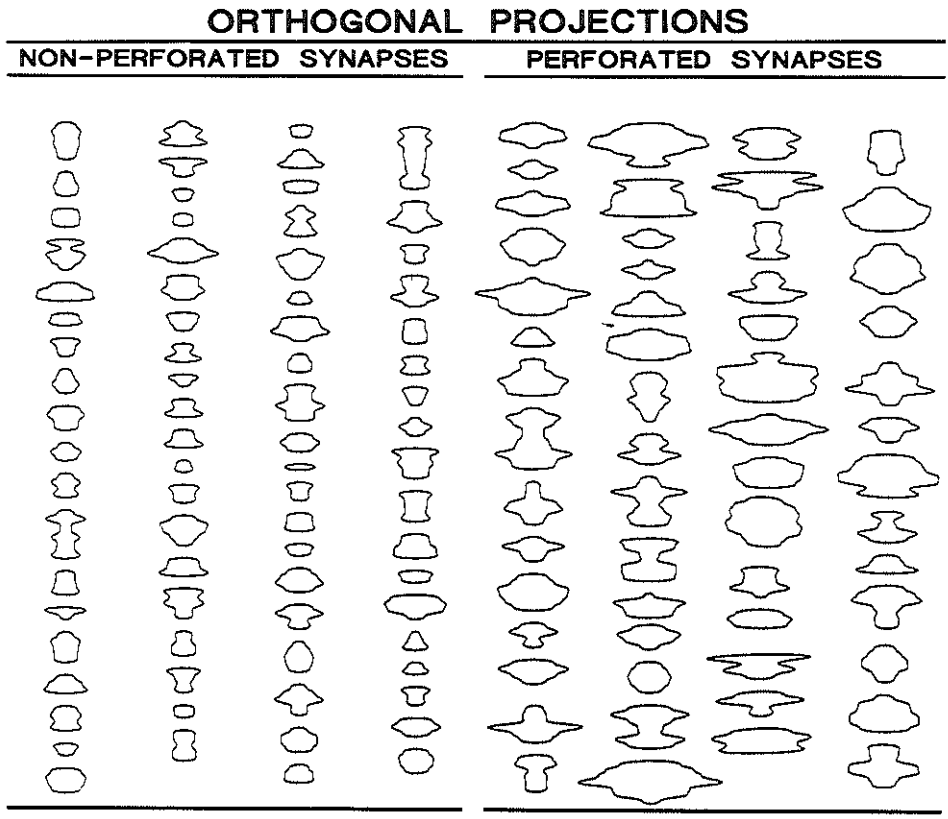

Figure 8. Randomly chosen examples of 2D reconstructions of orthogonal projections (shadows) of non-perforated and perforated synapses in the hippocampal CA3 area (stratum radiatum) of rats of four different age-groups (3, 12, 24 and 30 months).
From visual (qualitative) inspection of these synapse shadows it can be concluded that both synapse types deviate considerably from the presumed disc-shape and that the perforated synapses are larger than the non-perforated ones. Differences in shape of the shadows cannot be detected from qualitative inspection, only.

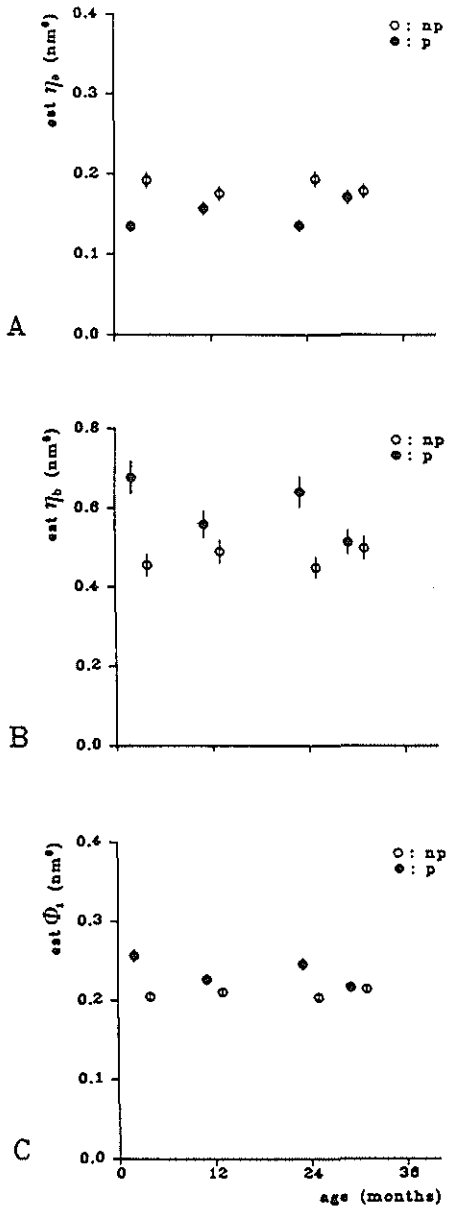

Figure 9. Relationship between estimates of

A. the normalized central moments with reference to the semi-major principle axis (est $E\eta_a$) (y-axis) and the age of the rats (x-axis),

B. the normalized central moments with reference to the semi-minor principle axis (est $E\eta_b$) (y-axis) and the age of the rats (x-axis),

C. the moment invariant est $E\Phi_1$ (= $E\eta_{02} + E\eta_{20}$) (y-axis) and the age of the rats (x-axis).

Est $E\eta_a$, est $E\eta_b$ and est $E\Phi_1$ are variables, independent of the size, shape and orientation of the investigated particles. Differences in these variables point at *differences* in *shape*.

PART IV

Appendix

DESCRIPTION OF PRACTICAL APPROACHES FOR THE QUANTIFICATION OF NEURONAL STRUCTURES

QUANTIFICATION OF SYNAPSES AND SYNAPTIC SUBSTRUCTURES

QUANTIFICATION OF SYNAPSES AND SYNAPTIC SUBSTRUCTURES (STERIO, 1984; CRUZ-ORIVE 1985).

A. QUANTIFICATION OF SYNAPSES[1]

1. *Total number of synapses per unit disector volume, $N_v(s)$*

For a detailed description of the estimation of the number of both simple non-perforated (n-ps) and complex perforated (ps) synapses using the disector method, the reader is referred to De Groot and Bierman, 1986 (in particular fig. 3 of this paper with corresponding text).

An unbiased estimate of the number of synapses per unit disector volume was obtained as follows:

$$\text{est } N_v = \sum_{i=1}^{n} Q_i^- \; / \sum_{i=1}^{n} h_i A_i \qquad \text{(A.1.1.)}$$

where

est N_v	=	estimated total number of particles per unit disector volume
n	=	number of disectors
Q_i^-	=	synapses (not synapse-fragments!) present in A_i (reference plane) but not in A_i (look-up plane)
h_i	=	distance in disector between A_i (reference plane) and A_i (look-up plane). In this case, h_i equals the thickness of one section; hence, h_i=Et' (=expected section thickness)
A_i	=	reference area of the reference plane in the i-th disector (i=1,2,...,n)

Provided V(disector) and V(reference volume) are obtained from identically treated tissue (see: Discussion), an unbiased estimate of the total number of synapses can be obtained as follows

$$\text{est } N = \text{est } N_v \; \text{est V(reference volume)} \qquad \text{(A.1.2.)}$$

est N	=	estimated total number of particles per total volume e.g. total number of synapses in CA3, stratum radiatum
est N_v	=	estimated total number of particles per unit disector volume
est V	=	estimated volume of the brain structure, e.g. the volume V of stratum radiatum of the hippocampal CA3 area (= reference volume).

[1]In this appendix the notation E is used for 'average mean' instead of for its literal meaning 'Expectatia', which is a mathematical term.

To avoid problems, encountered in different treatment of disector and reference volume tissue (see: Discussion), the following numerical density ratios, obtained in epon-embedded tissue, were estimated:
1) N_V(non-perforated synapses) / N_V(perforated synapses);
2) N_V("all" synapses, CA3 str. rad.) / N_V(pyr. neurons, CA3 str. pyr.);
3) N_V(pyr. neurons, CA1 str. pyr) / N_V(pyr. neurons, CA3 str. pyr.).

2. *Maximum intercept length of the synapses, Emaxl(s)*

The Q^- synapses were tracked through the series of sections and the observed maximum profile (=intercept) length, maxl, was measured using a semi-automatic image analysis system "Videoplan" (Kontron Messgeräte Eching, West Germany). Then,

$$\text{est Emaxl} = \left[\sum_{i=1}^{n} \sum_{j=1}^{Q_i^-} \text{maxl}_{ij} \right] / \sum_{i=1}^{n} Q_i^- \qquad \text{(A.2.1.)}$$

where

est Emaxl	=	estimated maximum synapse intercept length, observed in serial sections
n	=	number of disectors
maxl_{ij}	=	maximum intercept length of the j-th synapse in the i-th disector. Note that j runs from 1 to Q_i^-
Q_i^-	=	number of synapses, present in A_i(reference plane) but not in A_i(look-up plane)

It should be noted that, for circular disc-like synapses, maxl equals the diameter of the synaptic disc; for other shapes of synapses it is as close to the ideal as one can come for non-circular shapes (Braendgaard and Gundersen, 1986).

3. *Synapse perimeter length, EL(s)*

The size parameter EL was calculated from the ratio: est L_V / est N_V. For est N_V of this ratio an unbiased estimate of N_V, obtained by the disector method (see: Appendix, A1) was used.

To obtain est L_V, the following approach was followed. After identification of the synapse type by tracking the synapses through the series of sections, the number n_i of synapses present in A_i(reference plane) was counted.
An (uncorrected) length density was calculated as follows:

$$\text{est } L_V' = 4 \left(\sum_{i=1}^{m} n_i \right) / \sum_{i=1}^{m} A_i \qquad \text{(A.3.1.)}$$

where

est L_V'	=	estimated length density, uncorrected for capping and overprojection
m	=	number of series
n_i	=	number of synapses (not synapse-

fragments!) present in A_i (reference plane) and tracked through the series of sections

A_i = reference area of the reference plane in the i-th series

To correct for capping and overprojection:

$$\text{est } L_V = \text{est } L_V' \, [(Et'/EH) + \cos Z]^{-1} \qquad \text{(A.3.2.)}$$

where

est L_V = estimated length density corrected for capping and overprojection

Et' = expected section thickness (cf. De Groot, 1988)

EH = expected projected height (=linear projection) of the synapses

Z = capping angle for synapses

EH is calculated from:

$$\text{est } EH = \text{est } \tilde{EH}/\text{est } \cos Z \qquad \text{(A.3.3.)}$$

where

est $\tilde{EH}$ = estimated effective projected height of the synapses

$$\text{est } \tilde{EH} = (EN_A/\text{est } N_V) - Et' \qquad \text{(A.3.4.)}$$

where

EN_A = expected number of hit and observed synapses per unit area

est cos Z is obtained as follows:

$$\text{est } (\cos Z_i) = \text{est } [\cos \arcsin (\sin Z_i)] \qquad \text{(A.3.5.)}$$

$$\text{est } (\sin Z_i) = \sum_{i=1}^{m} \sum_{j=1}^{n_i} \text{minl}_{ij} / \sum_{i=1}^{m} \sum_{j=1}^{n_i} \text{maxl}_{ij} \qquad \text{(A.3.6.)}$$

where

minl_{ij} = shortest intercept length observed in serial sections for the j-th tracked synapse in the i-th series

maxl_{ij} = longest intercept length observed in serial sections for the j-th tracked synapse in the i-th series

In the present study the data of the minl_{ij} and maxl_{ij} of all synapses (i.e.

the Q-portions) of n rats per age group were pooled and the ratio of the pooled data was used to estimate sin Z for both synapse types separately.

4. *Synapse (presynaptic) surface area, ES(s)*

The size parameter ES was calculated from the ratio: est S_V/est N_V. For est N_V of this ratio an unbiased estimate of N_V, obtained by the disector method (see: Appendix, A1) was used.

From the number of n_i synapses counted in A_i(reference plane) (see: Appendix, A3) the intercept length l_{ij} was measured, using the Videoplan (see: Appendix, A2). An (uncorrected) surface density was calculated as follows:

$$\text{est } S_V' = (4\pi)\ EL_A \qquad \text{(A.4.1.)}$$

where

est S_V'	=	estimated surface density uncorrected for capping and overprojection
EL_A	=	expected intercept length of synapses per unit area

$$EL_A = \sum_{i=1}^{m} \sum_{j=1}^{n_i} l_{ij} \Big/ \sum_{i=1}^{m} A_i \qquad \text{(A.4.2.)}$$

where

EL_A	=	expected intercept length of synapses per unit area
m	=	number of series
n_i	=	number of synapses (not synapse-fragments!) present in A_i(reference plane) and tracked through the series of sections
l_{ij}	=	intercept length of the j-th synapse in the i-th series. Note that j runs from 1 to n_i
A_i	=	reference area of the reference plane in the i-th series

To correct for capping and overprojection:

$$\text{est } S_V = [\text{est } S_V' - (4/\pi) Et'(ED) \text{est } N_V] g(Z) \qquad \text{(A.4.3.)}$$

where

est S_V	=	estimated surface density corrected for capping and overprojection
Et'	=	expected section thickness (cf. De Groot, 1988)
ED	=	expected diameter of synaptic "disc"
est N_V	=	estimated number of synapses per unit

volume (see: Appendix, A1)

Z = capping angle for synapses

ED is obtained as follows:

$$ED = EL/\pi \qquad (A.4.4.)$$

where

EL = expected synapse perimeter length (see: Appendix, A3)

g(Z) is calculated as follows (Z in radials):

$$g(Z)=[1-(2/\pi)(Z-\sin Z \cos Z)]^{-1} \qquad (A.4.5.)$$

To calculate Z, see Appendix, A3

5. *Projected height (=linear projection) of the synapses, EH(s)*

The size parameter "projected height" of the synapses was calculated according the Sterio (1984, formula 4). For this, both the Q and the Q^- portions of the synapses determined for the estimation of the number of synapses (see: Appendix, A1) were used. The projected height of the synapses was estimated as follows:

$$\text{est } EH = \left[\sum_{i=1}^{n} (Q_i \, h_i) \right] / \sum_{i=1}^{n} Q_i^- \qquad (A.5.1.)$$

where

est EH = estimated projected height of the synapses

n = number of disectors

Q_i = number of synapses counted in A_i(reference plane)

h_i = distance in disector between A_i(reference plane) and A_i(look-up plane). In this case, h_i equals the thickness of one section; hence, h_i=Et'(=expected section thickness)

Q_i^- = number of synapses present in A_i(reference plane) but not in A_i(look-up plane) of the i-th disector

As pointed out by Sterio (1984), EH requires a random orientation distribution of either the investigated particles or the disectors. With respect to synapses in stratum radiatum of the hippocampal CA3 area, a random orientation distribution was assumed.

B. QUANTIFICATION OF SYNAPSE PERFORATIONS

1. *Number of perforations per perforated synapse, Ep_0*

An unbiased estimate of the number of synapse perforations (p) was also obtained according to Sterio (1984). However, in view of their low quantity and relatively small size the Q^- portion was determined in complete series (="stacks") of sections. For this, the reference area A_i of the first section of the series was compared with the same area in the adjacent second section to obtain the Q^- portion of the first disector of the stack (= $Q(1)^-$). This latter area, i.e. the look-up area of the first disector, subsequently served as reference area of the second disector and was compared with the third section of the stack to obtain $Q(2)^-$. This procedure was followed through the complete stack of n sections. Doing so, all sections of the stack -except for the first and last (=n-th) sections- first served as look-up plane of the one disector and then as reference plane of the next. A stack (=series) of n sections was thus composed of (n-1) disectors and resulted in (n-1) Q^- portions. In this study, a stack consisted of at least 15 adjacent serial sections; at least 5 stacks per animal were analyzed. An estimate of the number of synapse perforations per perforated synapse (ps) was then calculated as follows:

$$\text{est } Ep_0 = \left[\sum_{i=1}^{m} \left(\sum_{j=1}^{n_i} Q^-_{ij} \Big/ \sum_{j=1}^{n_i} h_{ij}\, A_{ij} \right) \Big/ m \right] / N_V(ps) \qquad \text{(B.1.1.)}$$

where

est Ep_0	=	estimated number of synapse perforations per perforated synapse
m	=	number of stacks (=series)
n_i	=	number of disectors in i-th stack
Q^-_{ij}	=	number of perforations, present in A_{ij}(reference plane) but not in A_{ij}(look-up plane) of the j-th disector in the i-th stack
h_{ij}	=	distance in disector between A_{ij}(reference plane) and A_{ij}(look-up plane). In this case, h_{ij} equals the thickness of one section; hence, h_{ij} = Et' (=expected section thickness)
A_{ij}	=	reference area of the reference plane in the j-th disector in the i-th stack
$N_V(ps)$	=	estimated number of perforated synapses (ps) per unit volume (see: Appendix, A1)

2. *Maximum intercept length of the perforations, E(maxl)(p)*

The same disectors, used to estimate E(maxl)(s) (= synapses) were used to estimate E(maxl)(p) (=perforations). Of all the perforations present in A_i(reference plane) but not in A_i(look-up plane) -i.e. the Q^- perforations- the maximum intercept length maxl was measured using the Videoplan (see: Appendix, A2). Then, est E(maxl)(p) was calculated in accordance with est

E(maxl)(s) (see Appendix, formula A.2.1.).

The perforations were observable in 1 to 3 serial sections depending on their size. For circular perforations, maxl represents the diameter of the perforation; for non-circular shapes it is as close to the ideal as one can come (Braendgaard and Gundersen, 1986).

Note, that "maxl" used also in De Groot and Bierman (1986) represents "maxB" in Cruz-Orive's (1985) paper.

3, 4. *Perforation perimeter length, EL(p) and perforation surface area, ES(p)*

The disectors used for E(maxl)(p) were also used to estimate EL(p) and ES(p). In principle, the procedures for EL(s) (see: Appendix, A3) and ES(s) (see: Appendix, A4) were used. However, EL(p) and ES(p) were obtained from the ratios est L'_V /est N_V. In other words: no corrections for overprojection and capping were carried out. In fact, assuming an overprojection of the E-PTA stained profiles of the "dense projection zone" implies an underprojection of the "dense projection free zone". Such a correction was not made. EL(p) and ES(p), in principle, are needed for the prediction of the number of dense projections per presynaptic surface area using the tile model (see: Appendix C2) and fluctuations in EL(p) and ES(p) will hardly affect the final outcome of formula C.2.1.

5. *Projected height (=linear projection) of the perforations, EH(p)*

est EH(p) was determined in accordance with formula A.5.1. where the estimation of EH(s) is given. In case of the perforations the Q and Q^- portions determined in stacks for the estimation of the number of perforations were used to estimate EH(p):

$$\text{est EH} = \sum_{i=1}^{m} \left[\left(\sum_{j=1}^{n_i} Q_{ij} \sum_{j=1}^{n_i} h_{ij} \right) / \sum_{j=1}^{n_i} Q^-_{ij} \right] / m \qquad \text{(B.5.1)}$$

where

est EH	=	estimated mean projected height of the perforations
m	=	number of stacks (=series)
Q_{ij}	=	number of perforations counted in A_{ij}(reference plane) of the j-th disector in the i-th stack
h_{ij}	=	distance in disector between A_{ij}(reference plane) and A_{ij}(look-up plane). In this case, h_{ij} = Et' (=expected section thickness)
Q^-_{ij}	=	number of perforations present in A_{ij}(reference plane) but not in A_{ij}(look-up plane) of the j-th disector in the i-th stack
n_i	=	number of disectors in i-th stack

Note that EH requires a random orientation distribution of either the perforations or the disectors (Sterio, 1984); a random orientation

distribution of the synapse perforations in stratum radiatum of the hippocampal CA3 area was assumed.

C. QUANTIFICATION OF THE NUMBER OF DENSE PROJECTIONS

1. *Estimation of the number of dense projections along the maximum intercept length E(nDP/maxl).*

After measuring the maximum intercept length (maxl) of the Q^- synapses (see: Appendix, A2) and the Q^- perforations (see: Appendix, B2) the number of dense projections along maxl was counted. Then, the estimated mean number of dense projections along maxl of the *dense projection zone* is

$$\text{est } E(nDP/maxl) = \{ \sum_{i=1}^{n} \sum_{j=1}^{Q_i^-} [nDP_{ij}/(maxl_{ij} - \text{est } Emaxl(p))] \} / \sum_{i=1}^{n} Q_i^- \qquad (C.1.1.)$$

where

n	=	number of disectors
Q_i^-	=	number of synapses, present in A_i(reference plane) but not in A_i(look-up plane)
$maxl_{ij}$	=	maximum intercept length of the j-th synapse in the i-th disector (j runs from 1 to Q_i^-)
est Emaxl(p)	=	estimated maximum intercept length of (Q^-) synapse perforations

To calculate est Emaxl(p) see: Appendix, A2 and B2. Note that in the case of non-perforated synapses, est Emaxl(p) in formula C.1.1. is zero.

2. *Number of dense projections per synapse, En_0: tile model*

The basis for the "tile" model (Cruz-Orive, 1985) is formed by the hypothesis that a dense projection and its surrounding hexagonal area (cf. e.g. Akert and Pfenniger, 1969; Akert et al., 1971; Akert, 1973; Vrensen et al., 1980) is a basic unit, involved in guiding the vesicular release of neurotransmitters. In the model an unbounded lattice of fundamental regions (= the hexagonal areas), each containing a fundamental domain (= a dense projection) is covered with a plane mobile figure of arbitrary connectivity (= the presynaptic surface area) (cf. Cruz-Orive, 1985, fig. 4). Using classical methods of integral geometry the expected number of fundamental domains completely inside the mobile figure, i.e. the expected number of dense projections on the presynaptic surface area, was calculated as follows:

$$En_0 = \{ [(ES) + (1 - Ep_0)a_1]/a_2 \} - b_1(EL)/(2\pi a_2) \qquad (C.2.1.)$$

where

En_0	=	expected number of dense projections per synapse
ES	=	expected area of the mobile figure, i.e. the area enclosed by the outer boundary (in the case of perforated synapses:

minus the area occupied by the perforation(s))

Ep_0 = expected number of perforations per synapse

a_1 = area of the fundamental domain, i.e. area occupied by a dense projection

a_2 = area of the fundamental region, i.e. the hexagon belonging to a dense projection

b_1 = boundary length (= perimeter length) of the fundamental convex domain i.e. a dense projection

EL = expected total perimeter length of the mobile figure, i.e. the perimeter length of the presynaptic surface area EL(s) (in the case of perforated synapses: plus the perimeter length of the perforations EL(p))

Note that Ep_0 = Eh in Cruz-Orive, 1985, formula 3.2. In the present paper Eh was replaced by Ep_0 to avoid confusion with h(disector) (See e.g.: Appendix, A1); b_1 in this paper = l_1 in Cruz Orive's paper to avoid confusion with synaptic intercept length, l(synapses).

To calculated a_1, a_2 and b_1, the intercept length of the base of the dense projections (b(BDP)) and of the space between two adjacent dense projections (b(iDP)) was measured in a number of synaptic profiles present in A_i(reference plane). Then,

$$a_1 = \pi\,(b(BDP)/2)^2 \qquad (C.2.2.)$$

$$a_2 = 2\sqrt{3}(b(BDP)/2+b(iDP)/2)^2 \qquad (C.2.3.)$$

$$b_1 = \pi\,(b(BDP)/2) \qquad (C.2.4.)$$

To estimate EL and ES of synapses and perforations see: Appendix, A3, A4, B3 and B4. To estimate Ep_0, see: Appendix, B1.

3. *Number of dense projections per synapse, En_0: conic model*

For the "conic" model, the dense projections were regarded as cone-like structures sitting on the presynaptic surface area. The expected number of dense projections (dp) per synapse (En_0) was obtained from the ratio $N_V(dp)/N_V(s)$. $N_V(dp)$ was obtained by counting the profiles of the dense projections observed in A_i(reference plane) and applying a correction for overprojection and capping:

$$\text{Est } N_V = \sum_{i=1}^{m} [n_i/(Et' + K\,EH)] \qquad (C.3.1.)$$

where

est N_V = estimated number of dense projections per

unit volume

m	=	number of series
n_i	=	number of dense projections present in A_i(reference plane)
Et'	=	expected section thickness (cf. De Groot, 1988)
K	=	truncation constant for dense projections
EH	=	expected projected height of the dense projections

Then, assuming cone-like particles with radius=BDP/2 and height=HDP, EH(dp) is :

$$EH=(b(BDP)/4)\{\pi+[b(HDP)/b(BDP)/2)]-\arctan\,[b(HDP)/(b(BDP)/2)]\} \qquad (C.3.2.)$$

where

b(BDP)	=	intercept length of the base of the dense projections
b(HDP)	=	intercept length of the height of the dense projections

D. (INDIRECT) QUANTIFICATION OF DIFFERENCES IN SYNAPTIC SHAPE: MEASUREMENTS ON "SYNAPSE ORTHOGONAL PROJECTIONS" (SHADOWS)

To obtain so called "orthogonal projections" of the Q$^-$portions of both non-perforated and perforated synapses, the following procedure was carried out. Q$^-$disector-sampled synapses were tracked in adjacent serial sections. In each section in which the "tracked" synapse appeared, the "chord length" (=shortest distance between the outer ends) of the intercepts (=profiles) was measured using the Videoplan (see: Appendix, A.2). "Symmetrical" reconstructions (= orthogonal projections) of the synapses were performed by a program (SYNMORF-DRAWING V4-90) written in the Fortran language by one of us (EPB B). In the reconstructions the centre-point of all intercept chord lengths of a tracked synapse -i.e. the chord length(s) of the DP zone(s) plus the chord length(s) of possible perforation(s)- are put on top of each other. The width of a drawn chord length equals the section thickness used. Hence, "symmetric" reconstructions result, comparable with "orthogonal projections" (part III, fig. 8). The hardware used was a VAX/VMS 8250-computer (Digital Equipment Corporation, Maynard, Massachusetts) and a ZETA8-plotter (NICOLET).

To test possible age-related changes in synaptic shape the following parameters were calculated for each orthogonal projection of the Q$^-$ synapses: the perimeter L, the area S (= m_{00}= 0-th order geometric moment), the normalized central moments with respect to x- and y-axis and with respect to the semi-major and semi-minor principle axis (η_{02}, η_{20}, η_a and η_b, respectively) and the moment invariant Φ_1, being a function of geometric moments and invariant under image translation, scaling and rotation. For these calculations an 8-connected-chaincode scheme (Freeman, 1960), coding the contour of the drawn synapse projection, was used. This coding was derived

from the coordinates of the drawing. The moments η_a, η_b and Φ_1 are invariant under image translation, scaling and rotation.

To obtain L, the corner count estimator, proposed by Dorst and Smeulders (1987, formula 24) was calculated.

$$L_c(n_e, n_o, n_c) = an_e + bn_o + cn_c \qquad \text{(D.1.1.)}$$

where

- L_c = corner count estimator
- n_e = number of even chaincode elements in the string of the contour
- n_o = number of odd chaincode elements in the string of the contour
- n_c = (corner count =) number of occurrences of consecutive chaincode elements in the string of the contour
- a,b,c = coefficients for the (n_e, n_o, n_c) characterization; in this case a = .980, b = 1.406 and c = -.091. For the derivation of a, b and c the reader is referred to the original paper of Dorst and Smeulders (1987), formulae 22-24.

In principle L_c is unbiased over an ensemble of long straight strings. In this case, the contour length of the orthogonal projections was approximated as a concatenated series of circular arcs. Although not designed for such situations, L_c is remarkably accurate (Dorst and Smeulders, 1987).

The 0-th order geometric moment m_{00} (=S) and the normalized central moments with respect to x- and y-axis and with respect to the semi-major and semi-minor principle axis (η_{02}, η_{20}, η_a and η_b, respectively) and the moment invariant Φ_1 were obtained as follows (Chen, 1990).

Basic knowledge learns that a digital image can be presented by moments of its intensity functions. The (K,L)-th (geometric) moment of an object in an image is defined by

$$m_{KL} = \sum_{i=1}^{N} \sum_{j=1}^{M} i^K j^L x_{ij} \qquad \text{(D.1.2.)}$$

where

- m = moment
- K,L = order indicators; the order of the moment equals K plus L
- N = number of coordinates in x direction
- M = number of coordinates in y direction
- i = x coordinate; i=1,2,3...N
- j = y coordinate; j=1,2,3...M
- x_{ij} = binary value at the point (i,j).

Note that
$x_{ij} = 1$, if point (i,j) is on or within (the contour of) the object
$x_{ij} = 0$, if point (i,j) is outside the object

The area (S) of the binary image of the object is represented by the 0-th order geometric moment m_{00} (K and L zero).

m_{00} together with the 1-st order geometric moments m_{10} and m_{01} locate the centroid (= centre of gravity = point i_o,j_o) of an object in the image. The centroid is defined by

$$i_o = m_{10} / m_{00} \qquad j_o = m_{01} / m_{00} \qquad \text{(D.1.3.)}$$

The centroid, together with th 2-th order geometric moments m_{02} and m_{20} (= axial quadratic surface moments with respect to x- and y-axis, respectively) were used to compute the central moments μ_{02}, μ_{11} and μ_{20}

$$\mu_{02} = m_{02} - m_{01}^2 / m_{00} \qquad \mu_{20} = m_{20} - m_{10}^2 / m_{00} \qquad \text{(D.1.4.)}$$

$$\mu_{11} = m_{11} - m_{01}\, m_{10} / m_{00}$$

The central moments μ_{02} and μ_{11} and μ_{20} were normalized for scaling as follows

$$\eta_{02} = \mu_{02} / \mu_{00}^2 \qquad \eta_{20} = \mu_{20} / \mu_{00}^2 \qquad \text{(D.1.5.)}$$

$$\eta_{11} = \mu_{11} / \mu_{00}^2$$

where

η_{KL} = normalized central moments with respect to axis K, L

The normalized central moments with respect to semi-major (a) and semi-minor (b) principle axis were calculated as follows

$$\eta_a = \eta_{20} \sin^2\phi - 2\, \eta_{11} [\sin\phi \cos\phi] + \eta_{02} \cos^2\phi \qquad \text{(D.1.6.)}$$

$$\eta_b = \eta_{20} \sin^2(\phi+\pi/2) - 2\, \eta_{11} [\sin(\phi+\pi/2) \cos(\phi+\pi/2)] + \eta_{02} \cos^2(\phi+\pi/2) \qquad \text{(D.1.7.)}$$

where

η_a = semi-major principle axis
η_b = semi-minor principle axis
ϕ = slope of the semi-major principle axis

The slope of the semi-major principle axis is calculated as follows

$$\phi = \tfrac{1}{2} \tan^{-1} [2\, \mu_{11} / (\mu_{20} - \mu_{02})] \qquad \text{(D.1.8.)}$$

For the sake of completeness the formulae to calculate the length of the

semi-major and semi-minor principle axis are given below (Hu, 1962).

$$a = ((\mu_{02} + \mu_{20} + [(\mu_{20} - \mu_{02})^2 + 4\,\mu_{11}^2]^{1/2}) \,/\, (\mu_{00}/2))^{1/2} \qquad \text{(D.1.9.)}$$

$$b = ((\mu_{02} + \mu_{20} - [(\mu_{20} - \mu_{02})^2 + 4\,\mu_{11}^2]^{1/2}) \,/\, (\mu_{00}/2))^{1/2} \qquad \text{(D.1.10.)}$$

The ratio of these length parameters of the principle axis can, like the ratio of the axis in the geometric x-(A) and y-directions (B) (De Groot et al., 1992), be used to derive information about the *actual* shape of the particle[2]. It is noted that the *ratio* a/b equals the *ratio* A/B.

The moment invariant Φ_1 was obtained

$$\Phi_1 = \eta_{02} + \eta_{20} \qquad \text{(D.1.11.)}$$

From the moments mentioned above only the resulting moments η_a, η_b and Φ_1 are independent upon location, size and orientation of the investigated particles. Differences between age-groups or between the two synapse types in the estimated mean values of the 3 variables can result only from differences in shape. However, it should be borne in mind that -although est $E\eta_a$, est $E\eta_b$ and est $E\Phi_1$ are unbiased variables characterizing the shape of an object- knowledge on the shape of the orthogonal projections cannot simply be extrapolated to the true shape of the synapses. Nevertheless differences in the shape of orthogonal projections clearly do reflect differences in the true shape of the synapse.

REFERENCES

Akert, K. (1973) Dynamic aspects of synaptic ultrastructure, Brain Res., 49: 511-518.

Akert, K. and Pfenniger, K. (1969) Synaptic fine structure and neural dynamics. In S.H. Barondes (Ed.), Cellular dynamics of the neuron, I.S.C.B. Symposium, Vol. 8, Academic Press, New York, pp. 245-260.

Akert, K., Kawana, E. and Bandri, C. (1971) ZIO-positive and ZIO-negative vesicles in nerve terminals. In Eränko (Ed.), Histochemistry of nervous transmission, Progress in Brain Research, Vol 34, Elsevier, Amsterdam, pp. 305-317.

Braendgaard, H. and Gundersen H.J.G. 1986 The impact of recent stereological advances on quantitative studies of the nervous system, J. Neurosc. Methods, 18: 39-78.

Chen, K. (1990) Efficient parallel algorithms for the computation of two-dimensional image moments, Pattern Recognition, 23(1/2): 109-119.

Cruz-Orive, L.M. (1985) Estimating particle number and size. In L.F. Agnati

[2] Note : In De Groot et al. (1992) the axis in the geometric x- and y-directions are erroneously called *principle* axis

and K. Fuxe (Eds.), Quantitative Neuro-anatomy in Transmitter Research, MacMillan Press, London, pp. 11-24.

De Groot, D.M.G. (1988) Comparison of methods for the estimation of the thickness of ultrathin tissue sections, J. Microsc., 151: 23-42.

De Groot, D.M.G. and Bierman, E.P.B. (1986) A critical evaluation of methods for estimating the numerical density of synapses, J. Neurosc. Methods, 18: 79-101.

De Groot, D.M.G., Bierman, E.P.B. and Saris-Wijnans, M.J. (1992) 2D Reconstruction of synapse orthogonal projections: Estimation of differences in shape using second order moment invariants, Acta Stereol., 11/Suppl I: 587-592.

Dorst, L. and Smeulders, A.W.M. (1987) Length estimators for digitized contours, Computer vision, graphics and image processing, 40: 311-333.

Freeman, H. (1960) On the encoding of arbitrary geometric configurations, IRE Trans. Electr. Comp., C10: 260-268.

Hu, M.K. (1962) Visual pattern recoqnition by moments invariants, IRE Trans. Inf. Theory, IT-8: 179-187.

Sterio, D.C. (1984) Estimating number, mean sizes and variations in size of particles in 3-D specimens using disectors, J. Microsc. 134: 127-136.

Vrensen, G., Nunez Cardozo, J., Müller, L. and Van der Want, J. (1980) The pre-synaptic grid: a new approach, Brain Res., 184: 23-40.

SUMMARY

SUMMARY

Quantitative stereological/morphometrical methods are used to study whether synaptic plasticity occurs in the hippocamus of the rat during normal ageing. The methods are evaluated and their usefulness for quantitative morphological assessment of neural structures is discussed.

Part I is an introduction to the thesis. The purpose of the thesis is given, as well as a brief description of the anatomical organization of the hippocampal formation and recent views on structure and function of perforated synapses.

Part II includes 5 different papers, dealing with different methodological problems encountered in the quantification of synapses of arbitrary morphology using stereological/morphometrical methods.

In **Part II, Chapter 1**, the bias introduced in the estimation of synapse number and size when complex-shaped 'perforated' synapses are not recognized as such is studied. Results obtained in random sections are compared with results obtained in serial sections. The results showed that, when the consequences for stereological work of the simultaneous presence of complex-shaped perforated and non-perforated synapses are not realized, synaptic profile length is underestimated and synaptic density is overestimated when measured on random ultrathin E-PTA sections. It is shown that this problem can be solved by using serial sections and a calculation method which makes no assumptions about synaptic size and shape.

In **Part II, Chapter 2**, improvements of the protocol for serial sectioning are described, as is the application of the 'serial section technique' to estimate numerical densities of arbitrarily-shaped synapses. It is shown how the efficiency of the technique can be improved for routine application. For this, the use of large serial sections, preinspected at the light microscopical level is proposed as well as a rotation holder, a calibrated micrometer and specific grids to carry and orientate the section in the electron beam. Together, these changes in the protocol overcome the problems of orientation within the tissue and facilitate recognition of the areas of interest in sequential sections.

The serial section technique to estimate the numerical density N_V of perforated and non-perforated synapses is nearly unbiased. It was concluded that the section thickness should be measured very precisely, and that, when carried out in the way described, the serial section technique for calculating N_V is no longer more laborious than conventional methods.

In **Part II, Chapter 3**, different methods to estimate the thickness of (ultra)thin tissue sections are described, evaluated and compared. In general, the section thickness t' will differ from the actual distance t between the two cuts that generate a section. Five different methods are evaluated experimentally using sections of ten different interference colours: the 'small-fold' technique, b) the 'electron scattering' method, c) interference microscopy with A) the Vicker's M86 scanning microinterferometer and B) the Jenoptik Amplival Interphako interference microscope and d) the 're-embedding' method.

Reliable, reproducible and comparable results are obtained with the small-fold technique,

with the Vicker's M86 scanning microinterferometer and with the electron scattering method. For the electron scattering method, standard testlines for the different settings of the electron microscope were developed. The results obtained with the Jenoptik Amplival Interphako interference microscope are reproducible, but show a constant difference in thickness compared with the other three techniques. The re-embedding method proved to be more laborious and slightly less reliable than the other techniques. Furthermore it is concluded that the variation in t' between sections of a particular interference colour (inter-section variation) is larger than the variation in t' within a section (intra-section variation).

In **Part II, Chapter 4**, the conventional 'unfolding' procedure (Cruz-Orive, 1983) to estimate the numerical density of synapses is compared with two recent methods, i.e. the serial section technique (Cruz-Orive, 1980) and the 'disector technique' (Sterio, 1984), which do not rely on assumptions regarding the size, shape and orientation of the synapse.

It is shown that, with respect to the distinction between different types of synapses, a size distribution of synapses derived by conventional means does not provide satisfactory results since the types and extent of biases are never known.

Consistently lower values for N_V are obtained with the disector technique compared with the results of the serial section technique. The main conclusion in this respect is that both techniques can be used to estimate synaptic densities, provided a reliable estimate of the section thickness is obtained and an appropriate sampling procedure is used.

In **Part II, Chapter 5**, a method is described providing information on differences or changes in the shape of arbitrarily-shaped synapses using measurements on 2D reconstructions of synapse orthogonal projections (shadows). It is concluded that, whatever the actual shape of the investigated synapses may be, the results of the measurements on their orthogonal projections show that there is a difference in size and shape between perforated and non-perforated synapses. Compared to 3D reconstruction, the proposed 2D reconstruction approach is rather simple and differences found in the shape of the shadows demonstrated with this method reflect differences in the shape of the synapse. The method certainly has its limitations, in particular, with respect to the orientation and distribution of the synapses in the tissue and it does not permit firm conclusions about the actual shape of the synapse as 3D reconstruction does. Nevertheless, the method may provide relevant information about synaptic morphology which can not be obtained by other means. In the present study, 3D reconstruction is hampered by alignment problems which, so far, were unsolvable.

In **Part III** the effect of age on several ultrastructural features of neurons, of non-perforated and of perforated synapses in the hippocampus of 3, 12, 24 and 30 months old rats is studied. Wherever possible, methods have been used providing unbiased estimates of the investigated parameters. To estimate number and size of these structures, some of the methods evaluated in Part II have been applied. Synapses and neurons have been counted in serial sections according to an 'unbiased counting rule' (Gundersen, 1977). To avoid biases introduced by age-related or procedure-related changes in the reference volume, number fractions of neurons and synapses have been

calculated since number fractions do not depend on changes in the reference space.
Also the number and size of 'synapse perforations' have been estimated.
Three methods to estimate the number of 'presynaptic dense projections' are applied, evaluated and compared. To our knowledge, this is the first study, to apply these methods.
Synapse 'shadows' are reconstructed to obtain (indirect) information about the shape of the synapses.

The relevance of the results with regard to synaptic plasticity and the ageing process is discussed. In general, the effect of age on the parameters measured is found to be mild. The following observations are made: 1) no change in the numerical relation between numbers of CA1 and CA3 pyramidal neurons; 2) no change in the numerical relation between numbers of CA3 synapses (stratum radiatum) and CA3 pyramidal neurons; 3) no change in the numerical relation between numbers of perforated and non-perforated synapses in CA3, stratum radiatum; 4) an increase in size of the non-perforated synapses; 5) no change in the number of perforations per perforated synapse; significantly larger perforations at high age (30 months); 6) an increase in numbers of presynaptic dense projections; 7) no change in size and shape of synapse shadows; the shape of both synapse types deviates considerably from the presumed disc-shape.

The perforated synapses are found to be larger and more complex than the non-perforated synapses.

The reliability and value of the different variables are discussed in relation to the effect of age on the neural structures studied. The results, taken together, show that the number of synapses per neuron in the hippocampal CA3 area is not affected by age. The efficacy of the synapses increases with age, expressed by an increase in the number of dense projections in the active zone (transmission zone), an increase in size of the active zone (non-perforated synapses) and a larger size of the perforation area in the active zone (perforated synapses) at high age (30 months). Impairment of synaptic circuitry in this area at 30 months is not likely to occur.

Part IV, the Appendix, includes an extensive description of all the stereological/morphometrical procedures and formulae, used in Part III to quantify (arbitrairily-shaped) synapses.

SAMENVATTING

SAMENVATTING

Gebruik makend van kwantitatief stereologische/morfometrische methoden is onderzocht of er in de hippocampus van de rat gedurende het normale verouderingsproces sprake is van synaptische plasticiteit. De gebruikte methoden zijn geëvalueerd en hun bruikbaarheid voor kwantitatief morfologisch onderzoek aan neurale structuren wordt besproken.

Deel I is een inleiding tot het proefschrift. De doelstellingen van het proefschrift en de meest recente ideeën over structuur en functie van geperforeerde synapsen zijn gegeven, alsmede een korte beschrijving van de anatomie van de hippocampus.

Deel II omvat een vijftal publicaties waarin methodologische problemen beschreven zijn die men zoal tegen kan komen wanneer voor het kwantificeren van synapsen die willekeurig van vorm zijn, bepaalde stereologische/morfometrische methoden gebruikt worden .

In **Deel II, Hoofdstuk 1,** is de bias (of onbekende willekeurige "fout") bestudeerd waarmee schattingen van aantal en grootte van synapsen zijn behept wanneer complexe, geperforeerde synapsen niet als zodanig worden herkend. De resultaten, verkregen uit metingen in random coupes, zijn vergeleken met die, verkregen in serie coupes. Uit deze resultaten is af te leiden dat, wanneer de gelijktijdige aanwezigheid van complexe, geperforeerde synapsen en van niet-geperforeerde synapses niet wordt onderkend, de profiel lengte van de synapsen zal worden onderschat en hun dichtheid overschat wanneer deze worden gemeten in random ultradunne, E-PTA gecontrasteerde coupes. Zoals is beschreven kan dit probleem worden voorkomen door gebruik te maken van serie-coupes en een berekeningsmethode waarbij geen aannames gedaan hoeven te worden met betrekking tot de vorm en de grootte van de synaps.

In **Deel II, Hoofdstuk 2,** staat beschreven welke verbeteringen aan te brengen zijn in het protocol voor het snijden van serie-coupes. Ook is de zgn. serie-coupe techniek voor het schatten van numerieke dichtheden, toegepast op synapsen die willekeurig van vorm zijn. Belicht is, hoe de efficiëntie te vergroten is om tot routinematig gebruik van de techniek te kunnen komen. Met name door gebruik te maken van grote serie-coupes die, alvorens bekeken te worden op electronenmicroscopisch niveau, op lichtmicroscopisch niveau worden gecontroleerd. Daarnaast wordt gebruik gemaakt van een rotatie houder, van een gecalibreerde micrometer en van speciale grids waarmee men zich snel kan oriënteren in de coupe na inbrenging in de electronenbundel. Met deze veranderingen in het protocol blijken de problemen betreffende orientatie in het weefsel te zijn opgelost. Het is op deze manier niet moeilijk relevante gebieden in opeenvolgende coupes te herkennen en te vervolgen. Met behulp van de serie-coupe-techniek blijkt een schatting van de numerieke dichtheid N_V van geperforeerde en niet-geperforeerde synapsen te verkrijgen te zijn, die nagenoeg vrij is van bias. Enerzijds is het duidelijk geworden dat de dikte van de coupe bepaald moet worden met een grote mate van nauwkeurigheid. Anderzijds is gebleken dat de serie-coupe techniek, mits uitgevoerd zoals beschreven staat, niet langer bewerkelijker en arbeidsrovender is dan de conventionele methoden als het gaat om het bepalen van numerieke dichtheden N_V.

In **Deel II, Hoofdstuk 3,** zijn verschilllende methoden beschreven voor het bepalen

van de dikte van (ultra)dunne weefsel coupes. De methoden zijn geevaluëerd en onderling vergeleken. In het algemeen zal de coupedikte t' verschillen van de werkelijke afstand t tussen de twee snijvlakken die in feite de coupe genereren. Vijf verschillende methoden zijn experimenteel geëvalueerd, daarbij gebruik makend van coupes van verschillende interferentie kleur. In totaal zijn er tien verschillende interferentie kleuren geselecteerd en is de dikte van de coupes met een van de betreffende kleuren onderzocht, gebruikmakend van de volgende technieken: a) de zgn. small-fold techniek, b) de electron-scattering methode, c) interferentie microscopie met A) de Vicker's M86 scanning microinterferometer en B) de Jenoptik Amplival Interphako interferentie microscoop en d) de re-embedding methode.
Betrouwbare, reproduceerbare en vergelijkbare resultaten worden verkregen met de small-fold techniek, met de Vicker's M86 scanning microinterferometer en met de electron-scattering methode. Voor de electron-scattering methode zijn, voor de verschillende instellingen van de electronenmicroscoop, standaard testlijnen ontwikkeld. Ook met de Jenoptik Amplival Interphako interferentie microscoop blijken reproduceerbare resultaten te verkrijgen te zijn. Echter, in vergelijking met de resultaten van de andere drie technieken laten zij een constant verschil in dikte van de coupe zien. De re-embedding methode blijkt arbeids-intensiever te zijn en iets minder betrouwbaar dan de andere technieken. Verder kon geconcludeerd worden dat de variatie in t' tussen coupes van een bepaalde interferentie kleur (inter-coupe variatie) groter is dan de variatie in t' binnen een coupe (intra-coupe variatie).

In **Deel II, Hoofdstuk 4**, wordt, voor het schattten van numerieke dichtheden van synapsen, de conventionele ontvouwings procedure (Cruz-Orive, 1983) vergeleken met twee recente methoden, n.l. de serie-coupe techniek (Cruz-Orive, 1980) en de disector techniek (Sterio, 1984). Voor beide laatste methoden behoeven geen aannames gemaakt te worden met betrekking tot de grootte, de vorm en de orientatie van de synaps.
Aangetoond is dat een verdeling van de grootte van synapsen, welke op conventionele wijze verkregen is, geen bevredigende resultaten oplevert. Dergelijke resultaten zijn behept met een bias waarvan de omvang onbekend is. Met de disector techniek werden, in vergelijking met de resultaten van de serie-coupe techniek, consequent lagere waarden voor N_V verkregen . Uiteindelijk is er wat dit betreft een belangrijke conclusie getrokken: beide technieken zijn te gebruiken om synaptische dichtheden te bepalen, op voorwaarde dat er een betrouwbare schatting van de coupe dikte wordt verkregen en er een correcte en adequate sampling-procedure gebruikt wordt.

In **Deel II, Hoofdstuk 5**, wordt een methode beschreven waarmee informatie te verkrijgen is over verschillen of veranderingen in de vorm van willekeurig gevormde synapsen. Bij deze methode wordt gebruik gemaakt van metingen aan 2D reconstructies van zgn. orthogonale projecties (schaduwen) van synapsen. Verschillen die met deze methode aangetoond worden in de 2D reconstructies (orthogonale projecties of schaduwen), reflecteren uiteindelijk verschillen in de vorm van de feitelijke synaps. Met deze methode is aangetoond dat er verschillen bestaan in vorm en grootte tussen geperforeerde en niet-geperforeerde synapsen. In vergelijking met 3D reconstructies is de voorgestelde methode relatief eenvoudig. De methode heeft zeker zijn beperkingen,

met name wat betreft de orientatie en verdeling van de synapsen in het weefsel. Bovendien kunnen er geen harde conclusies getrokken worden wat betreft de werkelijke vorm van de synaps zoals 3D reconstructies dat doen. Desalnietemin kan de methode relevante informatie opleveren met betrekking tot de morfologie van synapsen, welke op geen enkele andere manier te verkrijgen is. 3D reconstructie bleek in deze studie nl. praktisch onmogelijk te zijn door de tot nu toe onoverkomelijke uitlijningsproblemen van E-PTA-gecontrasteerde synapsen.

In **Deel III** is het effect van de leeftijd op verschillende ultrastructurele karakteristieken van neuronen, van niet-geperforeerde en van geperforeerde synapsen bestudeerd in de hippocampus van 3, 12, 24 en 30 maanden oude ratten. Waar mogelijk, zijn methodes gebruikt die schattingen van de te bestuderen parameters opleveren welke vrij zijn van bias. Enkele van de methoden voor het schatten van aantal en grootte van deze structuren welke in deel II geëvalueerd werden, zijn hier toegepast. Zowel synapsen als neuronen zijn geteld in serie-coupes volgens een zgn. 'unbiased counting rule' (Gundersen, 1977). Om bias te vermijden welke geintroduceerd wordt door leeftijds- of procedure-gerelateerde veranderingen in het referentie volume, zijn neuron- en synaps-'aantalfracties' berekend (d.w.z. ratio's van numerieke dichtheden van verschillende structuren) berekend aangezien aantalfracties niet afhankelijk zijn van veranderingen in het referentie volume.
Ook het aantal en de grootte van de zgn. perforaties in de geperforeerde synapsen zijn geschat.
Om het aantal presynaptische 'dense projections' per synaps te schatten zijn drie methoden toegepast, geëvalueerd en onderling vergeleken. Voor zover ons bekend is deze verouderings-studie de eerste studie waarin deze methoden worden toegepast.
Van de synapsen zijn ook 2D reconstructies gemaakt om (indirecte) informatie te verkrijgen over eventuele vormveranderingen van de synapsen.

Tenslotte wordt de relevantie van de resultaten met betrekking tot synaptische plasticiteit en het verouderingsproces besproken. In het algemeen blijkt het effect van de leeftijd op de gemeten parameters, zo er al een effect is waargenomen, gering te zijn. Er zijn geen veranderingen gevonden in de aantalfractie CA1/CA3 pyramide neuronen, de aantalfractie CA3 synapsen (stratum radiatum)/CA3 pyramide neuronen en de aantalfractie CA3 geperforeerde/CA3 niet-geperforeerde synapsen. Er is een toename gevonden in de grootte van de niet-geperforeerde synapsen. Geen veranderingen in het aantal perforaties per geperforeerde synaps maar wel significant grotere perforaties op hoge leeftijd (30 maanden) en ten slotte zijn er ook geen veranderingen gevonden in de vorm en de grootte van de 2D reconstructies van de synapsen; de vorm van de beide synaps typen blijkt echter aanzienlijk te verschillen van de voor-onderstelde schijf-vorm.

De geperforeerde synapsen blijken groter en meer complex te zijn dan de niet-geperforeerde.

De betrouwbaarheid en de waarde van de verschillende variabelen worden besproken in relatie tot het effect van de leeftijd op de bestudeerde neurale structuren. Uiteindelijk is er geconcludeerd dat het aantal synapsen per neuron in het CA3 gebied van de hippocampus niet wordt beinvloed door de leeftijd. De efficiëntie van de synapsen

daarentegen lijkt toe te nemen met de leeftijd, hetgeen afgeleid wordt uit het toenemen van het aantal dense projections in de zgn. "actieve zone" (transmissie zone), uit het toenemen van de grootte van de actieve zone (niet-geperforeerde synapsen) en uit het toenemen van de grootte van de perforaties (geperforeerde synapsen) m.n. op hoge leeftijd (30 maanden). Het lijkt dus niet waarschijnlijk dat er in het onderzochte hippocampus gebied op de leeftijd van 30 maanden sprake is van een "aftakelen" van het synaptisch circuit.

In **Deel IV**, de Appendix, worden alle stereologische/morfometrische procedures en formules welke gebruikt zijn in Deel III voor het kwantificeren van synapsen, arbitrair van vorm, in detail beschreven.

CURRICULUM VITAE

CURRICULUM VITAE

Name: De Groot, Didima M.G.

Title: Master of Sciences;

Address (office): TNO-Medical Biological Laboratory
Lange Kleiweg 139
(*mail*) P.O. Box 5815, 2280 HV Rijswijk

Address (private): Cerespark 1, 5844 AE Stevensbeek

Date of birth: July 02 1949

Country of birth: The Netherlands

Nationality: Dutch

EDUCATION:

- Technician Medical Research, 1967
- Technician Histo-pathology, 1969
- Technician Biochemistry, 1970
- Master of Sciences Biology (with honor), Catholic University of Nijmegen, 1978:
  Main subjects: - Chemical Cytology
  - Electron microscopy
  - Physiology
- Teaching Certificate Biology, Catholic University of Nijmegen, 1985

POSITIONS HELD:

University of Nijmegen, Lab. Submicroscopic Morphology (Head: Prof. Dr. A.M. Stadhouders)	1967-1972
Mental Hospital "Endegeest", Oegstgeest, Lab. Electron Microscopy (Head: Dr. G.F.J.M. Vrensen)	1972-1975
Study in Biology	1975-1978
Part Time Teaching at Breitner College Rotterdam and Scholen Gemeenschap Stevensbeek	1975-1977
TNO/MBL Rijswijk, Department of Pharmacology	1978-present

MAIN RESEARCH INTERESTS:

- Research on the mechanism(s) of brain damage induced by cholinesterase inhibitors of the organophosphorus type (so-called "nerve agents") using (quantitative) light microscopy and electron microscopy, EEG-analyses, pharmacological, biochemical and behavioural means.
- Stereology
- Ageing

PEER REVIEWED PUBLICATIONS

1 Vrensen, G.F.J.M. and **De Groot, D.M.G.**,Some aspects of efficiency of electron microscopic autoradiography with tritium. J. of Histochemistry and Cytochemistry, 18 (1970) 278-290.

2 Vrensen, G.F.J.M. and **De Groot, D.M.G.**, Quantitative stereology of synapses : a critical investigation. Brain Research, 58 (1973) 25-35.

3 Vrensen, G.F.J.M. and **De Groot, D.M.G.**, Phosphotungstic acid staining and the quantitative stereology of synapses. Electron microscopy and cytochemistry, eds. Wisse, E., Daems, W.Th., Molenaar, I. and van Duijn, P., (1973) North-Holland Publishing Company Amsterdam, The Netherlands, 255-258.

4 Vrensen, G.F.J.M. and **De Groot, D.M.G.**, Osmium-zinc iodide staining and the quantitative study of central synapses. Brain Research, 74 (1974) 131-142.

5 Vrensen, G.F.J.M. and **De Groot, D.M.G.**, The effect of dark-rearing and its recovery on synaptic terminals in the visual cortex of rabbits. A quantitative electron microscopic study. Brain Research, 78 (1974) 263-278.

6 Vrensen, G.F.J.M. and **De Groot, D.M.G.**, The effect of monocular deprivation on synaptic terminals in the visual cortex of rabbits. A quantitative electron microscopic study. Brain Research, 93 (1975) 15-24.

7 Vrensen, G.F.J.M., vanHof, M.W., and **De Groot, D.M.G.**, Visual performance and synapses in the visual cortex of rabbits. Brain Research Bulletin, 1 (1976) 603-604.

8 Vrensen, G.F.J.M. and **De Groot, D.M.G.**, Quantitative aspects of the synaptic organization of the superior colliculus in control and dark-reared rabbits. Brain Research, 134 (1977) 417-428.

9 Vrensen, G.F.J.M., **De Groot, D.M.G.** and Nunes-Gardozo, J., The postnatal development of neurons and synapses in the visual and motor cortex of rabbits. A quantitative light and electron microscopic study. Brain Research Bulletin, 2 (1977) 405-416.

10 **De Groot, D.M.G.** and Vrensen, G.F.J.M., Postnatal development of synaptic contact zones in the visual cortex of rabbits. Brain Research, 147 (1978) 362-369.

11 Vrensen, G.F.J.M. and **De Groot, D.M.G.**, Neuronale and synaptic development of the cerebral cortex of the rabbits. Abh. Akad. Wiss. DDR 5 (1979) 383-391.

12 Vrensen, G.F.J.M., **De Groot, D.M.G.** and Boesten, A., Electron microscopy in Neurobiology. In : Methods in Neurobiology, Vol. 2, Edited by Lahue, R., Plenun Publishing Corporation, 1981, 433-500.

13 Magchielse, T., Hooisma, J., Muijser, H., **De Groot, D.M.G.** and Stevens, W.F., Application of sterile electrophysiological techniques for the investigation of long term changes in innervated myotubes in culture. Tissue Culture in Neurobiology, (1980) eds. E. Giacobini et al., Raven Press, New York, 13-23.

14 Hooisma, J., **De Groot, D.M.G.**, Magchielse, T. and Muijser, H., Sensitivity of several cell systems to acrylamide. Toxicology, 17 (1980) 161-167.

15 Hooisma, J., De Krijger, J., **De Groot, D.M.G.**, Magchielse, T. and Muijser, H., Effects of extracts of denervated muscle on the morphology of cultured muscle cells. Neuroscience Letters, 22 (1981) 47-50.

16 Verwer, R.W.H. and **De Groot, D.M.G.**, The effect of shape assumptions on the estimation of the numerical density of synapses from thin sections. Progress in Brain Research, 55 (1983) 196-203.

17 **De Groot, D.M.G.** and Bierman, E.P.B., The complex-shaped "perforated" synapse, a problem in quantitative stereology of the brain. J. Microsc., 131 (1983) 355-360.

18 **De Groot, D.M.G.**, Lage concentraties neurotoxische stoffen stereologisch opgespoord. Project, 11 (1984) 441-444.

19 **De Groot, D.M.G.**, Disc-like and complex-shaped synapses: Number, size and dense projections. A critical note. Acta Stereol. 4 (1985) 147-151.

20 **De Groot, D.M.G.** and Bierman, E.P.B., A critical evaluation of methods for estimating the numerical density of synapses, J. Neurosc. Meth., 18 (1986) 79-101.

21 **De Groot, D.M.G.** and Bierman, E.P.B., Numerical changes in rat hippocampal synapses. An effect of "ageing" ? Acta Stereol, 6 III (1987) 53-58.

22 **De Groot, D.M.G.**, Comparison of methods for the estimation of the thickness of ultrathin tissue sections, J. Microsc., 151 (1988) 23-42.

23 **De Groot, D.M.G.**, Improvements of the serial section method in relation to the estimation of the numerical density of complex-shaped synapses. In A. Reith and T.M. Mayhew (Eds), Stereology and Morphometry in Electron Microscopy. Problems and Solutions. Hemisphere Publishing Corporation, New York, London, (1988) 135-158.

24 Myhrer, T. and **De Groot, D.M.G.**, Immobility-related hippocampal theta activity in rats during reaction to novelty. Scandinavian J. of Psychology, 29, (1988) 214-222.

25 **De Groot, D.M.G.**, Bierman, E.P.B. and Van Huygevoort, A.H.B.M., Involvement of acetylcholine and glutamate in soman-induced brain damage. Micron and Microscopica Acta, 21 (1990) 247-248.

26 **De Groot, D.M.G.** and Bierman, E.P.B. and Saris-Wijnans, M.L., 2D Reconstruction of synapse orthogonal projections: estimation of differences in shape using second order moment invariants. Acta Stereol., 11/suppl 1 (1992) 587-592.

27 Philippens, H.C.H.M., Melchers, B.P.C., **De Groot, D.M.G.** and Wolthuis, O.L.; Behavioral performance, brain histology and EEG-sequela after immediate combined atropine/diazepam treatment of soman-intoxicated rats. Pharmacology Biochemistry and Behavior, 42 (1992) 711-719.

28 **De Groot, D.M.G.**, Measuring ultrathin section thicknesses. Protocols in Electron Microscopy. Accepted for publication.

29 Vrensen, G.F.J.M., Müller, L. and **De Groot, D.M.G.**, Some histological Techniques to study neuronal connectivity and synaptic ultrastructure. Korsakov J. of Neuropathology and Psychiatry: accepted for publication (to be translated into russian).

CONTRIBUTIONS TO MEETINGS MEDICAL DEFENCE RESEARCH

- PROCEEDINGS NATO RESEARCH STUDY GROUP 3, PANEL VIII
- PROCEEDINGS MEDICAL DEFENSE BIOSCIENCE REVIEW

1 **De Groot, D.M.G.** and Wolthuis, O.L., The effect of atropine on soman-induced lesions in the central nervous system of the rat. Proceedings of the NATO Research Study Group 3, Panel VIII, Grafschaft FRG, 30 September -4 October 1985, Part 1, 282-290.

2 **De Groot, D.M.G.**, On the mechanism of soman-induced brain lesions: Preliminary results. Proceedings of the third German-Dutch Symposium " Schutz vor hochtoxischen Substanzen", Schmallenberg-Grafschaft, 29 September - 1 October 1986, 246-248.

3 **De Groot, D.M.G.** and Wolthuis, O.L., "Convulsions" and "EEG-seizures" in soman-intoxicated rats; the effect of atropine sulphate and N-methyl-atropine nitrate treatment. Proceedings of the NATO Research Study Group 3, Panel VIII, Gent Belgium, 27-30 April 1987, Part 1, 16.1-16.7.

4 **De Groot, D.M.G.**, Soman and brain damage : a quantitative morphological study. Proceedings of the NATO Research Study Group 3, Panel VIII, Washington DC USA, 26-29 September 1988, Part 1, 117-139.

5 **De Groot, D.M.G.**, Soman and brain damage. Additional findings and comments on earlier results. Proceedings of the NATO Research Study Group 3, Panel VIII, The Hague The Netherlands, 13-17 November 1989, Part 1, 17.1-17.25.

6 **De Groot, D.M.G.**, Bierman, E.P.B. and Van Huygevoort, A.H.B.M., Does acetylcholine potentiate glutamate-induced neuron degenration in brains of soman-poisoned rats? Proceedings of the NATO RSG III Meeting Grenoble (1991).

7 **De Groot, D.M.G.**, Bierman, E.P.B. Van Huygevoort, A.H.B.M. and Bruijnzeel, P.L.B., Involvement of NMDA receptors in soman-induced neuropathology. Medical Defense Bioscience Review 1993 (1), 277-283.

8 Blanchet, G., Lallement, G., Carpentier, P., **De Groot, D,M,G.**, Bodjarvan, N., Rondouin, G., Lerner-Natoli, M., Vignon, M., Sentenac-Roumanou; H.,, and Kamenka, J.M., Role of glutamatergic system in nerve agent intoxication, Proceedings Medical Defense Bioscience Review 2 (1993) 405-413.

REPORTS RESEARCH PROJECTS[1]

1 **De Groot, D.M.G.**, Hooisma, J., Muijser, H. and Stevens, W.F., Detection of the adverse effects of neurotoxic compounds with the aid of nerve and muscle cells maintained in tissue culture. MBL-Report 1978-13.

2 **De Groot, D.M.G.**, Hooisma, J., Meeter, E. and Muijser, H., Detection of the adverse effects of neurotoxic compounds. MBL-Report 1980-16.

3 **De Groot, D.M.G.**, The influence of the shape of the presynaptic grid on the number of synapses counted. MBL-Report 1982-7.

4 **De Groot, D.M.G.** and Wolthuis, O.L., The effect of atropine on soman-induced lesions in the central nervous system of the rat. MBL-Report 1987-2.

5 **De Groot, D.M.G.** and Wolthuis, O.L., "Convulsions" and "EEG-seizures" in soman-intoxicated rats; the effect of atropine sulphate and N-methyl-atropine nitrate treatment. MBL-Report 1987-16.

6 **De Groot, D.M.G.**, Comparison of methods for the estimation of the thickness of ultrathin tissue sections. MBL-Report 1987-17.

7 Van Wijk, C.A.M. and **De Groot, D.M.G.**, Subclinical doses of soman and brain damage : A morphological, biochemical and electroencephalographical study in rat. MBL-Report 1990-13.

8 **De Groot, D.M.G.**, Soman and brain damage. Additional findings and comments on earlier results. MBL-Report 1990-14.

9 **De Groot, D.M.G.** and Wolthuis, O.L., Atropine protects against soman-induced convulsions, suppresses EEG-seizure-activity and prevents seizure-related brain damage. MBL-Report 1990-15.

10 **De Groot, D.M.G.**, Bierman, E.P.B. and Van Huygevoort, A.H.B.M., Does acetylcholine potentiate glutamate-induced neuron degeneration in brains of soman-poisoned rats? MBL-Report 1991-7.

11 Wolthuis, O.W., Van Helden, H.P.M., Melchers, B.P.C. Busker, R.W. and **De Groot, D.M.G.**, The search for a therapy against soman-intoxication. MBL-Report 1993-44.

ABSTRACTS IN INTERNATIONAL JOURNALS

1 **De Groot, D.M.G.** and Bierman, E.P.B., Age-related morphometric changes in the CNS of the rat? Neuroscience Letters, 7 (1981) S434.

2 **De Groot, D.M.G.**, Age-related morphometric changes in the CNS of the rat? Acta Anatomica, 111/1-2 (1981) 51-52.

3 **De Groot, D.M.G.**, Age-related morphometric changes in the CNS of the rat? Neuroscience Letters, 10 (1982) S145,

4 **De Groot, D.M.G.**, Problems in the quantitative stereology of complex- shaped synapses. J. Ultramicroscopy, 14/4 (1984) 404-405.

5 **De Groot, D.M.G.**, Stereology of (ultra)structural elements. Estimation of number, size and dense projections of arbitrary synapses. J. Ultramicroscopy, 19 (1986) 117.

6 **De Groot, D.M.G.**, Stereology of synapses: number, size and dense projections. J. Anat., 149 (1986) 211.

[1] MBL-Reports are available at the Royal Library in The Haque